

The Influence of Season, Heating Mode and Slope Angle  
on Wildland Fire Behavior

Jonathan Ray Gallacher

A dissertation submitted to the faculty of  
Brigham Young University  
in partial fulfillment of the requirements for the degree of  
Doctor of Philosophy

Thomas H. Fletcher, Chair  
David O. Lignell  
David R. Weise  
W. Vincent Wilding  
Bradley C. Bundy

Department of Chemical Engineering

Brigham Young University

February 2016

Copyright © 2016 Jonathan Ray Gallacher

All Rights Reserved



## ABSTRACT

### The Influence of Season, Heating Mode and Slope Angle on Wildland Fire Behavior

Jonathan Ray Gallacher  
Department of Chemical Engineering BYU  
Doctor of Philosophy

Wildland fire behavior research in the last 100 years has largely focused on understanding the physical phenomena behind fire spread and on developing models that can predict fire behavior. Research advances in the areas of live-fuel combustion and combustion modeling have highlighted several weaknesses in the current approach to fire research. Some of those areas include poor characterization of solid fuels in combustion modeling, a lack of understanding of the dominant heat transfer mechanisms in fire spread, a lack of understanding regarding the theory of live-fuel combustion, and a lack of understanding regarding the behavior of flames near slopes.

In this work, the physical properties, chemical properties and burning behavior of the foliage from ten live shrub and conifer fuels were measured throughout a one-year period. Burn experiments were performed using different heating modes, namely convection-only, radiation-only and combined convection and radiation. Models to predict the physical properties and burning behavior were developed and reported. The flame behavior and associated heat flux from fires near slopes were also measured. Several important conclusions are evident from analysis of the data, namely (1) seasonal variability of the measured physical properties was found to be adequately explained without the use of a seasonal parameter, (2) ignition and burning behavior cannot be described using single-parameter correlations similar to those used for dead fuels, (3) moisture content, sample mass, apparent density (broad-leaf species), surface area (broad-leaf), sample width (needle species) and stem diameter (needle) were identified as the most important predictors of fire behavior in live fuels, (4) volatiles content, ether extractives, and ash content were not significant predictors of fire behavior under the conditions studied, (5) broadleaf species experienced a significant increase in burning rate when convection and radiation were used together compared to convection alone while needle species showed no significant difference between convection-only and convection combined with radiation, (6) there is no practical difference between heating modes from the perspective of the solid—it is only the amount of energy absorbed and the resulting solid temperature that matter, and (7) a radiant flux of  $50 \text{ kW m}^{-2}$  alone was not sufficient to ignite the fuel sample under experimental conditions used in this research, (8) the average flame tilt angle at which the behavior of a flame near a slope deviated from the behavior of a flame on flat ground was between  $20^\circ$  and  $40^\circ$ , depending on the criteria used, and (9) the traditional view of safe separation distance for a safety zone as the distance from the flame base is inadequate for fires near slopes.

Keywords: physical properties, live fuels, fuel growth patterns, ignition, fire behavior, seasonal burning behavior, radiation, convection, Coanda effect, fire attachment on slopes, safe separation distance, firefighter safety zone



## ACKNOWLEDGEMENTS

I thank my research advisor, Tom Fletcher, for his guidance, mentorship, motivation and support while completing this project. I acknowledge his effort in walking the line between teaching effective research skills and allowing me to grow through experience. I am thankful for his help and friendship on a personal and professional level. I am grateful to David Weise for his mentorship and for his willingness to share his vast knowledge in all areas of wildland fire, all while continuing his work at the Pacific Southwest Research Station in Riverside, CA. I thank the other members of my graduate committee, David Lignell, Vince Wilding and Brad Bundy, for their feedback and support.

I am grateful for the efforts of those who collected samples and sent them to our lab: Joey Chong, Gloria Burke and Bonni Corcoran from Riverside, CA; Scott Pokswinski from Newton, GA; and Sara McAllister, Matt Jolly and Rachael Kropp from Missoula, MT. I am grateful for the collaboration with faculty and students from the University of Alabama – Huntsville: Babak Shotorban, Bangalore Yashwanth, Shankar Mahalingam and Selina Ferguson. I am grateful to the many undergraduate students from BYU who helped with this project: Victoria Lansinger, Sydney Hansen, Samantha Smith, Kelly Wilson, Ashley Doll, Taylor Ellsworth, Kristen Nicholes, Marianne Fletcher, Aaron Bush, Timothy Snow and Colton Hickman. This project would not have been possible without the work of all the people mentioned herein. I note with special thanks the contributions of Victoria Lansinger and Sydney Hansen for the work they put in while I was busy with course work and the department qualifying exam. I also acknowledge the work of Devin Kimball and Brad Ripa in performing experiments to study the Coanda Effect.

I am grateful for the collaboration and friendship of other graduate students, namely Dallon Prince, Chen Shen, Robert Laycock, Aaron Lewis, He Yang and Dan Jack. I am also grateful for mentoring from other experts in the field of fire research, specifically Sara McAllister, Bret Butler and Mark Finney from the Missoula Fire Lab in Missoula, MT.

I acknowledge the support and encouragement I received from my family, particularly from my parents and my wife's parents. I thank my children, Rachel, Caleb and Spencer, whose happiness and excitement brightened many weary days. I especially thank my wife, Kiera, for being a rock of support, comfort and love. I also thank her for her patience in following me across the country to complete graduate school. Lastly, I thank my Heavenly Father and His son, Jesus Christ, for guidance from the Holy Ghost and for the chance to repent and change for the better.

This work was supported by Joint Fire Sciences Program (JFSP) Grant 11-1-4-14 through United States Department of Agriculture (USDA) Forest Service Pacific Southwest (PSW) Research Station agreement 11-JV-11272167-044 and Brigham Young University. Any opinions, findings, and conclusions or recommendations expressed in this dissertation are those of the graduate student and advisor and do not necessarily reflect the views of the JFSP or any other government funding agency.

## TABLE OF CONTENTS

List of Tables	viii
List of Figures	x
1 Introduction	1
2 Literature Review	5
2.1 Fuel Element Property Measurements and Modeling	5
2.2 Ignition and Burning of Wildland Fuels	9
2.2.1 Ignition Time and Temperature	9
2.2.2 Effect of Moisture on Ignition Characteristics and the Differences between Live and Dead Fuels	11
2.2.3 Effect of Heat Transfer Mode on Ignition	14
2.2.4 Ignition Summary	16
2.3 Wildland Fire Modeling	17
2.3.1 Statistical Models	18
2.3.2 Physical Models	18
2.3.3 Empirical Models	20
2.3.4 Simulation Models	22
2.3.5 Modeling Summary	23
2.4 Fire Fighter Safety Considerations	24
2.4.1 Current Safety Zone Models	25
2.4.2 The Coanda Effect and its Influence on Fire Behavior near Solid Surfaces	26
2.4.3 The Coanda Effect and Safety Zones	27
2.5 Summary	28
3 Objective and Tasks	29
3.1 Objective	29
3.2 Tasks	29
4 Physical Properties and Dimensions for Ten Shrub and Conifer Fuels to Predict Fire Behavior	31
4.1 Methods	31
4.1.1 Measurements	31
4.1.2 Physical Properties Model Development	38
4.2 Results and Discussion	42

4.2.1	Size and Shape Measurements	42
4.2.2	Chemical Composition Measurements	47
4.2.3	Dry Mass Distribution	49
4.2.4	Prediction Models	51
4.2.5	Uncertainty Analysis	55
4.3	Summary and Conclusions	59
5	The Effect of Heating Mode on Ignition and Burning of Ten Live Fuel Species	61
5.1	Methods	61
5.1.1	Experiment Description	61
5.1.2	Analysis of Heat Transfer Conditions	65
5.2	Results and Discussion	67
5.3	Summary and Conclusions	74
6	Seasonal Changes in Ignition and Burning of Live Fuels using Natural Variation in Fuel Characteristics	77
6.1	Methods	77
6.1.1	Experimental Setup	77
6.1.2	Model Development	78
6.2	Results and Discussion	79
6.2.1	Effects of Sample Condition, Season, Moisture Content and Species	79
6.2.2	Single Variable Regressions	84
6.2.3	Multi-variable Regressions	87
6.2.4	Uncertainty Analysis	100
6.3	Summary and Conclusions	102
7	The Influence of the Coanda Effect on Flame Attachment to Slopes and Firefighter Safety Zone Considerations	105
7.1	Methods	105
7.2	Results	110
7.2.1	Flame Behavior Measurement Results	111
7.2.2	Heat Flux Measurement Results	114
7.2.3	Dimensional Analysis	119
7.3	Discussion	127
7.4	Summary and Conclusions	129
8	Summary and Conclusions	131

8.1	Physical and Chemical Properties	131
8.2	The Effects of Heating Mode on Ignition	131
8.3	Seasonal Variations in Ignition and Burning Behavior	132
8.4	The Effect of Slope Angle on Fire Behavior	133
8.5	Recommended Future Work	135
	References	137
	Appendix	155
A.	Preliminary Riverside Results	156
A.	1 Introduction	156
A.	2 Experimental Methods	157
A.	2.1 Shrub Combustion Experiment	157
A.	2.2 Individual Leaf Combustion Experiment	159
A.	3 Shrub Combustion Modeling	160
A.	4 Results and Discussion	163
A.	4.1 Shrub Combustion Experiments	163
A.	4.2 Shrub Combustion Modeling	166
A.	5 Future Work	168
A.	6 Conclusions	168
A.	7 Acknowledgements	169
B.	Prediction Model Parity Plots	170
B.1	Physical Properties Models	170
B.2	Ignition and Burning Behavior Models—Best Overall Models	177
B.3	Ignition and Burning Behavior Models—Models Using Most Common Parameters	185
C.	Experimental Data	193
C.1	Physical and Chemical Properties Data	193
C.2	Ignition and Burning Data	193
C.3	Temperature Plateau Data	194
C.4	Data for Flame Behavior near Slopes	195
D.	Data Processing and Model Development Algorithms	196
D.1	Surface Area Measurement Algorithm	196
D.2	Physical Properties Model Development Algorithm	197
D.3	Ignition and Burning Model Development Algorithm	221



## LIST OF TABLES

Table 4-1: Measurement definitions	33
Table 4-2: Species tested.	34
Table 4-3: Yearly average and standard deviation for measured foliage characteristics— broadleaf species.	44
Table 4-4: Yearly average and standard deviation for measured foliage characteristics— needle species.	44
Table 4-5: Yearly average values of volatiles content, fixed carbon content, ash content and lipid content for manzanita, ceanothus, Douglas-fir, Gambel oak, fetterbush,	49
Table 4-6: Weibull distribution parameters for measured dry mass calculated using	51
Table 4-7: Fuel element property models for broadleaf species.	53
Table 4-8: Fuel element property models for needle species.	54
Table 4-9: Relative uncertainty and sources of measurement error for all the pre-burn measurements.	57
Table 4-10: Estimated model prediction error due to measurement uncertainty normalized by the root mean squared error (RMSE) for each model. RMC = relative moisture	58
Table 5-1: Flame characteristics derived from video data.	63
Table 5-2. Effect of heating mode on ignition variables. Table entries indicate the	68
Table 5-3: Yearly average and range for the time required to reach 50% mass remaining for each species for the three heating cases. All times are in seconds.	69
Table 5-4: Maximum surface temperature (°C) for each species averaged over the year.	70
Table 6-1: Ignition time order listed from shortest to longest. Ignition times are averaged as indicated by the column headings.	83
Table 6-2: Order of strongest average correlation to weakest average correlation for needle species for each of the six listed burning characteristics. MC = moisture content;	85
Table 6-3: Order of strongest average correlation to weakest average correlation for broadleaf species for each of the six listed burning characteristics. MC = moisture content;	86
Table 6-4. Significance of yearly trends by species.	87
Table 6-5: Adjusted R <sup>2</sup> values when regressing flame characteristics for (a) the best overall model and (b) the model using the most frequent parameters. C means there was no significant model beyond a constant.	88
Table 6-6: Best overall correlations for flame characteristics of ten species.	90
Table 6-7: Correlations for flame characteristics for ten species using most frequent parameters from best-fit correlations shown in Table 6-6.	94
Table 6-8: Relative uncertainty and sources of measurement error for all the burn experiment measurements.	101
Table 6-9: Estimated model prediction error due to measurement uncertainty normalized by the root mean squared error (RMSE) for each	102
Table 6-10: Estimated model prediction error due to measurement uncertainty normalized by the root mean squared error (RMSE) for	102

Table 7-1: Table of run conditions for all experiments.	107
Table 7-2: Measurement definitions.	108
Table 7-3: Dimensionless numbers relevant to fire behavior near slopes.	121
Table 7-4: Variable definitions for use in dimensionless group calculations and experiment characterization.	121
Table 7-5: Measured conditions for five documented wildland fires plus the control burns from the experiments presented in this work.	124
Table 7-6: Conditions for five documented wildland fires estimated from measured data, plus the control burns from the experiments presented in this work.	124
Table 7-7: Estimates of the dimensionless flame length and heat	125
Table A-1: Experimental data for 16 big sagebrush shrub combustion experiments.	163

## LIST OF FIGURES

Figure 4-1: Diagram of measurements for broadleaf species.	32
Figure 4-2: Diagram of measurements for needle species, including sagebrush and chamise.	33
Figure 4-3: Apparatus used to measure foliage density.	36
Figure 4-4: Panel showing processing steps for surface area calculations. The left panel is the normal image, the middle panel is the binary image, and the right panel is the leaf perimeter.	37
Figure 4-5: Ether extractives apparatus showing soxhlet, sampling-containing thimble, condenser, round-bottom flask, solvent, stir bar and heater.	39
Figure 4-6: Flow chart for fuel element property model development	41
Figure 4-7: Yearly patterns for foliage moisture content (MC) and relative moisture content (RMC) for fetterbush (Fet), gallberry (Gal), sand pine (SP), sagebrush (Sage), lodgepole pine (LP), Gambel oak (Goak), Douglas-fir (DF), chamise, (Cham), manzanita (Manz) and ceanothus (Cean).	43
Figure 4-8: Monthly surface area and width values for gallberry. Error bars indicate the standard deviation in the data.	45
Figure 4-9: Monthly density values for manzanita and Gambel oak. Error bars indicate the standard deviation in the data.	46
Figure 4-10: Monthly thickness values for manzanita, Gambel oak and fetterbush. Error bars indicate the standard deviation in the data.	46
Figure 4-11: Surface area to volume (SA:V) ratio measurements for Gambel oak, fetterbush, gallberry, ceanothus and manzanita. Values shown are in units of inverse centimeters. Error bars indicate the standard deviation in the data.	47
Figure 4-12: Volatiles content, fixed carbon content, ash content and lipid content for manzanita, ceanothus, Douglas-fir, Gambel oak, fetterbush, sand pine and gallberry. Reported values are mass fractions on a dry basis. California species are on the left, Southern in the middle, and Rocky Mountain on the right.	48
Figure 4-13: Dry mass data, probability distribution function (pdf), cumulative distribution function (cdf) and empirical distribution function (edf) for species from the California region (left panel) and Southern region (right panel).	50
Figure 4-14: Dry mass data, probability distribution function (pdf), cumulative distribution function (cdf) and empirical distribution function (edf) for species from the Rocky Mountain region.	51
Figure 4-15: Physical property predictions for manzanita.	55
Figure 4-16: Physical property predictions for Douglas-fir.	56
Figure 5-1: Schematic of flat-flame burner.	62
Figure 5-2: Flame height versus time curve for a single fetterbush run. Points in time identified by red circles include ignition time, time to maximum flame height, burnout time and maximum flame height. All times were measured relative to the start time ( $t = 0$ ).	63

Figure 5-3: Example of image processing. The visual image is on the left, the binary image with the flame perimeter identified is on the right. Only contiguous pixels containing flame were categorized as part of the flame.	64
Figure 5-4: Infrared image for a convection-only manzanita run. The leaf is in the middle of the image, glowing red.	64
Figure 5-5: Time required to reach 50% mass remaining versus heat flux for all three heating cases for all ten species.	71
Figure 5-6: Time required to reach 50% mass remaining versus heat absorbed for all three heating cases for all ten species.	71
Figure 5-7: Typical average surface temperature versus time plot for convection-only run. The red circle indicates the temperature plateau	73
Figure 5-8: Plateau temperature versus heat flux for five boradleaf species for the three heating cases.	74
Figure 6-1: Results of sample condition experiments for chamise branch segments. The left pane shows the time required to reach 50% mass remaining ( $t_{50}$ ); the right pane shows the t-test results for the different comparisons. Error bars represent one standard deviation. SDAN=slow drying, all needles; NDAN=no drying, all needles; NDHN=no drying, half needles; QDAN=quick drying, all needles; QDHN=quick drying, half needles.	80
Figure 6-2: Ignition time versus month (left column) and moisture content (right column). Manz = manzanita, Cean = ceanothus, Cham = chamise, Fet = fetterbush, Gal = gallberry, SP = sand pine, DF = Douglas-fir, Goak = Gambel oak, Sage = sagebrush, LP = lodgepole pine.	81
Figure 6-3: Ignition temperature versus month (left column) and moisture content (right column). Manz = manzanita, Cean = ceanothus, Cham = chamise, Fet = fetterbush, Gal = gallberry, SP = sand pine, DF = Douglas-fir, Goak = Gambel oak, Sage = sagebrush, LP =lodgepole pine.	82
Figure 6-4: Parity plots for ignition temperatures for manzanita. Best overall models are shown in the left column, models using the most common predictors are shown in the right column.	97
Figure 6-5: Parity plots for burning characteristics for manzanita. Best overall models are shown in the left column, models using the most common predictors are shown in the right column.	98
Figure 6-6: Parity plots for burning characteristics for Douglas-fir. Best overall models are shown in the left column, models using the most common predictors are shown in the right column.	99
Figure 6-7: Parity plots for ignition temperatures for Douglas-fir. Best overall models are shown in the left column, models using the most common predictors are shown in the right column.	100
Figure 7-1: Experimental apparatus showing fuel pan, flame, slope and heat flux sensor placement.	106
Figure 7-2: Schematic showing definitions of flame height, flame length and flame attachment zone.	109

Figure 7-3: Image processing example. The left image is the visual image from and experiment, the right image is the associated binary image.	110
Figure 7-4: Transient flame height data in centimeters (a) and radiative heat flux data in kilowatts per square meter (b) for a control run at 0° and 30 cm.	111
Figure 7-5: Flame length measured in centimeters. Each point represents the average of all burns for that angle and boundary condition. The error bars and dashed lines represent the 95% confidence interval.	112
Figure 7-6: Flame attachment length, measured in centimeters. Each point represents the average of all burns for that angle and boundary condition. The error bars and dashed lines represent the 95% confidence interval.	113
Figure 7-7: Fraction of run time with flame attached to slope. Each point represents the average of all burns for that angle and boundary condition. The error bars and dashed lines represent the 95% confidence interval.	113
Figure 7-8: Flame pulse frequency, measured in hertz (Hz). Each point represents the average of all burns for that angle and boundary condition. The error bars and dashed lines represent the 95% confidence interval.	114
Figure 7-9: Average radiative heat flux, measured in kilowatts per square meter (kW m <sup>-2</sup> ). Each point represents the average of all burns for that angle and boundary condition. The error bars and represent the 95% confidence interval.	116
Figure 7-10: Average convective heat flux, measured in kilowatts per square meter (kW m <sup>-2</sup> ). Each point represents the average of all burns for that angle and boundary condition. The error bars and represent the 95% confidence interval.	116
Figure 7-11: Average convective and radiative heat flux for bare metal and insulated slopes. Each point represents the average of all burns for that angle and boundary condition. The error bars and represent the 95% confidence interval.	117
Figure 7-12: Average and maximum total heat flux for bare metal and insulated slopes. Each point represents the average of all burns for that angle and boundary condition normalized against the mean and maximum values for the 0° control burn. The error bars and represent the 95% confidence interval.	119
Figure 7-13: Angle at which the deviation from control levels becomes significant for each the burn characteristics on the x-axis. Labels on the x-axis are those shown in Table 7-2. Pulse frequency is not shown here because there was no significant deviation from control levels.	120
Figure 7-14: Dimensionless flame attachment length ( $L_{Attach}$ ) versus slope angle. The solid line is the dimensionless attachment length for the control burns; the dashed line is the dimensionless flame length for the control burns.	122
Figure 7-15: Dimensionless heat flux upslope ( $Flux_{Attach}$ ) versus slope angle. The solid line is the dimensionless heat flux for the control burns; the dashed line is the heat release rate for the control burns.	123
Figure 7-16: Dimensionless flame attachment length ( $L_{Attach}$ ) versus slope angle. The solid line is the dimensionless attachment length for the control burns; the dashed line is the dimensionless flame length for the control burns. The triangles represent the estimates of flame attachment from reported data for five documented wildland fires.	126

Figure 7-17: Dimensionless heat flux upslope ( $\text{Flux}_{\text{Attach}}$ ) versus slope angle. The solid line is the dimensionless heat flux for the control burns; the dashed line is the heat release rate for the control burns. The triangles represent the estimates of heat flux from reported data for five documented wildland fires.	126
Figure A-1: Schematic illustration of the wind tunnel at the Pacific Southwest Research Station of Forest service in Riverside, CA (Lozano, 2011)	159
Figure A-2: Comparison of (a) picture of a manzanita shrub and (b) manzanita shrub simulated.	161
Figure A-3: Maximum solid temperature of each area with respect to time for a manzanita shrub combustion experiment with no wind.	165
Figure A-4: Burning big sagebrush stems after the foliage burnout.	165
Figure A-5: $\Delta z_{f,\text{max}}$ comparison of current model (box plots of minimum, first quartile, median, third quartile and maximum) and wind tunnel experiments (dots) (Prince, 2014)	167
Figure A-6: Burn time comparison of model simulations (box plots of minimum, first quartile, median, third quartile and maximum) and wind tunnel experiments (dots) (Prince, 2014)	167
Figure A-7: Comparison of predicted flame behavior in a manzanita shrub (left) using the semi-empirical shrub combustion model vs. the measured flame behavior in a wind tunnel.	168
Figure B-1: Parity plots for chamise	170
Figure B-2: Parity plots for sagebrush	170
Figure B-3: Parity plots for ceanothus	171
Figure B-4: Parity plots for fetterbush	172
Figure B-5: Parity plots for gallberry	173
Figure B-6: Parity plots for Gambel oak	174
Figure B-7: Parity plots for lodgepole pine	175
Figure B-8: Parity plots for sand pine	176
Figure B-9: Parity plots for ceanothus—best overall models	177
Figure B-10: Parity plots for chamise—best overall models	178
Figure B-11: Parity plots for fetterbush—best overall models	179
Figure B-12: Parity plots for gallberry—best overall models	180
Figure B-13: Parity plots for Gambel oak—best overall models	181
Figure B-14: Parity plots for lodgepole pine—best overall models	182
Figure B-15: Parity plots for sagebrush—best overall models	183
Figure B-16: Parity plots for sand pine—best overall models	184
Figure B-17: Parity plots for ceanothus—models using MCP	185
Figure B-18: Parity plots for chamise—models using MCP	186
Figure B-19: Parity plots for fetterbush—models using MCP	187
Figure B-20: Parity plots for gallberry—models using MCP	188
Figure B-21: Parity plots for Gambel oak—models using MCP	189
Figure B-22: Parity plots for lodgepole pine—models using MCP	190
Figure B-23: Parity plots for sagebrush—models using MCP	191

Figure B-24: Parity plots for sand pine—models using MCP	192
Figure C-1: Sample temperature plateau curves for all ten species. Broadleaf species are in the left column, needle species are in the right column.	194



## 1 INTRODUCTION

Knowledge of the role that wildland fire plays in shaping the landscapes in North America has dramatically increased over the past 60 years. With this knowledge, federal wildland fire policy in the United States has evolved. The focus a century ago was on fire suppression. Over the last century, this practice has resulted in an increase in fuel density in the form of forest litter and small shrubs, causing an escalation in fire intensity and a heightened awareness that more work is needed to understand the fundamentals of fire spread. Statistics from the National Interagency Fire Center (National Interagency Fire Center, 2014) support these conclusions. Data on area burned and suppression costs indicate these numbers have doubled over the last 20 years, from averages of 2.96 million acres and \$371 million between 1985 and 1989 to 5.86 million acres and \$1605 million between 2010 and 2014. While the cost and area burned has increased, the average number of fires has decreased, from 72,000 (1985-1989) to 65,000 (2010-2014). The trend of larger, more intense fires has not gone unnoticed. Most work in this area focuses on the causes of these “megafires” and steps to reduce their frequency (Maditinos and Vassiliadis, 2011; Adams, 2013; Flannigan et al., 2013; Williams, 2013; Liu et al., 2014; Stavros et al., 2014). While not specifically promoting the spread of megafires, some ecologists have argued that larger fires actually increase the health of forests and shrublands (Smith et al., 2011; Wan et al., 2014). The current US wildland fire policy reflects these ideas by holding paramount firefighter safety while recognizing the important

ecological functions of fire as well as the economic impact that fire management has on the budget (Bunsenberg, 2004; Stephens and Ruth, 2005; Fire Executive Council, 2009).

A key component of the current policy is the emphasis on risk management and decision support systems, which makes it imperative that our understanding of wildland fire be enhanced and the suite of fire models be improved. Efforts to model wildfires and predict their behavior have been largely successful for dead, homogenous fuel beds like dry grasslands and forest litter (Rothermel, 1972; Sullivan, 2009b). Modeling of fire spread in live vegetation is more difficult, and the lack of knowledge surrounding which physical phenomena drive fire spread in live fuels increases the uncertainty of the model (Finney et al., 2013). The differences between grasslands, forests, and shrublands add further difficulty to the problem. Since much of the western United States is covered by sparsely growing shrubs and small trees (LANDFIRE 1.2.0, 2010), it is vital to understand those differences so fire managers have more accurate information to guide their decisions.

Another major emphasis in fire policy is on firefighter safety. During the last 100 years, thousands of wildland firefighters have been killed or injured in the line of duty (Britton et al., 2013; Butler, 2014). Of the 900 deaths in that time, 427 were due to firefighter entrapment, the phenomenon that occurs when the fire passes over the firefighter's location (Fryer et al., 2013). While firefighter entrapment fatalities have declined over the last 50 years, they have not been eliminated (Butler, 2014). Butler (2014) summarized the current challenges in safety zone determination and listed, among other things, the lack of a theoretical understanding of fires in live fuels and the lack of understanding regarding the influence of slope angle on fire behavior as two critical areas where further research is needed. This knowledge will help firefighters better

understand where, and how fast, the fire is likely to spread and also help identify locations where firefighters will be safe if the fire behavior changes drastically.

The National Fire Decision Support Center identified five key areas of fire research that must be understood in order to improve fire models and thereby improve fire management strategies and fire fighter safety protocols. This dissertation presents the results of two years of experimental measurements focusing on two of those key areas, namely the ignition and burning behavior of live fuels and the differences between convection and radiation in heating live fuels to ignition. This dissertation also presents work to describe the behavior of fires near slopes and the influence this behavior has on firefighter safety.



## **2 LITERATURE REVIEW**

Ignition of wood and other cellulosic fuels has been studied for over 100 years. Research has been conducted in many areas that feed into a discussion of wildland fire, including fuel bed descriptions, requirements for ignition, conditions during burning, predictive modeling techniques (including rate of spread calculations), and fire fighter safety. The ultimate goal in wildfire research is two-fold: (1) to understand the physical phenomena that occur within wildfires, and (2) to develop models that can predict wildfire behavior. Both these research areas feed into fire fighter safety protocols. Each of the aforementioned research areas will be discussed briefly: Work to quantify and describe fuel and fuel-bed properties will be reviewed in Section 2.1; research into physical phenomena (requirements for ignition and conditions during burning) will be reviewed in Section 2.2; modeling techniques will be reviewed in Section 2.3; the influence of fire behavior near slopes and the resulting effect on firefighter safety zones will be reviewed in Section 2.4.

### **2.1 Fuel Element Property Measurements and Modeling**

Fuel characterization, including physical properties, chemical properties, fuel load, and fuel location, is an inherent part of any experimental or modeling effort to understand wildland fire behavior. Characterization of the solid fuel (i.e., grasses, shrubs and trees) can be divided into three categories: (1) allometric models, (2) three-dimensional (3D) fuel placement models, and (3) fuel element property models. A discussion of each category follows.

Allometric models can predict general fuel properties, such as fuel loading, canopy height, relative amounts of live and dead fuel, and biomass by size class. These models can be used in conjunction with remote sensing or ground cover data to describe general fuel properties over large areas. Considerable work has been done in this area. Most techniques are destructive and time intensive (Ludwig et al., 1975; Brown, 1976, 1978; Helgerson et al., 1988; Williams, 1989; Schlecht and Affleck, 2014). The main drawback of these models, beyond the labor necessary to develop them, is their limited applicability—the correlations are specific to both the fuel type and location. Efforts to improve these models and reduce the required labor through the use of remote sensing have received increased attention in recent years. Remote sensing data have been used to measure detailed information about individual plants and general information about large areas. Seielstad et al. (2011) found that remote sensing can be used to distinguish foliage and small branches from large branches in Douglas-fir. Skowronski et al. (2007); (2011) and Barbier et al. (2012) all discuss remote sensing models that predict properties like canopy bulk density for large areas of land with a high degree of accuracy. A different approach is to use plant growth theory to predict bulk properties. One such model is that developed by Bartelink (1998) which allows for growth predictions to be adjusted based on simulated growing conditions. While these models provide some necessary information to describe solid fuels, they do not provide all the necessary information. This is seen in the work by Wright (2013), in which prescribed burn plots with similar fuel loading and fuel type experienced widely different total burn areas even when accounting for weather variations.

Fuel placement models are those models that seek to capture the natural structure of plants and the resulting local fuel-density fluctuations. Research has shown fuel bulk density to be an important variable in fire propagation (Rothermel, 1972; White and Zipperer, 2010;

Marino et al., 2012). Work by Parsons et al. (2011) illustrated the need for accurate 3D fuel characterization. Using a stochastic fuel placement technique called FUEL3D, Parsons et al. (2011) showed that, for the same mass and volume, fire spread behaves very differently between fuel beds with homogeneous fuel density and those with variable fuel density. Schwilk (2003) found that cutting dead fuel from the shrub canopy and placing it on the ground significantly reduced fire intensity, and thus concluded that canopy structure, not just fuel load, affects fire behavior. Weise and Wright (2014) cite several other studies which indicate the importance of fuel arrangement. Prince et al. (2014) developed a fuel placement model for chamise and juniper based on fractal theory. They used bulk descriptors from Countryman and Philpot (1970) to provide guidance for the overall shrub properties, then built the shrub using the natural repeating patterns found in those species. While these models provide the location in 3D space of the shrub's trunk, branches and foliage, they do not provide a physical description of the various shrub parts that affect burning behavior.

Fuel element property models are those models that describe the physical, chemical, and shape properties of individual leaves or small branch segments. Chemical properties have received considerable attention (Hough, 1969; Behm et al., 2004), and include properties like heat capacity, thermal conductivity, and heat of combustion as well as chemical composition measurements like volatiles content, ash content, structural carbohydrates and ether extractives. Extensive work has been completed to measure and predict heat capacity and thermal conductivity for various species of wood (Forest Products Laboratory, 2010) but little has been done for foliage. Most models for foliage combustion use a form similar to those developed for wood (Fons, 1946; Engstrom et al., 2004; McAllister et al., 2012; Prince, 2014). Chemical composition and heat of combustion measurements for foliage are common (Countryman and

Philpot, 1970; Rothermel and Philpot, 1973; Countryman, 1982; Frandsen, 1983; Burgan and Sussot, 1991; Owens et al., 1998; Elder et al., 2011; Jolly et al., 2014). Work has been done to connect these measurements to flammability and is discussed in Section 2.2.2.

Physical and shape properties have received less attention than chemical properties. Work by Lyons and Weber (1993) indicated size, shape and orientation of fine fuels could affect burning behavior. Fons (1946) found that properties like surface area, fuel volume, and foliage density are important in fire behavior predictions. More recent work (Engstrom et al., 2004; Fletcher et al., 2007; Shen, 2013) showed fuel orientation and thickness can drastically influence ignition of shrub foliage. Despite the established effect of these physical properties and dimensions, there is a startling lack of data in the literature. Countryman and Philpot (1970) and Countryman (1982) provide excellent descriptions of some common California fuels, including fuel properties such as ash content, percent extractives, extractive heat content, density, surface area and volume, but did not report other geometrical properties. Wagtendonk et al. (1996) measured the diameter, specific gravity and surface-area-to-volume ratio for 19 coniferous species based on size class and age, but did not report other properties and did not specify if the needles were used for specific gravity and surface-area-to-volume measurements. Shen and Fletcher (2015) provided correlations for the geometrical properties of four fuel species to be used in fire spread models, but did not measure surface area or density, two properties that have been found to affect fire behavior (Fons, 1946; Lyons and Weber, 1993). Pickett (2008) measured physical dimensions for several fuels but did not report any prediction models for these properties, though Prince (2014) reported correlations for manzanita leaves. No other work has been done to measure or model the physical properties and dimensions of individual fine fuel

elements. This lack of data highlights the need to develop these prediction models for other fuel types so solid fuels can be characterized completely.

## **2.2 Ignition and Burning of Wildland Fuels**

Ignition and burning of live forest and shrub fuels are not well understood (Finney et al., 2013); our understanding must increase if accurate wildland fire prediction models are to be developed. Current research efforts in this area focus on two questions: (1) Does radiation or convection dominate in wildland fire spread, and (2) What causes the differences in burning behavior observed between species and between live and dead fuels. Section 2.2.1 discusses background work on ignition of wood fuels and foliage. The differences in burning behavior between live and dead fuels are discussed in Section 2.2.2. The effect of heating mode on ignition and burning is discussed in Section 2.2.3.

### **2.2.1 Ignition Time and Temperature**

Ignition time and temperature are two empirical phenomena used to describe rate of fire spread and amount of fuel consumed. Fundamentally, ignition (defined as the onset of a sustained, visible flame for the purposes of this discussion) occurs when molecules in the solid break down, enter the gas phase, mix with air and react. Since these phenomena are difficult to measure, ignition time and temperature are often used as an approximate way to capture these details. Ignition time is defined as the time elapsed between fuel sample exposure to elevated temperatures and ignition, and these values are used in modeling to simulate the ignition delay sequence—pre-heating followed by the onset of pyrolysis. Ignition temperature is defined as the fuel surface temperature when ignition occurs, and these values are used in modeling to represent the point at which pyrolysis rates are high enough to support a flame. It should be noted that

these two parameters are intimately linked with both the chemical composition and properties of the individual fuel samples as well as the experimental conditions under which they were measured. Thus, while these parameters provide a convenient way to discuss results, they do not convey the complex phenomena occurring during ignition (Smith and King, 1970).

Many studies have been performed during the last century on both wood fuels and foliage to determine these parameters, with the bulk of the literature focusing on ignition temperature. Experimental conclusions to date are mixed. Babrauskas (2002, 2003) compiled the results of ignition temperature experiments on wood fuels and foliage, respectively. After eliminating the experiments in which the fuel sample was pressed against a hot surface, the reported ignition temperatures ranged from 200-530°C for wood and 201-450°C for foliage. Babrauskas noted the large amount of scatter in the data and suggested that, in addition to variations in experimental setup and measurement techniques, sample condition (e.g. moisture content and size) and species could affect ignition temperature.

Wildland fire observations that species burn differently support Babrauskas's postulate that plant species could be one source of variation in measured ignition temperatures (Fletcher et al., 2007). However, results by Susott (1982) showed that material ground from various plant species has the same heat of combustion and similar TGA (thermogravimetric analysis) pyrolysis mass release curves, and should therefore burn similarly. Thus, one possible explanation for the observed differences in ignition properties is the shape and structure of the plant and the effect shape has on heat and mass transfer. However, this explanation has not been tested experimentally. Most empirical correlations used to predict ignition behavior, particularly for live fuels, are species specific (Xanthopoulos and Wakimoto, 1993; Dimitrakopoulos and

Papaioannou, 2001; Smith, 2005; Pellizzaro et al., 2007; Shen, 2013). Work must be done to understand the differences in ignition behavior between various species.

### **2.2.2 Effect of Moisture on Ignition Characteristics and the Differences between Live and Dead Fuels**

Investigation of the effect of moisture content on ignition has been studied extensively and supports Babrauskas' postulate that sample condition affects ignition. Moisture has been shown to increase both ignition time (Fons, 1950; Xanthopoulos and Wakimoto, 1993; Gill and Moore, 1996; Shu et al., 2000; Dimitrakopoulos, 2001) and ignition temperature (Moghtaderi et al., 1997; Catchpole et al., 2002; Smith, 2005) for various fuels. There are many possible reasons for this delay. Dilution of pyrolysis gases with non-combustible gases has been cited as a method for fire suppression (Fons, 1950; Browne, 1958; Catchpole et al., 2002; Lu et al., 2004; Ferguson et al., 2013). Ferguson et al. (2013) also show that gas-phase temperature is reduced as moisture increases, which should slow heat transfer to the surface and reduce the surface temperature. Haseli et al. (2011) and Leroy et al. (2010) have shown pyrolysis to be a strong function of surface temperature. A slight discrepancy seems to arise at this point in the discussion. Moisture increases ignition temperature, but also decreases the gas temperature surrounding the solid which should decrease the solid temperature. One possible explanation for this problem is that the rate of pyrolysis required to sustain a flame is greater due to dilution by water. Thus, ignition is delayed until the higher rate of pyrolysis is achieved and a higher average surface temperature is measured at ignition.

While these results are insightful, most of the previous research on moisture effects has been performed on dead fuels that have been pre-treated to a specified moisture content. Xanthopoulos and Wakimoto (1993) performed seasonal experiments on three western conifer

species. Fresh cut branch segments (10-15 cm in length) were burned in heated air at temperatures between 400 °C and 640 °C. Correlations were developed to predict ignition time based on air temperature and fuel moisture content. Results showed trends are non-linear and vary with species. Researchers at Brigham Young University (BYU) have collectively performed thousands of experiments on individual fuel elements in the last decade (Engstrom et al., 2004; Smith, 2005; Fletcher et al., 2007; Pickett, 2008; Pickett et al., 2009; Pickett et al., 2010; Cole et al., 2011; Prince, 2014; Prince and Fletcher, 2014; Shen and Fletcher, 2015). Samples, composed of individual leaves for leaf species and 4 – 6 cm branch segments (<6 mm diameter) for needle species, were burned in 1000 °C post-flame gases with 10 mol% oxygen to more closely resemble the conditions of wildland fires (Butler et al., 2004a). Initial experiments were used to compare live and dead fuels with similar moisture contents, describe qualitatively and quantitatively the physical changes that occur during live fuel combustion, and determine if flaming ignition would occur without direct flame contact. Observations regarding the link between live fuel ignition and moisture were also reported. Work by Fletcher et al. (2007) and Prince and Fletcher (2013) has shown live fuels release moisture differently than dead fuels. Water evaporation in dead fuels has been assumed complete in fine fuels once the sample temperature passes 100°C (Albini, 1967; Rothermel, 1972), but Fletcher et al. (2007) showed there is still a significant amount of moisture in live fuels when ignition occurs. Pickett (2008) showed water release still occurring at surface temperatures in excess of 200°C and Prince (2014) showed significant differences in the temperature profiles of live and dead foliage during ignition and burning even with the same moisture content. Work by McAllister et al. (2012) showed significant differences in the ignition behavior between live and dead pine needles. Additionally, work by Weise et al. (2005a) demonstrated live fuels can burn with moisture levels

in excess of 100% on a dry-weight basis while dead fuels are rarely able to sustain combustion when moisture content is above 30-35% (Hawley, 1926; Lindenmuth and Davis, 1973). Tiaz and Zeiger (2010) indicate plant response to environmental stresses like drought causes accumulation of non-structural carbohydrates within plant cells that could affect flammability. These differences have led researchers to postulate that there is significant interaction between the free water and the cells in live plants that does not occur in dead plants (McAllister et al., 2012; Prince and Fletcher, 2013). Finney et al. (2013) postulated that water release in live fuels is not complete until breakdown of the cellular structure occurs. Still other work has been done indicating root structure (Pellizzaro et al., 2007), plant dry mass (Jolly et al., 2014), chemical composition (Pyne et al., 1996; McAllister et al., 2012), tree sex (Owens et al., 1998) and post-fire regeneration strategy (Cowan, 2010) could have a larger effect on ignition of live fuels than moisture content, though results are mixed in work to quantify the effect of chemical composition (Alessio et al., 2008). Several studies have been published indicating flammability changes with season but not necessarily with moisture content (Philpot, 1969; Wright and Bailey, 1982; White, 1994; Rodriguez Anon et al., 1995; Bianchi and Defosse, 2015). White and Zipperer (2010) review work done on the flammability of live foliage and conclude moisture content has the largest effect on ignition (Etlinger and Beall, 2004; Weise et al., 2005b; Alessio et al., 2008). There are some dissenting opinions (Alexander and Cruz, 2013), but the general consensus is that live fuels burn differently than dead fuels and that moisture has a significant effect on burning characteristics for both live and dead fuels. In summary, a fundamental understanding of the physical processes that drive live fuel combustion is both absent and necessary if predictive models are to be developed.

Another difficulty in evaluating the effects of moisture levels on foliage combustion is the presence of light hydrocarbons (ether extractives such as fats, waxes and terpenoids) in live foliage (Philpot and Mutch, 1970; Susott, 1980). While structural carbohydrate (cellulose, hemicellulose, and lignin) content within foliage changes very little once a leaf is fully developed, levels of non-structural carbohydrates, extractives and water experience fluctuations in response to season and climatological conditions (Kozlowsk and Clausen, 1965; Little, 1970; Gilmore, 1977; Kainulainen et al., 1992; Jolly et al., 2014). These extractives have the highest heat content of any forest fuel (Nunez-Regueira et al., 2005) and often decompose and vaporize at temperatures much lower than accepted ignition temperatures. For example, Mardini et al. (1989) suggested decomposition temperatures of extractives as low as 50 °C. This early devolatilization could lead to an increase in flammability for live fuels, and the presence of these extractives is sometimes cited as the reason for the ability of live fuels to burn under conditions in which dead fuels do not burn (Finney et al., 2013). These phenomena must be understood if a fundamental understanding of wildfire spread is to be developed.

### **2.2.3 Effect of Heat Transfer Mode on Ignition**

Many experimentalists and modelers have concluded that radiation heat transfer dominates in large fires (Simms, 1960; Balbi et al., 2007; Silvani and Morandini, 2009; Paudel, 2013) and fires with little to no wind in homogeneous fuel beds (Morandini et al., 2001; Morvan and Dupuy, 2001; Sullivan et al., 2003; Morvan and Dupuy, 2004), but the relative effect of radiation and convection for fires outside these conditions is still unknown (Morandini et al., 2001; Sullivan et al., 2003). Much of the experimental work looking at heat transfer mode has focused on dead and woody fuels (Simms, 1960, 1963; McCarter and Broido, 1965; Simms and Law, 1967; Pagni, 1975; Moghtaderi et al., 1997; Morandini et al., 2001; Dupuy et al., 2003;

Gratkowski et al., 2006; Pitts, 2007; Reszka and Torero, 2008; Silvani and Morandini, 2009), with only a limited amount of work performed for live fuels and foliage (Stocks et al., 2004; McAllister et al., 2012). Experiments performed by Rothermel (1972) showed fuel pre-heating in no-wind and backing-fire situations, illustrating radiative heating and leading researchers to conclude that radiation is the dominant form of heat transfer for fire spread. However, other experiments have shown that, while pre-heating does occur due to radiation, the bulk of the temperature rise occurs within a few centimeters of the flame front in no-wind situations (Fang and Steward, 1969; Baines, 1990) and that significant amounts of pyrolyzates are not formed at the fuel temperatures associated with radiant pre-heating (Cohen and Finney, 2010). Anderson (1969) concluded that radiant heat flux can provide no more than 40% of the energy required for sustained fire spread. Engstrom et al. (2004) showed experimentally that flaming ignition can occur with convective heating without direct flame contact. Work in the past three years has shown that convection contributes significantly to intermittent fuel pre-heating and downward fire spread (Finney et al., 2015). Still other work has shown flame propagation to depend strongly on direct flame contact with un-burned fuel (Vogel and Williams, 1970; Carrier et al., 1991). Current operational fire spread models do not differentiate between heat transfer mechanisms (Sullivan, 2009b, c). This lack of consensus illustrates that a detailed understanding of heat transfer in fire spread and the mode driving that spread under various conditions is still missing (Finney et al., 2013).

One reason it is difficult to reach a consensus on heat transfer effects in wildland fire is that it is problematic to compare results from different data sets due to varying experimental conditions. For example, McAllister et al. (2012) report ignition characteristics of live fuels under radiant heating using the FIST apparatus. The experimental setup includes laminar air

flowing past the irradiated sample sitting on an insulated balance with an igniter downstream of the sample. The samples were covered in graphite powder to increase sample emissivity in the mid-IR wavelength range. Cohen and Finney (2010) exposed fuel samples to similar radiant heat fluxes as McAllister et al. (2012), but their samples were suspended in air next to the heat source and they did not use an igniter. The results from both papers are interesting and present useful information, but it is difficult to compare results between papers due to different experimental conditions. This is true for convection experiments as well, as seen when comparing the work published by Xanthopoulos and Wakimoto (1993) and Prince and Fletcher (2014). One question that has never been explored is whether or not the fuel sample responds similarly to radiation or convection under the same experimental conditions. The answer to this question can help facilitate comparison of experimental results between researchers worldwide.

Work to quantify the contributions of radiation and convection in live-shrub combustion is necessary to understand the basic theory of fire spread and to develop a model that accounts for both mechanisms of heat transfer. Additionally, exploration of radiant and convective heating of solid fuel samples under similar experimental conditions can help facilitate comparison of experimental results. The aim of this project is to explore the effect of heating mode on ignition and burning behavior to better understand what physical processes drive fire spread in live shrub and conifer fuels.

#### **2.2.4 Ignition Summary**

Ignition occurs when a fuel sample is heated to the point where pyrolysis rates are high enough to support a gaseous flame *and* a flammable mixture exists in the gas phase. Researchers and other fire professionals often simplify this problem by measuring an ignition time and temperature. These values are then used as empirical estimates of the time it takes to heat the

sample and the surface temperature when pyrolysis rates can support a continuous flame, respectively. While these approximations can capture general trends, they cannot explain the complex behavior observed in wildland fires. Additionally, ignition time and temperature values hold little physical meaning because they are dependent on experimental conditions (Finney et al., 2013). Moisture is known to cause an ignition delay, but the exact mechanisms at work are still a mystery. Moisture is assumed to be almost completely evaporated before ignition occurs in fine dead fuels, but a significant amount of moisture is still present at ignition in live fuels (Fletcher et al., 2007) and in larger dead woody fuels (Williams, 1953; Simms and Law, 1967).

The relative importance of the different heat transfer mechanisms in live-shrub fires is not well understood. Most early models assume radiation as the dominant heat transfer mechanism, but experiments have indicated convection (Baines, 1990; Weber, 1991) or direct flame contact (Fang and Steward, 1969; Vogel and Williams, 1970; Carrier et al., 1991) are also important in fire spread. A better understanding of these phenomena must be established if improved predictive models are to be developed.

### **2.3 Wildland Fire Modeling**

Wildfire models were summarized and categorized in 1991 as statistical, empirical and physical (Weber, 1991; Clark, 2008). In a review published in 2009, Andrew Sullivan suggested a fourth category be added that includes fire spread simulators and differentiated between physics only and physics and chemistry models (Sullivan, 2009c, b, a). For the purposes of this review, models will be categorized as statistical models, physical models, empirical models, and simulation models. Each has its own strengths and weaknesses, and each must be understood in order to follow current efforts in model development.

### **2.3.1 Statistical Models**

Statistical models are based on test fires and contain no explicit physical information. These models often take two forms—those developed for a specific fuel at specific conditions and those developed for several species over a broad range of conditions. The first kind are often very accurate for the conditions and fuels specified, but provide little information outside those conditions. The second kind provide ballpark information for a large number of fires, but aren't accurate enough to provide detailed information (Lindenmuth and Davis, 1973; Weber, 1991). The Canadian FBPS and Anderson et al. (2015) models are examples of statistical models (Wotton et al., 2009).

### **2.3.2 Physical Models**

Physical models are based largely in fundamental physics and chemistry principles (Sullivan, 2009a). Two basic approaches have been used in developing these models. The first approach is to solve the governing equations in 3D space while the second uses correlations to approximate the solutions to the governing equations.

As mentioned, models following the first approach seek to solve the basic transport equations. They also differentiate between different modes of heat transfer and give insight into fundamental interactions within the flaming zone (Clark, 2008). Current models on this scale are FIRETEC (Linn, 1997; Linn et al., 2005; Linn and Cunningham, 2005), FDS and its extension WFDS (McGrattan and Forney, 2005; Mell et al., 2005; Mell et al., 2007) and WRF-Fire/CAWFE (Coen et al., 2013; Coen and Riggan, 2014; Weise and Wright, 2014). Simulations using these models can be separated into two categories based on their grid and domain size. The small-scale simulations use grid cells 1 centimeter in size and cover a domain up to a bush or tree

(approximately 1-10 meters). These simulations provide useful insights into fundamental interactions on leaf-scale (so far as the information is included in the models) but lack the complex characteristics of large-scale fires and the fire/wind/atmosphere interactions (Clark, 2008). The large-scale simulations use grid cells on the meter scale and cover domains on the hundred meter (or “hill-side”) scale. These simulations include the complex, large-scale dynamics that small-scale physical models lack, but are computationally expensive and do not include small-scale chemical and physical interactions. Clark et al. (2010) generated a sub-grid thermodynamic equilibrium combustion model based on the mixture fraction to interface with FIRETEC, with the hope that greater detail could be added to the combustion chemistry without increasing computational time. While this effort was largely successful, Clark et al. (2010) highlight the lack of wildfire data available to successfully validate theirs or any such model. These models can provide useful insights into physical phenomena, but use of these models assumes the authors knew enough about the physical phenomena to model them correctly. Additionally, high computational costs make these models ineffective except in prescribed burns, for post-fire analysis, or for academic purposes (Sullivan, 2009a).

The second approach, used by Albini and Brown (1996); (Balbi et al., 1999); Butler et al. (2004b); Balbi et al. (2007), and Balbi et al. (2009) is similar in concept to empirical models, but these models use enough physical detail to be classified as physical models. These models generally include detail about different modes of heat transfer (Albini, 1985, 1986; Butler et al., 2004b; Balbi et al., 2007) or chemical kinetics (Balbi et al., 1999) but do not solve the governing equations. Considerable effort is being put into development of these models with the hope of producing a model that is computationally fast but generally applicable. This effort has been met with varying amounts of success, but a widely applicable model has not yet been produced.

### 2.3.3 Empirical Models

Empirical models are compilations of lab-scale experiments into correlations that seek to account for variables such as wind, slope, fuel type, and moisture content in predicting the rate of fire spread (Weber, 1991; Clark, 2008). These models are essentially point-source models, where energy released by one fuel element is transferred to a neighboring fuel element, thereby initiating the combustion sequence for that fuel element (Fons, 1946; Rothermel, 1972; Albini, 1985; Catchpole et al., 1998; Pickett, 2008). Fons (1946) was the first to attempt a mathematical model for fire spread. His model treats fire spread as successive ignitions, with particle ignition time and distance between particles as the two governing parameters. This is the simplest empirical model and contains many shortcomings. Rothermel (1972) used the same premise as Fons in defining how fire spread occurs but included much more detail when he developed a model based on the data from Frandsen (1971). Rothermel introduced a heat of ignition parameter that defines how much energy must be absorbed by a particle to raise the surface temperature to its measured ignition temperature, assuming water vaporization occurs at 100 °C. Rothermel's formulation forms the basis for most fire spread models developed in the last forty years. Examples of these models used in the United States include BEHAVE (Rothermel, 1972), FIRECAST (Cohen, 1986), BehavePlus (Andrews, 2007; Andrews, 2008), FARSITE (Finney, 1998) and HFIRE (Peterson, 2009). One thing that makes Rothermel's model so unique is the use of field measurement inputs regarding fuel type, fuel density, wind speed and others. However, Rothermel's model assumes homogeneous, continuous fuel that is contiguous to the ground, such as pine needle litter or grass, and ignores the effect of moisture within the fuel except in delaying the fuel temperature rise while water evaporation occurs. Several models have been developed since Rothermel completed his model; three are noted here. Albini (1985, 1986)

developed models that account for radiative pre-heating, pre-cooling, and convective pre-cooling, respectively. This improvement allows his models to predict pre-heating that occurs in front of the flame in no-wind conditions, but still maintains the basic assumptions made by Rothermel. Butler et al. (2004b) developed a closed form version of Albini's model that was compared with data collected during the International Crown Fire Modeling Experiment (Stocks et al., 2004). This model accurately predicts the effect of fuel and environmental variables but over predicts the rate of spread. Catchpole et al. (1998) improved Rothermel's heat of ignition term by including both the water heat of vaporization and the fuel moisture content. While this change improves the model, it still uses the basic set of assumptions originally made by Rothermel. Smith (2005), Pickett (2008), and Prince and Fletcher (2014) showed water evaporation in live leaves occurs at fuel surface temperatures between 200 °C and 300 °C depending on the species being studied. Prince (2014) developed a single-leaf devolatilization model based on the Chemical Percolation Devolatilization (CPD) model (Fletcher et al., 1992) that accounts for within-leaf mass transfer effects, a distribution of leaf surface temperatures, within-leaf heat transfer effects, and different water release mechanisms for free and bound water. His model also differentiates mass loss between water, cellulose, hemi-cellulose and lignin. While some of the assumptions in the model have not been validated, the model matches experimental data and illustrates the complexity occurring during live fuel combustion. This model is the first of its kind, and more work must be done to verify the assumptions, extend the model to other species, and develop a theoretical basis for live fuel combustion.

Recent work at BYU by Pickett (2008) involved experiments in fuel samples from southern California, Utah, and the southeastern United States. In these experiments, individual fuel samples (leaf-scale) were burned and flame characteristics (ignition temperature, ignition

time, flame height, flame duration) were measured. These characteristics were included in a semi-empirical model produced in Pickett's work (Pickett, 2008). Pickett's model, like other empirical models, is computationally fast but limited in application. It does not differentiate between the various modes of heat transfer and accounts for transport phenomena and oxygen consumption only so far as observations can capture. It does, however, account for fire spread in both the horizontal and vertical directions in non-continuous fuel, while other models (Rothermel, 1972; Albini, 1985) assume a one dimensional, continuous fuel bed with fire spread only in the horizontal direction. Fletcher et al. (2007) extended the model to three dimensions. It is also unique in that it models fire spread by flame-fuel interactions rather than by solving simplified forms of the governing equations. This allows spatial variations that naturally occur in plants to be included as a basic function of the model (Pickett, 2008). Prince (2014) added more realistic flame merging behavior and an energy balance that accounts for differences in experimental conditions. Shen et al. (2015) added a better description of individual fuel element locations through the use of L-systems and laser scanning, and extended the model to chamise and sagebrush. While these adjustments to the basic approach are promising, the BYU model needs further development before it can predict wildfire behavior with enough accuracy to be used by fire managers in the field. Three specific areas of needed improvement include: (1) the effect of moisture on flame characteristics, (2) the differences in flame behavior resulting from different modes of heat transfer, and (3) the general effect of species.

#### **2.3.4 Simulation Models**

The goal of fire spread simulations is to take a statistical or empirical model (usually one dimensional), generalize it to a two dimensional form, and provide an algorithm for fire spread on a landscape scale with inputs about the details of the landscape (Sullivan, 2009c). Thus, the

operational fire spread models that are said to be statistical or empirical (i.e., FARSITE) are actually a combination of a simulation model that propagates fire in 2D space and a 1D (usually) statistical or empirical fire spread model based on experimental data. Fire propagation is modeled using one of three methods—the raster, vector, and level-set methods. The raster method models the fire propagation using a set of discrete cells on the fire perimeter that affect only their nearest neighbors and spread radially outward. The vector method uses a vector of linked points to approximate the fire line. Fire spread in the vector method is modeled as small fires at the individual points on the fire line that grow as ellipses in the direction of fire spread. After a specified time step, the fire line is re-defined by connecting the forward edge of each ellipse and the process is repeated (Sullivan, 2009c). The level-set method uses an Eulerian formulation to model the motion of an interface through time—the idea is to generate a surface (the level set function) and allow it to move through time. The part of the surface that intersects a specified plane is the interface in that plane. Thus, at any point in time, the interface (fire line) is found by finding the place where the plane intersects the level set function (Adalsteinsson and Sethian, 1999). Rehm and McDermott (2009) present one example of the application of this method. The major drawback here, like that which occurs with the physical models, is the lack of data with which to validate the model combined with the high computational costs for some of the models (Clark, 2008; Sullivan, 2009c).

### **2.3.5 Modeling Summary**

The four modeling approaches presented here encompass the broad spectrum of current fire spread models, and each approach has its own strengths and weaknesses. Statistical models are the simplest in construct in that they contain no physical information and make no attempt to solve the governing equations. They have been used in some operational models (Wotton et al.,

2009) but generally do not provide highly detailed or highly accurate information outside the conditions for which they were developed. Empirical models contain some physical information and seek to solve the basic conservation equations through the use of correlations. They provide the basis for the current operational codes like BehavePlus and FARSITE, but do not accurately predict fire spread in live, non-continuous fuel beds. Physical models include the most detail and can provide useful information about fire spread, though data available for validation is scarce and the models are only as accurate as the assumptions they use. Simulation models include more detailed geographic information, but are only as good as their propagation algorithm and the empirical or statistical model upon which they are based. As improvements are made to computing equipment, physical and simulation models will move closer to being able to produce real-time solutions, though Andrews (2007) suggests improvements to computational power alone will not be enough to allow physical models to overtake empirical and statistical models for use in fire management. In short, fire spread modeling can give valuable insight into wildland fires, but no model currently in use is completely adequate to describe the complex nature of fire spread.

#### **2.4 Fire Fighter Safety Considerations**

During the last 100 years, thousands of wildland firefighters have been killed or injured in the line of duty (Britton et al., 2013; Butler, 2014). Of the 900 deaths in that time, 427 were due to firefighter entrapment, the situation in which a fire passes over the firefighter's location (Fryer et al., 2013). Improved safety protocols throughout the last century combined to decrease entrapment fatalities, but recent fires like the 2001 Thirty-Mile fire, the 2006 Esperanza fire, and the 2013 Yarnell Hill fire demonstrate that the risk of entrapment still exists. One of these safety protocols is the identification of firefighter safety zones, defined as “a preplanned area of

sufficient size and suitable location that is expected to protect fire personnel from known hazards without using fire shelters” (National Wildfire Coordinating Group, 2004). While the definition works well in theory, the task of defining a safe zone in the field is difficult, and involves estimating fire behavior. This difficulty was illustrated in a survey conducted by Steele (2000), in which firefighters were shown pictures of vegetation and given descriptions of environmental conditions and asked to predict the size of the safety zone. The resulting safety zone sizes varied by three orders of magnitude. This illustrates the need for better understanding of practical definitions of safety zones.

#### **2.4.1 Current Safety Zone Models**

From its definition, the size of a safe zone depends strongly on fire behavior, but the practical application of choosing a safety zone is difficult. Work to develop methods to identify safe zones has increased in recent years, including work to determine the effect of clothing properties on safe heating levels (Raimundo and Figueiredo, 2009), determination of safety zones using terrestrial laser scanning (Dennison et al., 2014), and calculation of safe separation distances (SSD) using heat transfer models (Green and Schimke, 1971; Butler and Cohen, 1998; Zarate et al., 2008; Billaud et al., 2011; Rossi et al., 2011). A short discussion of some of the recent SSD models follows.

Butler and Cohen (1998) developed a model to calculate radiant heat flux from a fire front using the solid-flame assumption. They used  $7 \text{ kW m}^{-2}$  as the safe heating limit and concluded that a rule of thumb for safe zones is four times the flame height. Zarate et al. (2008) developed a similar radiation model for the thirteen Rothermel fuel classes and several Mediterranean fuels. They used  $4.7 \text{ kW m}^{-2}$  as the safe heating limit for people without protective clothing and concluded safe distances range from 15 m to 100 m, depending on the

fuel type, with a mean SSD of 4.8 flame heights. Rossi et al. (2011) developed another similar radiant heating model and used a safe heating limit of  $5 \text{ kW m}^{-2}$ . They conclude the SSD varies from 2.35 to 10 times the flame height, depending on the assumed flame temperature. Butler (2014) summarized these and other models and identified several areas of needed improvement, one of which is the inclusion of convection in safety zone size calculations.

#### **2.4.2 The Coanda Effect and its Influence on Fire Behavior near Solid Surfaces**

Convection has long been known to occur in wildland fires, but until recently, radiation was considered the dominant form of heat transfer for both fire spread and safety zone determination. Current work now emphasizes the combination of both heat transfer modes (Sullivan, 2009a; Butler, 2014). One scenario in which convection becomes extremely important is fire near slopes and hills. This is due to the Coanda effect, the phenomenon first noticed by Henry Coanda in 1910, in which a jet entering quiescent fluid attaches to a nearby solid object (McLean, 2012). The Coanda effect is caused by inhibited entrainment of ambient fluid near the solid. This lack of entrainment on one side of the jet causes a pressure gradient to develop normal to the flow direction that causes the jet to attach to the surface (McLean, 2012).

Extensive work has been done studying the Coanda effect in various applications, including nozzle flows (Sunol et al., 2015), coastal water flow (Lalli et al., 2010), swirled flame behavior and stability (Singh and Ramamurthi, 2009), indoor ventilation systems (van Hooff et al., 2012), and structure fires (Himoto et al., 2009; Tang et al., 2012; Hu et al., 2013). The King's Cross fire in London, England is a tragic example of fire behavior near a slope. This fire started as a small fire near the base of an escalator shaft. The fire quickly spread up the escalator, resulting in 31 fatalities and over 100 injuries. The behavior seen in the King's Cross fire was caused by a combination of the Coanda effect and flashover, the heating of solid fuel away from the flame

until it reaches its ignition point and the fire spreads nearly instantaneously over a large area (Drysdale et al., 1992; Moodie, 1992; Carvel, 2008).

Fire-wall interactions have been studied extensively in structural fire research (Chao and Wu, 2000; Himoto et al., 2009; Tang et al., 2012; Hu et al., 2013; Gao et al., 2015; Ji et al., 2015). Most of these studies deal with insulated vertical walls and ceilings to explore how the fire might spread within a building. While these studies provide useful background information, they are not directly applicable to scenarios in which the Coanda effect would play a major role in wildland fires. Only a few studies regarding the Coanda effect have been performed that apply more directly to wildland fires. Fox and Stewart (1978) showed increasing heat transfer for a given burner velocity as the slope angle increased from  $60^\circ$  to  $80^\circ$  from the horizontal. Viegas (2004) showed that fires are affected by a nearby slope with an angle greater than  $20^\circ$  and exhibit surface attachment at slopes greater than  $30^\circ$ . Viegas noted that flame-surface attachment occurred even in the absence of other factors favoring blowup-type behavior. Since fires frequently occur in rugged terrain, a better understanding is needed regarding how the Coanda effect influences fire behavior near a slope.

### **2.4.3 The Coanda Effect and Safety Zones**

As already noted, the effect of convection on safety zone determination has been identified as a major short coming of current safety zone guidelines (Butler, 2014). The added influence of the Coanda effect on safety zones near slopes and hills has never been studied. This must be understood if better safety zone guidelines are to be developed. This literature review has led to the formation of two specific questions regarding the Coanda effect and wildland fires, namely (1) what is the effect of flame attachment on the heat flux on slopes near a fire and how does this affect safety zone size, and (2) can computational fluid dynamics (CFD) codes predict

fire behavior near slopes accurately enough to be used to explore topographical configurations and environmental conditions not suited for laboratory work. This work presents preliminary results aimed at answering the first question; the second question is the focus of recommended future work.

## **2.5 Summary**

While much has been learned about fire spread in the last century, there is still much that is not well understood; this knowledge gap is accentuated in modeling efforts due to computational limitations. Some of these areas include (1) the seasonal changes in moisture content and the resulting effect on ignition behavior, (2) the relative importance of convection and radiation in fire spread and their individual and combined effect on ignition, and (3) firefighter safety in rugged terrain. This information is crucial in the development of a theory of live fuel combustion and rigorous, yet computationally effective fire spread models that can help reduce both the cost of and damage from wildfires.

This literature review has led to the proposal of three questions which were the focus of this PhD research: (1) What are the seasonal changes in burning behavior and can they be attributed to variation in moisture levels? (2) How does radiation affect ignition? (3) How does fire behavior change near slopes and how does this change in behavior affect firefighter safety zones?

### **3 OBJECTIVE AND TASKS**

#### **3.1 Objective**

This research was focused on understanding the differences and relative importance of heating mode in live-fuel combustion and the fundamental reason(s) that live fuels burn differently than dead fuels. This understanding will help in two major areas of ongoing fire research: (1) to develop a theoretical understanding of live-fuel combustion, and (2) to develop accurate, fast fire behavior models.

#### **3.2 Tasks**

These objectives were achieved by completion of the following tasks:

1. Measure physical and chemical properties of ten live fuels representing major wildland fuel types over a one-year period to determine seasonal differences
2. Develop correlations to predict the physical and chemical properties used as inputs to fire spread models
3. Measure the effect of heating mode on the ignition and burning behavior of ten live fuels
4. Determine the effect of season (moisture content) on the ignition and burning behavior of ten live fuels over a one-year period
5. Identify physical and chemical properties that have an individual effect of ignition and burning behavior

6. Develop correlations to prediction ignition and burning behavior of ten live fuels
7. Determine the influence of slope on fire behavior and discuss the impact of this behavior on firefighter safety.

Data for physical and chemical properties, as well as the correlations to predict those properties, are presented in Chapter 4 (Tasks 1 and 2). The results discussing the differences in burning behavior stemming from different heating modes are shown in Chapter 5 (Task 3). Chapter 6 contains the data and results regarding season and the individual and combined effects of pre-burn measurements on ignition and burning behavior (Tasks 4-6). Data and results from flame-slope experiments are discussed in Chapter 7. The data in Chapters 4 and 6 will be submitted to the Forest Service Research Data Archive for permanent storage.

## **4 PHYSICAL PROPERTIES AND DIMENSIONS FOR TEN SHRUB AND CONIFER FUELS TO PREDICT FIRE BEHAVIOR<sup>1</sup>**

Physical and chemical properties play an important role in burning behavior of live fuels, and prediction models for these properties are useful in describing the solid fuels in fire behavior models. Physical and chemical properties data for live fuels are available for some species, but prediction models are almost non-existent. One of the goals of this dissertation was to measure the chemical and physical properties of the ten fuels studied herein, and develop prediction models for some of the physical properties that are inputs in fire models.

### **4.1 Methods**

#### **4.1.1 Measurements**

Physical dimensions (see Figure 4-1, Figure 4-2 and Table 4-1), moisture content, relative moisture content, surface area, volatiles content, ash content, ether extractives content and apparent density were measured at the BYU Wildfire Lab in Provo, UT each month over a one-year period for ten live fuels (see Table 4-2). On average, 25 replicates were completed each month. All measurements were made within 48 hours of sample collection—non-local species were sealed in plastic bags and shipped overnight to Provo. The plastic bags were kept sealed

---

<sup>1</sup> This chapter is under review for publication in *Forest Science*

and out of direct sunlight until measurements could be made. The ten species were categorized as broadleaf species or needle species based on the shape of the foliage (see Table 4-2). Broadleaf samples consisted of whole, undamaged leaves while needle samples consisted of 2-6 cm branch tips with the foliage attached. Sagebrush was categorized as a needle species because the fuel element used in this work was a section of branch with the foliage attached, even though sagebrush foliage is comprised of small leaves and not needles. A branch segment was used because previous work on sagebrush showed that individual leaves did not burn well (Shen, 2013). Foliage samples were also categorized as new (current year) growth or old (previous year) growth.

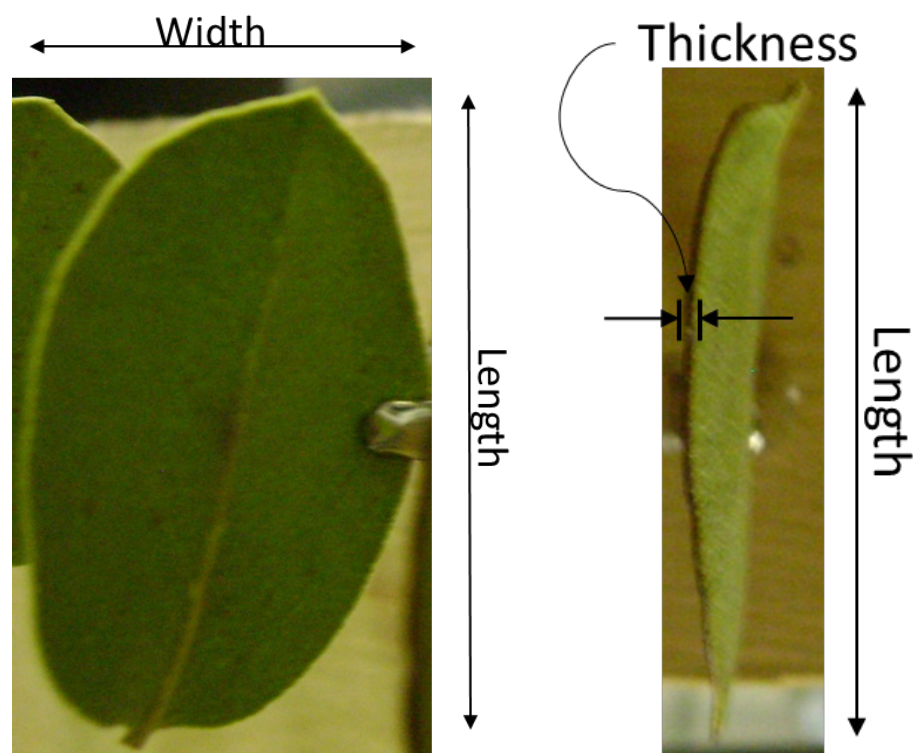


**Figure 4-1: Diagram of measurements for broadleaf species.**

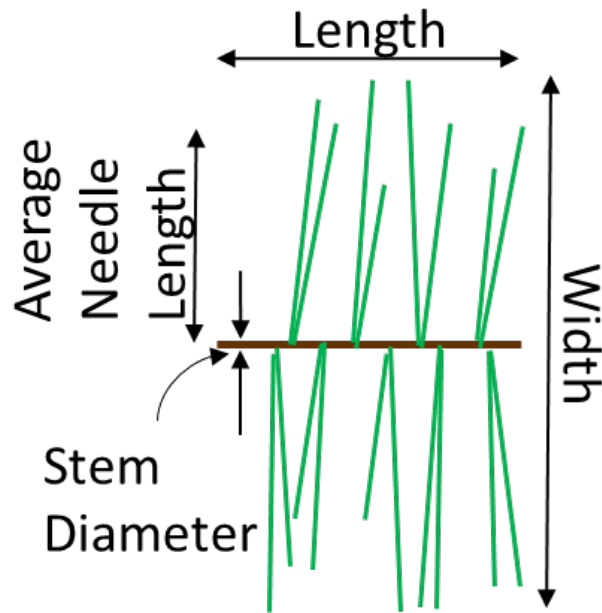


Figure 4-2: Diagram of measurements for needle species, including sagebrush and chamise.

Table 4-1: Measurement definitions

Property	Broadleaf species	Needle species	Chamise and sagebrush
<b>Length</b>	Distance from leaf base to leaf tip (cm).	Length of stem (cm).	Length of stem (cm).
<b>Width</b>	Largest distance in direction perpendicular to length (cm).	Largest distance between needle tips normal to length (cm).	N/A
<b>Thickness</b>	Measured using calipers without crossing the main vein (mm).	N/A	N/A
<b>Needle length</b>	N/A	Average needle length on the sample (cm).	N/A
<b>Stem diameter</b>	N/A	Diameter of stem (mm).	Diameter of stem (mm).
<b>Mass</b>	Mass of sample (g).	Mass of sample (g).	Mass of sample (g).

**Table 4-2: Species tested.**

Species	Region	Sampling Location	Type	Year
<b>chamise</b> ( <i>Adenostoma fasciculatum</i> )	California	Riverside, CA	Needle	1
<b>manzanita</b> ( <i>Arctostaphylos glandulosa</i> )	California	Riverside, CA	Broadleaf	2
<b>ceanothus</b> ( <i>Ceanothus crassifolius</i> )	California	Riverside, CA	Broadleaf	2
<b>Douglas-fir</b> ( <i>Pseudotsuga menziesii</i> var. <i>glauca</i> )	Rocky Mountain	Missoula, MT	Needle	2
<b>big sagebrush</b> ( <i>Artemisia tridentata</i> )	Rocky Mountain	Provo, UT	Needle	1
<b>lodgepole pine</b> ( <i>Pinus contorta</i> )	Rocky Mountain	Missoula, MT	Needle	1
<b>gambel oak</b> ( <i>Quercus gambelii</i> )	Rocky Mountain	Provo, UT	Broadleaf	2
<b>gallberry</b> ( <i>Ilex glabra</i> )	Southern	Crestview, FL	Broadleaf	2
<b>fetterbush</b> ( <i>Lyonia lucida</i> )	Southern	Crestview, FL	Broadleaf	2
<b>sand pine</b> ( <i>Pinus clausa</i> )	Southern	Crestview, FL	Needle	2

Scientific names cited from USDA, NRCS. 2015. The PLANTS Database (<http://plants.usda.gov>, 31 March 2015). National Plant Data Team, Greensboro, NC 27401-4901 USA. Year 1 = April 2012-March 2013, Year 2 = April 2013-March 2014.

Physical dimensions include mass, length, width and thickness for broadleaf species and mass, length, width, needle length and stem diameter for needle species. See Table 4-1 for definitions. Moisture content (MC) was measured on a dry basis (see Equation 4-1) using a Comptrac Max1000 analyzer<sup>2</sup> with a drying temperature of 95°C and a minimum sample size of 1 gram. Relative moisture content (RMC) was measured on a turgid basis (see Equation 4-2); turgid mass (mass of sample when fully saturated with water) was determined by soaking the sample in water for 24 to 48 hours before weighing. The minimum sample size for RMC was also 1 gram. Because several leaves or branch sections were necessary to reach the required minimum weight, the reported MC and RMC were an average of the fuel elements used in the measurements.

<sup>2</sup> The use of trade or firm names in this publication is for reader information and does not imply endorsement by the U.S. Department of Agriculture of any product or service.

$$MC = 100 \left( \frac{\text{fresh mass} - \text{dry mass}}{\text{dry mass}} \right) \quad (4-1)$$

$$RMC = 100 \left( \frac{\text{fresh mass} - \text{dry mass}}{\text{turgid mass} - \text{dry mass}} \right) \quad (4-2)$$

#### 4.1.1.1 Density

Density was measured using Archimedes principle that the force exerted on a submerged object is equal to the mass of the displaced fluid (Ryan and Pickford, 1978; Sackett, 1980; Fernandes and Rego, 1998). The sample was submerged in silicone oil (Dow Corning 704 Diffusion Pump Fluid) rather than water to prevent the plant sample from absorbing the liquid into pores on the sample surface and to prevent fluid evaporation during mass measurements. Only whole leaves or needles were used, and three replicates were performed for each species each month. Using the sample mass, the weight of the displaced fluid and the fluid density, the sample density was calculated using Equation 4-3, in which  $\rho$  is density,  $m$  is mass,  $V$  is volume, *sample* refers to the sample, *displaced* refers to the fluid displaced by the sample and *fluid* refers to bulk fluid properties.

$$\rho_{\text{sample}} = \frac{m_{\text{sample}}}{V_{\text{sample}}} = \frac{m_{\text{sample}}}{V_{\text{displaced}}} = \frac{m_{\text{sample}}}{m_{\text{displaced}} * \rho_{\text{fluid}}} \quad (4-3)$$

Aluminum 6061 rectangular blanks were used to verify the measurement accuracy. The density of aluminum 6061 is 2.72 gm cm<sup>-3</sup> (Narender et al., 2013). The measured density was 2.72 ± 0.008 g cm<sup>-3</sup>. The reported density is the average of 10 replicates, the ± is the 95% confidence interval on the mean calculated using the standard error of the mean and a Student t-value of 2.262 (9 df). The agreement between the measured value and the literature value indicates this is a valid method for density measurement. Density was measured only for year 2 species. The apparatus used to measure density is shown in Figure 4-3.

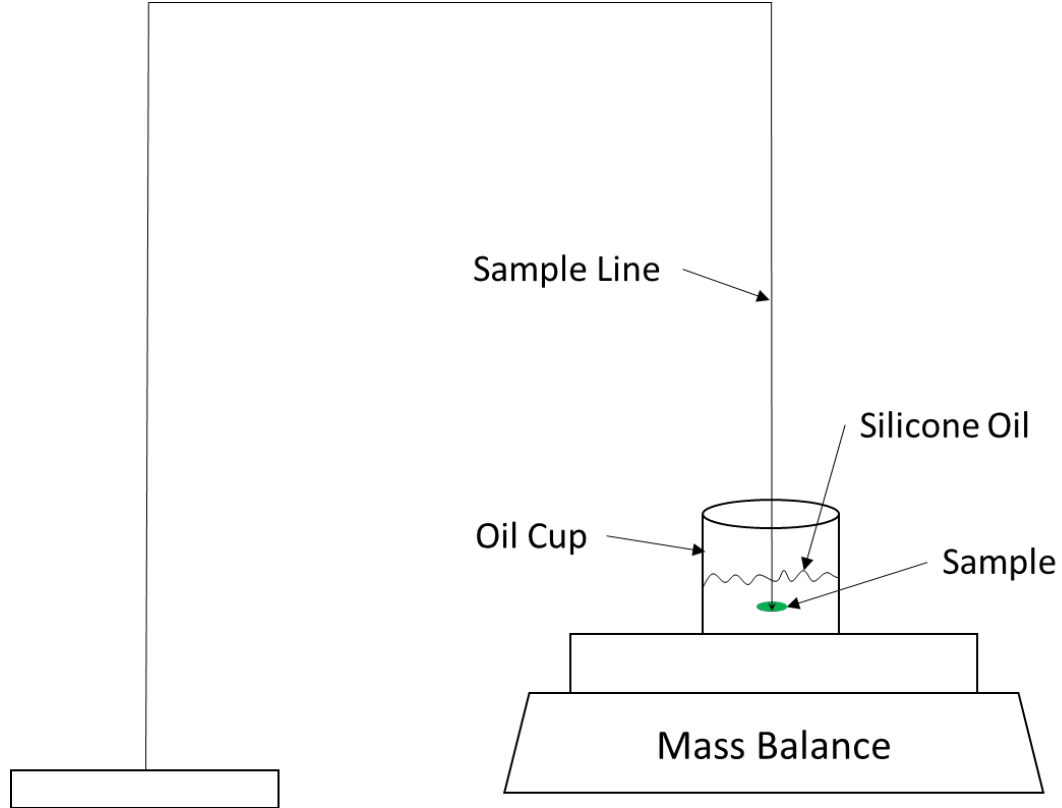


Figure 4-3: Apparatus used to measure foliage density.

#### 4.1.1.2 Surface Area

External surface areas for broadleaf species were obtained using images of each sample. The surface area of one side of each leaf and the leaf perimeter were measured using in-house computer vision algorithms written in MATLAB (2014a, The Mathworks Inc). The total surface area was then calculated using Equation 4-4, where  $SA_{total}$  is the total external surface area,  $SA_{side}$  is the external surface area measured from the image,  $P$  is the leaf perimeter and  $t$  is the leaf thickness. Figure 4-4 contains images showing the sequence of processing steps for finding the total surface area, including the normal image, the black and white binary image, and the image identifying the leaf perimeter. The surface area to volume ratio was found for broadleaf

species by dividing the surface area by the leaf volume. The leaf volume was obtained by multiplying half the surface area by the leaf thickness.

$$SA_{total} = 2 SA_{side} + P * t \quad (4-4)$$

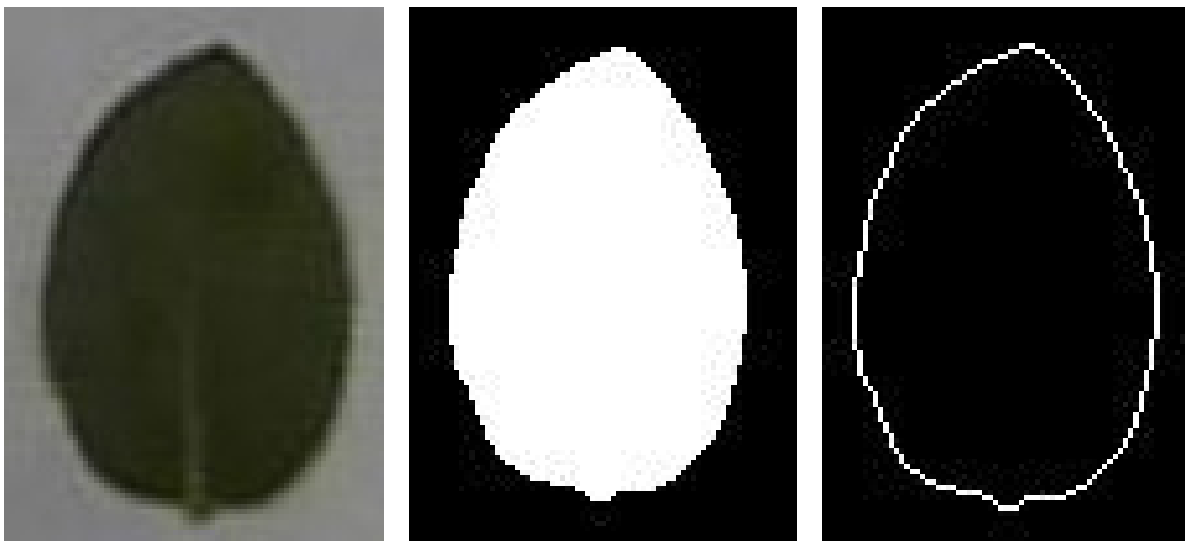


**Figure 4-4: Panel showing processing steps for surface area calculations. The left panel is the normal image, the middle panel is the binary image, and the right panel is the leaf perimeter.**

#### **4.1.1.3 Ether Extractives**

Ether extractives were measured for manzanita, Douglas-fir, Gambel oak and fetterbush using a procedure similar to that outlined in the AOAC Handbook (Horwitz and Latimer, 2005) with diethyl ether as the solvent. The procedure was modified slightly to be compatible with available resources at BYU. These modifications include the following:

1. Whole fuel elements, the glassware and the thimble were dried for 48 – 72 hours at 50 °C.
2. Approximately 0.5 grams of ground, dried sample was added to each thimble.
3. The soxhlet was run for 18 – 24 hours at a nominal rate of 2 drops per second.

The soxhlet operates essentially as a continuous liquid-solid extraction. Solvent (diethyl ether in this case) is boiled from the round bottom flask up into the condenser and down into the thimble. When the liquid level in the thimble area reaches the height of the drain tube, the solvent with the extracted material drains into the flask and the process repeats. Because of the time required to measure ether extractives, only two replicates were performed each month for the four species previously mentioned. The ether extractives content was reported as a fraction of the sample dry mass. The apparatus used to measure ether extractives is shown in Figure 4-5.

#### **4.1.1.4 ASTM Analysis**

Volatiles content and ash content were measured using ASTM procedures for volatiles content and ash; fixed carbon was calculated by difference. Three replicates were performed each month on each of the Year 2 species (Table 4-2). These measurements are reported on a dry basis. To avoid fuel-bed and particle shape effects in the proximate analysis measurements, needle species samples were cut to nominally 5 mm lengths while broad leaf species samples were hole-punched (Prince and Lewis, 2013). Approximately 0.35 g of sample were used for each replicate.

#### **4.1.2 Physical Properties Model Development**

The models developed here are designed to predict the size and shape characteristics of the individual fuel elements measured as part of this study. Moisture content is a typical input for most fire models and is used as the starting point for the models developed in this work. A moisture content value is usually available to the researchers and fire suppression experts using these models. Sample dry mass is also used as an input parameter for all the prediction models reported herein, but the dry mass is obtained using the specified moisture content and a

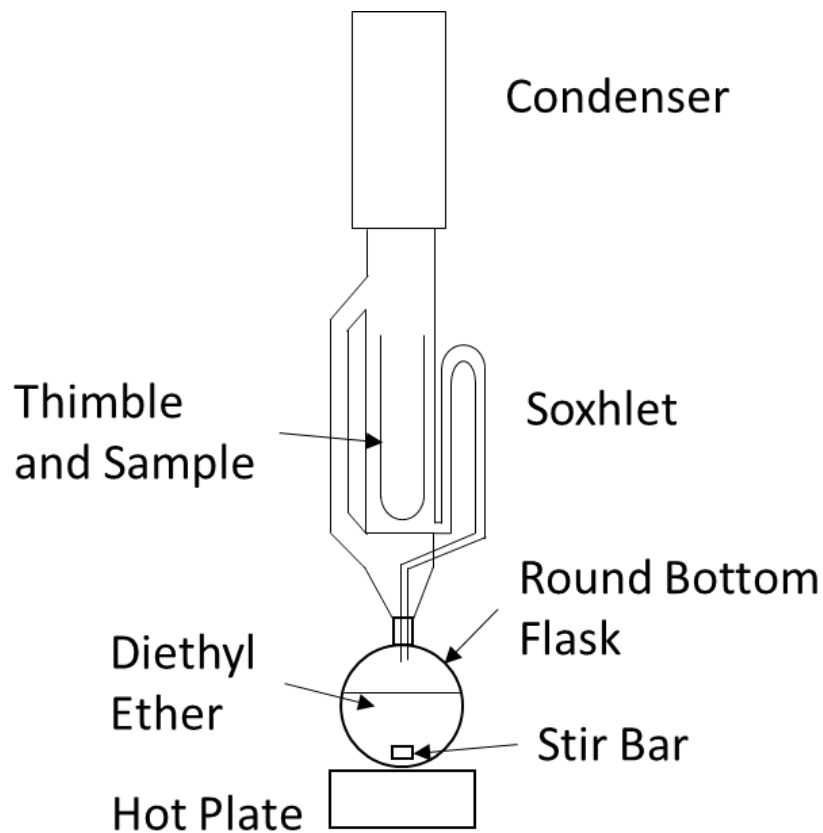


**Figure 4-5: Ether extractives apparatus showing soxhlet, sampling-containing thimble, condenser, round-bottom flask, solvent, stir bar and heater.**

distribution of measured dry masses as described below. Before any model development, however, it was first necessary to determine if there were seasonal changes in the measured data. The determination of seasonal changes in the data was accomplished using non-linear mixed effects models. In these types of models, the user must first specify the model form before solving for both the fixed and random effects and testing the model significance. Several model forms were used to allow for the presence of different seasonal trends. The possible models included month as the independent variable with the following possible transformations: nothing, square, absolute value, power, sine and cosine. The significance of a model was determined by comparing the F-statistic, the ratio of explained variance to unexplained variance, with the critical F-value at a 99% significance level. If the resulting models were significant, and a

constant was not within the data range for each month, the presence of a seasonal pattern was confirmed.

The dry mass of each sample was calculated using Equation 4-1. From the dry mass data for a set of samples, the Weibull probability density function and the cumulative Weibull distribution function were determined for each species using Equations 4-5 and 4-6, respectively, where  $a$  and  $b$  are the density function parameters found using the maximum likelihood estimate. This distribution can be used to determine the dry mass for a modeled fuel element, which serves as the other input parameter for the model user (see below).

$$f(x; a, b) = \frac{b}{a} \left(\frac{x}{a}\right)^{b-1} e^{-\left(\frac{x}{a}\right)^b} \quad (4-5)$$

$$f(x; \alpha, \beta) = 1 - e^{-\left(\frac{x}{a}\right)^b} \quad (4-6)$$

Prediction models were developed for relative moisture content, density, length, width, needle length, thickness, stem diameter and surface area. Approximately 500 models were developed for each species parameter using both forward and backward stepwise regression, and the best model for each parameter was selected using the adjusted  $R^2$  value and the Bayesian Information Criterion (BIC). The procedure for building a set of models for each species is shown in Figure 4-6. To start, the moisture content and dry mass were used to calculate fresh mass and water mass. Next, a model for relative moisture content was found using stepwise regression with moisture content and fresh, dry, and water mass as possible predictors. Thereafter, models for length, width, needle length, thickness and stem diameter were developed simultaneously using the five previously defined values as predictor variables within the stepwise regression procedure. The response variable (length, width, etc...) with the best fit was

then added to the set of predictor variables and new models were developed for the remaining response variables using the six previously defined predictor variables. This process was repeated until models were developed for each of the response variables. Once this model selection loop was complete, models for surface area and foliage density were found via stepwise regression using all previously defined variables as predictor variables. Within each model, moisture content ( $M$ ) and relative moisture content ( $R$ ) are proportions; length ( $L$ ), width ( $W$ ) and needle length ( $N$ ) are in units of centimeters; thickness ( $t$ ) and stem diameter ( $D$ ) are in units of millimeters; surface area ( $SA$ ) is in units of square centimeters; and fresh mass ( $m_f$ ), dry mass ( $m_d$ ) and water mass ( $m_w$ ) are in units of grams.

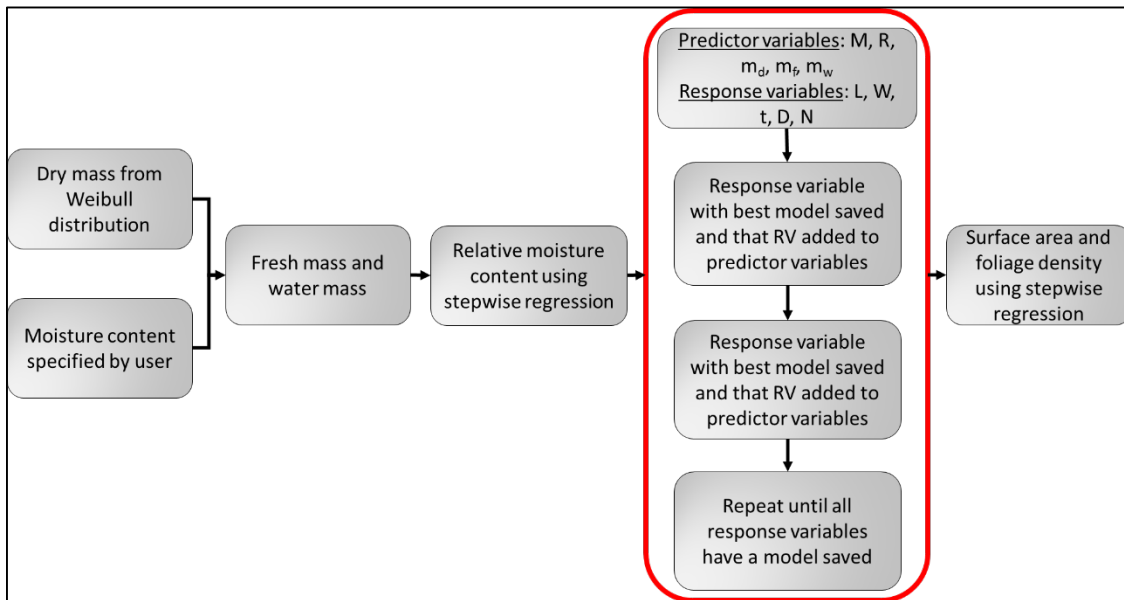


**Figure 4-6: Flow chart for fuel element property model development**

The framework for using the presented models is similar to that for model development shown in Figure 4-6. To start, the model user specifies a moisture content and the probability distribution described by Equations 4-5 and 4-6 is used to specify the dry mass. Fresh mass and water mass can be calculated directly using the moisture content and dry mass. The other sample

properties (relative moisture content, length, width, needle length, thickness, stem diameter, density and surface area) can then be found using the equations presented.

## **4.2 Results and Discussion**

A small sample of the pre-burn data are presented in this chapter. The complete data set is presented in Appendix C.1.

### **4.2.1 Size and Shape Measurements**

Seasonal moisture content and relative moisture content data are shown in Figure 4-7 for the ten samples. Samples from the same region of the country exhibited similar but not identical curves. California species had the lowest moisture content on average. Coniferous species (lodgepole pine, Douglas-fir, and sand pine) had consistently higher MC than other species from the same region. California and Rocky Mountain species had the lowest moisture content during the summer and fall months while Southern species experienced a maximum in MC during late summer. The lone deciduous species, Gambel oak, showed a strong relationship between moisture content and the growing season. The local fire seasons are March through December for the Southern California region (all year during drought years), May/June through October for the Rocky Mountain region and March through November for the Southern region (Hull et al., 1966; Werth, 2015). Moisture content is usually lowest during the local fire season, though the agreement is far from perfect. Relative moisture content tracks moisture content very closely for Southern California species throughout the entire year. Relative moisture content for Rocky Mountain species loosely tracked, but was usually 20 – 30% lower, than moisture content. Relative moisture content for Southern species exhibited little change throughout the year, and

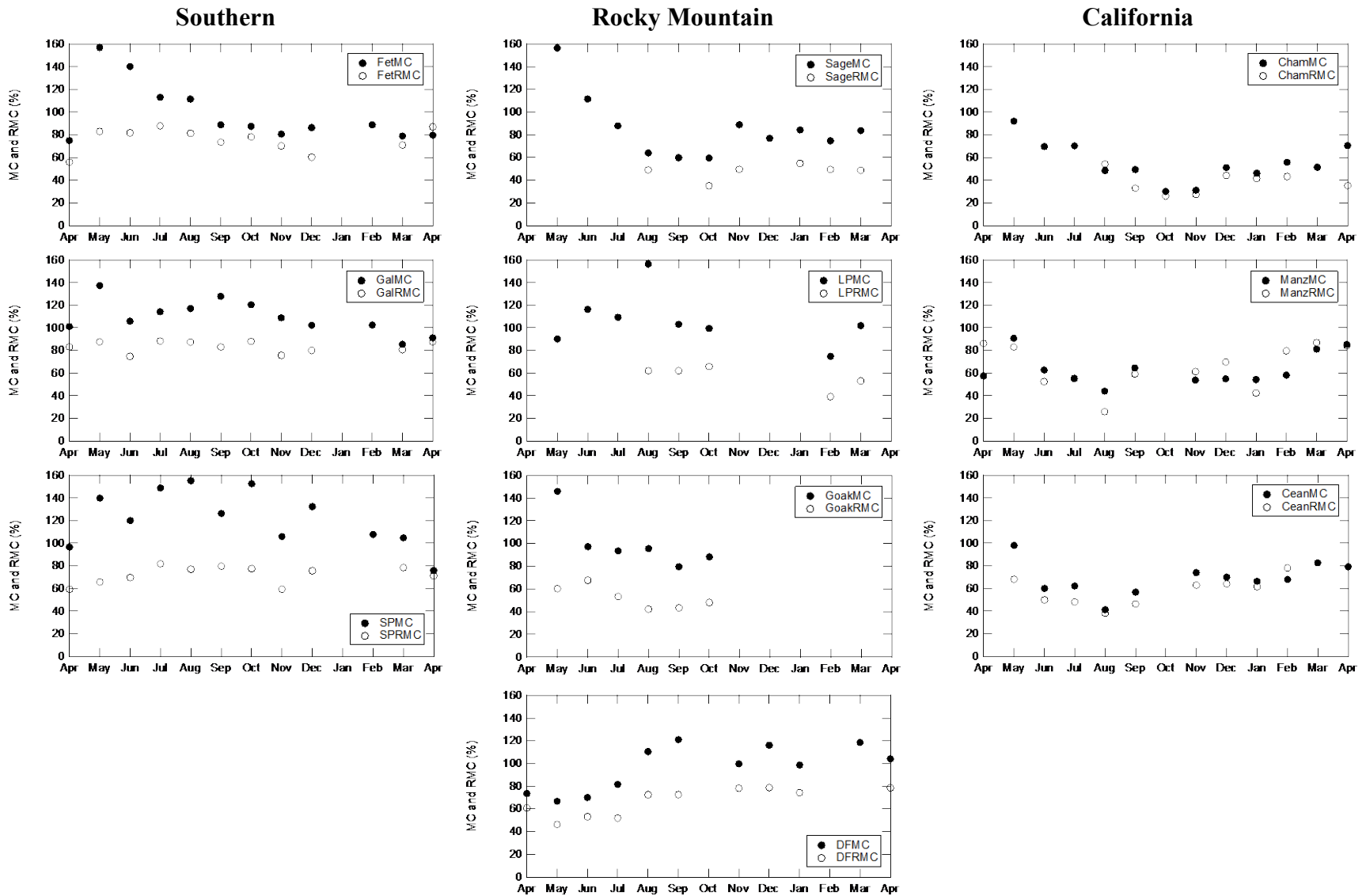


Figure 4-7: Yearly patterns for foliage moisture content (MC) and relative moisture content (RMC) for fetterbush (Fet), gallberry (Gal), sand pine (SP), sagebrush (Sage), lodgepole pine (LP), Gambel oak (Goak), Douglas-fir (DF), chamise, (Cham), manzanita (Manz) and ceanothus (Cean).

did not track the high moisture content measurements in the spring. Moisture content was found to change less than 5% over 48 hours from the sample collection time using local species, so the foliage samples tested in this dissertation are believed to be similar to foliage that is still attached to the plant. Only 13% of the non-moisture sample characteristics exhibited seasonal changes. The yearly average and standard deviation for the sample characteristics without seasonal trends are shown in Table 4-3. Non-moisture characteristics that exhibited a seasonal trend are marked in Table 4-3 and Table 4-4 with “Graph” and are shown in Figure 4-8 through Figure 4-10.

**Table 4-3: Yearly average and standard deviation for measured foliage characteristics—broadleaf species.**

Species	Density (g cm <sup>-3</sup> )	Length (cm)	Width (cm)	Thickness (mm)	Surface Area (cm <sup>2</sup> )	Fresh Mass (g)
manzanita	Graph	3.77±0.56	2.14±0.46	Graph	13.0±4.30	0.33±0.13
ceanothus	0.99±0.03	1.60±0.28	1.23±0.23	0.57±0.11	3.18±0.97	0.09±0.04
gambel oak	Graph	6.51±1.63	4.33±1.36	Graph	29.8±15.08	0.23±0.13
fetterbush	0.89±0.04	5.25±1.06	2.51±0.63	Graph	19.2±8.01	0.28±0.12
gallberry	0.89±0.03	3.89±0.73	Graph	0.32±0.06	Graph	0.12±0.05

**Table 4-4: Yearly average and standard deviation for measured foliage characteristics—needle species.**

Species	Density (g cm <sup>-3</sup> )	Length (cm)	Width (cm)	Needle Length (cm)	Stem Diameter (mm)	Fresh Mass (g)
Douglas-fir	0.95±0.03	3.00±0.97	4.28±0.70	2.01±0.50	1.44±0.45	0.60±0.26
lodgepole pine	--	2.24±0.45	8.57±2.45	5.44±0.97	3.14±1.00	1.33±0.47
big sagebrush	--	4.42±0.47	--	--	1.22±0.39	0.22±0.13
chamise	--	3.93±0.59	--	--	1.05±0.30	0.14±0.07
sand pine	0.98±0.03	2.47±0.92	7.02±2.35	5.60±1.09	1.35±0.41	0.67±0.25

Significant monthly trends were found for density (manzanita and Gambel oak), surface area (gallberry), thickness (manzanita, Gambel oak and fetterbush) and width (gallberry), as shown in Figure 4-8 through Figure 4-10. Surface area and width for gallberry both followed a similar trend (see Figure 4-8); large leaves were observed in April, small leaves in July and

relatively large leaves from August to the next April. Density for manzanita was high in April, decreased rapidly to a low in August, and then increased slowly through March (see Figure 4-9). Density for Gambel oak showed the opposite trend, with lows in May and October and a high in August. Thickness for manzanita, Gambel oak and fetterbush all showed the same pattern: high in the spring, low in the summer, then increasing slowly through the rest of the sample period (see Figure 4-10). Changes in density and thickness for manzanita compared to Gambel oak show some interesting relationships. Thickness and density for manzanita seemed to be correlated fairly well with each other ( $R^2 = 0.76$ ), but the observed seasonal changes did not correlate solely to changes in MC ( $R^2_{\text{density}} = 0.25$ ,  $R^2_{\text{thickness}} = 0.12$ ). The trends for Gambel oak thickness and density were not well correlated ( $R^2 = 0.10$ ). The trend for Gambel oak thickness is at least partly due to MC ( $R^2 = 0.40$ ) while that for density had no relationship to MC ( $R^2 = 0.00$ ). The  $R^2$  values presented here represent the amount of variation in the response variable that is accounted for by the associated linear regression model.

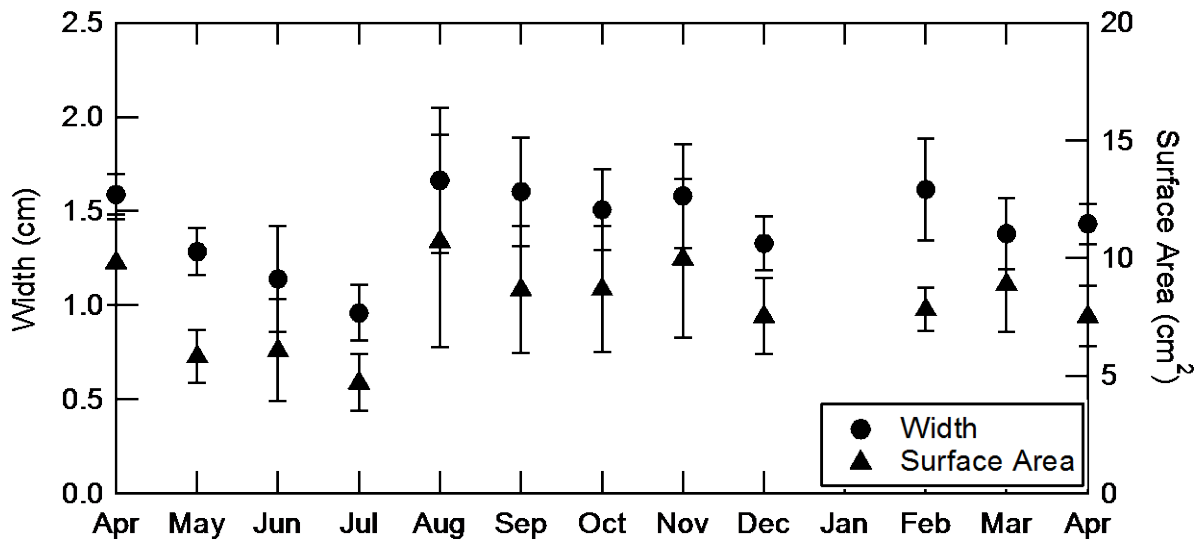


Figure 4-8: Monthly surface area and width values for gallberry. Error bars indicate the standard deviation in the data.

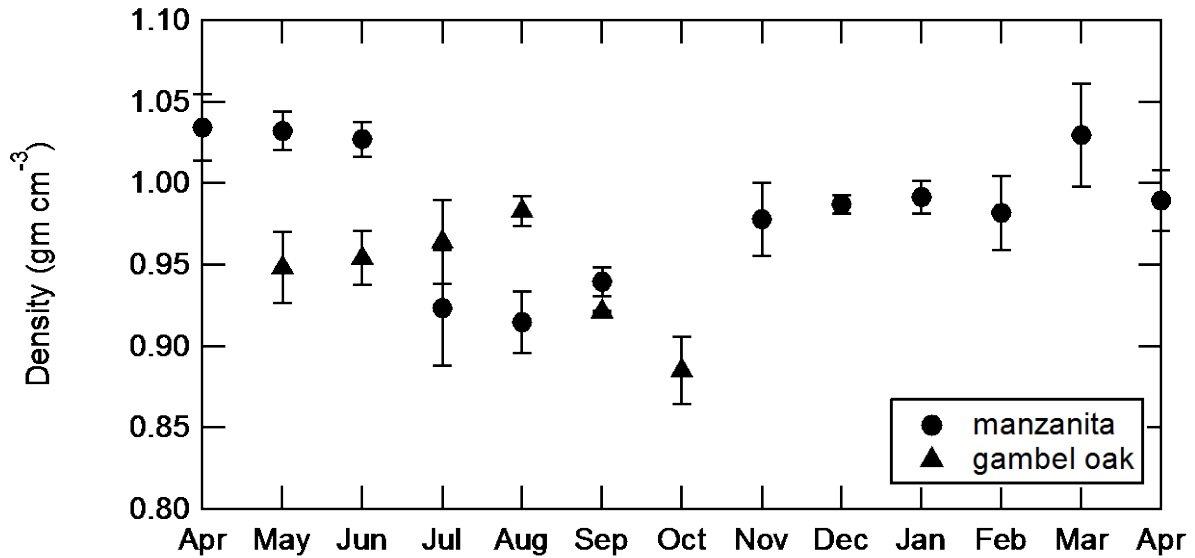


Figure 4-9: Monthly density values for manzanita and Gambel oak. Error bars indicate the standard deviation in the data.

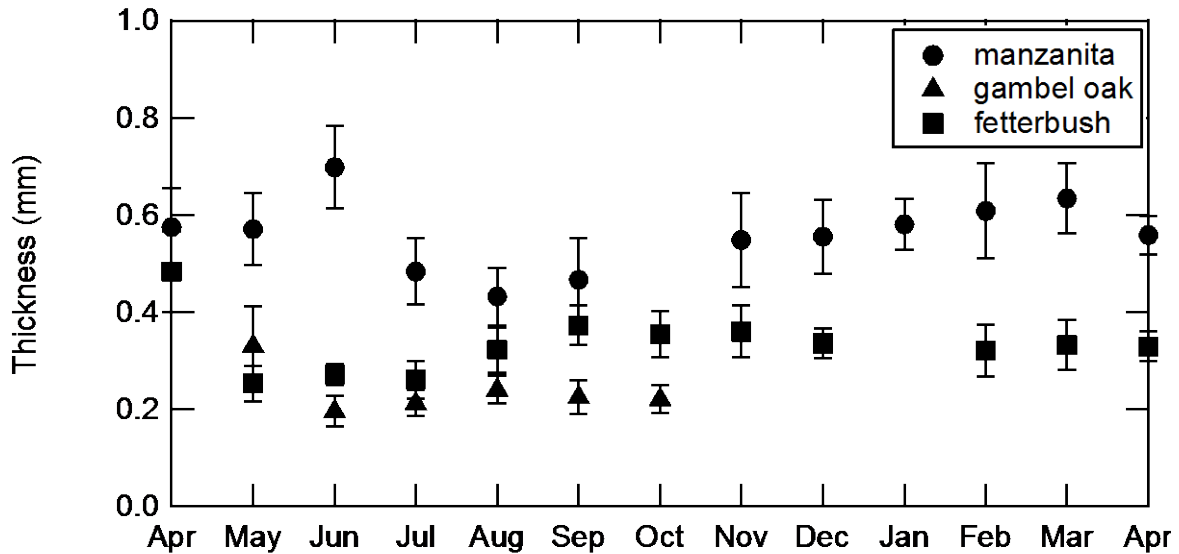


Figure 4-10: Monthly thickness values for manzanita, Gambel oak and fetterbush. Error bars indicate the standard deviation in the data.

Surface area to volume (SA:V) ratio measurements are shown in Figure 4-11 for all five broadleaf species. The SA:V ratio varies during the spring and summer but levels off during the fall and winter months. Species from the same location have nearly identical trends. Gambel oak

consistently exhibited the largest SA:V ratio with the exception of May, when the leaves were still forming. Fetterbush and gallberry had similar SA:V ratios to that for Gambel oak during the spring and early summer, but those values dropped during fall and winter. Manzanita and ceanothus had consistently lower SA:V ratios than the other broadleaf species.

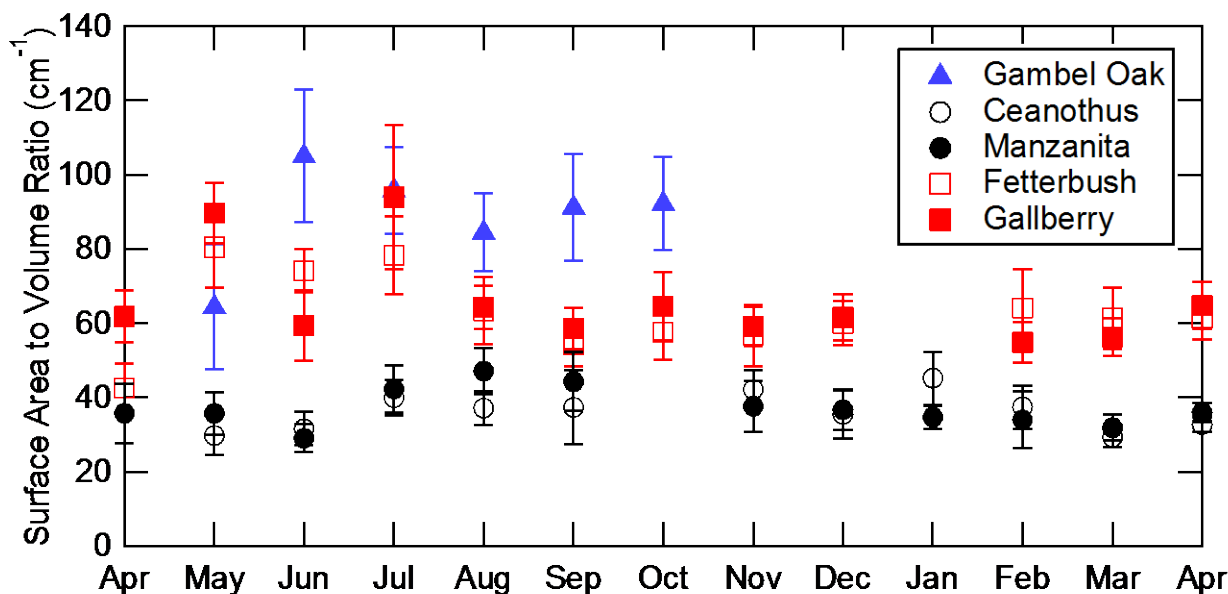


Figure 4-11: Surface area to volume (SA:V) ratio measurements for Gambel oak, fetterbush, gallberry, ceanothus and manzanita. Values shown are in units of inverse centimeters. Error bars indicate the standard deviation in the data.

#### 4.2.2 Chemical Composition Measurements

Data for volatiles content, fixed carbon content, ash content and lipid content are reported as mass fractions on a dry basis and are shown in Figure 4-12. Aside from Gambel oak, which shows an 8% change in volatiles and fixed carbon content, chemical composition measurements were constant throughout the year. The yearly mean for each measurement is shown in Table 4-5. The chemical composition measurements reported here show minimal differences between species. Susott et al. (1975) and Susott (1982) showed 17 different foliage samples all had

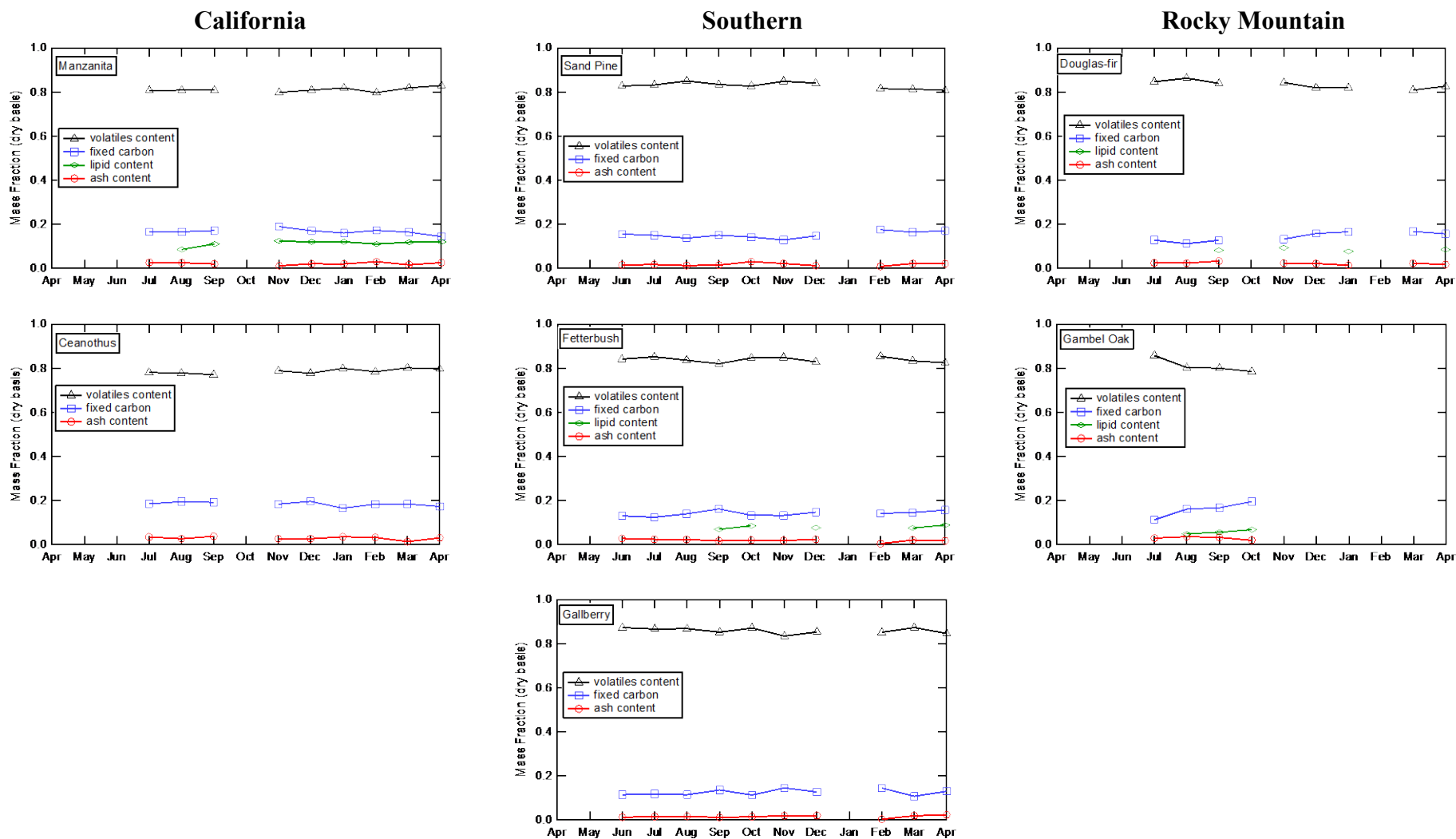


Figure 4-12: Volatiles content, fixed carbon content, ash content and lipid content for manzanita, ceanothus, Douglas-fir, Gambel oak, fetterbush, sand pine and gallberry. Reported values are mass fractions on a dry basis. California species are on the left, Southern in the middle, and Rocky Mountain on the right.

similar heats of combustion and mass release curves. The result that the ten species studied herein all have similar volatiles contents agrees with results by Susott (Susott et al., 1975; Susott, 1982), and provides evidence that foliage samples are chemically similar. The result that different species are chemically similar has important implications for fire modeling. Many physics-based models simplify surface chemistry through the use of one-step and two-step devolatilization models and by assuming generic properties for the solid fuel (Morvan and Dupuy, 2001; Mell et al., 2007). While these simplified models were shown to be inadequate for predicting mass loss in live manzanita leaves (Prince, 2014), it is possible that more sophisticated surface chemistry models would also predict similar mass loss behavior between species. These results are at odds with reported differences in burning behavior between species (Fletcher et al., 2007); future work must be done to understand these differences.

**Table 4-5: Yearly average values of volatiles content, fixed carbon content, ash content and lipid content for manzanita, ceanothus, Douglas-fir, Gambel oak, fetterbush, sand pine and gallberry.\***

<b>Species</b>	<b>Volatiles Content</b>	<b>Fixed Carbon Content</b>	<b>Ash Content</b>	<b>Lipid Content</b>
<b>Sand pine</b>	0.830	0.152	0.018	---
<b>Douglas-fir</b>	0.833	0.144	0.023	0.085
<b>Ceanothus</b>	0.786	0.184	0.029	---
<b>Manzanita</b>	0.811	0.167	0.022	0.114
<b>Fetterbush</b>	0.839	0.141	0.020	0.079
<b>Gallberry</b>	0.859	0.126	0.016	---
<b>Gambel oak</b>	0.812	0.159	0.029	0.058

\* All values are reported on a dry basis

### 4.2.3 Dry Mass Distribution

The estimated parameter values, the 95% confidence intervals on the means and the p-value from the Kolmogorov-Smirnov test are shown in Table 4-6. All the species except ceanothus are statistically verified as Weibull distributions at the 95% confidence level while ceanothus is verified at the 90% confidence level. There were no distinct seasonal trends in the

mass data (see Table 4-3 and Table 4-4), so the distribution is valid for the entire year. Plots containing the collected data, probability density function (pdf), empirical cumulative distribution function (edf) and theoretical cumulative distribution function (cdf) are shown in Figure 4-13 (left panel) for California species, Figure 4-13 (right panel) for Southern species and Figure 4-14 for Rocky Mountain species.

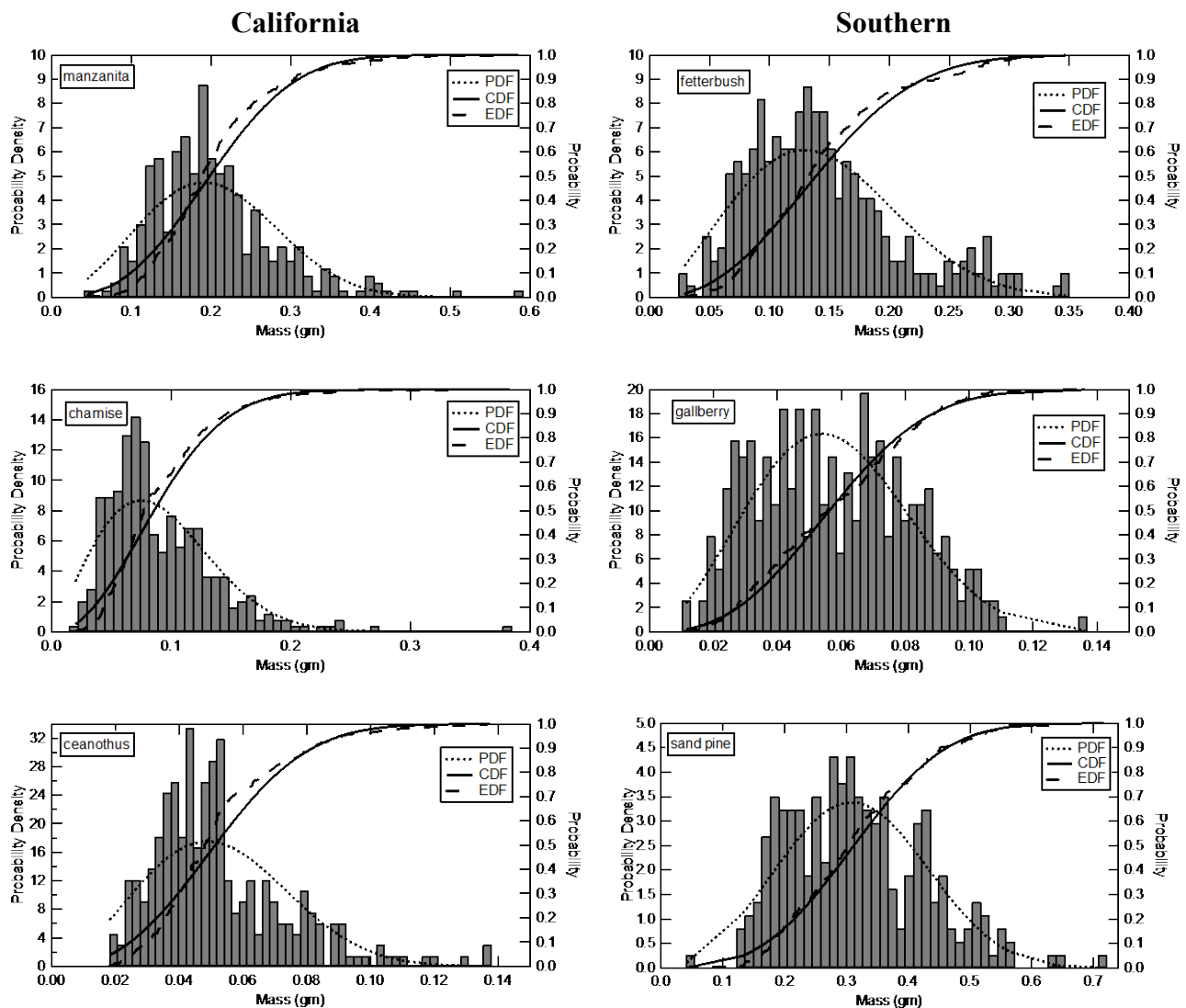


**Figure 4-13: Dry mass data, probability distribution function (pdf), cumulative distribution function (cdf) and empirical distribution function (edf) for species from the California region (left panel) and Southern region (right panel).**

**Table 4-6: Weibull distribution parameters for measured dry mass calculated using Equations 4-5 and 4-6.**

Species	$a \pm CI$	$b \pm CI$	p-Value
manzanita	$0.227 \pm 0.010$	$2.699 \pm 0.216$	0.158
ceanothus	$0.059 \pm 0.003$	$2.574 \pm 0.217$	0.045
Douglas-fir	$0.352 \pm 0.019$	$2.300 \pm 0.201$	0.479
chamise	$0.102 \pm 0.006$	$2.091 \pm 0.158$	0.166
gambel oak	$0.133 \pm 0.012$	$1.848 \pm 0.231$	0.944
big sagebrush	$0.135 \pm 0.009$	$1.816 \pm 0.152$	0.455
lodgepole pine	$0.727 \pm 0.037$	$2.785 \pm 0.264$	0.687
sand pine	$0.352 \pm 0.015$	$3.047 \pm 0.272$	0.881
fetterbush	$0.162 \pm 0.008$	$2.409 \pm 0.203$	0.329
gallberry	$0.065 \pm 0.003$	$2.638 \pm 0.236$	0.838

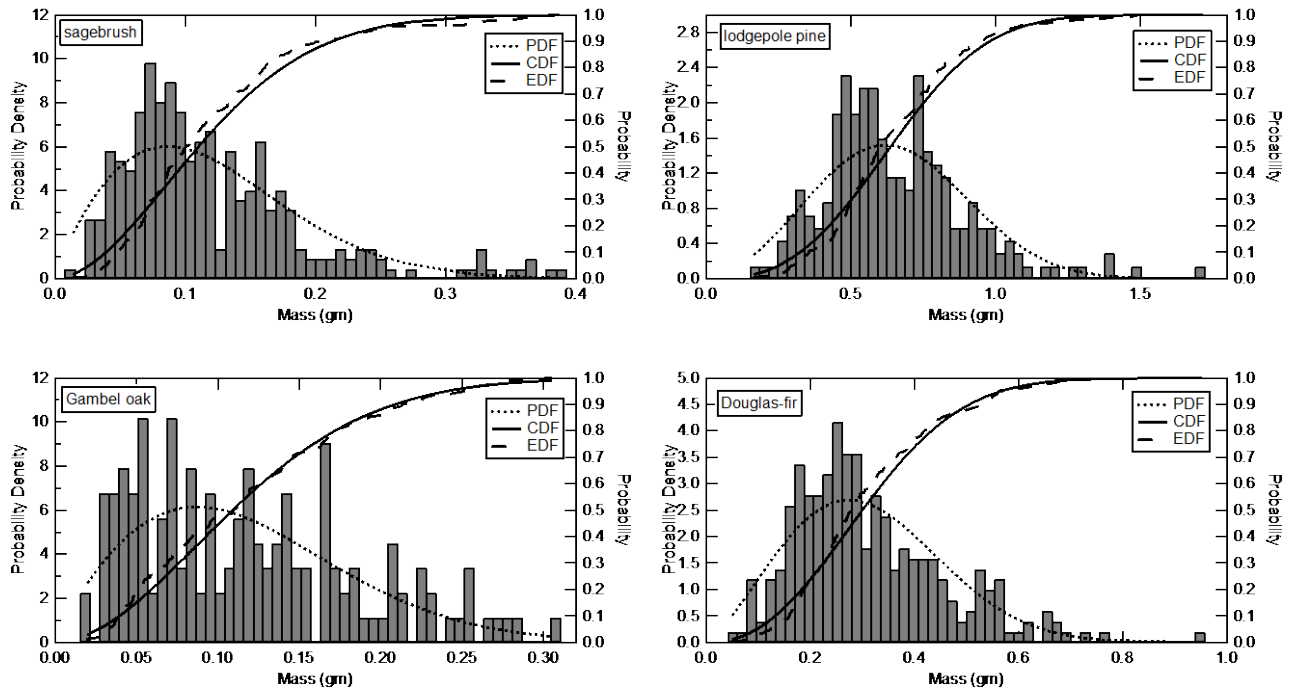


**Figure 4-14: Dry mass data, probability distribution function (pdf), cumulative distribution function (cdf) and empirical distribution function (edf) for species from the Rocky Mountain region.**

#### 4.2.4 Prediction Models

The prediction models for the various fuel element characteristics are shown in Table 4-7 (Broadleaf) and Table 4-8 (Needle). The models are reported in the order in which they were developed and are intended to be used. The strength of these models is shown by the amount of

data variation accounted for by the model. For the overall collection of models, 36% have an  $R^2$  values greater than 0.7 and 72% have an  $R^2$  value greater than 0.5. When broken out by species type, 50% of the broad leaf species models have an  $R^2$  value greater than 0.7 and 90% of the models greater than 0.5. The needle species were less successful, with 17% and 48% of the models having an  $R^2$  value greater than 0.7 and 0.5, respectively. The difference between needle and broadleaf species models likely could have been overcome if the number of needles per sample was measured for the needle species.

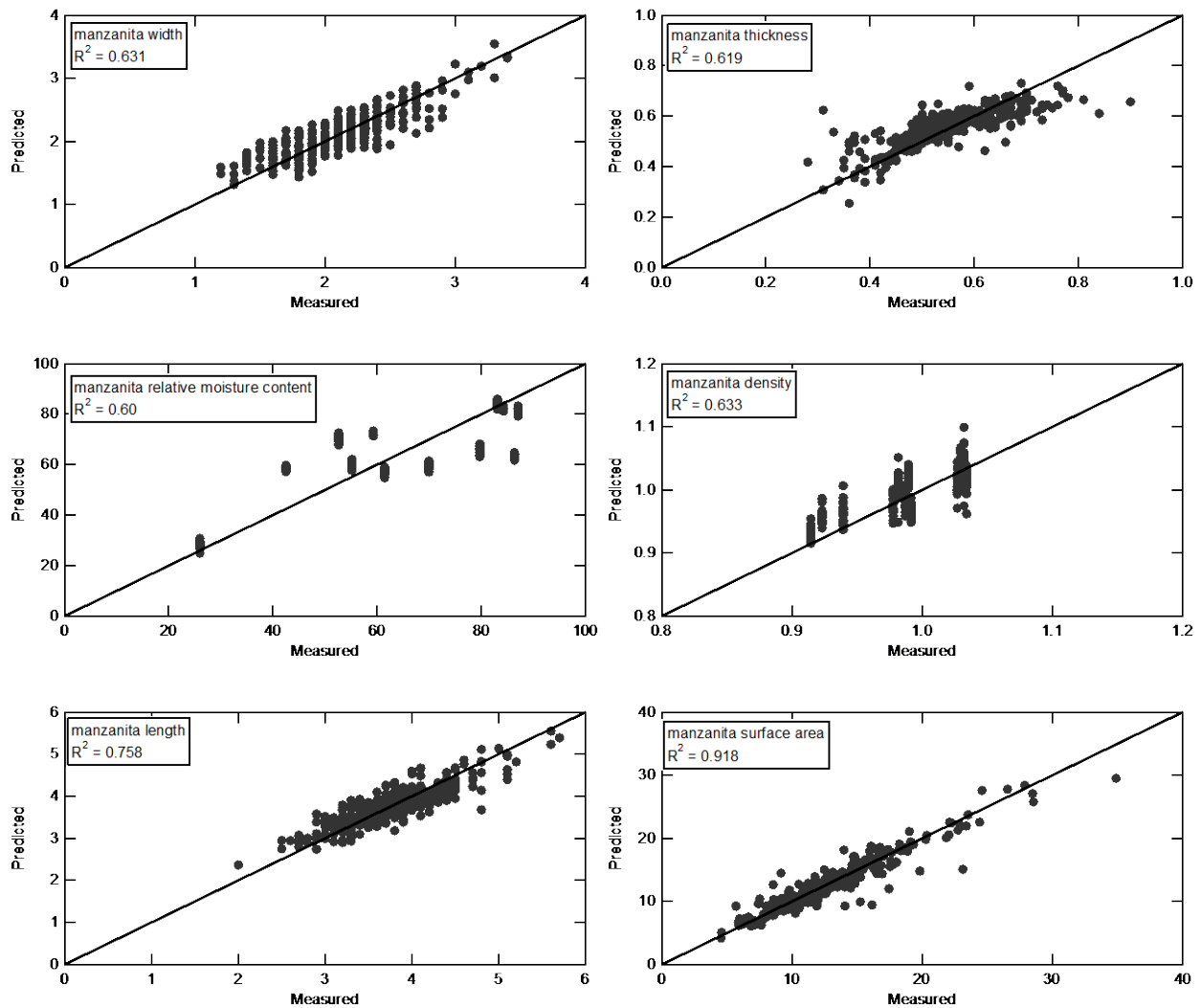
None of the models developed here contain a seasonal parameter. While this lack of a seasonal parameter is not typical for plant growth models or models predicting plant characteristics (Adams, 2014), the constancy of the measured data throughout the year made the inclusion of a seasonal parameter unnecessary. The measured characteristics that did change with season were accompanied by changes in other characteristics (usually moisture content) so that the single prediction model is valid for the whole year. Some of the needle species, particularly sand pine, did exhibit some visual seasonal variation in the shape and size of individual fuel samples that was not captured by the statistical test for seasonal trends. However, there is enough scatter in the data for sand pine that the differences based on growing season are indistinguishable from the general trends reported here. Parity plots for all the manzanita and Douglas-fir models are shown in Figure 4-15 and Figure 4-16, respectively. Model parity plots for the other eight species are shown in Appendix B.1.

Table 4-7: Fuel element property models for broadleaf species.

Parameter	R <sup>2</sup> <sub>Adj</sub>	Model
<b>Ceanothus</b>		
RMC	0.676	$0.568 + 32.11\sqrt{m_w} - 42.20\sqrt{m_f} + 28.28\sqrt{m_d}$
Length	0.615	$0.781 + 0.356R^2 - 0.494 \ln(M) + 13.48m_w$
Width	0.523	$4.04 - 2.95\sqrt{m_w} + 0.703 \ln(m_d) + 0.286 \ln(R)$
Thickness	0.508	$0.671 - 38.42\sqrt{m_d} - 0.039L - 29.31\sqrt{m_w} - 0.499\sqrt{W} + 50.13\sqrt{m_f}$
Density	0.523	$1.28 - 0.124 \ln(m_f) - 0.039R^2 - 0.096t^2 + 0.163 \ln(m_w)$
SA	0.873	$-0.776 + 143.8m_d^2 + 1.35W + 1.14L$
<b>Fetterbush</b>		
RMC	0.411	$4.41 + 2.94 \ln(m_w) - 5.23 \ln(m_f) + 2.28 \ln(m_d)$
Length	0.841	$8.67 + 0.656 \ln(R) + 2.08 \ln(m_d) + 0.935M^2$
Width	0.809	$82.15\sqrt{m_w} + 69.49\sqrt{m_d} - 102.1\sqrt{m_f}$
Thickness	0.662	$1.499 + 0.307 \ln(m_f) - 0.298 \ln(L) - 0.293 \ln(W)$
Density	0.737	$0.626 - 0.793 \ln(m_d) + 0.792 \ln(m_f) - 0.198MC^2 - 0.112R^2$
SA	0.948	$-4.92 + 20.09m_f^2 + 5.56W + 0.289L^2$
<b>Gallberry</b>		
RMC	0.214	$-5.86 - 7.51 \ln(m_w) + 6.69M^2 + 7.57 \ln(m_d) - 6.05 \ln(m_w) * M^2 + 6.01 \ln(m_d) * M^2$
Width	0.74	$0.446 - 37.28m_d^2 + 0.174M^2 + 7.53m_f$
Length	0.714	$-8.503 + 4.165 \ln(m_w) + 37.69\sqrt{m_d} - 7.03 \ln(m_f)$
Thickness	0.597	$0.443 - 0.318R^2 + 0.623\sqrt{m_f} - 0.087 \ln(L)$
Density	0.599	$1.393 - 8.89m_w^2 - 11.18m_d - 0.115M^2 + 6.17m_f - 0.455\sqrt{R}$
SA	0.905	$152.1m_w^2 - 2.40R + 1.54L + 1.60W^2$
<b>Gambel Oak</b>		
RMC	0.443	$133.3 - 438.5\sqrt{M} - 441.1 \ln(m_d) + 441.1 \ln(m_f)$
Length	0.912	$4.073R^2 + 16.31\sqrt{m_d}$
Width	0.838	$9.388\sqrt{m_f}$
Thickness	0.72	$0.090 - 23.85\sqrt{m_d} + 32.22\sqrt{m_f} - 21.46\sqrt{m_w} - 0.088 \ln(R)$
Density	0.879	$204.6 - 3.98 \ln(m_w) - 695.6 \ln(m_d) - 0.199R^2 - 688.4\sqrt{M} + 699.6 \ln(m_f)$
SA	0.937	$60.4m_w + 0.371W^2 + 0.335L^2$
<b>Manzanita</b>		
RMC	0.6	$-18.77 - 63.74 \ln(m_f) + 63.77 \ln(m_d) + 63.84\sqrt{M}$
Length	0.758	$1.232 + 4.48\sqrt{m_f}$
Width	0.631	$0.414 - 89.38\sqrt{m_w} - 0.264R^2 - 111.3\sqrt{m_d} + 145.8\sqrt{m_f}$
Thickness	0.619	$2.555 - 0.365\sqrt{L} - 0.296M + 0.398 \ln(m_w) - 0.338 \ln(W)$
Density	0.633	$0.858 + 0.0813R^2 + 0.817m_w^2 + 0.215t - 0.1996m_d$
SA	0.918	$-4.79 - 2.425 \ln(t) + 1.016W^2 + 12.51m_f + 1.993L$

**Table 4-8: Fuel element property models for needle species.**

Parameter	R <sup>2</sup> <sub>Adj</sub>	Model
<b>Chamise</b>		
RMC	0.631	$3.208 - 3.246M + 1.656 \ln(m_w) - 1.66 \ln(m_d)$
Diameter	0.576	$1.039 - 1.50M^2 + 8.97m_w$
Length	0.392	$-28.32 - 6.48 \ln(M) - 69.87 \ln(m_d) - 32.00R + 70.62 \ln(m_f)$ $+ 0.655 \ln(M) * \ln(m_d) - 45.13 \ln(M) * R$
Density		<i>Not measured for year 1 species</i>
<b>Douglas-fir</b>		
RMC	0.846	$-1.28 + 4.164 \ln(m_f) - 4.182 \ln(m_d) - 0.89M^2$
Length	0.723	$4.041 + 29.32m_w^2 - 4.33R^2 - 20.78m_w^2 * \sqrt{m_f}$
NL	0.421	$14.34\sqrt{R} - 9.05\sqrt{M} + 9.833 \ln(m_d) * \sqrt{R} - 7.47 \ln(m_d) * \sqrt{M}$
Width	0.524	$1.564m_w + 1.15N + 2.94R - 0.748R * \ln(L)$
Diameter	0.418	$-1.14 \ln(m_f) + 0.176W^2 - 2.435N - 0.261\sqrt{m_d} * W^2 + 4.49\sqrt{m_d}$ $* N$
Density	0.303	$-1.064 + 1.13\sqrt{M} + 0.156 \ln(R) + 1.30 \ln(m_f) - 1.32 \ln(m_w)$
<b>Lodgepole Pine</b>		
RMC	0.773	$5.89 + 7.62 \ln(m_w) - 3.36 \ln(M) - 7.62 \ln(m_f)$
Diameter	0.614	$34945\sqrt{m_f} - 2719\sqrt{m_d} - 2218\sqrt{m_w} + 999.6\sqrt{m_d} * R^2 - 1004\sqrt{m_w}$ $* R^2$
Length	0.524	$4.24 - 1.55M^2 + 1.05\sqrt{m_w} - 4.22R^2 - 0.856\sqrt{D} + 3.92M^2 * R^2$
NL	0.45	$-248.8 + 383.4 \ln(m_f) - 13.35\sqrt{R} - 374.8 \ln(m_d) - 268.7 \ln(M)$ $* \sqrt{R} - 9.52 \ln(m_d) * \sqrt{R}$
Width	0.31	$(94.56 + 47.66M + 151.2 \ln(m_d) - 205.1 \ln(m_f) + 0.0073L^2$ $+ 53.81 \ln(m_w))^{-1}$
Density		<i>Not measured for year 1 species</i>
<b>Sagebrush</b>		
RMC	0.821	$-46.96 + 158.8 \ln(m_d) + 157.4\sqrt{M} - 158.8 \ln(m_f)$
Diameter	0.493	$-0.811M^2 + 4.35 \ln(m_f) - 4.004 \ln(m_d)$
Length	0.493	$5.78\sqrt{R} - 2334\sqrt{m_w} + 1213\sqrt{m_d} - 2452M^2 * \sqrt{m_w} + 3563M^2$ $* \sqrt{m_d}$
Density		<i>Not measured for year 1 species</i>
<b>Sand Pine</b>		
RMC	0.24	$0.738 + 4.65m_w^2 - 2.264m_f^2 + 4.083m_d^2$
Length	0.634	$5.26 - 3.58M^2 + 12.22 \ln(R) + 1.143M^2 * \sqrt{m_w} + 11.42M^2 * \ln(R)$
Width	0.355	$9.11 - 4.37 \ln(L) + 5.09m_f^2 - 11.78R * m_w^2$
NL	0.481	$6.34 + 1.57M^2 - 6.84 \ln(m_f) + 1.89 \ln(W) + 8.02 \ln(m_d)$
Diameter	0.224	$41.46 - 33.16\sqrt{M} - 42.07\sqrt{R} - 3.144\sqrt{L} - 2.37\sqrt{N} + 38.44\sqrt{M} * \sqrt{R}$ $+ 1.850\sqrt{L} * \sqrt{N}$
Density	0.571	$0.841 - 0.0675 \ln(M) - 0.0014L^2 - 0.0011W + 0.202\sqrt{R}$



**Figure 4-15: Physical property predictions for manzanita.**

#### 4.2.5 Uncertainty Analysis

As with any experimental work, it is important to explore the effect of measurement error on both the measured values themselves and on the models which use the data. Table 4-9 details both the sources of error and the relative magnitude of those errors for each pre-burn measurement. Within the table, the relative uncertainty entries represent the measurement uncertainty normalized by the measured value averaged across all species and months. The

maximum relative uncertainty is 33% for the ash content measurements, and is largely due to the small amount of ash contained in the samples. Other than ash, all the other relative uncertainties are below 5%, indicating the natural scatter in the data is far more important than measurement uncertainty in developing prediction models.

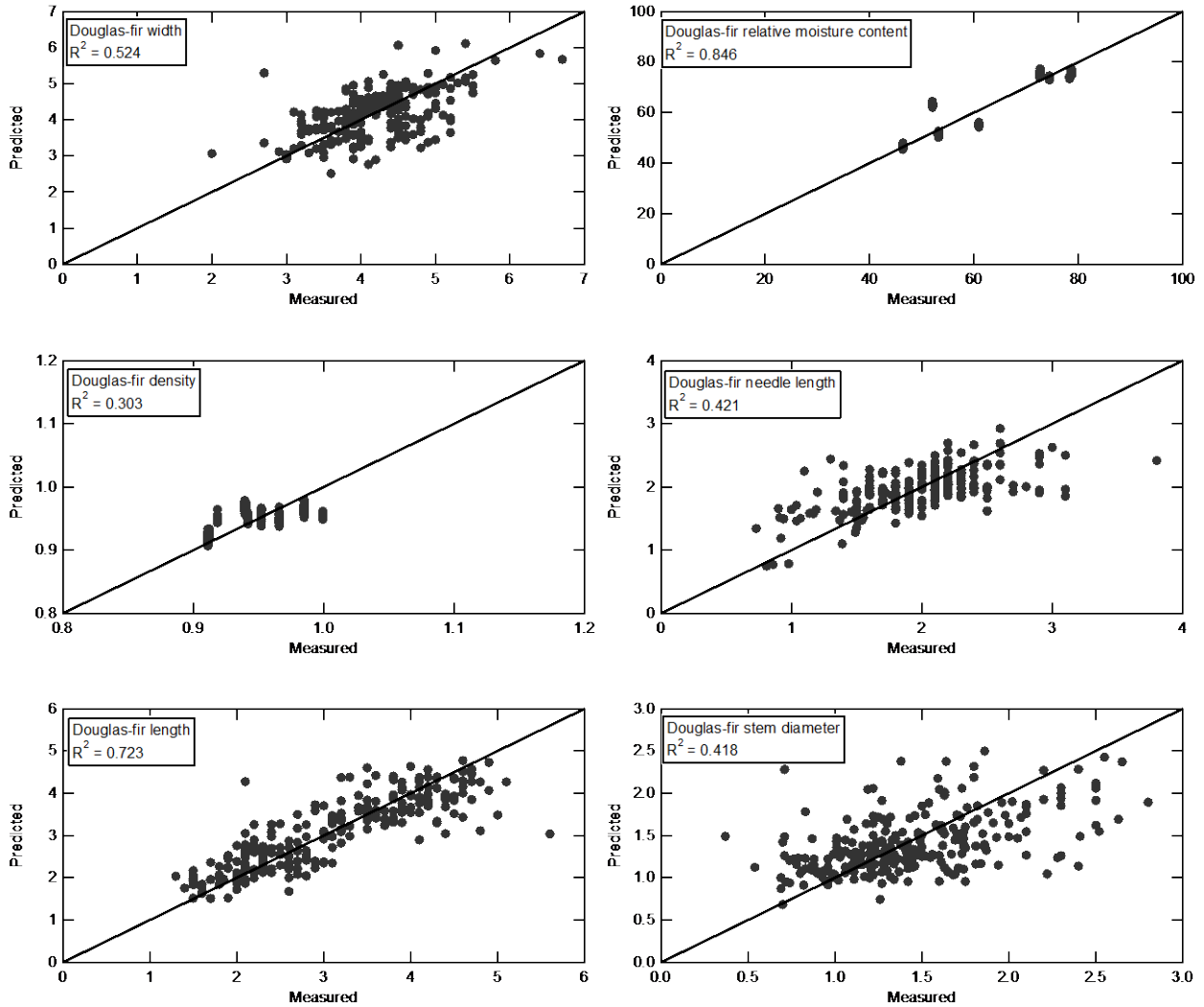


Figure 4-16: Physical property predictions for Douglas-fir.

**Table 4-9: Relative uncertainty and sources of measurement error for all the pre-burn measurements.**

<b>Measurement</b>	<b>Relative Uncertainty</b>	<b>Sources of Error</b>
<b>Moisture content</b>	0.0001	Computrac runs drying program and reports moisture content. Error is that reported by manufacturer
<b>Relative moisture content</b>	0.0017	Error source is the sensitivity of the mass balance
<b>Density</b>	0.0053	Error source is the sensitivity of the mass balance
<b>Length</b>	0.014	Error comes from the tick mark spacing on the ruler
<b>Width</b>	0.015	Error comes from the tick mark spacing on the ruler
<b>Needle length</b>	0.011	Error comes from the tick mark spacing on the ruler
<b>Thickness</b>	0.025	Error comes from the specification on the caliper
<b>Stem diameter</b>	0.006	Error comes from the specification on the caliper
<b>Surface area</b>	0.017	Error comes from user input on the algorithm's reference length scale and from the error on the thickness measurement
<b>Fresh mass</b>	0.0005	Error source is the sensitivity of the mass balance
<b>Dry mass</b>	0.001	Error source is the sensitivity of the mass balance
<b>Water mass</b>	0.001	Error source is the sensitivity of the mass balance
<b>Lipid content</b>	0.04	Error source is the sensitivity of the mass balance
<b>Volatiles content</b>	0.0012	Error source is the sensitivity of the mass balance
<b>Fixed carbon content</b>	0.013	Error source is the sensitivity of the mass balance
<b>Ash content</b>	0.33	Error source is the sensitivity of the mass balance

The entries in Table 4-10 represent the estimate of the model error due to measurement uncertainty, using analytical propagation of error techniques, divided by the root mean squared error (RMSE) of the residuals between the data and the prediction. Thus, a table entry greater than one (highlighted in the table) indicates that the estimated effect of measurement uncertainty is greater than the average model residual. The entries listed in Table 4-10 for Gambel oak relative moisture content and density are high because the model agreement with the data is very good, with  $R^2$  values near 1, and hence the RMSE value is close to zero. Only the entries in the Table 4-10 for sagebrush (RMC and length) and lodgepole pine (diameter) are greater than one and have relatively high RMSE values. The average for the entries with values less than one is 0.11. The results in Table 4-10 indicate the same conclusion drawn from Table 4-9, namely, that

the measurement uncertainty does not have a large effect on the prediction models show in Table 4-7 and Table 4-8.

**Table 4-10: Estimated model prediction error due to measurement uncertainty normalized by the root mean squared error (RMSE) for each model. RMC = relative moisture content, NL = needle length, SA = surface area.**

Species	RMC	Length	Width	NL	Diameter	Thickness	SA	Density
Manzanita	0.161	0.0016	0.125	--	--	0.558	0.143	0.096
Ceanothus	0.128	0.0101	0.004	--	--	0.50	0.404	0.052
Fetterbush	0.014	0.0023	0.090	--	--	0.685	0.161	0.014
Gallberry	0.086	0.012	0.029	--	--	0.131	0.188	0.141
Gambel oak	1.94	0.012	0.002	--	--	0.242	0.011	18.8
Douglas-fir	0.020	0.015	0.137	0.007	0.008	--	--	0.092
Lodgepole pine	0.043	0.033	0.009	0.176	10.8	--	--	--
Sand pine	0.018	0.057	0.115	0.122	0.258	--	--	0.026
Sagebrush	1.83	1.78	--	--	0.003	--	--	--
Chamise	0.011	0.063	--	--	0.005	--	--	--

One shortcoming of the foregoing model development is that many of the models suffer from multicollinearity, which occurs when the predictor variables are dependent on one another. Multicollinearity can be identified in several ways, two of which are the condition number of the data matrix being greater than 30 and the absolute value of the Pearson product-moment correlation coefficient between variables being close to one. The model for ceanothus relative moisture content is one such model (condition number = 1e16; correlation coefficient = 0.975). This issue is inherent in any data set comparable to the one presented here due to plant growth patterns, and therefore cannot be avoided when trying to develop prediction models for foliage characteristics. However, the models can still be useful for prediction purposes as long as the relationships between measured characteristics in the model-development dataset are similar to the relationships between characteristics in the model-use dataset (Gujarati, 2003). The

propagation of error analysis results shown in Table 4-10 indicate the multicollinearity seen in the prediction models is at least partially mitigated by the fact that the measurement errors are generally independent and do not have a large effect on the model predictions. This does not account for the interdependence of the measured variables, but without influence from measurement uncertainty, the author claims the same interdependence would exist in a similar data set and the models are therefore valid. For example, a sample with more moisture would generally be thicker and more massive, a longer sample would also have a higher surface area, and so on.

### **4.3 Summary and Conclusions**

Physical and chemical properties for 10 live fuels were measured throughout a one-year period, including moisture content, relative moisture content, apparent density, length, width, thickness, stem diameter, needle length, surface area, surface area to volume ratio, mass, volatiles content, fixed carbon content, ash content and lipid content. An alternate method for measuring foliage apparent density using oil instead of water was developed and used. Whole-leaf surface area measurements are reported that do not require approximating the sample with an idealized shape. Foliage dry mass distributions were developed that allow the user to calculate the dry mass for a single leaf or branch tip. Prediction models were developed for each measured property based on sample dry mass and moisture content. Most measured sample characteristics did not change throughout the year, making the use of a seasonal parameter in model development unnecessary. Sample characteristics that did change throughout the year were associated with changes in the other characteristics (usually moisture content) so that the models developed here are accurate for the entire year. It is anticipated that these models can be used in

conjunction with bulk fuel description models and fuel placement models to describe the fuel matrix in detail for comprehensive fire spread models.

## 5 THE EFFECT OF HEATING MODE ON IGNITION AND BURNING OF TEN LIVE FUEL SPECIES<sup>3</sup>

### 5.1 Methods

#### 5.1.1 Experiment Description

Combustion experiments (25 replicates for each species) were performed each month in the flat flame burner (FFB) apparatus at Brigham Young University (BYU) (see Figure 5-1). In total, ten species were tested over a two-year period. Experiments were performed each month using three heating cases: convection only, radiation only, and both convection and radiation combined. Pre-burn measurements, including moisture content, relative moisture content, mass, density, length, width, needle length, stem diameter, thickness and surface area, are described in Section 4.1.1. Video images, mass and temperature data were collected using the apparatus shown in Figure 5-1. Samples were individually weighed and placed within the apparatus. The water-cooled FFB produced exhaust gases at 1000°C and 10 mol% oxygen that flowed past the sample suspended on a holding rod using an alligator clip. The holding rod was connected to a Mettler Toledo XS204 Cantilever mass balance. Mass data were continuously measured using National Instruments Labview 8.6 software. A glass cage surrounding the sample prevented ambient air from being entrained in the FFB exhaust gases. An Omega K-type thermocouple (0.013 mm diameter, 0.05 s response time) was used to measure the gas temperature. Smith

---

<sup>3</sup> This chapter is under review for publication in *Combustion Science and Technology*

(2005) corrected these temperature measurements for thermocouple radiation losses and found the losses to be small at these temperatures. An Omega QH-101060 radiant panel was used to provide a  $50 \text{ kW m}^{-2}$  flux at the sample location; radiant heat flux was measured using a Medtherm 64-series heat flux sensor.

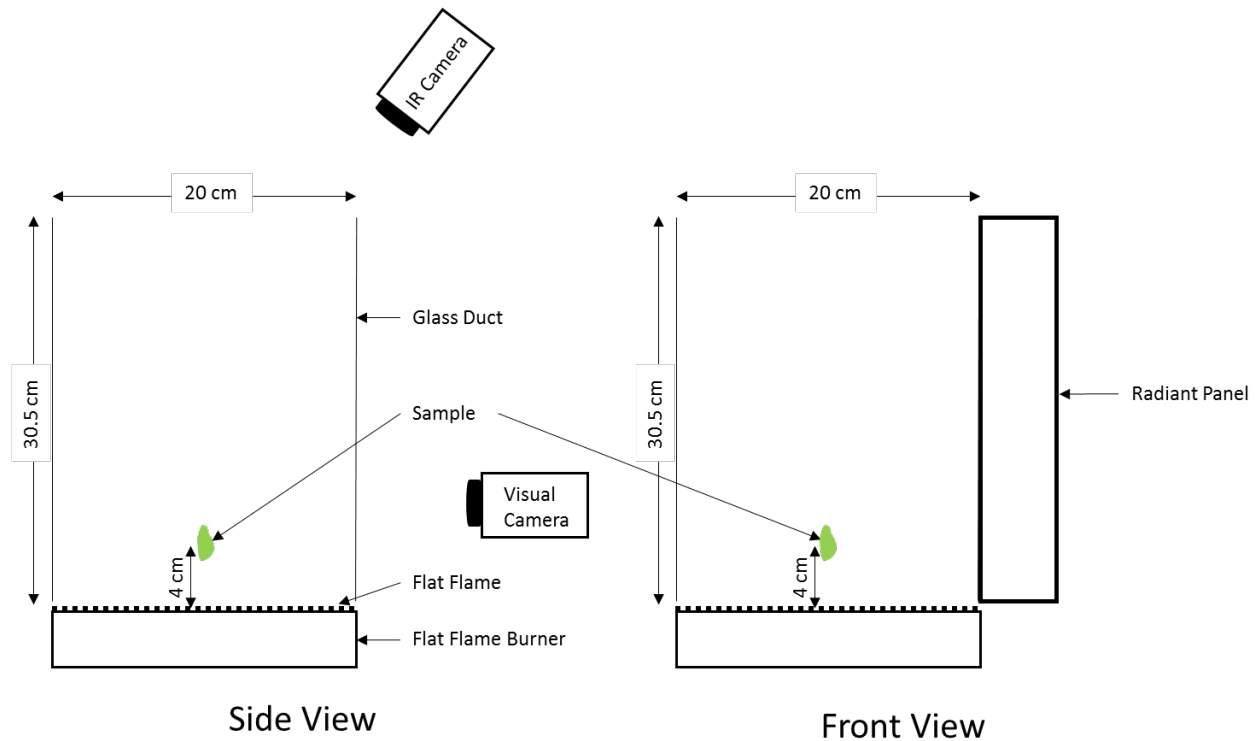


**Figure 5-1: Schematic of flat-flame burner.**

Flame videos were captured using a Panasonic SDR S50 Camcorder; surface temperature videos were collected using a FLIR A20M infrared camera. Visual and infrared video data were post-processed to extract the burn characteristics listed in Table 5-1. Flame characteristics listed in Table 5-1 are illustrated in Figure 5-2. A visual image and its associated binary image are shown in Figure 5-3 to demonstrate image processing techniques. Figure 5-4 contains an infrared image with its associated temperature scale. A few experiments with radiant fluxes of  $60 \text{ kW m}^{-2}$

and  $35 \text{ kW m}^{-2}$  were performed using Gambel oak to further explore the effects of heating mode versus heat flux.

**Table 5-1: Flame characteristics derived from video data.**

Variable	Description
Ignition Time ( $t_{ig}$ )	Time when a visible, sustained flame appears (s).
Burnout Time ( $t_{bo}$ )	Time when the flame disappears (s).
Maximum Flame Height (MFH)	Height of tallest flame during a run (cm).
Time to Max Flame Height ( $t_{mfh}$ )	Time when tallest flame occurs (s).
Surface Temperature ( $T_{ig}$ )	Average surface temperature at time of ignition ( $^{\circ}\text{C}$ ).
Maximum Ignition Temperature ( $T_{ig,max}$ )	Maximum surface temperature at the time of ignition ( $^{\circ}\text{C}$ ).
Fraction Remaining at Ignition ( $X_{ig}$ )	Mass at ignition divided by initial mass (fraction).
Mass Loss Rate at Ignition ( $\dot{m}_{ig}$ )	Instantaneous mass loss rate at ignition divided by initial mass ( $\% \text{ s}^{-1}$ ).

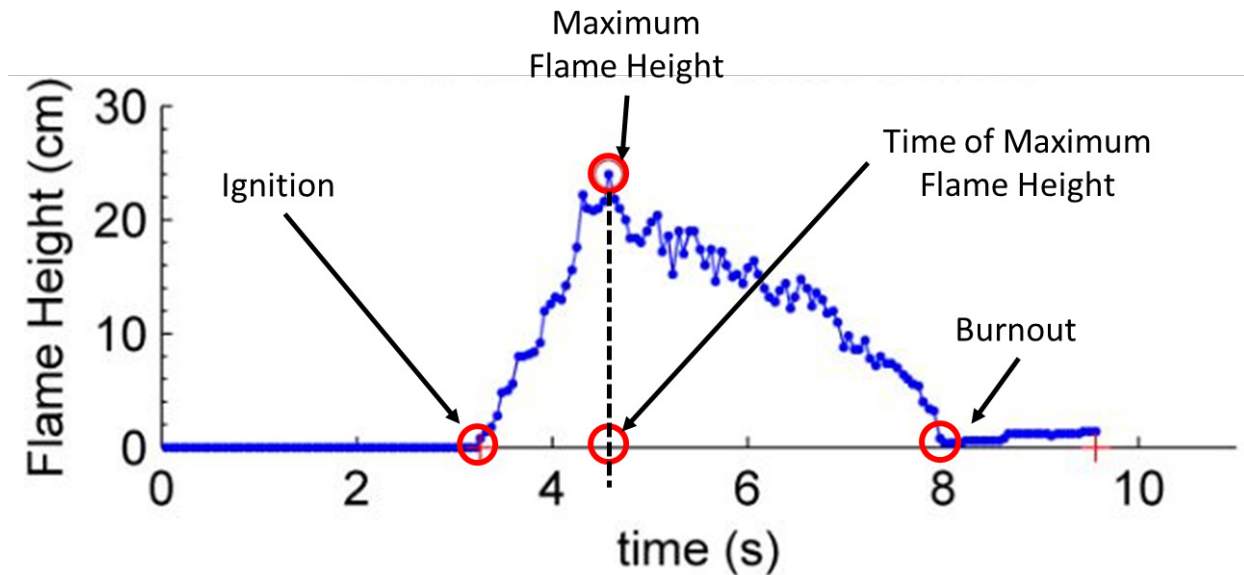


**Figure 5-2: Flame height versus time curve for a single fetherbush run. Points in time identified by red circles include ignition time, time to maximum flame height, burnout time and maximum flame height. All times were measured relative to the start time ( $t = 0$ ).**

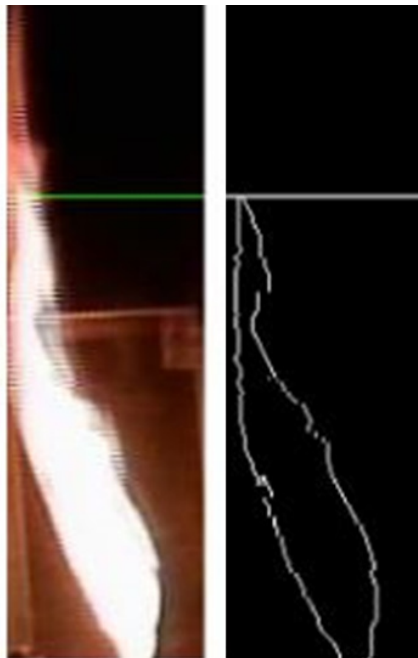


Figure 5-3: Example of image processing. The visual image is on the left, the binary image with the flame perimeter identified is on the right. Only contiguous pixels containing flame were categorized as part of the flame.

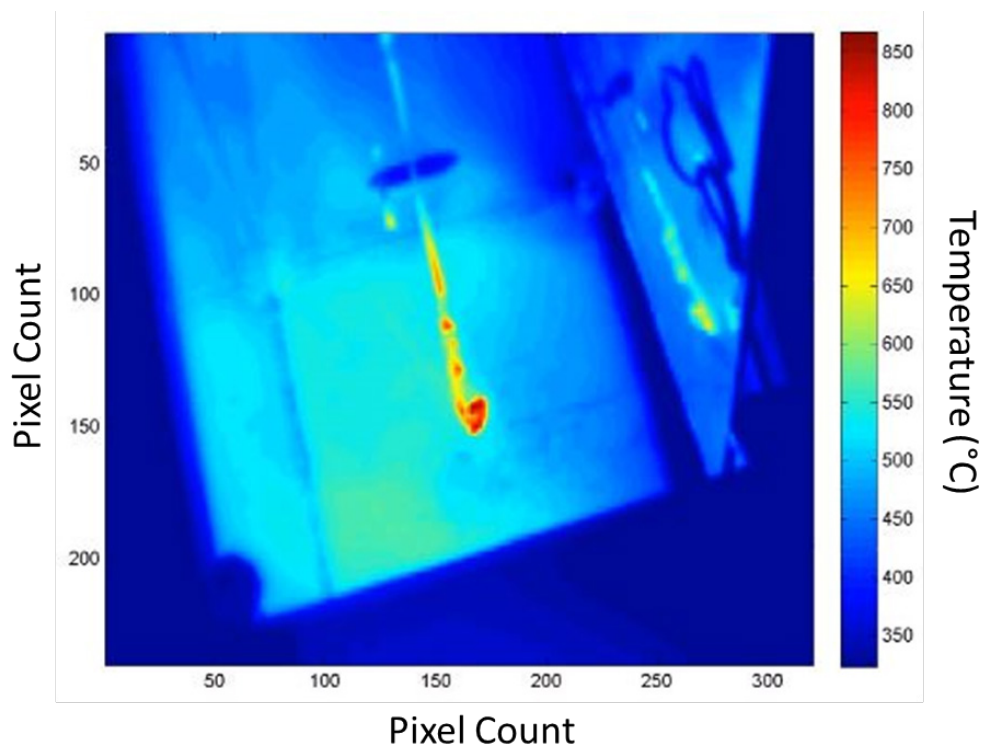


Figure 5-4: Infrared image for a convection-only manzanita run. The leaf is in the middle of the image, glowing red.

## 5.1.2 Analysis of Heat Transfer Conditions

### 5.1.2.1 Convective Heat Flux

A further comparison of heating modes is possible by looking at heat flux and heat absorbed for the different heating cases. An energy balance similar to that outlined by Engstrom et al. (2004) was used to calculate the initial convective heat flux for both broadleaf and needle species. The overall energy balance is shown in Equation 5-1, in which  $m_{fuel}$  is the mass of the solid fuel,  $C_p$  is heat capacity,  $T$  is temp,  $t$  is time,  $\dot{h}$  is the convection coefficient adjusted to include the blowing factor,  $A$  is the surface area,  $\epsilon$  is the emissivity,  $\sigma$  is the Stefan-Boltzman constant,  $\dot{m}_{rxn}$  is the mass loss rate due to chemical reactions,  $\Delta H_{rxn}$  is the heat of reaction,  $\dot{m}_{vap}$  is the mass loss rate due to evaporation,  $\Delta H_{vap}$  is the heat vaporization,  $g$  refers to the gas phase far from the solid,  $fuel$  refers to the fuel itself, and  $surr$  refers to the surrounding surfaces that interact with the solid through radiation.

$$m_{fuel}C_p \frac{dT}{dt} = \dot{h}A(T_g - T_{fuel}) + \epsilon\sigma A(T_{surr}^4 - T_{fuel}^4) + \dot{m}_{rxn}\Delta H_{rxn} + \dot{m}_{vap}\Delta H_{vap} \quad (5-1)$$

Calculating the initial heat flux for a convection-only experiment simplifies the energy balance considerably by ignoring radiative heating between the sample and surrounding surfaces, chemical reactions, evaporation, and high mass transfer rates (blowing factor). Though not shown in Equation 5-1, conductive heating is also ignored. The simplified form of the energy balance is shown in Equation 5-2, in which  $q$  is heat transferred to the solid fuel,  $h$  is the standard convection coefficient and all other terms are as defined above.

As seen in Equation 5-2, it is possible to calculate the heat flux without knowing the convection coefficient by using the heating rate data for the solid fuel. This is necessary because

there are no correlations to determine the convection coefficient for a live leaf or needle species sample. The final simplified equation used in this analysis is shown in Equation 5-3, in which  $q''$  is the heat flux,  $\Delta x$  is the sample thickness,  $\rho$  is density and all other terms are as defined above.

$$q = m_{fuel} C_p \frac{dT}{dt} = hA(T_g - T_{fuel}) \quad (5-2)$$

$$q'' = \rho \Delta x C_p \frac{dT}{dt} \quad (5-3)$$

Detailed surface temperature measurements for dead manzanita leaves in a vertical orientation were taken from Prince (2014) while density and thickness were measured to be  $700 \text{ kg m}^{-3}$  and  $0.436 \text{ mm}$ , respectively. Heat capacity was calculated using the correlation for wood developed by Dunlap (1912) and used by Engstrom et al. (2004). This correlation is shown in Equation 5-4, in which  $C_p$  is heat capacity ( $\text{kJ kg}^{-1} \text{ }^\circ\text{C}^{-1}$ ) and  $T$  is temperature ( $^\circ\text{C}$ ).

$$C_p = 1.11 + 0.00486T \quad (5-4)$$

Detailed surface temperature measurements for a dead Douglas-fir sample were not available, so the convective flux was calculated using the convection coefficient for a cylinder in cross flow shown in Equation 5-5, in which  $Nu_D$  is the Nusselt number,  $Re_D$  is the Reynolds number and  $Pr$  is the Prandlt number (Incropera et al., 2007).

$$Nu_D = 0.989 Re_D^{0.33} Pr^{\frac{1}{3}} \quad (5-5)$$

### 5.1.2.2 Radiative Heat Flux

The measured radiative flux of  $50 \text{ kW m}^{-2}$  (uncertainty is 0.5%) was used for the broadleaf samples. Since the needle samples are in a different orientation than broadleaf samples relative to the heating panel, the radiative flux for the needle species was calculated using the

view factor for a single needle. The convective and radiative fluxes were used to estimate the flux for the different heating cases. The heat absorbed was calculated by multiplying the heat flux by the surface area. The surface area used for the radiative flux was half that used for the convective flux, since only one side of the sample was exposed to radiation.

## 5.2 Results and Discussion

A comparison of several flame characteristics between convection-only and combined convection and radiation burns is shown in Table 5-2. The data for this table are shown in Appendix C.2. The entries in Table 5-2 indicate the percentage of months in which there was a significant difference between convection-only and combined burns at a 95% confidence level. A stark contrast was observed between the broadleaf species and the non-broadleaf species for ignition time ( $t_{ig}$ ) and time to maximum flame height ( $t_{mfh}$ ). The difference between convection-only and combined burns for the three other reported variables (MFH,  $X_{ig}$ ,  $m_{i,g}$ ) was less obvious, but the overall result was that the added radiation had a much larger effect on broadleaf species than on non-broadleaf species. Radiation alone was never sufficient to ignite a fuel sample without a pilot ignition source, so it was not possible to compare ignition or flame characteristics for radiation-only experiments. The samples heated only with radiation simply pyrolyzed and then charred.

**Table 5-2. Effect of heating mode on ignition variables. Table entries indicate the percentage of months that radiation and convection burns ignited differently from convection-only burns at a 95% confidence level.**

	Species	$t_{ig}$	$t_{mfh}$	MFH	$X_{ig}$	$m_{ig}$
<b>Broadleaf</b>	Manzanita	92	83	83	25	42
	Ceanothus	100	91	100	45	18
	Gambel oak	83	100	83	50	17
	Fetterbush	100	100	8	17	25
	Gallberry	92	100	0	17	58
<b>Non-broadleaf</b>	Dougals-fir	9	27	27	0	9
	Sand pine	25	25	8	0	17
	Chamise	33	25	17	17	0
	Sagebrush	22	22	22	11	11
	Lodgepole pine	50	25	13	38	13

Table 5-3 shows the yearly average and range for the time required to reach a mass fraction remaining of 50% ( $t_{50}$ ). As seen in the table, the difference in  $t_{50}$  between convection-only, combined, and radiation-only burns follows the same behavior as that seen in Table 5-2 for ignition; radiation helps broadleaf species heat, and hence react, faster but not needle-like species. This difference in heating characteristics between needle and broadleaf species suggests that models must include a careful description of solid fuel characteristics rather than assuming the fuel to be a porous media and assigning bulk radiative properties, which is commonly assumed in physics-based simulations (Sullivan, 2009a). These results also suggest that models must include convective heat transfer in addition to radiative heat transfer (Weber, 1991; Sullivan, 2009a).

**Table 5-3: Yearly average and range for the time required to reach 50% mass remaining for each species for the three heating cases. All times are in seconds.**

	Species*	Convection		Combined		Radiation	
		Mean	Range	Mean	Range	Mean	Range
<b>Broadleaf</b>	Manzanita	8.8	4.1 – 15	5.8	3.6 – 13	18	15 – 43
	Ceanothus	6.6	2.3 – 18	4.4	2.8 – 9.7	26	25 – 91
	Gambel oak	2.7	2.0 – 4.9	1.8	1.1 – 4.1	9.5	7.9 – 74
	Fetterbush	4.2	2.8 – 7.4	2.7	1.4 – 7.8	15	4.0 – 123
	Gallberry	3.5	2.1 – 6.3	2.3	1.6 – 4.3	18	10 – 76
<b>Non-broadleaf</b>	Dougals-fir	3.3	1.7 – 8.3	2.3	1.8 – 8.7	45	18 – 339
	Sand pine	2.8	0.8 – 11	2.3	1.3 – 8.0	25	7.7 – 146
	Chamise	5.8	2.9 – 18	3.7	2.4 – 17	34	29 – 164
	Sagebrush	8.7	3.0 – 26	3.5	4.4 – 13	33	29 – 124
	Lodgepole pine	3.6	0.3 – 22	1.9	1.9 – 20	20	33 – 124

Although Table 5-2 and Table 5-3 show there is a clear difference in ignition and mass loss characteristics between the three heating cases, the difference is not because the radiation-only experiments lack sufficient energy to reach pyrolysis or surface oxidation temperatures. This is seen in Table 5-4, in which the maximum surface temperatures for each species each month, averaged over the year, are reported. There is a large difference in maximum temperature for radiation-only burns compared to either convection-only or combined burns, but that temperature is still high enough for surface reactions to occur. Thus, the difference in mass loss rate is not because the temperature does not reach pyrolysis temperatures, as reported for small wood sticks and excelsior in Cohen and Finney (2010). Temperature data for radiation-only experiments performed on needle species were not reported because the IR camera resolution was not high enough to clearly see individual needles.

**Table 5-4: Maximum surface temperature (°C) for each species averaged over the year.**

<b>Species</b>	<b>Convection</b>	<b>Combined</b>	<b>Radiation</b>
<b>Douglas-fir</b>	807	808	--
<b>ceanothus</b>	765	807	646
<b>chamise</b>	654	773	--
<b>fetterbush</b>	757	816	647
<b>gallberry</b>	771	804	616
<b>Gambel oak</b>	788	818	661
<b>lodgepole pine</b>	837	830	--
<b>manzanita</b>	789	826	755
<b>sagebrush</b>	765	795	--
<b>sand pine</b>	807	828	--

The convective heat flux was found to be 75 kW m<sup>-2</sup> for a dead manzanita leaf and 137 kW m<sup>-2</sup> for a dead Douglas-fir needle. The calculated radiative flux for a dead Douglas-fir needle was found to be 66 kW m<sup>-2</sup>. Figure 5-5 shows the time required to reach 50% mass remaining versus initial heat flux for all ten species studied. The heat flux found for manzanita was assumed to be valid for all broadleaf species and the heat flux for Douglas-fir was assumed to be valid for all needle species. Each species exhibits a similarly shaped but species-specific curve between mass loss and heat flux, indicating heating rate plays an important role in mass loss. An interesting pattern emerges when mass loss is compared with heat absorbed (heat flux multiplied by the appropriate surface area), as seen in Figure 5-6. The mass remaining data for all the needle species in Figure 5-6 seem to lie on the same heat absorbed curve. The t<sub>50</sub> data for manzanita, fetterbush and Gambel oak seem to lie on the same curve in Figure 5-6, while gallberry and ceanothus seem to lie on a slightly different curve. The existence of two curves for the broadleaf species is likely due to the assumption that the convective flux for a manzanita leaf is the same for all leaf species tested. In reality, shape and surface characteristics will cause each leaf to have a unique convective heat flux. The effect of these differences is also seen in the scatter in the t<sub>50</sub> data for needle species.

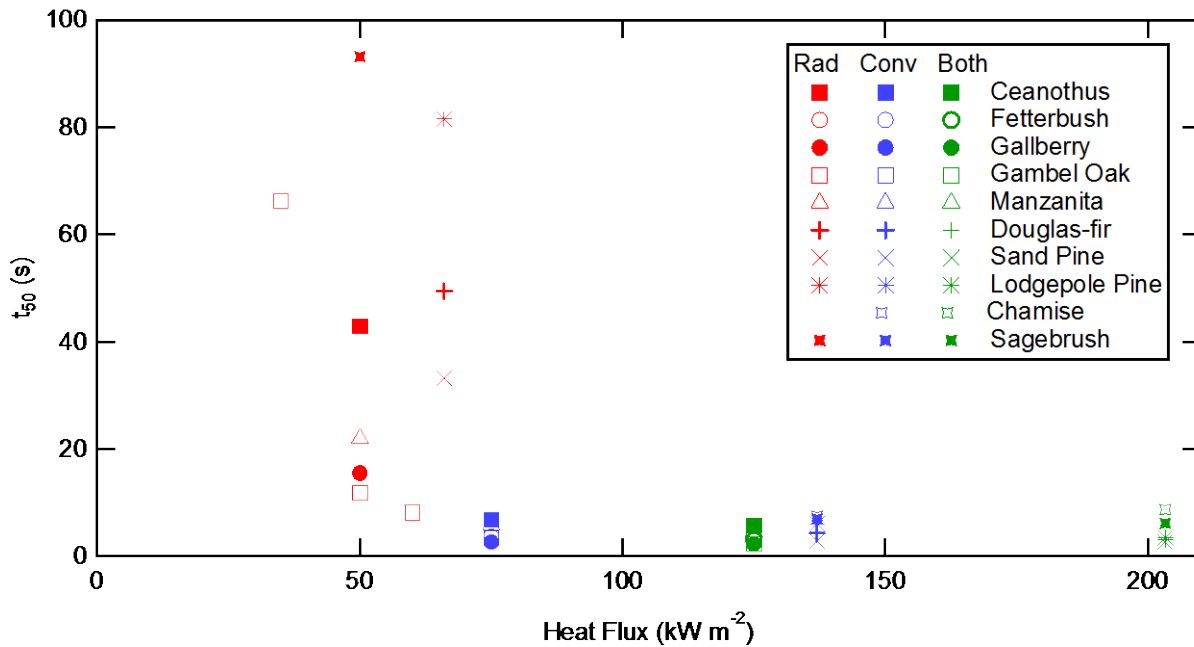


Figure 5-5: Time required to reach 50% mass remaining versus heat flux for all three heating cases for all ten species.

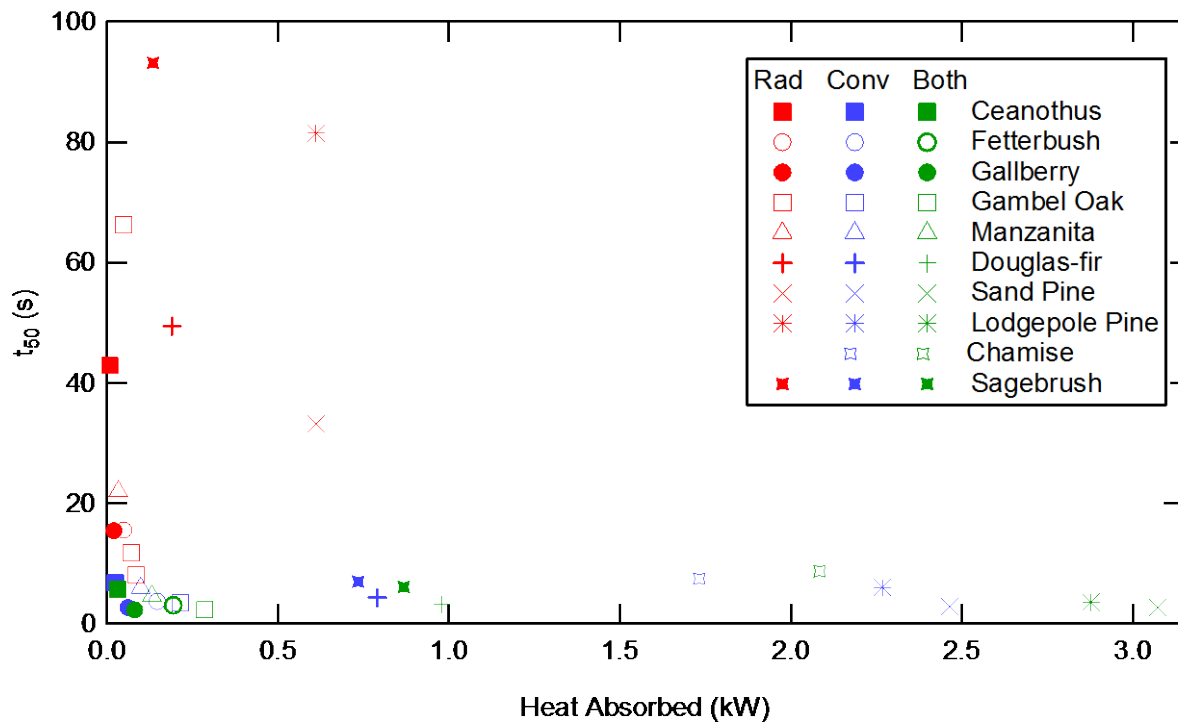


Figure 5-6: Time required to reach 50% mass remaining versus heat absorbed for all three heating cases for all ten species.

One result from these figures is that, from the perspective of the solid, the type of energy (i.e., radiation versus convection) is not important; only the amount of energy absorbed that matters. However, the lack of ignition for the radiation-only experiments, even though the solid temperature reached surface oxidation temperatures, indicates that there is a difference between heating modes from the perspective of the gas phase. The average maximum temperature of the gases surrounding the solid in these radiation-only experiments was 140 °C, which is not hot enough to cause the pyrolyzates to ignite. However, it is likely that in a wildland fire ignition sources exist that will ignite pyrolysis gases.

Another result from this analysis is seen by comparing Figure 5-5 and Figure 5-6. When the mass loss data are compared using heat absorbed data rather than heat flux data, the effects of species and heating mode drop out. The differences in experimental setup and fuel type have been cited as major reasons for the large variations in reported values for ignition time and ignition temperature (Babrauskas, 2003). Comparison of combustion data using heat absorbed provides a basis to compare results across heating modes and potentially across species, provided the experiments yield similar boundary conditions.

A comparison between heating mode and heating rate was also accomplished using surface temperature measurements. A typical surface temperature versus time plot is shown in Figure 5-7; sample curves for each species are shown in Appendix C.3. Due to an issue with absolute time stamps, it was not possible to match the time required to reach 50% mass remaining (Table 5-3, Figure 5-5 and Figure 5-6) with the associated surface temperature. However, the temperature plateau, the area circled in red in Figure 5-7, occurs in nearly all experiments and is a repeatable and recognizable point on the temperature-time curve. The temperature at the start of the plateau for all heating cases for each of the five broadleaf species

is shown in Figure 5-8. As seen in the figure, the temperature plateau occurs at higher temperatures as the heating rate increases. The phenomenon of increasing surface temperature as heating rate increases for a given reaction is also seen in coal research (Fletcher et al., 1992) and, although this phenomenon has not been demonstrated previously for live fuels, is not surprising. The fact that the relationship between the temperature plateau and heat flux is almost linear is another piece of evidence to suggest there is no difference between radiation and convection from the perspective of the solid.

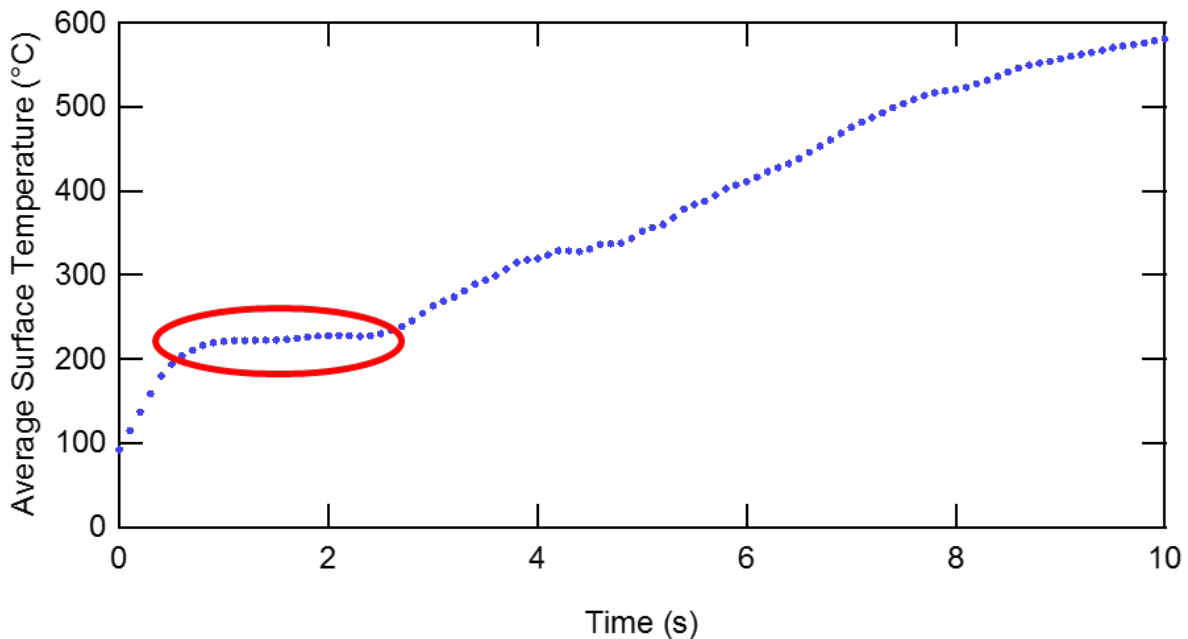


**Figure 5-7: Typical average surface temperature versus time plot for convection-only run. The red circle indicates the temperature plateau**

While it is possible internal energy and mass transfer gradients influenced the reported surface temperatures, a one-dimensional heat conduction calculation indicates the mean internal temperature gradients are approximately 10 °C or less. In this calculation, measured surface temperatures were used to calculate the heat flux through the solid at each time step. The thermal conductivity was determined using the method described by Forest Products Laboratory (2010).

More important than the internal temperature gradient for this analysis, the linear temperature-flux relationship is preserved and the conclusion that there is no difference in solid heating patterns between heating modes is supported.

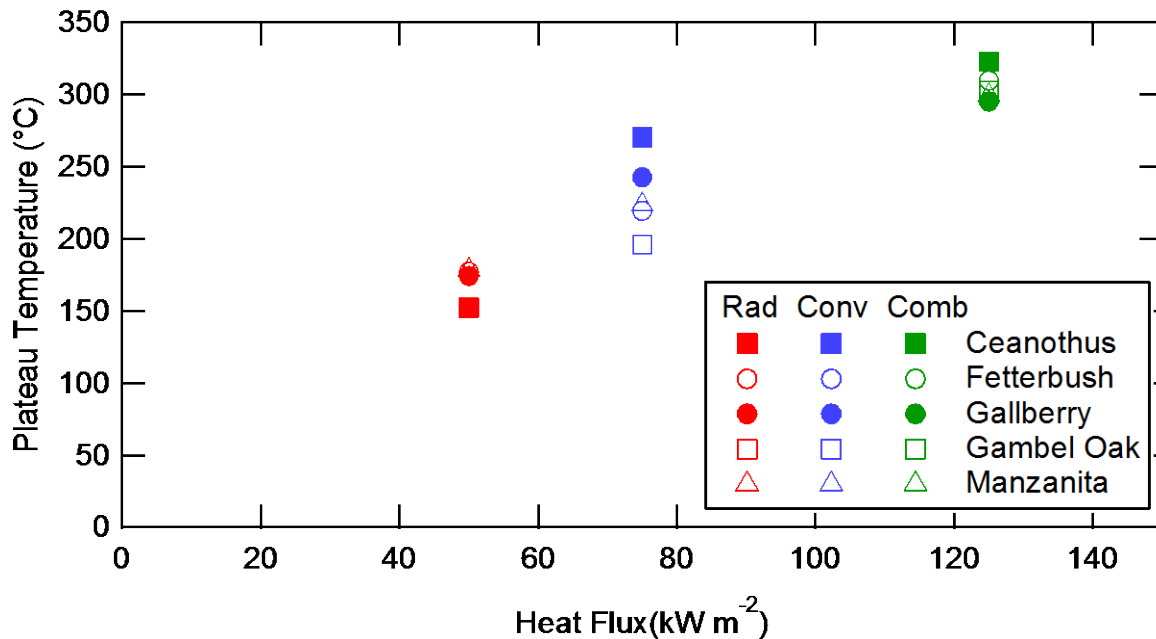


Figure 5-8: Plateau temperature versus heat flux for five broadleaf species for the three heating cases.

### 5.3 Summary and Conclusions

Ignition and burning behavior for ten live fuels was studied in a flat-flame burner apparatus to test the effect of heat transfer mode on live fuel combustion. Experiments were performed over a two-year period to see if and how the ignition and burning behavior changed throughout the year in response to the different heating cases. The heating cases were using a convection-only heat source, a radiation-only heat source, and both heat sources together.

Ignition did not occur in any of the unpiloted radiation-only experiments. Inclusion of a radiant flux in the convective environment of a flat-flame burner significantly decreased observed ignition times for broadleaf species but not for non-broadleaf species. Differences in

the behavior of broadleaf species and non-broadleaf species was also seen when comparing the time required to reach 0.5 mass fraction remaining. These results do not indicate radiation was unimportant, but rather that additional modes of heat transfer were needed to cause ignition under the conditions studied in this work. A comparison of mass remaining and surface temperature data with heat flux and heat absorbed data indicate it is the amount of energy rather than the type of energy that matters for surface reactions and mass loss. Comparing time to reach 50% mass remaining with heat absorbed presents an intriguing option for comparing experimental results across heating modes as long as the experimental conditions yield similar boundary conditions.



## **6 SEASONAL CHANGES IN IGNITION AND BURNING OF LIVE FUELS USING NATURAL VARIATION IN FUEL CHARACTERISTICS<sup>§</sup>**

Live fuels have been shown to burn differently than dead fuels, but neither a theoretical explanation for those differences nor an accurate prediction model has been developed. One area of study that can help explain the differences between live and dead fuels is to explore the changes in burning behavior of live fuels throughout the year. The information in this chapter details work to identify the most important pre-burn measurements to predict fire behavior in live fuels over a one-year period. This knowledge can be used in fire suppression and fire prevention (e.g. prescribed burning) efforts.

### **6.1 Methods**

#### **6.1.1 Experimental Setup**

Experimental methods for pre-burn and combustion measurements were described in Sections 4.1.1 and 5.1.1, respectively, and are therefore not repeated here. The analyses presented in this chapter were limited to the convection-only experiments.

---

<sup>§</sup> This chapter is under review for publication in *Combustion Science and Technology*

### 6.1.2 Model Development

Both single and multiple parameter prediction models were developed to describe the following aspects of the burning behavior, namely time to ignition ( $t_{ig}$ ), average surface temperature at ignition ( $T_{ig}$ ), maximum surface temperature at ignition ( $T_{ig,max}$ ), maximum flame height (MFH), time to maximum flame height ( $t_{MFH}$ ), burnout time ( $t_{BO}$ ) and normalized mass loss rate at ignition ( $\dot{m}_{ig}$ ). Definitions of these burning characteristics are given in Table 5-1. Surface temperature has also been shown to have large spatial variations during the burning of live foliage, with ignition initially occurring on only part of the leaf (Prince and Fletcher, 2013). However, many ignition temperature measurements do not measure the spatial variation in surface temperature. Correlations for both average surface temperature at ignition and maximum surface temperature at ignition (assuming the location of maximum temperature corresponds to the localized ignition point) were developed. One-parameter models were developed using simple linear regression. The F-statistic, p-value, and confidence interval on the slope were used to determine if the slope term and regression model were significant.

Forward and backward stepwise regression was used to develop correlations with multiple parameters. One of the goals of this analysis was to identify the most important parameters that affect ignition. To this end, 500 separate correlations were developed by randomly selecting four parameters for use in each model and by randomly selecting a transformation of the data for those parameters. To develop the models, the parameters were first assigned to groups based on type of measurement to reduce the chance of multicollinearity. The groups were: (1) moisture content, relative moisture content and water mass; (2) fresh mass and dry mass; (3) length, width and surface area; (4) needle length, stem diameter, thickness and density; and (5) lipid content, volatile fraction, fixed carbon and ash content. For each

correlation, four of the five groups were randomly chosen, then a parameter from each of those four groups was randomly selected. Once the parameters were identified, a data transformation was applied to the data for each parameter. The transformations were: (1) no change; (2) square root of the data; (3) square of the data; (4) natural log of the data; and (5) inverse of the data. Once the data and data transformations were assigned, stepwise regression was performed to develop a correlation to fit the selected data to each of the burning characteristics listed above.

Once the 500 correlations were created, the correlation with the highest adjusted  $R^2$  for each burning characteristic for each species was identified. The parameters in each of the highest  $R^2$  value correlations were pooled and the most common parameters were identified. The data were organized by sampling location in order to identify the most common composition-type predictors (e.g. moisture content and fixed carbon, from groups 1, 2 and 5 defined above). The data were organized by species type (broadleaf or needle) in order to identify the most common size predictors (e.g. density and length, from groups 3 and 4 above). These most common parameters were then chosen as the set of most important parameters, and new correlations were developed for each of the temperature and flame characteristics listed in Table 5-1.

## **6.2 Results and Discussion**

### **6.2.1 Effects of Sample Condition, Season, Moisture Content and Species**

Results comparing sample condition for chamise branch segments are shown in Figure 6-1. Specifically, the time required to reach 50% mass remaining ( $t_{50}$ ) is shown on the left and the t-test results for the different comparisons are shown on the right. In the figure, the error bars represent one standard deviation; measurement uncertainty is 0.2 s. As seen in the figure, the difference in drying method (SDAN:QDAN) was insignificant while the difference in amount of

foliage was significant. It is interesting to note that removing half the needles for the undried samples resulted in a large and significant difference in time to reach 50% mass remaining, while time to reach 50% mass remaining for the dried samples with half the needles removed was indistinguishable from the time needed to reach 50% mass remaining for the dried samples with all the needles attached. This illustrates two important points: (1) there is a large difference in mass loss behavior between live and dead fuel moisture levels, and (2) effects of foliage loss were only distinguishable at live-fuel moisture levels.

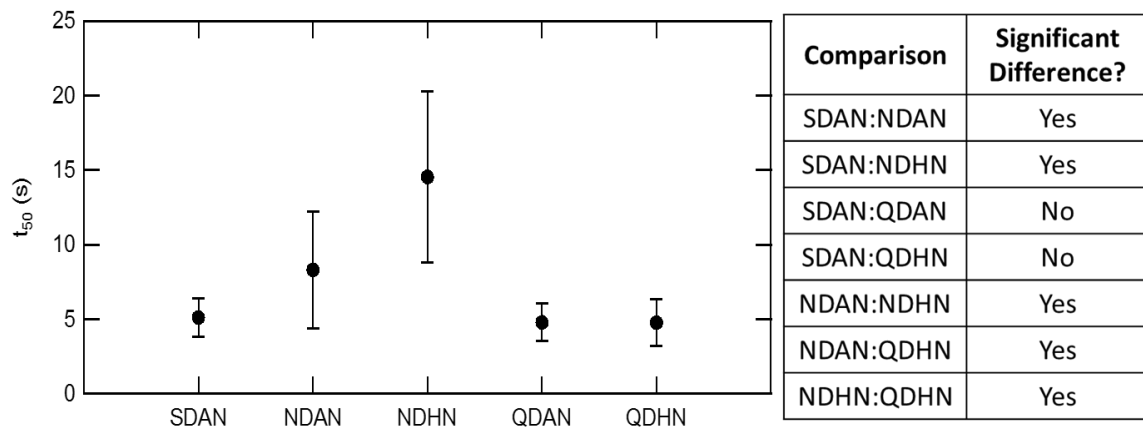


**Figure 6-1: Results of sample condition experiments for chamise branch segments. The left pane shows the time required to reach 50% mass remaining ( $t_{50}$ ); the right pane shows the t-test results for the different comparisons. Error bars represent one standard deviation. SDAN=slow drying, all needles; NDAN=no drying, all needles; NDHN=no drying, half needles; QDAN=quick drying, all needles; QDHN=quick drying, half needles.**

Measured ignition time and temperature data versus month and moisture content are shown in Figure 6-2 and Figure 6-3, respectively. As seen in the figures, the species from the California region (manzanita, ceanothus, and chamise) all have a strong dependence on season and moisture content for ignition time (Figure 6-2a,d) but not ignition temperature (Figure 6-3a,d). The species from the Southern region all show a similar dependence on season for ignition temperature (Figure 6-3b). There is no recognizable relationship between moisture

content and ignition temperature (Figure 6-3e) or ignition time (Figure 6-2e) for any Southern species. Non-California species do not show a relationship between ignition time and moisture content (Figure 6-2e,f). In general, needle species exhibit a shorter ignition time but show no consistent difference for ignition temperature. These observations yield three important results: (1) seasonal changes had a large effect on ignition behavior, (2) the seasonal changes that affect ignition were not captured by measuring moisture content alone, and (3) ignition behavior is species-specific, although there are observations that indicate both location and sample type can influence ignition behavior.

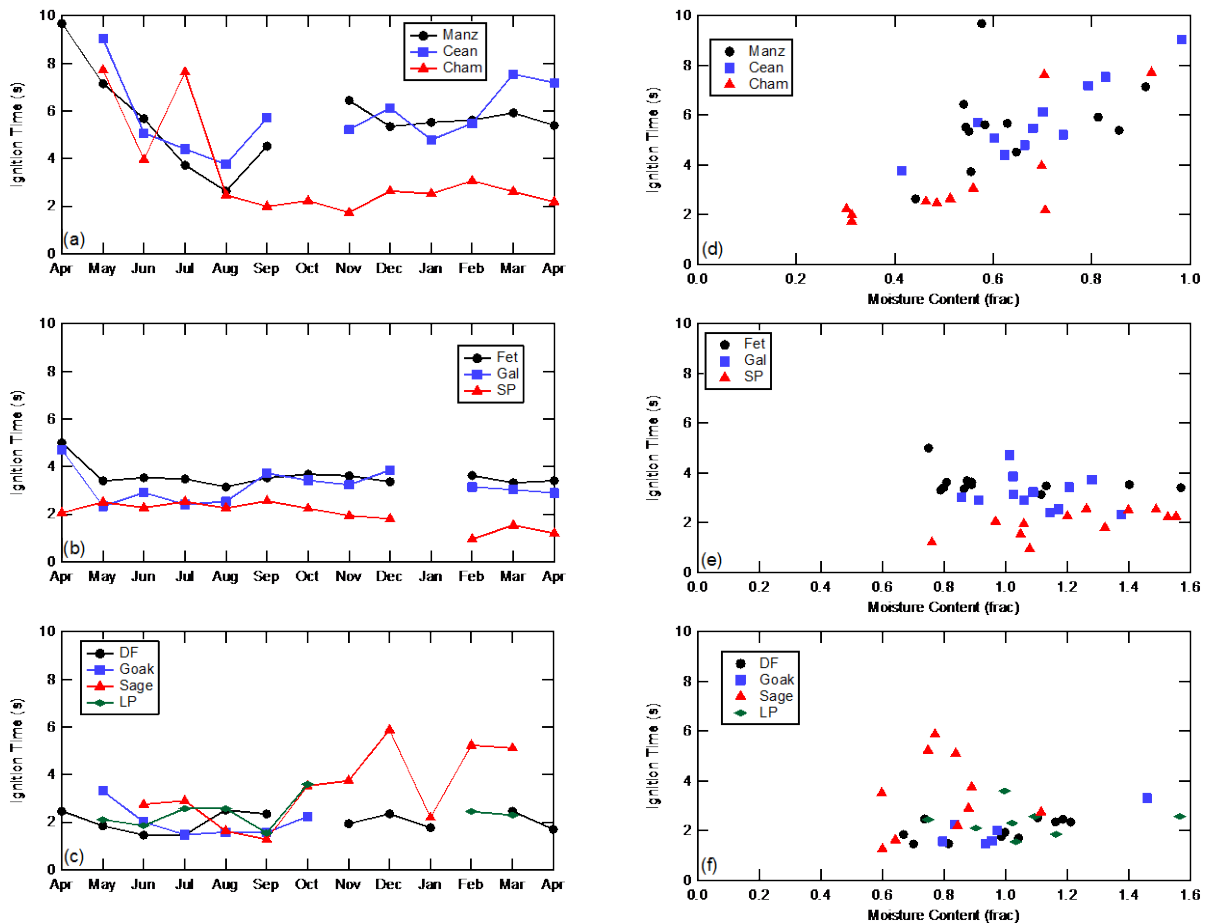


**Figure 6-2: Ignition time versus month (left column) and moisture content (right column). Manz = manzanita, Cean = ceanothus, Cham = chamise, Fet = fetterbush, Gal = gallberry, SP = sand pine, DF = Douglas-fir, Goak = Gambel oak, Sage = sagebrush, LP = lodgepole pine.**

Table 6-1 shows the order of ignition times listed in ascending order. Ignition times were averaged in four ways: (1) over the entire year; (2) over the local fire season; (3) over the local non-fire season; and (4) from May to October. The local fire season is March through December for southern California, March through November for Florida, May through October for Utah and June through October for Montana. Several important observations can be made from the

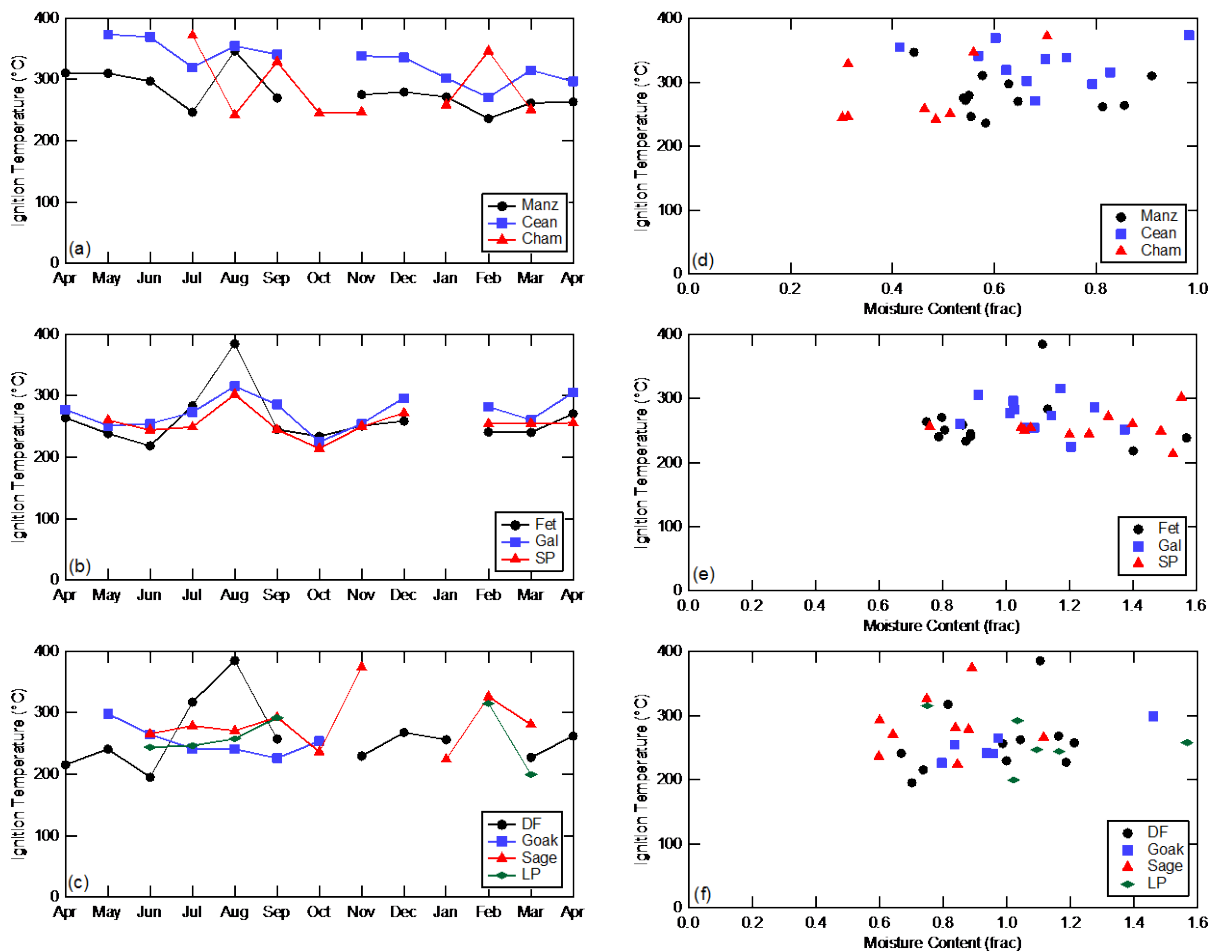


**Figure 6-3: Ignition temperature versus month (left column) and moisture content (right column). Manz = manzanita, Cean = ceanothus, Cham = chamise, Fet = fetterbush, Gal = gallberry, SP = sand pine, DF = Douglas-fir, Goak = Gambel oak, Sage = sagebrush, LP =lodgepole pine.**

table, namely (1) the order of most flammable to least flammable changes throughout the year, (2) some species ignite faster during the non-fire season than during the fire season (e.g. sand pine and lodgepole pine) and (3) in general, needle species ignite faster than broadleaf species.

The results from Table 6-1, together with those from Figure 6-2 and Figure 6-3, indicate that while heat transfer conditions play a major role in ignition, seasonal changes in foliage condition also affect ignition. Some of these seasonal changes evident in the data appear to be due to changes that occur on time-scales longer than one year, such as an extended drought. These long-term changes are seen readily in the difference in ignition time for chamise and manzanita when comparing measurements made in April at the beginning and end of the sampling period. These results also indicate that ignition behavior must be related to plant physiology on a deeper level than just moisture content. Each species exhibits unique ignition behavior, though it is unclear whether that behavior is due to species-specific composition and physiological behavior or some other phenomenon.

**Table 6-1: Ignition time order listed from shortest to longest. Ignition times are averaged as indicated by the column headings.**

<b>All Year</b>	<b>Fire Season</b>	<b>Non-fire Season</b>	<b>May-Oct</b>
sand pine	Douglas-fir	sand pine	Douglas-fir
Douglas-fir	Gambel oak	Douglas-fir	Gambel oak
Gambel oak	sand pine	lodgepole pine	lodgepole pine
lodgepole pine	sagebrush	chamise	sand pine
gallberry	lodgepole pine	fetterbush	sagebrush
chamise	gallberry	gallberry	gallberry
sagebrush	chamise	sagebrush	fetterbush
fetterbush	fetterbush	ceanothus	chamise
manzanita	manzanita	manzanita	manzanita
ceanothus	ceanothus	---*	ceanothus

\* Gambel oak only had leaves from May to October

### 6.2.2 Single Variable Regressions

Single parameter prediction models were developed to describe the following aspects of the burning behavior, namely time to ignition ( $t_{ig}$ ), average surface temperature at ignition ( $T_{ig}$ ), maximum surface temperature at ignition ( $T_{ig,max}$ ), maximum flame height (MFH), time to maximum flame height ( $t_{MFH}$ ), burnout time ( $t_{BO}$ ) and normalized mass loss rate at ignition ( $\dot{m}_{ig}$ ). Results for simple linear regression models are summarized in Table 6-2 and Table 6-3 for needles species and broadleaf species, respectively. Each entry in each column in both tables represents the relationship between that pre-burn measurement (e.g. moisture content) and the burning characteristic at the top of the column (e.g. ignition time). The entries in each column are shown in order of highest adjusted  $R^2$  value to lowest adjusted  $R^2$  value averaged across all species of the type specified for the given table. The maximum average adjusted  $R^2$  value for each column (average adjusted  $R^2$  value between the burning characteristic and the first pre-burn measurement listed) is shown in the second row of both tables. The significance or lack thereof for each one-parameter model is not indicated because the entries are listed by average adjusted  $R^2$  value, and the one-parameter interactions that are significant for one species are not necessarily significant for another species.

As seen in the tables, all the average one-parameter models for the needle species account for less than 25% of the variation in the data and all but one of the average one-parameter models for the leaf species account for 33% or less of the data variation. The poor fit of the single-parameter models is also seen in the widely varying order of the pre-burn measurements in the table entries. While there are some interactions that make sense, the overall result is that one-parameter models cannot predict the ignition and burning behavior of live fuels.

**Table 6-2: Order of strongest average correlation to weakest average correlation for needle species for each of the six listed burning characteristics. MC = moisture content; RMC = relative moisture content.**

<b>t<sub>ig</sub></b>	<b>t<sub>MFH</sub></b>	<b>t<sub>BO</sub></b>	<b>T<sub>ig</sub></b>	<b>MFH</b>	<b>m<sub>ig</sub></b>
<b>0.15</b>	<b>0.18</b>	<b>0.21</b>	<b>0.22</b>	<b>0.24</b>	<b>0.07</b>
MC	water mass	fresh mass	Density	Width	dry mass
water mass	Volatiles	dry mass	Fixed Carbon	dry mass	fresh mass
Volatiles	Fixed Carbon	water mass	Volatiles	Needle Length	water mass
Fixed Carbon	fresh mass	Width	water mass	RMC	Width
Density	Width	Length	Ash	fresh mass	Density
fresh mass	dry mass	RMC	MC	Length	Stem Diameter
Width	Stem Diameter	Stem Diameter	Lipid	MC	Length
dry mass	MC	MC	fresh mass	water mass	MC
Ash	RMC	Needle Length	Length	Volatiles	Needle Length
Length	Length	Density	dry mass	Fixed Carbon	Volatiles
RMC	Density	Ash	Stem Diameter	Density	Fixed Carbon
Stem Diameter	Ash	Volatiles	Needle Length	Lipid	RMC
Needle Length	Needle Length	Fixed Carbon	RMC	Stem Diameter	Ash
Lipid	Lipid	Lipid	Width	Ash	Lipid

Table 6-4 contains the simple linear regression results for each species for the variable combinations shown in the column headings of Table 6-4. The purpose of Table 6-4 is to give more detail than that shown in Table 6-2 and Table 6-3 for a few of the more common or interesting one-parameter models. These models were compared to a model that assumed a constant value to see if the trend was significant at a 95% confidence level. Zeros in the table indicate relationships with no statistical significance. Non-zero entries indicate the sign of the slope for the associated model—P for a statistically significant positive slope and N for a negative slope. The current ignition paradigm based on dead fuels is that ignition time and normalized mass loss at ignition increase as moisture content increases while maximum flame height decreases (McAllister et al., 2012). The expected behavior for dead fuels is shown in the

last row of Table 6-4. Relative moisture content measurements for dead fuels are not possible, so there is no current paradigm relating relative moisture content to burning behavior for dead fuels.

**Table 6-3: Order of strongest average correlation to weakest average correlation for broadleaf species for each of the six listed burning characteristics. MC = moisture content; RMC = relative moisture content; SA = surface area; SA:V = surface area to volume ratio.**

<b>t<sub>ig</sub></b>	<b>t<sub>MFH</sub></b>	<b>t<sub>BO</sub></b>	<b>T<sub>ig</sub></b>	<b>MFH</b>	<b>m<sub>ig</sub></b>
<b>0.29</b>	<b>0.33</b>	<b>0.55</b>	<b>0.10</b>	<b>0.31</b>	<b>0.12</b>
thickness	Water mass	Water mass	Lipid	SA	Fresh mass
MC	Fresh mass	Fresh mass	RMC	Width	Dry mass
SA:V	thickness	Dry mass	MC	Dry mass	Water mass
Water mass	Dry mass	SA	Length	Length	thickness
Lipid	SA:V	Length	Width	Fresh mass	SA:V
RMC	Lipid	thickness	Dry mass	MC	Lipid
Density	Length	SA:V	Fixed Carbon	Water mass	Length
Fresh mass	SA	Width	Volatiles	RMC	SA
Dry mass	MC	Density	SA	thickness	Density
Ash	Density	MC	Fresh mass	Fixed Carbon	RMC
Length	RMC	Lipid	thickness	Volatiles	MC
Width	Width	RMC	Density	SA:V	Ash
SA	Ash	Ash	Water mass	Density	Width
Fixed Carbon	Volatiles	Volatiles	SA:V	Lipid	Volatiles
Volatiles	Fixed Carbon	Fixed Carbon	Ash	Ash	Fixed Carbon

Ceanothus, Gambel oak, Douglas-fir and chamise all exhibited a positive correlation between ignition time and moisture content while the other six species show no correlation at a 95% significance level, indicating a simple relationship between moisture content and ignition is not adequate to describe ignition in live fuels. Manzanita and ceanothus exhibited a positive trend between ignition time and relative moisture content while the other eight species showed no significant relationship. Only Douglas-fir and Gambel oak exhibited statistically significant

relationships between maximum flame height and moisture content. Fetterbush, gallberry and manzanita showed significant trends between normalized mass loss at ignition and ignition time, while no significant trends were seen between normalized mass loss at ignition and moisture content. The observed behavior is very different from expected behavior if live fuels behaved as wet, dead fuels and further highlights the inability of one-parameter models to predict burning behavior in live fuels.

**Table 6-4. Significance of yearly trends by species.**

<b>Species</b>	<b>tig (s) vs MC</b>	<b>tig (s) vs RMC</b>	<b>MFH (cm) vs MC</b>	<b>m<sub>ig</sub> (%/s) vs MC</b>	<b>m<sub>ig</sub> (%/s) vs tig(s)</b>
<b>Manzanita</b>	0	P	0	0	N
<b>Ceanothus</b>	P	P	0	0	0
<b>Douglas-fir</b>	P	0	N	0	0
<b>Gambel Oak</b>	P	0	N	0	0
<b>Fetterbush</b>	0	0	0	0	N
<b>Gallberry</b>	0	0	0	0	N
<b>Sand Pine</b>	0	0	0	0	0
<b>Chamise</b>	P	0*	0	0	0
<b>Sagebrush</b>	0	0*	0	0	0
<b>Lodgepole Pine</b>	0	0*	0	0	0
<b>Wet Wood (expected)</b>	P	--	N	P	P

\*RMC was added to the pre-burn measurement suite in August, 2012

### 6.2.3 Multi-variable Regressions

Because the one-parameter models were not able to account for more than a third of the variability in the data, multi-parameter models were developed. Table 6-5 contains the adjusted  $R^2$  values for the multi-parameter models when regressing the flame characteristics using (a) the best overall models and (b) the models using the most common parameters (MCP) from procedure (a). Moisture content, sample mass, apparent density (broad-leaf species), surface area (broad-leaf), sample width (needle species) and stem diameter (needle) were identified as the

**Table 6-5: Adjusted R<sup>2</sup> values when regressing flame characteristics for (a) the best overall model and (b) the model using the most frequent parameters. C means there was no significant model beyond a constant.**

Species	(a) Best Overall Model						(b) Model Using Most Frequent Parameters					
	t <sub>ig</sub>	T <sub>ig</sub>	T <sub>ig,max</sub>	MFH	tMFH	tBO	t <sub>ig</sub>	T <sub>ig</sub>	T <sub>ig,max</sub>	MFH	tMFH	tBO
<b>Manzanita</b>	0.75	0.55	0.61	0.75	0.68	0.56	0.546	0.204	0.16	0.65	0.71	0.553
<b>Ceanothus</b>	0.794	0.481	0.372	0.743	0.905	0.676	0.793	0.18	0.071	0.719	0.891	0.598
<b>Douglas-fir</b>	0.303	0.571	0.692	0.342	0.254	0.50	0.307	0.315	0.419	0.272	0.278	0.509
<b>Gambel Oak</b>	0.664	0.472	0.186	0.432	0.86	0.81	0.624	0.434	0.153	0.425	0.821	0.812
<b>Fetterbush</b>	0.537	0.379	0.058	0.431	0.417	0.459	0.319	C	C	0.354	0.341	0.36
<b>Gallberry</b>	0.733	0.152	0.223	0.683	0.743	0.511	0.727	0.158	0.055	0.656	0.739	0.454
<b>Sand Pine</b>	0.434	0.294	0.247	0.58	0.624	0.639	0.351	C	0.041	0.416	0.61	0.641
<b>Chamise</b>	0.554	0.286	0.305	0.617	0.502	0.449	0.554	0.286	0.301	0.558	0.456	0.283
<b>Sagebrush</b>	0.449	0.285	0.247	0.403	0.589	0.403	0.226	0.057	C	0.262	0.486	0.338
<b>Lodgepole Pine</b>	0.489	0.315	0.309	0.384	0.36	0.30	0.111	0.066	C	0.261	0.179	0.069

most important predictors of fire behavior. In general, the models for ignition time and flame characteristics are more robust than those for temperature. This is partly due to the fact that foliage samples bend and move during burning and thus the entire sample surface was not always visible to the IR camera during the run. On average, the models using the most frequent parameters accounted for 12% less of the variation in the dependent variable, on an absolute scale, than the best overall models. If the models for temperature ( $T_{ig}$ ,  $T_{ig,max}$ ) are not included, the change in the amount of variation accounted for by using the best-parameter models reduces to 8%. This small loss in model strength (amount of variation accounted for by the model) seems to indicate that the set of best predictors is valid for model development. The change to the model strength using the set of best predictors for each species was not the same, however. Ceanothus, Douglas-fir, Gambel oak, gallberry, sand pine and chamise experienced minimal changes in model strength; manzanita experienced large changes in model strength for the ignition time and ignition temperature models and minimal change for the other models; while fetterbush, lodgepole pine and sagebrush experienced large changes in model strength with the resulting models losing much of their prediction capabilities. It is important to note that lipid content, volatile fraction, fixed carbon and ash content did not show up in the set of best parameters. In fact, lipid content showed up in only 5% of the best overall models, while fixed carbon and ash content showed up in 2% of the best overall models and volatile fraction did not show up at all.

The best overall correlations are shown in Table 6-6; the MCP correlations are shown in Table 6-7. Within each model, moisture content ( $M$ ), relative moisture content ( $R$ ), volatiles content ( $V_f$ ), fixed carbon ( $FC_f$ ), ash content ( $A_f$ ), and lipid content ( $l_f$ ) are proportions; length ( $L$ ), width ( $W$ ) and needle length ( $N$ ) are in units of centimeters; thickness ( $t$ ) and stem diameter

( $D$ ) are in units of millimeters; surface area ( $SA$ ) is in units of square centimeters; and fresh mass ( $m_f$ ), dry mass ( $m_d$ ) and water mass ( $m_w$ ) are in units of grams.

**Table 6-6: Best overall correlations for flame characteristics of ten species.**

Variable	Adjusted R <sup>2</sup>	RMSE	F-statistic
	Correlations		
<b>Manzanita</b>			
$t_{ig}$	0.748	0.787	70.4
	$13.04 + 6.33 \ln(l_f) + 10.47t^2 + 10.02L^{-1}$		
$T_{ig}$	0.554	27.2	44.4
	$182.24 + 567.5SA^{-1} + 26.05R^{-1}$		
$T_{ig,max}$	0.608	37.6	37.2
	$713.36 + 184.84t - 52.62\sqrt{SA} - 306.3\sqrt{R}$		
$t_{MFH}$	0.753	1.54	61.9
	$-0.726 + 7.97\sqrt{m_f} + 0.0577A_f^{-1} + 3.07R + 14.14t^2$		
$t_{BO}$	0.681	2.57	78.5
	$-60.41 + 30.42m_f + 73.78\sqrt{\rho} - 0.3886SA$		
MFH	0.559	2.8	47.1
	$52.74 + 30.19\sqrt{m_d} - 43.96\rho - 5.61R$		
<b>Ceanothus</b>			
$t_{ig}$	0.794	0.785	105
	$2.703 + 6.08M^2 - 1.027SA + 27.89\sqrt{m_f} - 4.989\rho^2$		
$T_{ig}$	0.481	26.7	33.7
	$392.6 - 123.8R^2 + 143.6t - 88.04\sqrt{W}$		
$T_{ig,max}$	0.372	40.6	16.7
	$366.3 + 110.4R^2 + 35.65W^2 + 152t^2 - 147.1R^2W^2$		
$t_{MFH}$	0.743	1.5	104
	$-0.116 - 3.185W + 5.696t + 62.87\sqrt{m_w}$		
$t_{BO}$	0.905	1.16	341
	$-6.759 - 0.2210SA^2 + 8.091t + 103.7\sqrt{m_w}$		
MFH	0.676	1.59	56.9
	$-6.533 + 5.984\sqrt{SA} + 121.2m_f - 262.4m_w + 1.241t^{-1}$		
<b>Douglas-fir</b>			
$t_{ig}$	0.303	0.576	14.5
	$1.044 + 0.806M^2 + 2.202\sqrt{m_f} - 1.035\ln(W)$		
$T_{ig}$	0.571	44.2	37.9
	$-676.9 - 335.5\sqrt{m_f} + 973.8\rho^{-1} + 584.2m_w$		
$T_{ig,max}$	0.692	63.8	47.5
	$-852.4 - 795.2\sqrt{m_f} + 89.92\sqrt{L} + 1214\rho^{-1} + 1319m_w$		
$t_{MFH}$	0.342	1.69	16.4
	$-7.763 + 3.295M^2 + 12.76\rho^2 + 2.729\ln(m_f)$		
$t_{BO}$	0.254	4.34	11.5
	$31.16 - 2.18m_f - 9.635\sqrt{W} + 6.580M^2$		
MFH	0.5	6.22	27.4
	$-15.20 - 24.69R^2 + 17.69\sqrt{m_d} + 17.88\sqrt{W}$		

**Table 6-6: Continued**

Variable	Adjusted R <sup>2</sup>	RMSE	F-statistic
	Correlations		
<b>Gambel oak</b>			
t <sub>ig</sub>	0.664	0.495	27.2
	$5.743 - 0.4425\sqrt{SA} - 16.95\sqrt{m_d} + 25.004\sqrt{m_w} - 4.408\rho^2$		
T <sub>ig</sub>	0.472	25.2	16.2
	$166.2 - 900.1\sqrt{m_f} + 811.6SA^{-1} + 1446\sqrt{m_w}$		
T <sub>ig,max</sub>	0.186	58.1	4.9
	$-380.9 + 676.7\rho^{-1} - 1026m_f + 2160m_w$		
t <sub>MFH</sub>	0.432	0.71	11.1
	$-7.047 + 18.34\sqrt{\rho} - 2.944\ln(L) + 2.414M + 1.951\ln(m_f)$		
t <sub>BO</sub>	0.86	0.606	164
	$2.988 + 17.41\sqrt{m_f} - 0.5803L$		
MFH	0.81	3.47	114
	$23.99 + 6.579\ln(SA) - 24.36M$		
<b>Fetterbush</b>			
t <sub>ig</sub>	0.537	0.509	24.7
	$5.698 - 0.5205t^{-1} + 125.2SA^{-1} - 2.220m_f - 32.43t^{-1} * SA^{-1} + 0.5465t^{-1} * m_f^{-1}$		
T <sub>ig</sub>	0.379	52.6	9.4
	$558230 - 768240l_f^2 - 61716\ln(R) - 504280\rho^{-1} + 86668l_f^2 * \ln(R) + 694810l_f^2 * \rho^{-1}$		
T <sub>ig,max</sub>	0.0584	104	2.84
	$418.2 + 475.4m_f - 71.6\sqrt{SA} + 205.2R^2$		
t <sub>MFH</sub>	0.431	0.862	36.7
	$6.77 + 7.152W^{-1} + 2.75\ln(m_f)$		
t <sub>BO</sub>	0.417	1.37	34.7
	$11.67 + 6.42W^{-1} + 3.78\ln(m_f)$		
MFH	0.459	5.12	47.3
	$13.61 - 4.153M^2 + 20.69\ln(W)$		
<b>Gallberry</b>			
t <sub>ig</sub>	0.733	0.439	90.5
	$-6.106 - 2.188\sqrt{SA} + 9.424\rho + 20.18\sqrt{m_f}$		
T <sub>ig</sub>	0.152	32.1	5.16
	$151.5 + 366.2L^{-1} + 343.2\ln(\rho) + 125.2R^2 - 1.035m_d^{-1}$		
T <sub>ig,max</sub>	0.223	53.1	9.88
	$1470 + 137.2\ln(m_d) - 307.7t - 312.04\sqrt{L}$		
t <sub>MFH</sub>	0.683	0.615	56.5
	$-2.889 - 273.8m_w^2 - 2.521\sqrt{SA} + 54.07m_f + 11.02\rho$		
t <sub>BO</sub>	0.743	0.78	95.2
	$10.56 - 0.4432SA - 8.163\rho^{-1} + 40.55\sqrt{m_d}$		
MFH	0.511	4.19	52.3
	$-17.72 + 8.017\sqrt{SA} + 22.07R^2$		

Table 6-6: Continued

Variable	Adjusted R <sup>2</sup>	RMSE	F-statistic
	Correlations		
<b>Sand pine</b>			
t <sub>ig</sub>	0.434	0.54	21.3
	$-4.517 - 0.3297m_f^{-1} - 1.918M^{-1} - 0.3179\sqrt{W} + 9.660\rho$		
T <sub>ig</sub>	0.294	27.9	10.5
	$36933 - 37131\sqrt{\rho} - 25944R^{-1} + 148.7L^{-1} + 26218\sqrt{\rho} * R^{-1}$		
T <sub>ig,max</sub>	0.247	47.6	6.95
	$52847 + 172.2L^{-1} - 22.61m_f^{-1} - 51448\rho^{-1} - 62518\sqrt{R} + 61198\rho^{-1} * \sqrt{R}$		
t <sub>MFH</sub>	0.58	1.26	29.8
	$1.936 - 1.299m_d^{-1} + 4.998\sqrt{M} + 12.68\ln(\rho) - 12.72W^{-1} + 6.101m_d^{-1} * W^{-1}$		
t <sub>BO</sub>	0.624	2.68	58.4
	$6.142 - 0.6101m_w^{-1} - 3.261D^{-1} + 40.77W^{-1}$		
MFH	0.639	6.09	47.1
	$-6.281 + 17.25\ln(W) + 5.455\ln(m_f) - 9.974\ln(M) + 8.518D^{-1}$		
<b>Chamise</b>			
t <sub>ig</sub>	0.554	1.43	60
	$0.5147 + 7.196M^2 + 13.15m_f^2$		
T <sub>ig</sub>	0.286	48.6	11.8
	$226.5 + 379.2m_f^2 + 189.4M^2$		
T <sub>ig,max</sub>	0.305	79	12.9
	$189.8 + 379.6M^2 + 306.5\sqrt{m_d}$		
t <sub>MFH</sub>	0.617	2.72	47.2
	$7.597 + 12.45\sqrt{m_f} - 1.405L + 438.9m_w^2$		
t <sub>BO</sub>	0.502	3.65	29.9
	$15.57 + 362m_w + 26.43\sqrt{m_d} - 5.746\sqrt{L}$		
MFH	0.449	2.45	15.7
	$22.09 - 1.774R^{-1} + 3.995\ln(m_f) - 6.188D^2 + 2.405R^{-1} * D^2$		
<b>Sagebrush</b>			
t <sub>ig</sub>	0.449	1.45	25.2
	$6.889 - 2.268M^{-1} + 9.638\sqrt{m_d} - 0.2050L^2$		
T <sub>ig</sub>	0.285	45.4	8.77
	$-66.13 + 106.6M^{-1} + 29.49m_f + 919.6L^{-1} - 20.79M^{-1} * m_f^{-1}$		
T <sub>ig,max</sub>	0.247	93.8	9.55
	$-2416 + 1918M^{-1} + 12998L^{-1} - 8793M^{-1} * L^{-1}$		
t <sub>MFH</sub>	0.403	4.27	21
	$-4.803 + 31.49m_d - 7.005M^{-1} + 85.51L^{-1}$		
t <sub>BO</sub>	0.589	6.19	43.5
	$61.74 - 26.55\ln(L) + 195.6m_d^2 - 7.489M^{-1}$		
MFH	0.403	3.72	21.1
	$14.28 - 121.1m_w + 209.2m_f^2 - 386.8m_w * m_f^2$		

**Table 6-6: Continued**

Variable	Adjusted R <sup>2</sup>	RMSE	F-statistic
	Correlations		
<b>Lodgepole pine</b>			
t <sub>ig</sub>	0.489	0.598	14.4
	$1.771 + 0.1106D^2 - 0.7138m_f + 2.204R^2$		
T <sub>ig</sub>	0.315	59.9	8.35
	$507.3 - 74.76m_f^{-1} - 5.158N^2$		
T <sub>ig,max</sub>	0.309	89.6	4.58
	$1006 - 92.66N + 302.4R^2 - 548.5W^{-1} - 121.2m_f^{-1}$		
t <sub>MFH</sub>	0.384	1.01	11.9
	$19.15 - 11.47M - 0.2721W - 36.94D^{-1} + 36.16M * D^{-1}$		
t <sub>BO</sub>	0.36	3.4	8.88
	$5.759 + 0.1703D^2 + 3.078m_f^2 - 0.1140D^2 * m_f^2$		
MFH	0.3	7.45	7.01
	$-301.8 + 145.7m_d + 213.9\sqrt{L} + 231.2M - 86.90m_d * \sqrt{L} - 153.1\sqrt{L} * M$		

Sample parity plots are shown in Figure 6-4 through Figure 6-7 below. Parity plots for manzanita ignition temperatures and burning characteristics are shown in Figure 6-4 and Figure 6-5, respectively. Parity plots for Douglas-fir burning characteristics are shown in Figure 6-6 while parity plots for Douglas-fir ignition temperatures are shown in Figure 6-7. In Figure 6-4 through Figure 6-7, the parity plots for the best overall models are shown in the left column and the parity plots for the models using the most common predictors are shown in the right column. The plots shown in Figure 6-4 through Figure 6-7 reiterate the data reported in Table 6-5: (1) the best overall models are generally stronger than the models using the most common predictors, but not by much, and (2) the temperature models are generally weaker than models describing burning characteristics. Parity plots for the other eight species are shown in Appendix B.2.

**Table 6-7: Correlations for flame characteristics for ten species using most frequent parameters from best-fit correlations shown in Table 6-6.**

Variable	Adjusted R <sup>2</sup>	RMSE	F-statistic
	Correlation		
<b>Manzanita</b>			
t <sub>ig</sub>	0.546	1.43	44.7
	$10.85 + 4.534\ln(m_f) + 10.75\rho^2 - 4.173\ln(SA)$		
T <sub>ig</sub>	0.204	39.1	28.9
	$229.7 + 608.8SA^{-1}$		
T <sub>ig,max</sub>	0.16	64.6	21.7
	$322.5 + 870.4SA^{-1}$		
t <sub>MFH</sub>	0.65	1.94	68.3
	$40.83 + 3.845M^2 + 10.27\ln(m_f) - 6.922\ln(SA)$		
t <sub>BO</sub>	0.71	2.45	89.9
	$36.73 + 38.06\sqrt{m_f} - 34.55\rho^{-1} - 0.4024SA$		
MFH	0.553	2.82	46
	$56.98 - 5.947M^2 + 6.817\ln(m_f) - 28.03\rho^2$		
<b>Ceanothus</b>			
t <sub>ig</sub>	0.793	0.787	104
	$-11.76 + 6.095M^2 + 27.86\sqrt{m_f} + 9.466\rho^{-1} - 1.028SA$		
T <sub>ig</sub>	0.18	33.5	8.81
	$130.5 + 22.36M^{-1} + 311.4\sqrt{m_f} + 206.8SA^{-1}$		
T <sub>ig,max</sub>	0.0709	49.3	5.08
	$637 + 66.88M^2 - 249.9\rho^2$		
t <sub>MFH</sub>	0.719	1.56	93.2
	$1.419 + 4.869M^2 + 60.57\sqrt{m_f} - 6.1\sqrt{SA}$		
t <sub>BO</sub>	0.891	1.24	295
	$-6.059 + 7.493M^2 + 83.86\sqrt{m_f} - 2.364SA$		
MFH	0.598	1.8	81.4
	$7.255 - 9.406M + 6.148\ln(SA)$		
<b>Douglas-fir</b>			
t <sub>ig</sub>	0.307	0.574	14.8
	$-1.51 + 0.7996M^2 + 2.205\sqrt{m_f} + 4.446W^{-1}$		
T <sub>ig</sub>	0.315	55	21
	$341.8 - 103.3M^{-1} + 76.82\ln(m_f)$		
T <sub>ig,max</sub>	0.419	86.8	32.4
	$437.9 - 144.1M^{-1} + 172.8m_f^2$		
t <sub>MFH</sub>	0.272	1.75	12.6
	$8.335 - 3.682M^{-1} - 1.217m_f^{-1} + 13.60W^{-1}$		
t <sub>BO</sub>	0.278	4.26	9.95
	$12.94 + 5.838M^2 - 2.146m_f^{-1} + 4.17D^{-1} - 0.22W^2$		
MFH	0.509	6.18	33.2
	$-28.12 + 19.14M^{-1} + 13.23\sqrt{m_f} + 4.016W$		

**Table 6-7: Continued**

Variable	Adjusted R <sup>2</sup>	RMSE	F-statistic
	Correlation		
<b>Gambel oak</b>			
t <sub>ig</sub>	0.624	0.523	23
	$26.14 - 3.385M^{-1} + 1.327\ln(m_f) - 14.78\sqrt{\rho} - 1.266\ln(SA)$		
T <sub>ig</sub>	0.434	26.1	14
	$398.8 - 120.8M^{-1} + 208.3m_f^2 - 1.158SA$		
T <sub>ig,max</sub>	0.153	59.3	5.61
	$-201 - 100.1M^{-1} + 610.8\rho^{-1}$		
t <sub>MFH</sub>	0.425	0.714	10.8
	$-1.454 - 3.006M^{-1} + 2.171\ln(m_f) + 18.56\sqrt{\rho} - 1.636\ln(SA)$		
t <sub>BO</sub>	0.821	0.684	123
	$11.68 + 3.552\ln(m_f) + 31.03SA^{-1}$		
MFH	0.812	3.46	116
	$10.94 - 10.59M^2 + 6.516\ln(SA)$		
<b>Fetterbush</b>			
t <sub>ig</sub>	0.319	0.662	24.7
	$13.85 + 2.663\ln(m_f) - 2.327\ln(SA)$		
T <sub>ig</sub>	----	59.7	----
	264.5		
T <sub>ig,max</sub>	----	106	----
	364.7		
t <sub>MFH</sub>	0.354	0.94	14.8
	$17.66 + 0.7458M^2 + 3.901\ln(m_f) + 8.006\ln(\rho) - 1.455\sqrt{SA}$		
t <sub>BO</sub>	0.341	1.45	53.4
	$12.65 + 2.501\ln(m_f)$		
MFH	0.36	5.67	29.4
	$0.1303 - 3.213M^2 + 10.75\ln(SA)$		
<b>Gallberry</b>			
t <sub>ig</sub>	0.727	0.436	92.4
	$-2.013 + 19.98\sqrt{m_f} + 5.393\rho^2 - 2.16\sqrt{SA}$		
T <sub>ig</sub>	0.158	31.8	5.58
	$-128.9 + 72.87M^{-1} - 2129m_f + 384.7\rho + 0.4201SA^2$		
T <sub>ig,max</sub>	0.0552	57.3	6.73
	$73.83 + 343.7\rho^2$		
t <sub>MFH</sub>	0.656	0.641	66.6
	$-3.149 + 23.85\sqrt{m_f} + 4.75\rho^2 - 0.4288SA$		
t <sub>BO</sub>	0.739	0.771	98.2
	$-3.15 + 32.92\sqrt{m_f} + 4.482\rho^2 - 0.5333SA$		
MFH	0.454	4.36	43.8
	$-6.294 + 3.154M^2 + 7.97\sqrt{SA}$		

**Table 6-7: Continued**

Variable	Adjusted R <sup>2</sup>	RMSE	F-statistic
	Correlation		
<b>Sand pine</b>			
t <sub>ig</sub>	0.351	0.578	20.1
	$3.394 + 1.568\ln(M) - 0.9688D^{-1} - 0.5011\ln(W)$		
T <sub>ig</sub>	-----	33.2	-----
	254.8		
T <sub>ig,max</sub>	0.0405	53.2	5.26
	$362.9 - 23.51m_f^{-1}$		
t <sub>MFH</sub>	0.416	1.49	25.7
	$0.2356 + 0.6804M^2 + 1.066m_f^2 + 14.37W^{-1}$		
t <sub>BO</sub>	0.61	2.73	82.3
	$4.862 - 3.555D^{-1} + 39.65W^{-1}$		
MFH	0.641	6.08	47.3
	$-17.71 + 11.53M^{-1} + 5.734\ln(m_f) + 8.724D^{-1} + 17.13\ln(W)$		
<b>Chamise</b>			
t <sub>ig</sub>	0.554	1.43	60
	$0.5147 + 7.196M^2 + 13.15m_f^2$		
T <sub>ig</sub>	0.286	48.6	11.8
	$226.5 + 189.4M^2 + 379.2m_f^2$		
T <sub>ig,max</sub>	0.301	79.2	12.6
	$200.8 + 341.2M^2 + 247.6\sqrt{m_f}$		
t <sub>MFH</sub>	0.558	2.86	61
	$4.278 + 6.105M^2 + 81.63m_f^2$		
t <sub>BO</sub>	0.456	3.7	80.5
	$10.88 + 96.78m_f^2$		
MFH	0.283	2.7	19.7
	$12.23 + 1.388M^{-1} + 3.012\ln(m_f)$		
<b>Sagebrush</b>			
t <sub>ig</sub>	0.266	1.67	33.3
	$0.1315 + 6.728\sqrt{m_f}$		
T <sub>ig</sub>	0.0572	52.1	5.73
	$267.4 + 3.325m_f^{-1}$		
T <sub>ig,max</sub>	---	108	---
	416.2		
t <sub>MFH</sub>	0.262	4.75	32.5
	$5.605 + 17.85m_f$		
t <sub>BO</sub>	0.486	6.92	85.2
	$12.84 + 58.51m_f^2$		
MFH	0.338	3.92	23.7
	$14.05 - 5.576M^2 + 22.04m_f^2$		

**Table 6-7: Continued**

Variable	Adjusted R <sup>2</sup>	RMSE	F-statistic
	Correlation		
<b>Lodgepole pine</b>			
t <sub>ig</sub>	0.111	0.764	9.75
	$1.62 + 5.4111W^{-1}$		
T <sub>ig</sub>	0.0661	59.5	4.47
	$174.4 + 87.83M^{-1}$		
T <sub>ig,max</sub>	---	96.9	---
	384.5		
t <sub>MFH</sub>	0.261	1.1	9.26
	$9.412 + 0.8091\ln(m_f) - 0.0414D^2 - 1.438\sqrt{W}$		
t <sub>BO</sub>	0.179	3.3	8.62
	$4.667 + 3.332m_f + 4.036D^{-1}$		
MFH	0.069	8.59	6.19
	$28.62 + 7.117\ln(m_f)$		

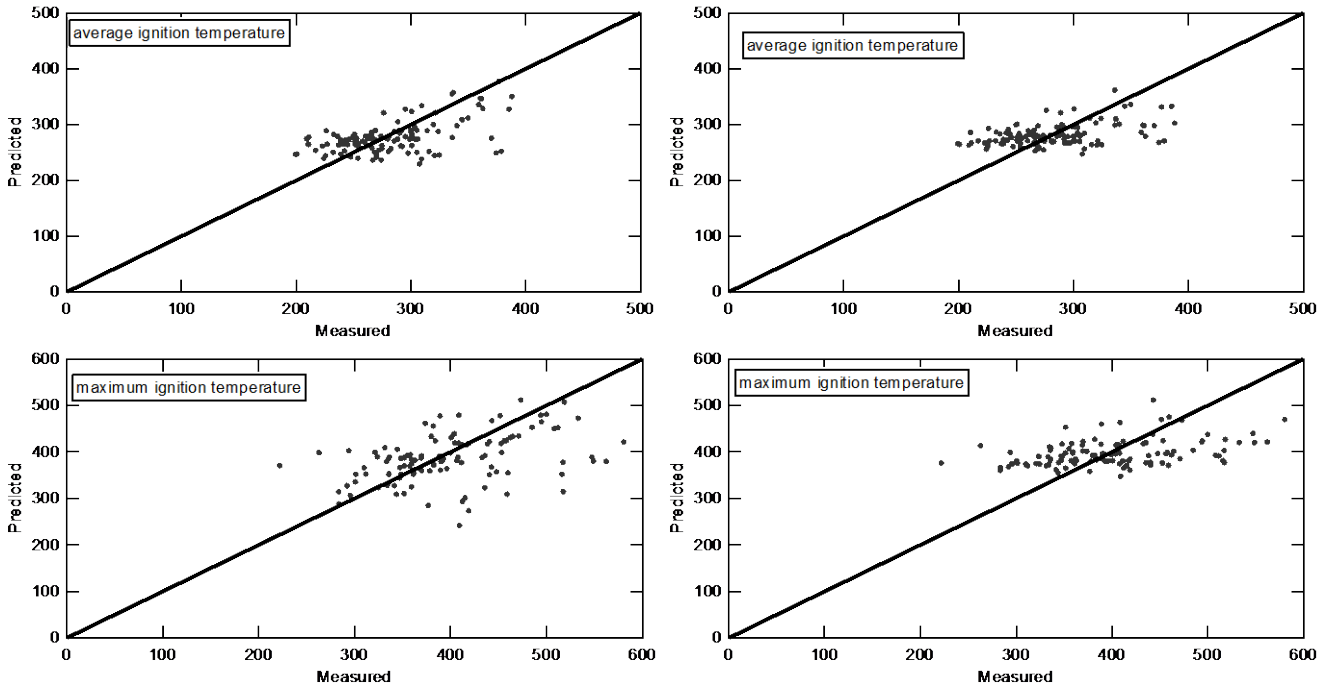


**Figure 6-4: Parity plots for ignition temperatures for manzanita. Best overall models are shown in the left column, models using the most common predictors are shown in the right column.**

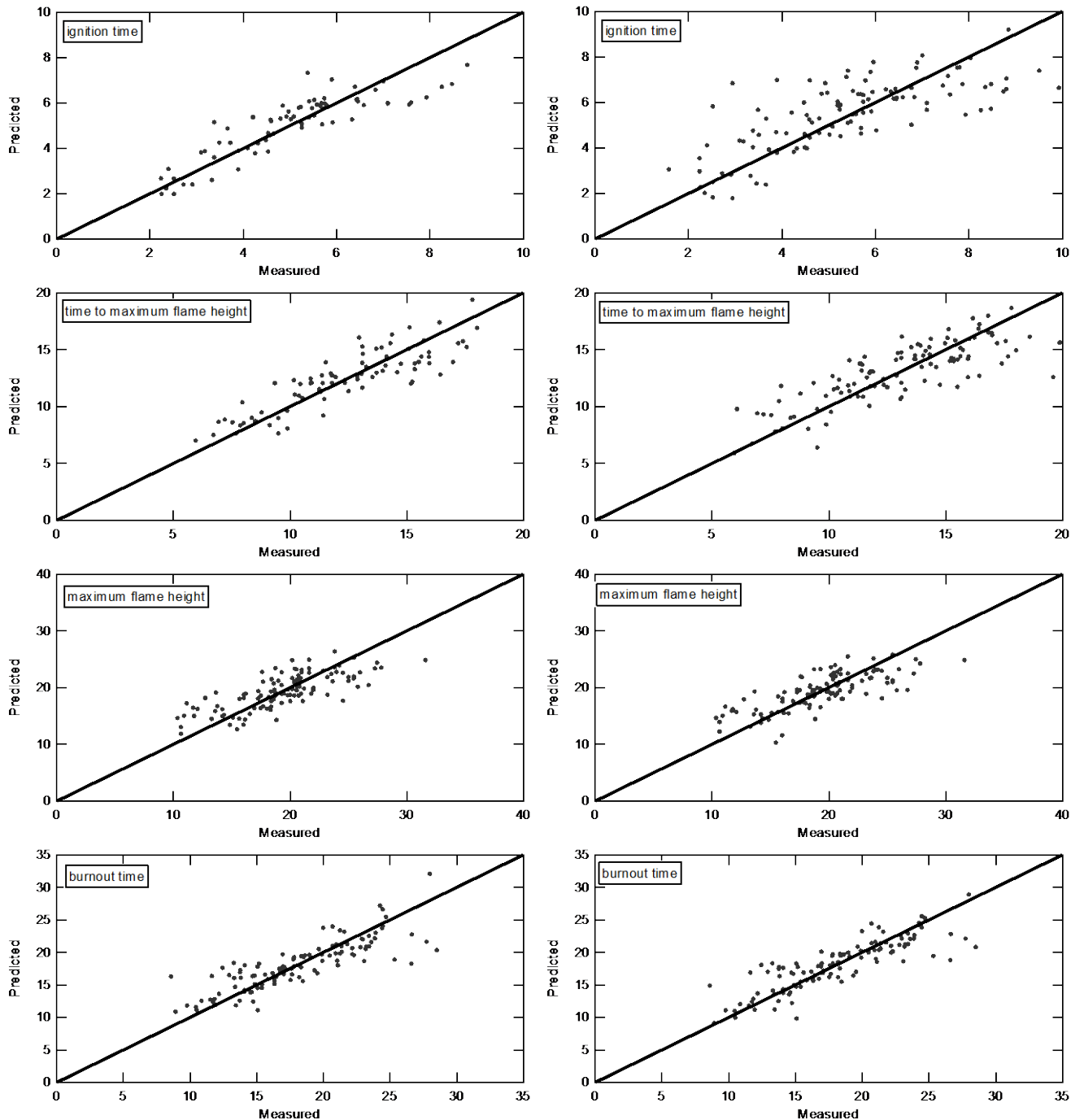


**Figure 6-5: Parity plots for burning characteristics for manzanita. Best overall models are shown in the left column, models using the most common predictors are shown in the right column.**

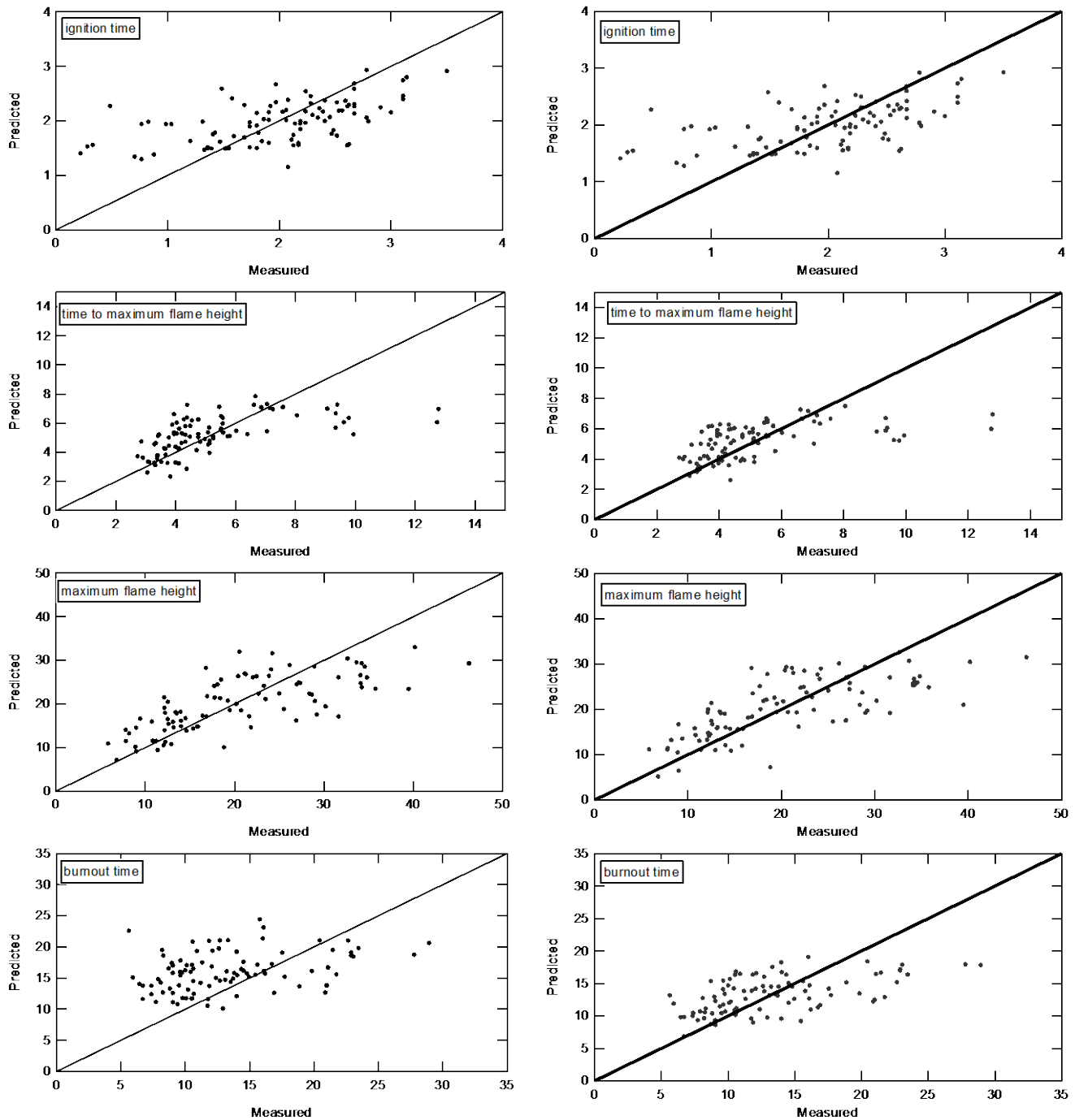


**Figure 6-6: Parity plots for burning characteristics for Douglas-fir. Best overall models are shown in the left column, models using the most common predictors are shown in the right column.**

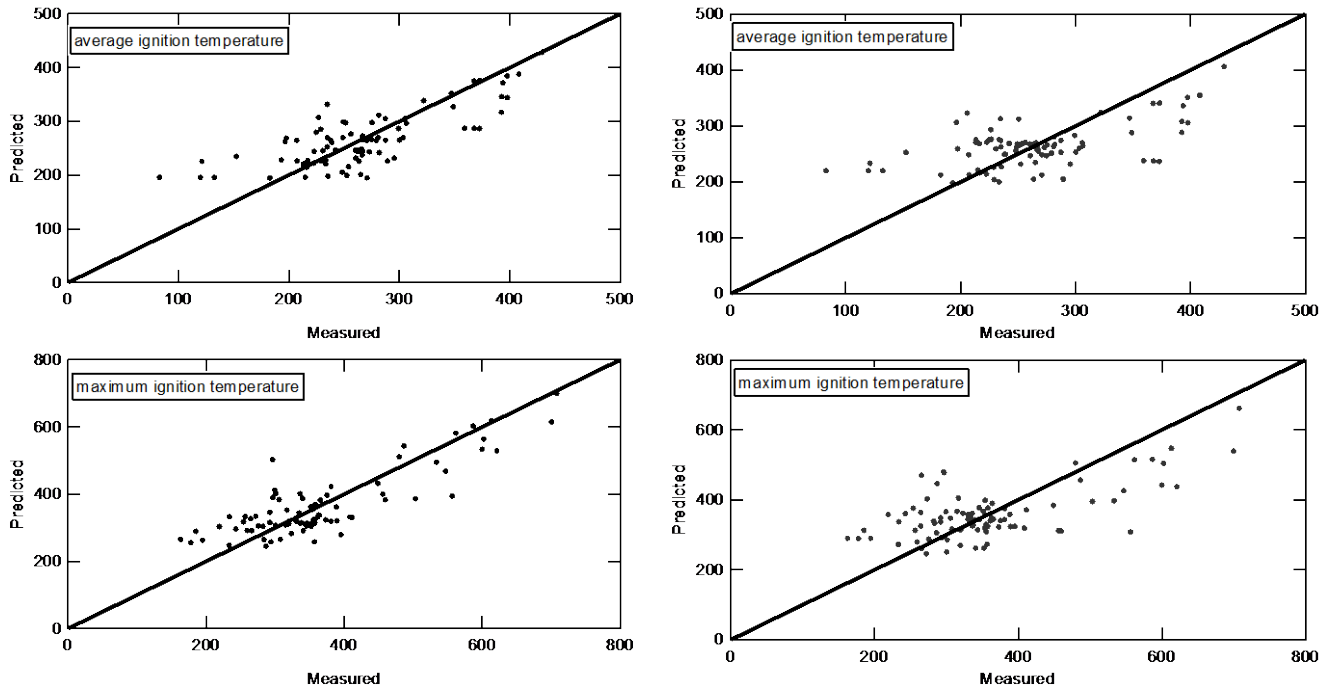


**Figure 6-7: Parity plots for ignition temperatures for Douglas-fir. Best overall models are shown in the left column, models using the most common predictors are shown in the right column.**

#### 6.2.4 Uncertainty Analysis

As discussed in Chapter 4, it is important to quantify the effects of measurement error on model performance. Table 6-8 shows the relative uncertainty and sources of error for each of the burn measurements. As with the pre-burn measurements, the relative uncertainty entries represent the measurement uncertainty normalized by the measured value averaged across all species and months. The maximum relative uncertainty for burn measurements is 9.6%, indicating the natural scatter in the data is far more important than measurement uncertainty in developing prediction models.

**Table 6-8: Relative uncertainty and sources of measurement error for all the burn experiment measurements.**

<b>Measurement</b>	<b>Relative Uncertainty</b>	<b>Sources of Error</b>
<b>Ignition time</b>	0.011	Error is one time stamp
<b>Ignition temperature</b>	0.02	Error is that reported by FLIR for their camera and errors in which a single pixel contained part sample and part background
<b>Time to maximum flame height</b>	0.005	Error is one time stamp
<b>Time to burnout</b>	0.003	Error is one time stamp
<b>Maximum flame height</b>	0.096	Error comes from user input on the algorithm's reference length scale. Error from flame flickering and interlaced video files were avoided by using only "connected" flame pixels
<b>Gas temperature</b>	0.0275	Error is that reported by manufacturer plus radiation losses from the thermocouple bead
<b>Mass during run</b>	0.05	Error is the sensitivity of the mass balance, the buoyant force exerted on the sample by the post-flame gases, and the shaking caused by moving the FFB (this source of error is mostly eliminated in data processing)

The entries in Table 6-9 and Table 6-10 represent the estimate of the model error due to measurement uncertainty, using analytical propagation of error techniques, divided by the root mean squared error (RMSE) of the residuals between the data and the prediction for the best overall models and the models using the most common predictors, respectively. Seven of the best overall models and five of the MCP models have entries greater than one (highlighted in the tables) in Table 6-9 and Table 6-10, respectively. The three main reasons for these high values are particularly strong models (resulting in a low RMSE), large model coefficients (this is particularly true for the ignition temperature correlations), and correlations having several terms. The average for the rest of the entries are 0.22 and 0.24, respectively, indicating the results in Table 6-9 and Table 6-10 also show measurement uncertainty does not have a large effect on the prediction models show in Table 6-6 and Table 6-7.

**Table 6-9: Estimated model prediction error due to measurement uncertainty normalized by the root mean squared error (RMSE) for each of the best overall models.**

Species	<b>t<sub>ig</sub></b>	<b>T<sub>ig</sub></b>	<b>T<sub>ig,max</sub></b>	<b>t<sub>MFH</sub></b>	<b>t<sub>BO</sub></b>	<b>MFH</b>
<b>Manzanita</b>	0.441	3.629	0.237	0.075	0.191	0.081
<b>Ceanothus</b>	0.362	0.178	0.131	0.143	0.118	0.869
<b>Fetterbush</b>	10.46	1.003	0.171	0.381	0.222	0.183
<b>Gallberry</b>	1.367	0.634	0.326	1.120	0.202	0.465
<b>Gambel oak</b>	0.262	7.787	0.065	0.335	0.045	0.476
<b>Douglas-fir</b>	0.091	0.091	0.125	0.037	0.113	0.149
<b>Lodgepole pine</b>	0.004	0.004	0.334	0.019	0.000	0.025
<b>Sand pine</b>	0.111	0.393	0.235	0.256	0.759	0.156
<b>Sagebrush</b>	0.007	0.883	1.495	0.901	0.195	0.008
<b>Chamise</b>	0.001	0.001	0.001	0.040	0.088	0.001

**Table 6-10: Estimated model prediction error due to measurement uncertainty normalized by the root mean squared error (RMSE) for each of the MCP models.**

Species	<b>t<sub>ig</sub></b>	<b>T<sub>ig</sub></b>	<b>T<sub>ig,max</sub></b>	<b>t<sub>MFH</sub></b>	<b>t<sub>BO</sub></b>	<b>MFH</b>
<b>Manzanita</b>	0.767	3.893	3.368	0.893	0.113	0.050
<b>Ceanothus</b>	0.391	1.544	0.025	0.982	0.484	0.854
<b>Fetterbush</b>	0.879	--	--	0.430	0.0002	0.474
<b>Gallberry</b>	1.305	0.071	0.030	0.208	0.206	0.457
<b>Gambel oak</b>	0.747	0.012	0.052	0.704	11.342	0.471
<b>Douglas-fir</b>	0.388	0.0003	0.0004	0.389	0.013	0.033
<b>Lodgepole pine</b>	0.354	0.0002	--	0.066	0.012	8e-5
<b>Sand pine</b>	0.060	--	4e-5	0.482	0.739	0.156
<b>Sagebrush</b>	0.0004	6e-6	--	0.0004	0.001	0.001
<b>Chamise</b>	0.001	0.001	0.001	0.003	0.003	0.0002

### 6.3 Summary and Conclusions

Ignition and burning behavior for ten live fuels were studied in a flat-flame burner apparatus. Experiments were performed over a two-year period to test the effect of season (specifically moisture content) on ignition and burning behavior. The hypothesis was that moisture content would not change ignition and burning behavior except by increasing time to ignition (behavior of wet wood).

Sample condition experiments indicate that amount of foliage matters for live fuels but not for dead fuels. Results comparing ignition and burning characteristics with moisture content and season were mixed. Ceanothus, Gambel oak, Douglas-fir and chamise all exhibited a positive correlation between ignition time and moisture content while the other six species show no correlation at a 95% significance level, indicating a simple relationship between moisture content and ignition is not adequate to describe ignition in live fuels. However, linear stepwise models capture much of the variability in ignition behavior. The results presented here indicate the most important predictors for ignition and flame behavior are moisture content, sample mass, apparent density (broad-leaf species), surface area (broad-leaf), sample width (needle species) and stem diameter (needle). The data also indicate lipid content, volatile fraction, fixed carbon and ash content are not significant predictors of the ignition and burning behavior characteristics measured under the conditions studied. Additionally, ignition behavior of live fuels in different seasons but at the same moisture content was different. These results suggest a relationship between moisture content and ignition that is different for live fuels than the relationship typically seen in dead fuels. It is possible some of seasonal influences on burning behavior seen in this work are due to changes that occur on a larger time-scale than one year, such as a multi-year drought or gradual change in soil composition. Additional combustion experiments and detailed physiological measurements are suggested to improve theoretical understanding of fire spread in live fuels. In the absence of a theoretical understanding, simple statistical models were developed that describe fire behavior accurately and that use as inputs the same information currently used in most fire models.



## **7 THE INFLUENCE OF THE COANDA EFFECT ON FLAME ATTACHMENT TO SLOPES AND FIREFIGHTER SAFETY ZONE CONSIDERATIONS<sup>5</sup>**

Improved safety protocols throughout the last century combined to decrease entrapment fatalities, but recent fires like the 2001 Thirty-Mile fire, the 2006 Esperanza fire, and the 2013 Yarnell Hill fire demonstrate that the risk of entrapment still exists (Butler, 2014). One reason often cited as contributing to entrapments is the influence of the Coanda effect, or more generally, the behavior of fires near slopes. The Coanda effect is the phenomenon in which a jet entering quiescent fluid attaches to a nearby solid object due to inhibited entrainment of ambient fluid near the solid. Little is known about the influence of the Coanda effect on wildland fire behavior. Specifically, there is a lack of knowledge regarding how the Coanda effect influences firefighter safety zone considerations in rugged terrain. This chapter presents results for small-scale burn experiments testing the effect of slope angle, slope boundary condition and distance from flame base on fire behavior and heat flux upslope from the fire. The results from the small-scale burn experiments point to several research areas that need further attention.

### **7.1 Methods**

Experiments were performed using the apparatus shown in Figure 7-1. Five milliliters of heptane in a nominally 12 cm long by 7 cm wide stainless steel pan were used as the fuel for all experiments. A nominally 30 cm long by 20 cm wide metal sheet, blackened from previous burn

---

<sup>5</sup> This chapter is under review for publication in *Combustion Science and Technology*

experiments, was used for the slope. Half inch thick fire board was attached to the back of the metal slope for the insulated slope experiments. Slope angle, boundary condition and flux sensor distance were varied as shown in Table 7-1. Slope angles varied from 0 degrees to 63 degrees or slopes of 0% to 196% from horizontal. Measurement angles were more closely spaced for the lower angles to better understand the effects of slopes at grades more typical of hills. Bare metal and insulated slopes were used to bracket the expected conductive and reflective properties of a real hill-side. The distance from the flame base to the heat flux sensor was varied to establish a better estimate of the added heat due to the presence of a slope and the effect of the added heat on safety zone size. The distance between flame base and flux sensor was limited to between 24 cm and 30 cm due to flame impinging on the sensor and the length of the slope, respectively. The

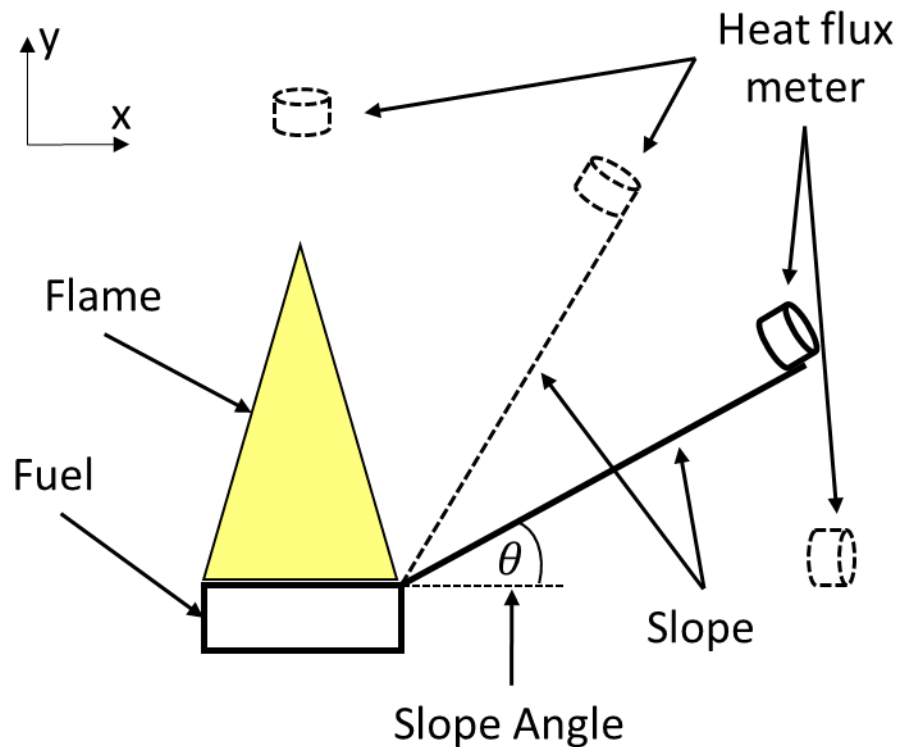


**Figure 7-1: Experimental apparatus showing fuel pan, flame, slope and heat flux sensor placement.**

“control” boundary condition listed in Table 7-1 indicates experiments performed in the absence of a slope. These flame and heat flux measurements are the base-level measurements with which all other experimental data are compared. One run was performed for each boundary condition, slope and distance. This resulted in four replicates for flame data for each slope and boundary condition, eight replicates for flame data for the control experiment, and one measurement of heat flux for each boundary condition, slope and distance.

**Table 7-1: Table of run conditions for all experiments.**

<b>Slope angle from horizontal (degrees)</b>	<b>Slope angle from horizontal (% grade)</b>	<b>Boundary condition</b>	<b>Distance from flame base (cm)</b>
90	infinite	Control	26, 30
60	173	Control	26, 30
30	58	Control	26, 30
0	0	Control	26, 30
63	196	Bare Slope	24,26,28,30
54	138	Bare Slope	24,26,28,30
45	100	Bare Slope	24,26,28,30
36	73	Bare Slope	24,26,28,30
27	51	Bare Slope	24,26,28,30
23	42	Bare Slope	24,26,28,30
19	34	Bare Slope	24,26,28,30
15	27	Bare Slope	24,26,28,30
10	18	Bare Slope	24,26,28,30
0	0	Bare Slope	24,26,28,30
63	196	Insulated Slope	24,26,28,30
54	138	Insulated Slope	24,26,28,30
45	100	Insulated Slope	24,26,28,30
36	73	Insulated Slope	24,26,28,30
27	51	Insulated Slope	24,26,28,30
23	42	Insulated Slope	24,26,28,30
19	34	Insulated Slope	24,26,28,30
15	27	Insulated Slope	24,26,28,30
10	18	Insulated Slope	24,26,28,30

Transient flame data were captured using a Samsung HMX-F90 video camera with a frame rate of 30 frames per second. Total and radiant heat flux data were measured using a water-cooled 64-series Medtherm heat flux sensor with a measurement frequency of one hertz and a response time on the order of one millisecond. Convective heat flux data were obtained from the difference between total and radiative fluxes. The sensor was controlled by and data were written to text files using Labview 8.6 software. Video and heat flux data were post-processed using in-house computer vision algorithms to extract the measurements defined in Table 7-2. Flame pulse frequency was defined as the number of times the flame length was longer than 1.4 times the average flame length divided by the number of time steps in the run. Flame attachment was determined by the presence of the flame in the flame attachment zone; flame attachment length was defined as the distance from the flame base to the point highest up the slope in which flame was present in the flame attachment zone. The flame attachment zone is an area near the slope whose size was defined using manual comparisons between the raw video data and the processed data. For the analyses presented in this work, the flame attachment zone was determined to be a trapezoid with a height of 1.5 cm.

**Table 7-2: Measurement definitions.**

<b>Measurement</b>	<b>Definition</b>
Flame height (FH)	Distance from flame base to flame peak in the y-direction (cm).
Flame length (FL)	Distance from flame base to flame peak (cm).
Flame attachment length (FA)	Distance up the slope that the flame is attached (cm).
Flame attachment time ( $t_{FA}$ )	Fraction of time flame is attached to the slope.
Flame pulse frequency ( $f_{pulse}$ )	Frequency of flame pulsation (Hz).
Heat flux ( $q''$ )	Total and radiative energy flux at specified distance from flame base ( $\text{kW m}^{-2}$ ).

A schematic illustrating the method for determining flame height, flame length, and flame attachment zone is shown in Figure 7-2. An example of the video processing is shown in Figure 7-3, in which the visual image and its associated binary image with the flame identified are shown in the left and right panels, respectively. Only the steady-state portion of the burn data were used. Typically, this was approximately 30 seconds during the middle of the run. Experimental data are reported in Appendix C.4.

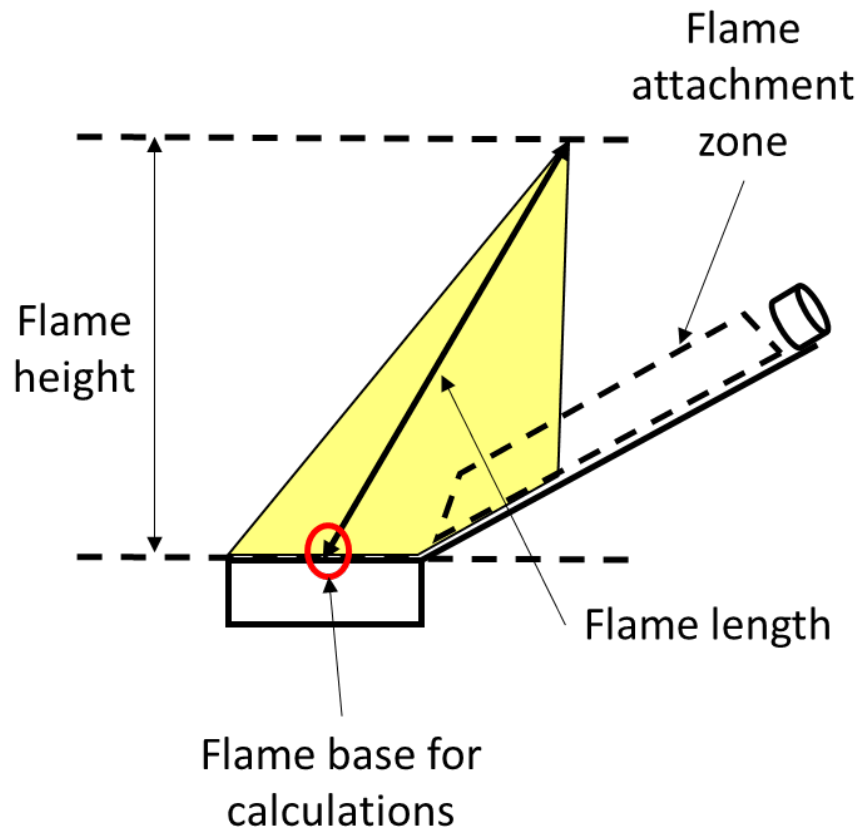


**Figure 7-2: Schematic showing definitions of flame height, flame length and flame attachment zone.**

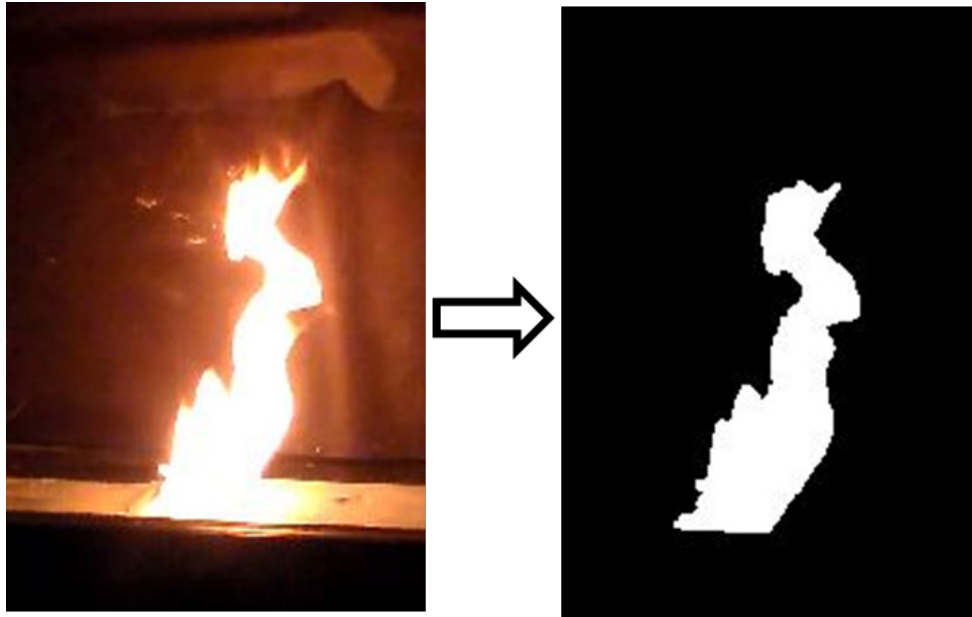


**Figure 7-3: Image processing example. The left image is the visual image from an experiment, the right image is the associated binary image.**

## **7.2 Results**

Raw data from one of the control runs with the heat flux sensor at  $0^\circ$  and 30 cm are shown in Figure 7-4. As shown in Figure 7-4a, large fluctuations were observed in the flame height data over time. Though not explicitly shown in the figure, the fluctuations are characterized by the puffing behavior typical of pool fires (Henriksen et al., 2008). Another pertinent observation can be made from Figure 7-4, namely the difference in measurement frequency between the video data and the heat flux data. This difference prohibits tracking the heat flux from individual flame fluctuations, but important information can still be learned from these data regarding fire behavior near slopes and how that behavior might influence safety zone size.

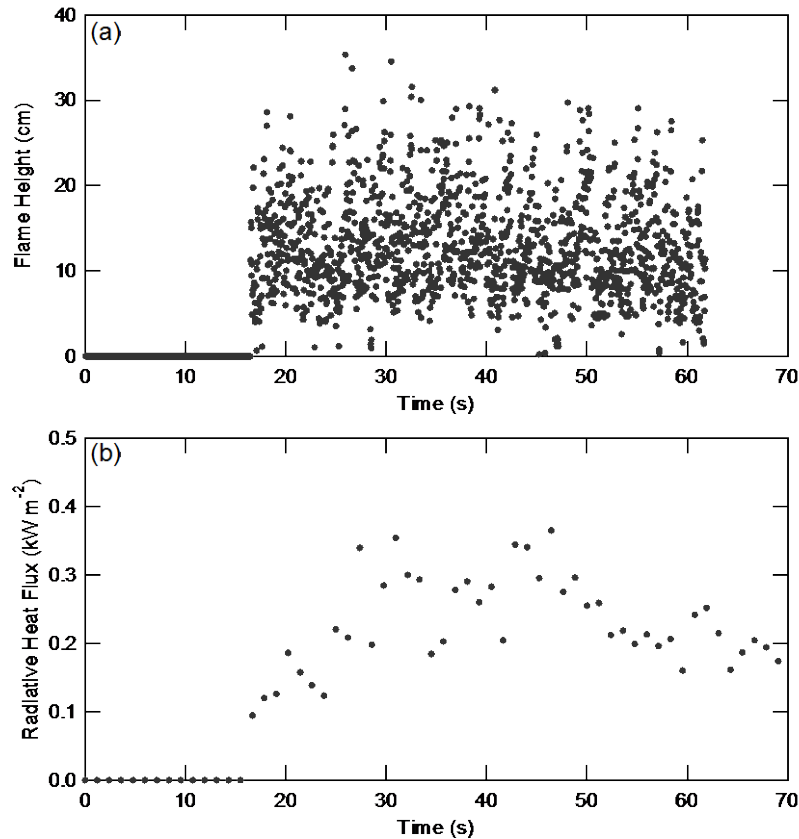


**Figure 7-4: Transient flame height data in centimeters (a) and radiative heat flux data in kilowatts per square meter (b) for a control run at 0° and 30 cm.**

### 7.2.1 Flame Behavior Measurement Results

Mean flame length is shown in Figure 7-5. The points in each figure represent the average value for all experiments for each angle and boundary condition. Within the figure, dots are burns with a bare metal slope and squares are burns with an insulated metal slope. The line indicates the average flame length for the eight control burns. The error bars and dashed lines represent the 95% confidence interval for each point. The mean flame length is significantly different (defined here as non-overlapping confidence intervals) from the control at a slope angle of 36° for both boundary conditions. Except for a few isolated angles, there is no significant, consistent difference between boundary conditions. It is clear from this figure that flames become longer as slope angle increases.

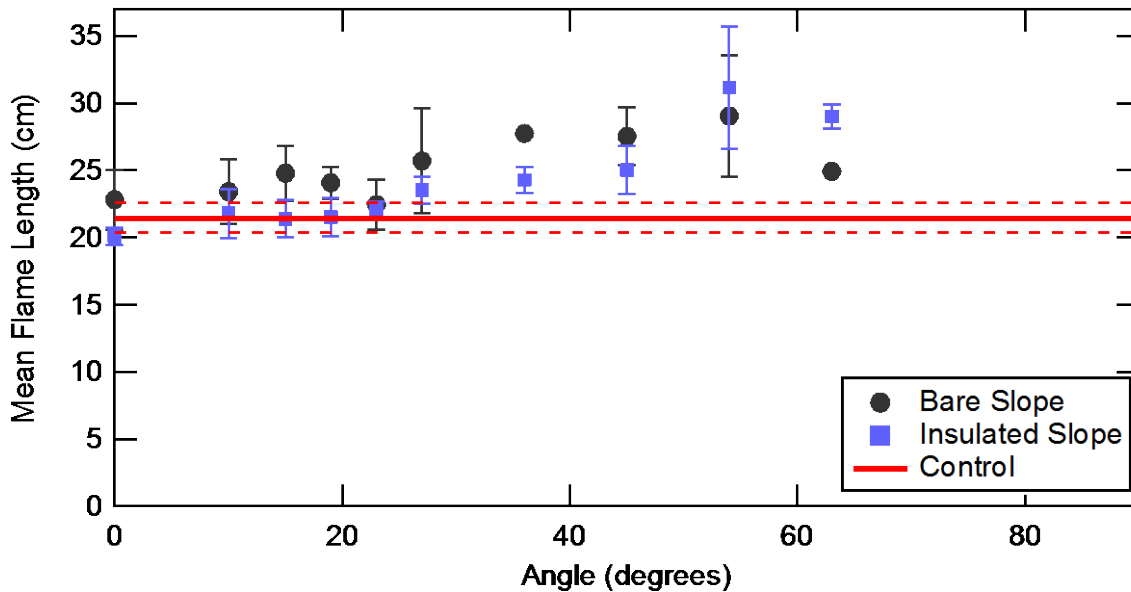


**Figure 7-5: Flame length measured in centimeters. Each point represents the average of all burns for that angle and boundary condition. The error bars and dashed lines represent the 95% confidence interval.**

The mean flame attachment length for each angle and boundary condition is shown in Figure 7-6. Figure 7-7 shows the fraction of time the flame is attached to the slope. Here again, the points in each figure represent the average value for all experiments for each angle and boundary condition. Within the figure, dots are burns with a bare metal slope and squares are burns with an insulated metal slope. The line indicates the average flame height or flame length for the eight control burns. The error bars and dashed lines represent the 95% confidence interval for each point. The flame attachment length shows a much stronger dependence on slope angle than either flame height or flame length, deviating from the control average at 19°. The same result is seen in Figure 7-7 for fraction of time the flame is attached to the slope. The flames attach higher up the slope and spend more time attached to the slope as the angle of the slope increases. As in Figure 7-5, there is no significant difference between boundary conditions for flame attachment length or fraction of time the flame is attached to the slope.

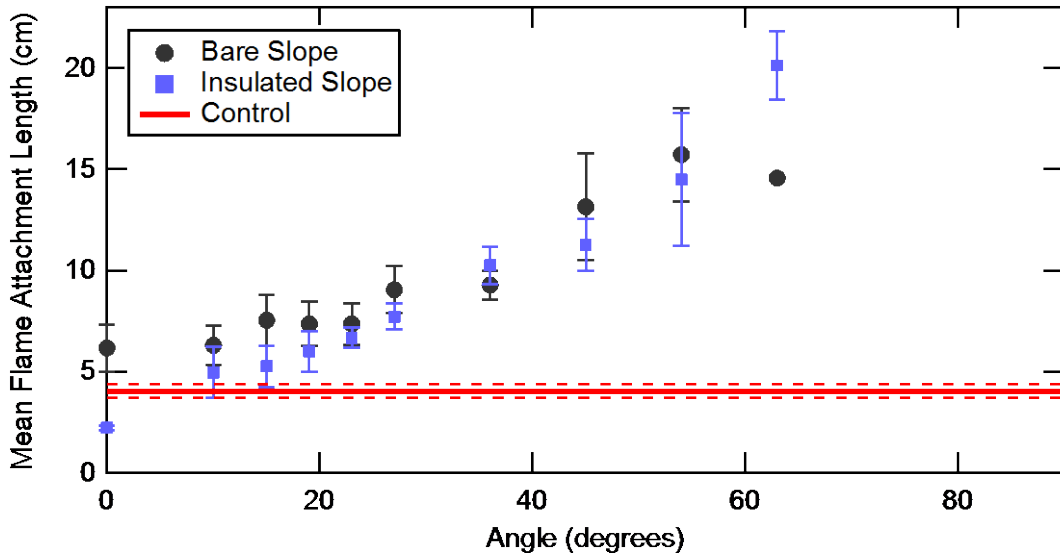


Figure 7-6: Flame attachment length, measured in centimeters. Each point represents the average of all burns for that angle and boundary condition. The error bars and dashed lines represent the 95% confidence interval.

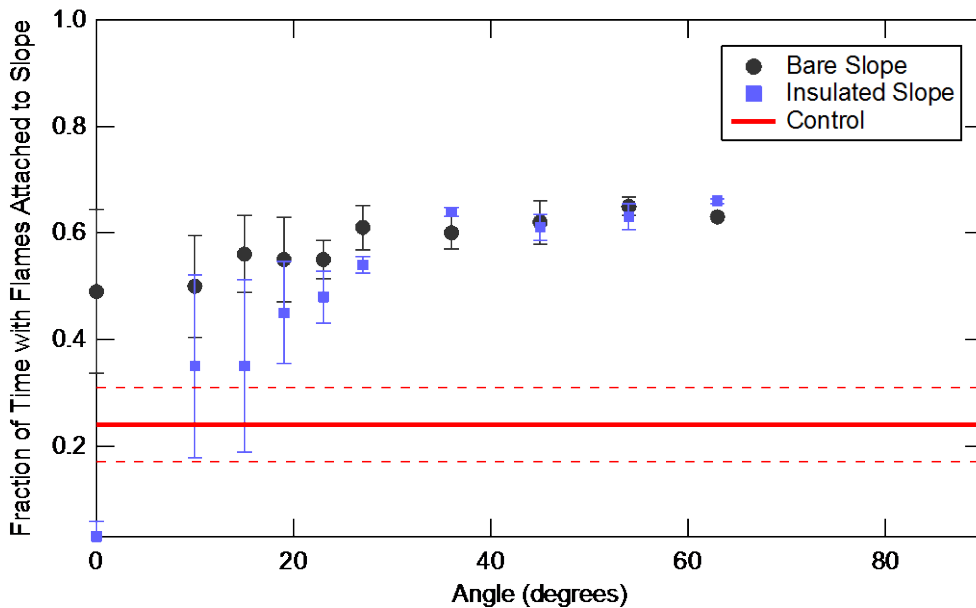
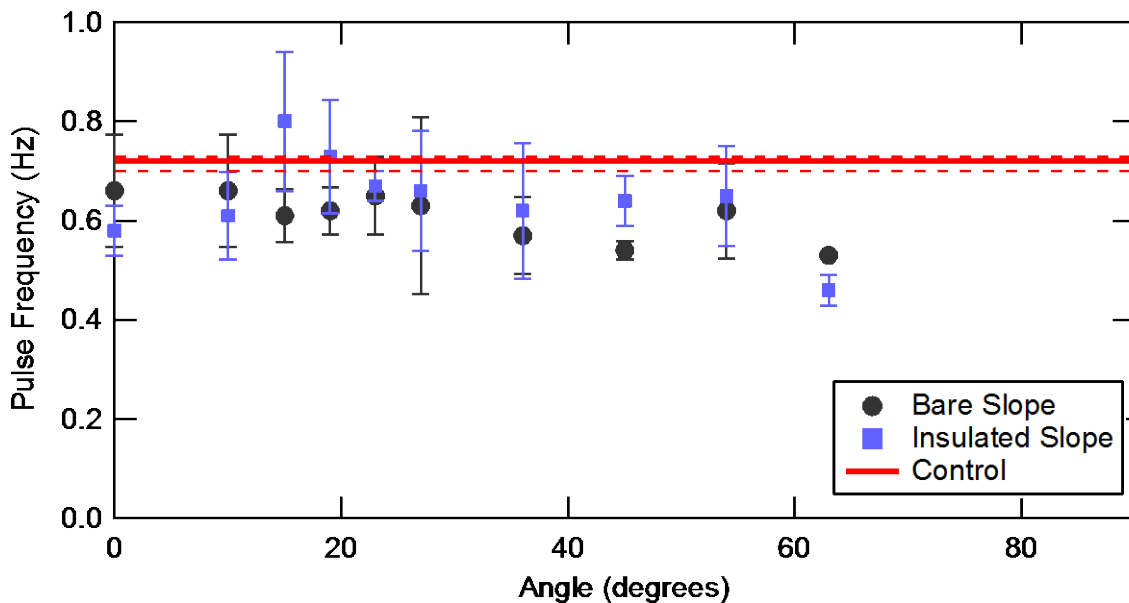


Figure 7-7: Fraction of run time with flame attached to slope. Each point represents the average of all burns for that angle and boundary condition. The error bars and dashed lines represent the 95% confidence interval.

Flame pulse frequency is shown in Figure 7-8. The same symbol convention is used in Figure 7-8 as was used in Figure 7-5 through Figure 7-7. Pulse frequency results were mixed. Six of the ten slope angles for the bare slope boundary condition were significantly different than the

control experiments while only two of the ten slope angles for the insulated slope boundary condition were significantly different than the control experiments. The two boundary conditions were different from each other in only two of the ten slope angles. The pulse frequency for each angle and boundary condition was not significantly different than the pulse frequency for the neighboring angles except for the 63° slope case. Based on these observations, the overall result is that the pulsation frequency did not change between boundary conditions or across slope angle, though the reduction in pulse frequency for the 63° slope case could indicate slope angle begins to influence pulsation frequency at high slope angles.



**Figure 7-8: Flame pulse frequency, measured in hertz (Hz). Each point represents the average of all burns for that angle and boundary condition. The error bars and dashed lines represent the 95% confidence interval.**

### 7.2.2 Heat Flux Measurement Results

The radiative and convective heat fluxes for each boundary condition, averaged across sensor distance for each angle, are shown in Figures 7-9 and 7-10, respectively. The same

symbol convention is used in Figures 7-9 and 7-10 as was used in Figure 7-5 through Figure 7-8. Three important observations can be made from the data in Figure 7-9, namely (1) there is no difference in radiative heat flux between boundary conditions, (2) control radiative levels change with viewing angle, presumably due to path length through the flame, and (3) radiation levels with the slope present are always higher than radiation levels without the slope, except in the  $0^\circ$  case. Observation 1 is not surprising given the similar results from previous figures. Observation 2 is also not surprising, and, while the difference in radiative heat flux between  $0^\circ$  and  $60^\circ$  is slight, it is significant and serves as validation that the results presented here agree with known physics principles. The behavior seen in observation 3 is comprised of two regimes. For angles below  $36^\circ$ , the difference between the slope experiments and the control experiments is significant but small. This change is likely due to a slight increase in radiative path length (observation 2) combined with a small amount of radiation reflected from the slope surface. At angles  $36^\circ$  and above, radiative heat flux increases sharply compared to control levels. This is the point at which flame length and flame attachment time increase, and the increase in radiative flux is largely due to an increase in radiative path length.

An even stronger dependence on slope angle is observed for convective heat flux in Figure 7-10. As seen in the figure, convective heat flux remains near zero until the slope angle reaches  $45^\circ$ , at which point there is a rapid rise in convective flux as the slope angle increases further. Thus, the presence of a slope has two effects on heat flux (radiative and convective) and both must be considered in determining safety zone size.

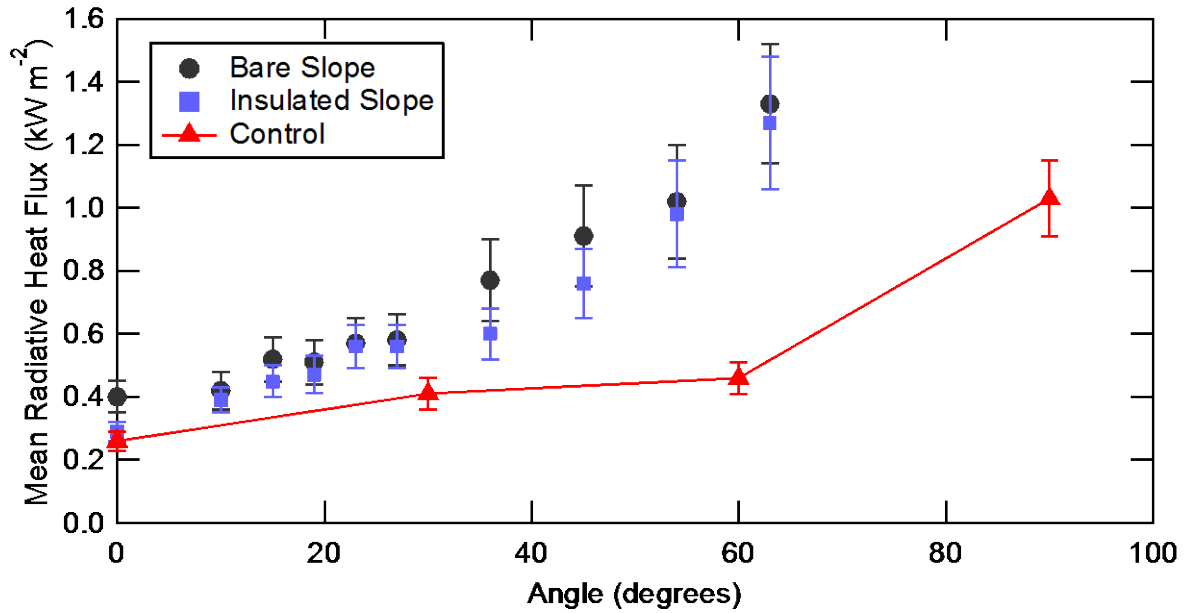


Figure 7-9: Average radiative heat flux, measured in kilowatts per square meter ( $\text{kW m}^{-2}$ ). Each point represents the average of all burns for that angle and boundary condition. The error bars and represent the 95% confidence interval.

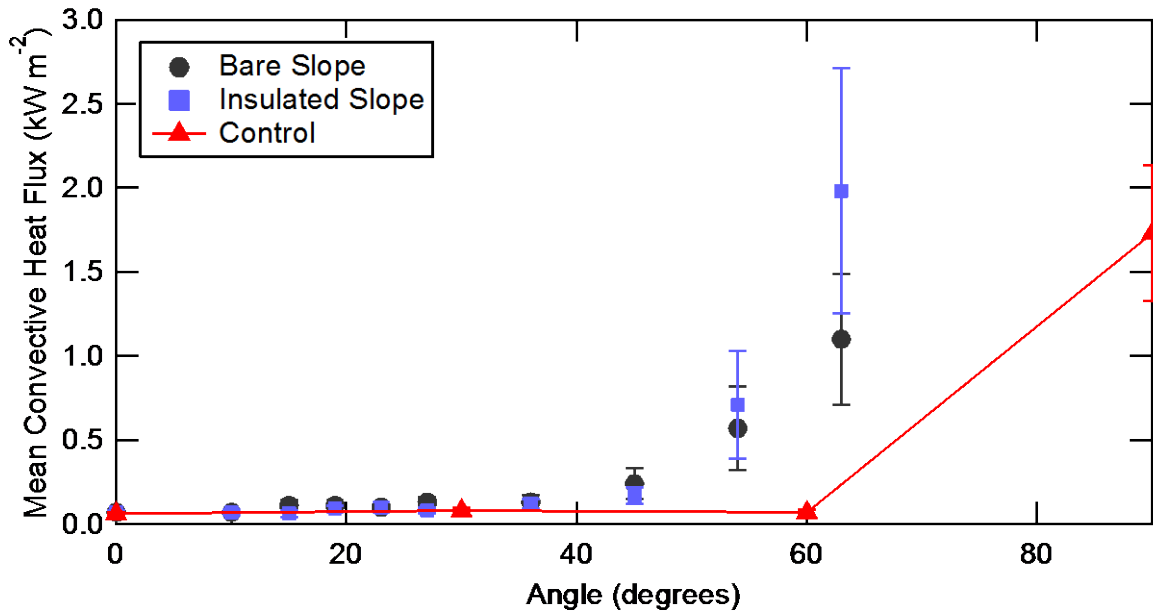
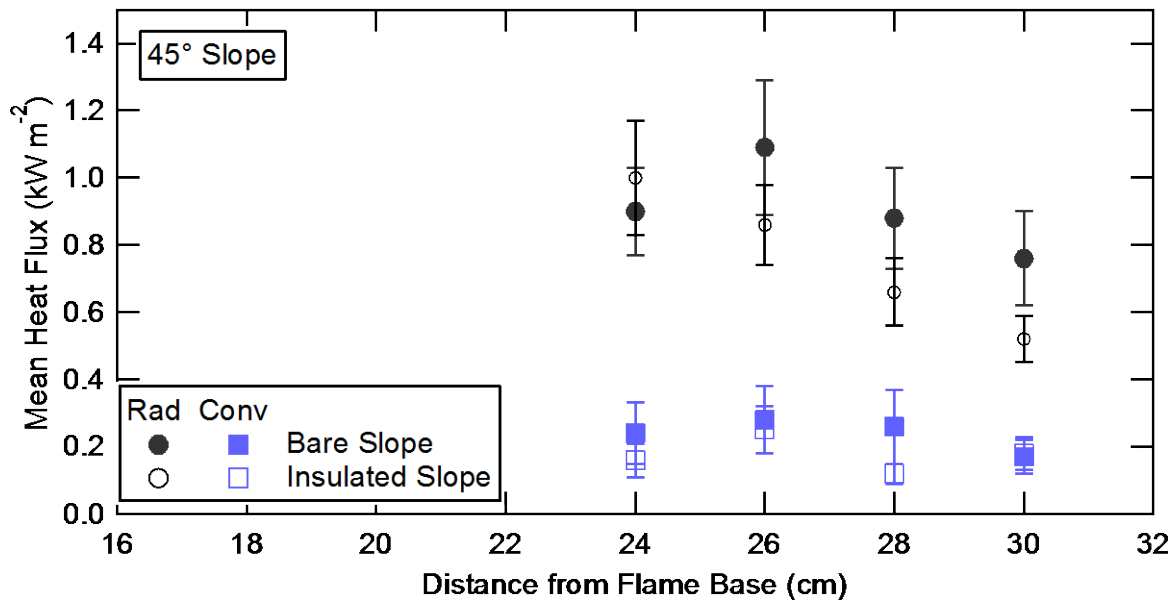


Figure 7-10: Average convective heat flux, measured in kilowatts per square meter ( $\text{kW m}^{-2}$ ). Each point represents the average of all burns for that angle and boundary condition. The error bars and represent the 95% confidence interval.

The effect of distance on radiative and convective heat flux is shown for the  $45^\circ$  case in Figure 7-11. Within the figure, circles represent radiative heat flux, squares represent convective

heat flux, closed symbols indicate experiments with a bare metal slope and open symbols indicate experiments with an insulated metal slope. The data in Figure 7-11 indicate that heat flux changes with respect to distance, as expected. This behavior is seen in the data for other angles as well. However, it is difficult to draw conclusions regarding the combined effect of distance and fluid flow on heat flux on slopes due to the limited range of distances available in the experimental apparatus. This does not indicate the effect of distance is unimportant, but rather that the effect of distance should be explored at a larger scale than that used herein.



**Figure 7-11: Average convective and radiative heat flux for bare metal and insulated slopes. Each point represents the average of all burns for that angle and boundary condition. The error bars and represent the 95% confidence interval.**

Given the small size of the experiments performed as part of this work, it is not surprising the mean measured heat fluxes do not reach an unsafe limit. The utility of these experiments lies mainly in illustrating the fire and heat flux behavior that can occur in fires near slopes. However, due to the low measurement frequency of the heat flux sensor, it is possible the actual mean heat flux was higher than that reported here and just not captured by the meter. This effect can be

partially explored by examining the maximum heat flux measured during each run. Those values are  $3.5 \text{ kW m}^{-2}$  for radiation and  $14 \text{ kW m}^{-2}$  for convection. While these are instantaneous individual values and therefore not the heat flux that would be seen continually, they still reach dangerous levels and therefore are worth noting. A more detailed look at maximum heat flux measured during each run is shown in Figure 7-12. Figure 7-12 contains the mean and maximum total (radiation and convection combined) heat flux measurements normalized to the mean and maximum control burn measurements taken at a  $0^\circ$  slope angle (analogous to a fire a level terrain). The total heat flux is used rather than showing individual heating modes because it is the total energy transfer rather than the type of heating that matters in determining the safe separation distance from a fire. Each “mean” data point represents the average of all data points for all distances at the given angle and boundary condition. Each “maximum” data point represents the maximum value from each run averaged across all distances at the given angle and boundary condition. Although it is difficult to see in the figure, the mean and maximum total flux reach two times the control level at a  $23^\circ$  slope angle. The deviation continues to grow, reaching 10 times the control level for the mean flux and 30 times the control level for the maximum flux. As in previous figures, there is no significant, consistent difference between boundary conditions.

The flame and heat flux data are summarized in Figure 7-13, Specifically, Figure 7-13 shows the angle at which the specified flame characteristic deviated from the control flame characteristic. Three main results can be seen in the figure, namely: (1) for most of the flame characteristics examined, there was no difference between a bare slope and an insulated slope, (2) the average angle at which the deviation from the control experiment occurred was between

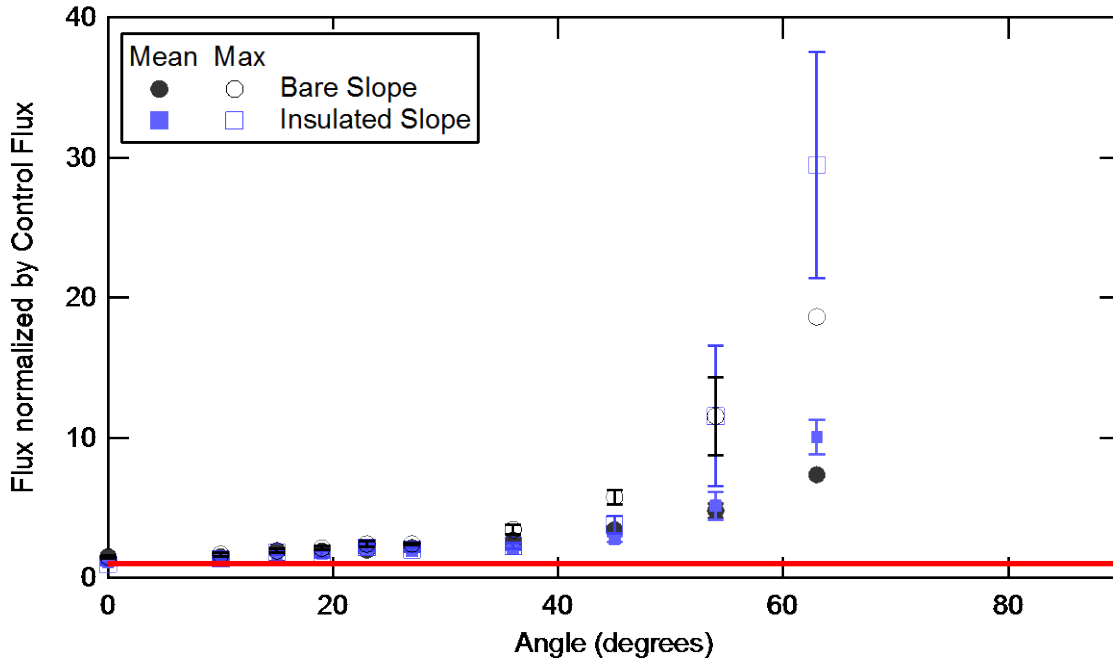


**Figure 7-12: Average and maximum total heat flux for bare metal and insulated slopes. Each point represents the average of all burns for that angle and boundary condition normalized against the mean and maximum values for the 0° control burn. The error bars and represent the 95% confidence interval.**

20° and 40°, depending on the criteria used, (3) the traditional view of safe separation distance as being the distance from the flame base seems inadequate for fires near slopes. The last result follows from the attachment behavior of flames near slopes; if the fire is attached to the slope and leaning toward the firefighter, the distance from the flame itself is much shorter than the distance from the flame base.

### 7.2.3 Dimensional Analysis

Given the difference in scale between the fires presented in this work and fires that would pose a risk to firefighters in the field, it was necessary to perform dimensional analysis to see the applicability of these data to larger fires. Table 7-3 contains the dimensionless groups often associated with fire behavior ( $Fr$ ,  $St$ ,  $Q^*$ ,  $L_{flame}^*$ ) as well as dimensionless numbers specific to

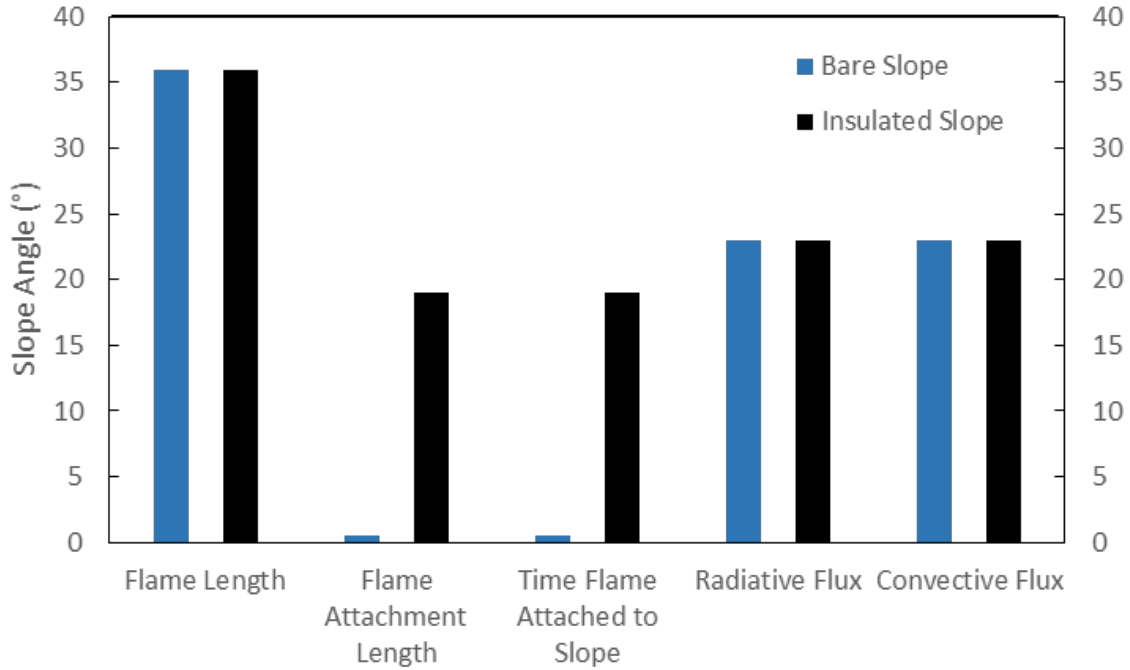


**Figure 7-13: Angle at which the deviation from control levels becomes significant for each the burn characteristics on the x-axis. Labels on the x-axis are those shown in Table 7-2. Pulse frequency is not shown here because there was no significant deviation from control levels.**

work with fires near slopes ( $L_{attach}^*$ ,  $q^{''*}$ ,  $S_A$ ,  $f_s$ ). Table 7-4 contains the values for intermediate variables necessary to calculate values of the dimensionless groups. Within the two tables,  $\frac{A}{F_{st}}$  is the stoichiometric air to fuel ratio,  $V_{fuel}$  is the fuel volume (5 mL),  $A_{cs}$  is the cross-sectional area of the fuel pan,  $m_{fuel}$  is the burning rate of the fuel,  $\Delta H_{comb}$  is the heat of combustion of the fuel,  $T_\infty$  is the ambient temperature,  $C_{p_\infty}$  is the constant pressure heat capacity at the ambient temperature,  $\rho_\infty$  is the density of air at ambient temperature and pressure,  $g$  is the gravitational acceleration constant and  $f$  is the flame pulsation frequency.

**Table 7-3: Dimensionless numbers relevant to fire behavior near slopes.**

Dimensionless Group	Value	Definition	Notes
<b>Froude number (Fr)</b>	1.006e-5	$\frac{v_e}{\sqrt{gd_j}}$	Standard definition, source (Hamins et al., 1995)
<b>Strouhal number (St)</b>	9384	$\frac{fd_j}{v_e}$	Standard definition, source (Hamins et al., 1995)
<b>Heat release rate (<math>Q^*</math>)</b>	0.784	$\frac{\dot{Q}}{\rho_\infty C_{p_\infty} T_\infty \sqrt{gd_j^5}}$	Standard definition, control burn, source (Heskestad, 1996)
<b>Flame length (<math>L_{flame}^*</math>)</b>	2.075	$\frac{L_{flame}}{d_j}$	Standard definition, control burn
<b>Flame attachment length (<math>L_{attach}^*</math>)</b>	Varies	$\frac{L_{attach}}{d_j}$	
<b>Heat flux upslope (<math>q^{''*}</math>)</b>	Varies	$\frac{\dot{q}''}{\rho_\infty C_{p_\infty} T_\infty \sqrt{gd_j}}$	
<b>Slope angle (<math>S_A</math>)</b>	Varies	Angle of slope from horizontal	
<b>Fuel stoichiometry (<math>f_s</math>)</b>	0.0619	$\frac{1}{1 + \frac{A}{F_{st}}}$	Fuel specific, source (Turns, 2011)

**Table 7-4: Variable definitions for use in dimensionless group calculations and experiment characterization.**

Variable	Value	Definition	Notes
<b>Burn Duration (<math>t_{burn}</math>)</b>	58.8 s	Duration of burn	All runs have same duration
<b>Velocity (<math>v_e</math>)</b>	1.013e-5 m s <sup>-1</sup>	$\frac{V_{fuel}}{t_{burn} A_{cs}}$	Assumes plug flow from fuel surface
<b>Diameter (<math>d_j</math>)</b>	0.1034 m	Diameter of circle whose area is the same as my burner	
<b>Heat Rate (<math>\dot{Q}</math>)</b>	2.578 kJ s <sup>-1</sup>	$m_{fuel} \dot{\Delta} H_{comb}$	

Figure 7-14 shows the dimensionless flame attachment length versus slope angle for each of the experimental conditions defined previously. Figure 7-15 shows the dimensionless heat

flux upslope from the fire versus slope angle. The solid line in each figure represents the value of the dimensionless quantity for the control burns (flame attachment length and heat flux upslope); the dashed line represents the dimensionless flame length and heat release rate, respectively. As seen in Figure 7-14, the dimensionless flame attachment length varies from the control flame attachment length to near the value of the standard dimensionless flame length. The dimensionless heat flux upslope from the fire (Figure 7-15) varies over an order of magnitude, but is still two orders of magnitude less than the standard dimensionless heat release rate. Using the data from these two figures, Equations 7-1 and 7-2 were developed to relate the dimensionless flame attachment length and heat flux to the standard definitions of dimensionless flame length and heat release rate. The  $R^2$  value for each correlation is shown directly below the equation.

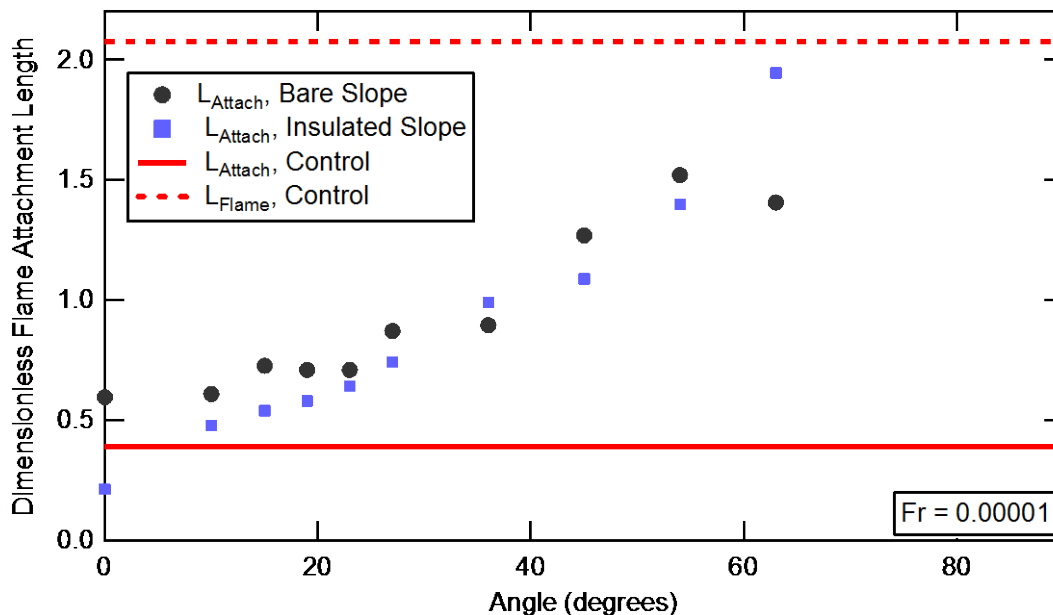


**Figure 7-14: Dimensionless flame attachment length ( $L_{Attach}$ ) versus slope angle. The solid line is the dimensionless attachment length for the control burns; the dashed line is the dimensionless flame length for the control burns.**

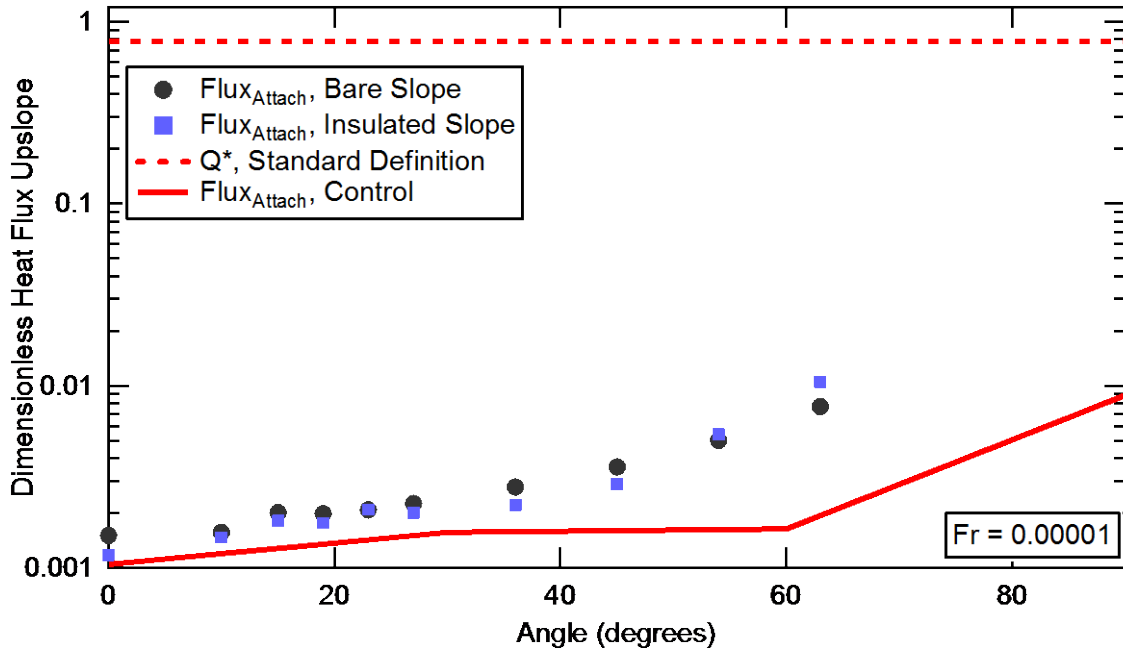


Figure 7-15: Dimensionless heat flux upslope ( $Flux_{Attach}$ ) versus slope angle. The solid line is the dimensionless heat flux for the control burns; the dashed line is the heat release rate for the control burns.

$$L_{Attach}^* = 0.1962 e^{0.0233S_A} L_{flame}^* \quad (7-1)$$

$$R^2 = 0.83$$

$$q^{''*} = 0.0014 e^{0.0281S_A} Q^* \quad (7-2)$$

$$R^2 = 0.90$$

Using Equations 7-1 and 7-2, it is possible to compare fire behavior data from documented wildland fires to what would be expected based on the work presented here. Data from five fires in which entrapment occurred were taken from the analysis completed by Butler (2014). Raw data, including ambient temperature ( $T_{\infty}$ ), terrain slope, wind speed, fuel load, fuel type and fuel heat of combustion ( $\Delta H_{comb}$ ) are shown in Table 7-5. Table 7-6 contains estimates of the flame height (FH) and rate of spread (ROS) for the five fires, as well as information

calculated from the data in Table 7-5, including jet diameter ( $d_j$ ), ambient heat capacity ( $C_{p_\infty}$ ), ambient density ( $\rho_\infty$ ), fuel burning rate ( $\dot{m}_{fuel}$ ) and heating rate ( $\dot{Q}$ ). Table 7-7 contains the resulting dimensionless flame length ( $L_{flame}^*$ ) and heat release rate ( $Q^*$ ).

**Table 7-5: Measured conditions for five documented wildland fires plus the control burns from the experiments presented in this work.**

Fire	$T_\infty$ (K)	Slope ( $^\circ$ )	Wind ( $m\ s^{-1}$ )	Fuel load ( $kg\ m^{-2}$ )	Fuel Type	$\Delta H_{comb}$ ( $MJ\ kg^{-1}$ )
<b>Baxter [2011]</b>	284	0	3	0.4	Grass	17.4 <sup>1</sup>
<b>Butte</b>	292	5	3.6	3	Lodgepole	21.53 <sup>2</sup>
<b>South Canyon</b>	300	31	15	1.5	Gambel oak	21.53
<b>Mann Gulch</b>	309	24	8	0.4	Timber/grass	17.4
<b>Battlement Creek</b>	306	22	13	1.5	Gambel oak	21.53
<b>Control</b>	295	0	0	5 mL	Heptane	45.0 <sup>3</sup>

<sup>1</sup>source (Overholt et al., 2014). <sup>2</sup>source (Susott et al., 1975). <sup>3</sup>source (Hamins et al., 1995).

**Table 7-6: Conditions for five documented wildland fires estimated from measured data, plus the control burns from the experiments presented in this work.**

Fire	$d_{jet}$ (m)	$C_{p_\infty}$ ( $J\ kg^{-1}\ K^{-1}$ )	$\rho_\infty$ ( $kg\ m^{-3}$ )	$\dot{m}_{fuel}$ ( $kg\ s^{-1}$ )	$\dot{Q}$ (MW)	ROS ( $m\ s^{-1}$ )	FH (m)
<b>Baxter [2011]</b>	1.66	1005	0.982	0.332	5.78	0.83	1.5
<b>Butte</b>	7.88	1005	1.01	0.443	9.54	0.985	80
<b>South Canyon</b>	14.3	1005	0.918	0.641	13.8	2.85	22.5
<b>Mann Gulch</b>	6	1005	1.01	0.48	8.35	3	7
<b>Battlement Creek</b>	5	1005	0.900	0.225	4.84	1	12
<b>Control</b>	0.103	1005	1.03	5.78e-5	0.0026	--	0.215

**Table 7-7: Estimates of the dimensionless flame length and heat release rate for five documented wildland fires and the control burns from the experiments presented in this work.**

<b>Fire</b>	$L_{flame}^*$	$Q^*$
<b>Baxter [2011]</b>	0.904	1.853
<b>Butte</b>	10.15	0.059
<b>South Canyon</b>	1.579	0.021
<b>Mann Gulch</b>	1.167	0.097
<b>Battlement Creek</b>	2.4	0.10
<b>Control</b>	2.075	0.784

The expected flame attachment and heat flux behavior for the five documented wildland fires were calculated using the results in Table 7-7 and Equations 7-1 and 7-2. The expected behavior is shown in Figure 7-16 and Figure 7-17 along with the data collected as part of this work. As seen in Figure 7-16, the dimensionless flame attachment lengths for all but the Butte fire are within 50% of the dimensionless flame attachment length for small-scale fires. The dimensionless heat flux values (Figure 7-17) for the five documented wildland fires are an order of magnitude lower than the small-scale experimental fires for all but the Baxter [2011] fire. Given the error associated with estimating information for actual fires, and the fact that half the parameters needed for this analysis were not measured for the five documented wildland fires analyzed here, the agreement between the small-scale fires measured for this work and the large-scale wildfires is surprising. While this work is by no means all-encompassing, it provides a basis from which to analyze other fire data and perform other experiments and model simulations in the future.

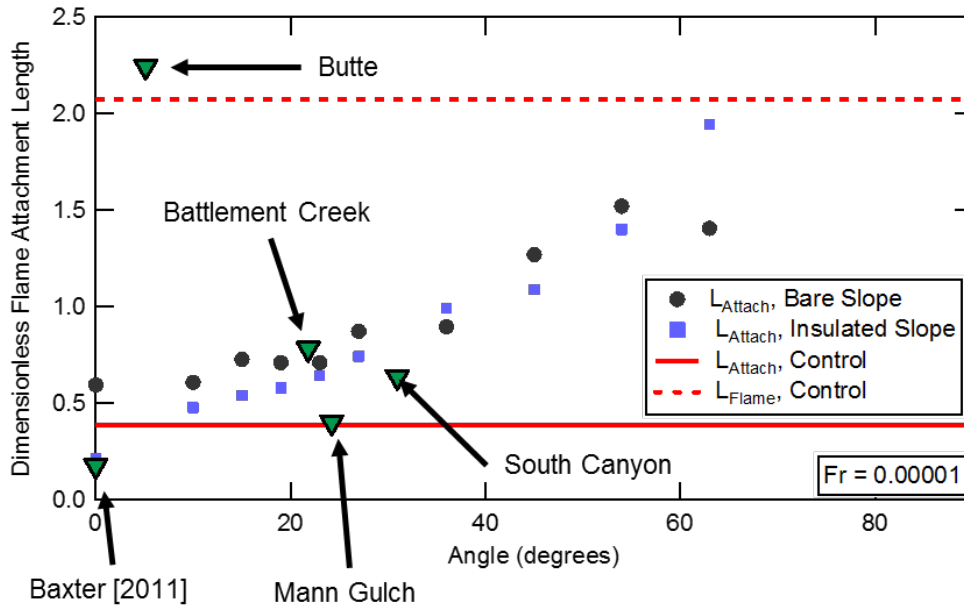


Figure 7-16: Dimensionless flame attachment length ( $L_{Attach}$ ) versus slope angle. The solid line is the dimensionless attachment length for the control burns; the dashed line is the dimensionless flame length for the control burns. The triangles represent the estimates of flame attachment from reported data for five documented wildland fires.

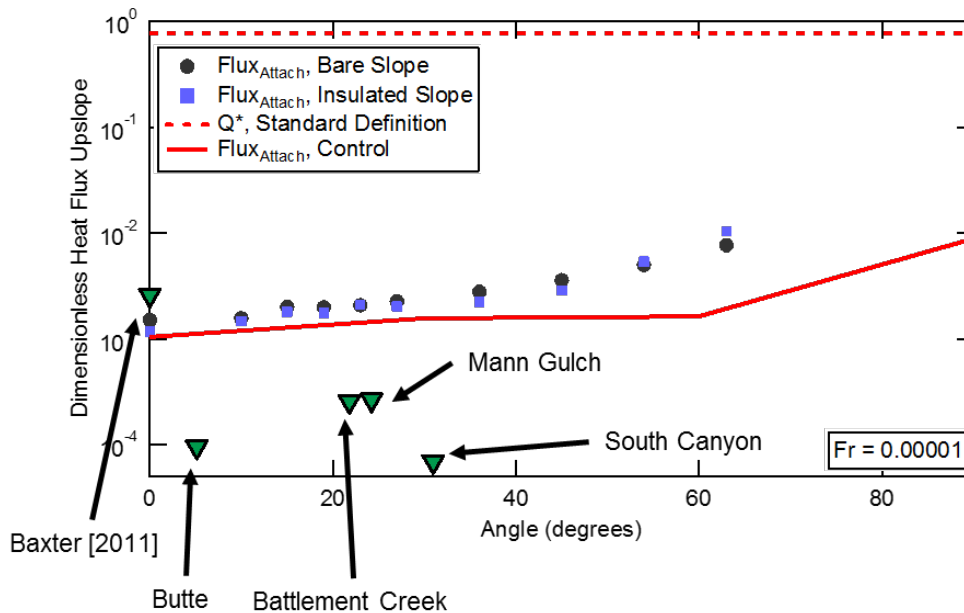


Figure 7-17: Dimensionless heat flux upslope ( $Flux_{Attach}$ ) versus slope angle. The solid line is the dimensionless heat flux for the control burns; the dashed line is the heat release rate for the control burns. The triangles represent the estimates of heat flux from reported data for five documented wildland fires.

### 7.3 Discussion

The results presented here agree with the results presented in the literature, namely that fire behavior is affected by the presence of a slope at low angles and that more work needs to be done before accurate adjustments to safety zone sizes can be made (Viegas, 2004; Butler, 2014). Several important considerations for future work are evident from the presented data, including: (1) more detailed work on the effects of distance and boundary condition, (2) the effect of flame pulsation on firefighter safety, (3) the effect of fuel properties (heat of combustion, solid versus liquid fuel), (4) the effect of scale, (5) the ability of physics-based fire models to accurately predict fire behavior near slopes, and (6) the inclusion of the Coanda effect in operational fire models. Each idea is discussed in the following paragraphs.

While the effects of distance and slope boundary condition are consistent throughout the results presented herein, it is likely that some of the results are specific to the apparatus used and do not reflect conditions as they might exist in the field. The effect of distance was small in these results; it is likely the effect of distance would be more pronounced at larger length scales. This is true for slope boundary condition as well. From a heat transfer perspective, it follows that an insulated boundary condition would cause lower heat loss to the environment and should result in a change flame behavior. It is not likely that a truly adiabatic boundary condition would ever exist in a wildland fire, but experimental data using a highly conductive slope and an insulated slope should bracket the behavior that would be seen in an actual fire. While the two boundary conditions studied were not significantly different in any of the burn characteristics measured, it is possible that a difference in flame behavior would exist if the “insulated” boundary condition was actually adiabatic.

Current safety zone models report radiative heat flux from a static flame. The effect of flame pulsation is not included in any of the models (Butler, 2014). While heat flux pulsation behavior was not captured consistently by the sensor used in this work, the combination of flame pulsation and maximum heat flux data indicate flame pulsation could have a large effect of safety zone size. This raises the question of the human response to intermittent heating. Is there a curve that defines the injury limit for the combination of heat flux and pulsation frequency? How much cooling would occur in the breaks between high heat fluxes? Finney et al. (2015) reported that fine fuel element heating to ignition in wildland fires is due in large part to intermittent heating. What effect does this have on firefighter safe considerations?

The effect of fuel properties and scale on fire behavior run together, and so will be discussed together. Wildland fires are often classified based on the relative influence of wind and buoyancy. The phrase used for this classification is the “power of the fire” versus the “power of the wind” (Pyne et al., 1996). A similar phrase could be used for fire behavior near slopes, except in this case the “power of the fire” is not competing with the Coanda effect, but rather the power of the fire enhances the Coanda effect. For example, van Hooff et al. (2012) reported that the Coanda effect increased with increasing Reynolds number. Thus, as flames get larger, the response of the flame is likely to be stronger attachment and higher heating upslope. Other considerations in the categories of fuel properties and scale include the influence of flame size on radiation (as the flames get larger, the radiation becomes more intense due to an increase in radiative path length) and the influence of fuel type (radiation from solid fuels would be present in wildland fires but not in pool fires). The dimensional analysis presented in this work illustrates the need for better understanding of scale and provides a foundation for further dimensional analysis and experimental work.

The ability of fire models to account for the Coanda effect is crucial to the development of better firefighter safety protocols. This is true for physics-based models and operational models. The ability of physics- and chemistry-based fire models to accurately predict fire behavior near slopes has not been explored. Once full-physics models have been verified to accurately account for the Coanda effect, these models can be used to explore conditions and scales not practical for experimental work and will hopefully lend important insights into firefighter safety. Work must also be done to add the influence of the Coanda effect into operational fire models so this knowledge can be applied in the field.

The preceding discussion identified several ideas for future work. They must all be understood to enhance firefighter safety.

#### **7.4 Summary and Conclusions**

Little is known about the influence of the Coanda effect on wildland fire behavior. Specifically, there is a lack of knowledge regarding how the Coanda effect influences firefighter safety zone considerations in rugged terrain. This chapter presents results for small-scale burn experiments testing the effect of slope angle, slope boundary condition and distance from flame base on fire behavior. The angle at which the specified flame characteristic deviated from the control flame characteristic is shown in Figure 7-13. This figure summarizes the results reported in this work and illustrates three main conclusions based on the experiments performed herein: (1) for most of the flame characteristics examined, there was no difference between a bare slope and an insulated slope, (2) the average angle at which the deviation from the control experiment occurred was between 20° and 40°, depending on the criteria used, (3) the traditional view of safe separation distance as being the distance from the flame base seems inadequate for fires near slopes. The last conclusion follows from the attachment behavior of flames near slopes; if the

fire is attached to the slope and leaning toward the firefighter, the distance from the flame itself is much shorter than the distance from the flame base.

While not specifically addressing the question of safety zone size, this work serves to identify several areas for future work so the question of safety zone size can be addressed adequately. These areas include: (1) more detailed work on the effects of distance and boundary condition, (2) the effect of flame pulsation on firefighter safety, (3) the effect of fuel properties (heat of combustion, solid versus liquid fuel), (4) the effect of scale, (5) the ability of fire models to accurately predict fire behavior near slopes, and (6) the inclusion of the Coanda effect in operational fire models. Each of these areas must be explored to better understand fire behavior near slopes and to better predict the size of safety zones for firefighters.

## **8 SUMMARY AND CONCLUSIONS**

### **8.1 Physical and Chemical Properties**

Physical and chemical properties for ten live fuels were measured throughout a one-year period. An alternate method for measuring foliage apparent density using oil instead of water was developed and used. Whole-leaf surface area measurements are reported that do not require approximating the sample with an idealized shape. Foliage dry mass distributions were developed that allow the user to calculate the dry mass for a single leaf or branch tip. Prediction models were developed for each measured property based on sample dry mass and moisture content. Most measured sample characteristics did not change throughout the year, making the use of a seasonal parameter in model development unnecessary. Sample characteristics that did change throughout the year were associated with changes in the other characteristics (usually moisture content) so that the models developed here are accurate for the entire year. It is anticipated that these models can be used in conjunction with bulk fuel description models and fuel placement models to describe the fuel matrix in detail for comprehensive fire spread models.

### **8.2 The Effects of Heating Mode on Ignition**

Ignition and burning behavior for ten live fuels were studied in a flat-flame burner apparatus to test the effect of heat transfer mode on live fuel combustion. Experiments were performed over a two-year period to see if and how the ignition and burning behavior changed in response to the different heating cases. The heating cases were using a convection-only heat

source, a radiation-only heat source, and both heat sources together. The convective heat flux was estimated to be  $75 \text{ kW m}^{-2}$  for a dead manzanita leaf and  $137 \text{ kW m}^{-2}$  for a dead Douglas-fir needle. The radiative heat flux was measured to be  $50 \text{ kW m}^{-2}$  for leaf species and calculated to be  $66 \text{ kW m}^{-2}$  for needle species.

Ignition did not occur in any of the unpiloted radiation-only experiments. Inclusion of a radiant flux in the convective environment of a flat-flame burner significantly decreased observed ignition times for broadleaf species but not for non-broadleaf species. This same behavior was seen when comparing the time required to reach 50% mass remaining. These results do not indicate radiation was unimportant, but rather that additional modes of heat transfer were needed to cause ignition under the conditions studied in this work. A comparison of mass remaining and surface temperature data with heat flux and heat absorbed data indicate it is the amount of energy rather than the type of energy that matters for surface reactions and mass loss. The data comparing mass loss with heat flux and heat absorbed measurements indicate it is possible to compare experimental results across heating modes provided the boundary conditions are similar. This is a critical first step in standardizing wildland fire experiments and knowledge transfer.

### **8.3 Seasonal Variations in Ignition and Burning Behavior**

Ignition and burning behavior for ten live fuels were studied in a flat-flame burner apparatus. Experiments were performed over a two-year period to test the effect of season (specifically moisture content) on ignition and burning behavior. The hypothesis was that moisture content would not change ignition and burning behavior except by increasing time to ignition, which is the observed behavior of wet wood.

Results comparing ignition and burning characteristics with moisture content and season were mixed. Ceanothus, Gambel oak, Douglas-fir and chamise all exhibited a positive correlation between ignition time and moisture content while the other six species show no correlation at a 95% significance level, indicating a simple relationship between moisture content and ignition is not adequate to describe ignition in live fuels. However, linear stepwise models capture much of the variability in ignition behavior. The results presented here indicate the most important predictors for ignition and flame behavior are moisture content, sample mass, apparent density (broad-leaf species), surface area (broad-leaf), sample width (needle species) and stem diameter (needle). The data also indicated lipid content, volatile fraction, fixed carbon and ash content were not significant predictors of the ignition and burning behavior measured under the conditions studied. Additionally, ignition behavior of live fuels in different seasons but at the same moisture content was different. These results suggest a relationship between moisture content and ignition that is different for live fuels than the relationship typically seen in dead fuels. Some of the seasonal influences on burning behavior seen in this work appear to be due to changes that occur on a larger time-scale than one year, such as a multi-year drought or gradual change in soil composition. Additional combustion experiments and detailed physiological measurements are suggested to improve theoretical understanding of fire spread in live fuels. In the absence of a theoretical understanding, simple statistical models were developed that describe fire behavior accurately and that use as inputs the same information currently used in most fire models.

#### **8.4 The Effect of Slope Angle on Fire Behavior**

Little is known about the influence of the Coanda effect on wildland fire behavior. Specifically, there is a lack of knowledge regarding how the Coanda effect influences firefighter

safety zone considerations in rugged terrain. Results for small-scale burn experiments testing the effect of slope angle, slope boundary condition and distance from flame base on fire behavior were presented as part of this dissertation. Four main conclusions follow from this work: (1) for most of the flame characteristics examined, there was no difference between a bare slope and an insulated slope, (2) the average angle at which the deviation from the control experiment occurred was between 20° and 40°, depending on the criteria used, (3) the dimensional analysis performed herein, although approximate due to the need to estimate some parameters for documented wildland fires, shows promise for comparing small-and large-scale fires, and (4) the traditional view of safe separation distance as being the distance from the flame base seems inadequate for fires near slopes. The last conclusion follows from the attachment behavior of flames near slopes; if the fire is attached to the slope and leaning toward the firefighter, the distance from the flame itself is much shorter than the distance from the flame base.

While these results do not answer the question of safety zone size directly, their utility lies in the identification of future research efforts that, when understood more fully, will help answer the question of safe separation distance. Several of these areas include: (1) more detailed work on the effects of distance and boundary condition on safety zone size based on fire scale, (2) the effect of flame pulsation on firefighter safety, (3) the effect of fuel properties (heat of combustion, solid versus liquid fuel), (4) the effect of scale, including using a non-dimensional analysis for wildland fire scaling, (5) the ability of fire models to accurately predict fire behavior near slopes, and (6) the inclusion of the Coanda effect in operational fire models and firefighter safety training modules. Each of these areas must be explored to better understand fire behavior near slopes and to better predict the size of safety zones for firefighters.

## 8.5 Recommended Future Work

Several questions that warrant further investigation have been identified as part of this work. They are presented below, categorized as work to improve the BYU Bush Model (Prince, 2014), work to develop a theoretical understanding of live-fuel combustion and work to develop better firefighter safety protocols.

- **BYU Bush Model**
  - Evaluate the use of LiDAR for fine-scale fuel placement.
  - Explore the effect of fuel canopy gaps with varying fire intensity.
  - Validate the Bush Model using landscape-scale data. Explore the use of remote sensing using UAV's for landscape mapping in fire models.
- **Live-Fuel Combustion Theory**
  - The combined results from all the live-fuel experiments presented in this dissertation indicate observed differences in ignition and burning behavior between species might be due to differences in fluid flow characteristics, and therefore heat and mass transfer rates, rather than to fundamental differences between plant species. Explore this idea using CFD or other models.
  - Measure the pyrolysis products of live fuels to identify possible differences between species.
  - Perform a more complete analysis of plant physiology as it affects combustion behavior. In particular, explore the burning behavior differences between C<sub>3</sub>, C<sub>4</sub> and crassulacean acid metabolism (CAM) plants.
- **Firefighter Safety Protocols**

- Perform more detailed work on the effects of distance and boundary condition.  
Work involving boundary conditions will help to bracket possible fire behavior and heat flux levels; work on distance is what will ultimately be used to determine safe separation distances.
- Explore the effect of flame and heat flux pulsation on firefighter safety.
- Explore the effect of fuel properties (heat of combustion, solid versus liquid fuel) and scale on firefighter safety.
- Evaluate the ability of fire models to accurately predict fire behavior near slopes and add the ability if necessary. This will allow testing of fire, terrain and environmental conditions not feasible in laboratory or field tests.
- Include the influence of the Coanda effect in operational fire models and the safe zone determination rules used in the field.

## REFERENCES

- Adalsteinsson, D. and J. A. Sethian, "The Fast Construction of Extension Velocities in Level Set Methods," *Journal of Computational Physics*, **148**(1), 2-22 (1999).
- Adams, M. A., "Mega-Fires, Tipping Points and Ecosystem Services: Managing Forests and Woodlands in an Uncertain Future," *Forest Ecology and Management*, **294**, 250-261 (2013).
- Adams, T., "Using Terrestrial LiDAR to Model Shrubs for Fire Behavior Simulation," MS Thesis, College of Forestry and Conservation, University of Montana (2014).
- Albini, F. A., "A Physical Model for Firespread in Brush," *Proceedings of the International Combustion Institute*, **11**, 553-560 (1967).
- Albini, F. A., "A Model for Fire Spread in Wildland Fuels by Radiation," *Combustion Science and Technology*, **42**(5-6), 229-258 (1985).
- Albini, F. A., "Wildland Fire Spread by Radiation - a Model Including Fuel Cooling by Natural Convection," *Combustion Science and Technology*, **45**(1-2), 101-113 (1986).
- Albini, F. A. and J. K. Brown, "Mathematical Modeling and Predicting Wildland Fire Effects," *Combustion Explosion and Shock Waves*, **32**(5), 520-533 (1996).
- Alessio, G. A., J. Penuelas, M. De Lillis and J. Llusia, "Implications of Foliar Terpene Content and Hydration on Leaf Flammability of *Quercus Ilex* and *Pinus Halepensis*," *Plant Biology*, **10**(1), 123-128 (2008).
- Alexander, M. E. and M. G. Cruz, "Assessing the Effect of Foliar Moisture on the Spread Rate of Crown Fires," *International Journal of Wildland Fire*, **22**, 415-427 (2013).
- Anderson, H. E., "Heat Transfer and Fire Spread," Research Paper INT-69, Intermountain Forest and Range Experimenta Station, Ogden, UT, USDA Forest Service (1969).
- Anderson, W. R., M. G. Cruz, P. M. Fernandes, L. Mccaw, J. A. Vega, R. A. Bradstock, L. Fogarty, J. Gould, G. McCarthy, J. B. Marsden-Smedley, S. Matthews, G. Mattingley, H. G. Pearce and B. W. van Wilgen, "A Generic, Empirical-Based Model for Predicting Rate of Fire Spread in Shrublands," *International Journal of Wildland Fire*, **24**(4), 443-460 (2015).

- Andrews, P. L., "BehavePLUS Fire Modeling System: Past, Present, and Future," Proceedings of the 7th Symposium on Fire and Forest Meteorology, Bar Harbor, MA (2007).
- Andrews, P. L., "Behaveplus Fire Modeling System, Version 4.0: Variable," General Technical Report RMRS-GTR-213WWW, Rocky Mountain Research Station, Fort Collins, CO, USDA Forest Service (2008).
- Babrauskas, V., "Ignition of Wood: A Review of the State of the Art," *Journal of Fire Protection Engineering*, **12**, 163-189 (2002).
- Babrauskas, V., Ignition Handbook, San Diego, CA, Fire Science Publishers, (2003).
- Baines, P. G., "Physical Mechanisms for the Propagation of Surface Fires," *Mathematical and Computer Modelling*, **13**(12), 83-94 (1990).
- Balbi, J.-H., J.-L. Rossi, T. Marcelli and P.-A. Santoni, "A 3D Physical Real-Time Model of Surface Fires across Fuel Beds," *Combustion Science and Technology*, **179**(12), 2511-2537 (2007).
- Balbi, J. H., P. A. Santoni and J. L. Dupuy, "Dynamic Modelling of Fire Spread across a Fuel Bed," *International Journal of Wildland Fire*, **9**(4), 275-284 (1999).
- Balbi, J. H., F. Morandini, X. Silvani, J. B. Filippi and F. Rinieri, "A Physical Model for Wildland Fires," *Combustion and Flame*, **156**(12), 2217-2230 (2009).
- Barbier, N., P. Coueron, J. P. Gastelly-Etchegorry and C. Proisy, "Linking Canopy Images to Forest Structural Parameters: Potential of a Modeling Framework," *Annals of Forest Science*, **69**(2), 305-311 (2012).
- Bartelink, H. H., "A Model of Dry Matter Partitioning in Trees," *Tree Physiology*, **18**(2), 91-101 (1998).
- Behm, A. L., M. L. Duryea, A. J. Long and W. C. Zipperer, "Flammability of Native Understory Species in Pine Flatwood and Hardwood Hammock Ecosystems Amd Implications for the Wildland-Urban Interface," *International Journal of Wildland Fire*, **13**, 355-365 (2004).
- Bianchi, L. O. and G. E. Defosse, "Live Fuel Moisture Content and Leaf Ignition of Forest Species in Andean Patagonia, Argentina," *International Journal of Wildland Fire*, **24**, 340-348 (2015).
- Billaud, Y., A. Kaiss, J. L. Consalvi and B. Porterie, "Monte Carlo Estimation of Thermal Radiation from Wildland Fires," *International Journal of Thermal Sciences*, **50**(1), 2-11 (2011).
- Britton, C., C. F. Lynch, J. Torner and C. Peek-Asa, "Fire Characteristics Associated with Firefighter Injury on Large Federal Wildland Fires," *Annals of Epidemiology*, **23**(2), 37-42 (2013).

- Brown, J. K., "Estimating Shrub Biomass from Basal Stem Diameters," *Canadian Journal of Forest Research*, **6**, 153-158 (1976).
- Brown, J. K., "Weight and Density of Crowns of Rocky Mountain Conifers," Research Paper INT-197, Intermountain Forest and Range Experiment Station, Ogden, UT, USDA Forest Service (1978).
- Browne, F. L., "Theories of the Combustion of Wood and Its Control: A Survey of the Literature," Report Number 2136, Forest Products Laboratory, Madison, WI, USDA Forest Service (1958).
- Bunsenberg, G., "Wildfire Management in the United States: The Evolution of a Policy Failure," *Review of Policy Research*, **21**, 145-156 (2004).
- Burgan, R. E. and R. A. Sussot, "Influence of Sample Processing Techniques and Seasonal Variation on Quantities of Volatile Compounds of Gallberry, Saw-Palmetto, and Wax Myrtle," *International Journal of Wildland Fire*, **1**(1), 57-62 (1991).
- Butler, B. W. and J. D. Cohen, "Firefighter Safety Zones: A Theoretical Model Based on Radiative Heating," *International Journal of Wildland Fire*, **8**(2), 73-77 (1998).
- Butler, B. W., J. Cohen, D. J. Latham, R. D. Schuette, P. Sopko, K. S. Shannon, D. Jimenez and L. S. Bradshaw, "Measurements of Radiant Emissive Power and Temperatures in Crown Fires," *Canadian Journal of Forest Research*, **34**(8), 1577-1587 (2004a).
- Butler, B. W., M. A. Finney, P. L. Andrews and F. A. Albini, "A Radiation-Driven Model for Crown Fire Spread," *Canadian Journal of Forest Research*, **34**(8), 1588-1599 (2004b).
- Butler, B. W., "Wildland Firefighter Safety Zones: A Review of Past Science and Summary of Future Needs," *International Journal of Wildland Fire*, **23**(3), 295-308 (2014).
- Carrier, G. F., F. E. Fendell and M. F. Wolff, "Wind-Aided Firespread across Arrays of Discrete Fuel Elements. 1. Theory," *Combustion Science and Technology*, **75**, 31-51 (1991).
- Carvel, R., "Lessons Learned from Catastrophic Fires in Tunnels," *Proceedings of the Institution of Civil Engineers-Civil Engineering*, **161**(6), 49-53 (2008).
- Catchpole, W. R., E. A. Catchpole, B. W. Butler, R. C. Rothermel, G. A. Morris and D. J. Latham, "Rate of Spread of Free-Burning Fires in Woody Fuels in a Wind Tunnel," *Combustion Science and Technology*, **131**(1-6), 1-37 (1998).
- Catchpole, W. R., E. A. Catchpole, A. G. Tate, B. W. Butler and R. C. Rothermel, "A Model for the Steady Spread of Fire through a Homogeneous Fuel Bed," IV International Conference on Forest Fire Research, Coimbra, Portugal (2002).
- Chao, Y. C. and C. Y. Wu, "A Study of the Interaction between a Jet Flame and a Lateral Wall," *Combustion Science and Technology*, **158**, 93-113 (2000).

- Clark, M. M., "Development and Evaluation of a Sub-Grid Combustion Model for a Landscape Scale for 3D Wildland Fire Simulator," PhD Dissertation, Chemical Engineering, BYU (2008).
- Clark, M. M., T. H. Fletcher and R. R. Linn, "A Sub-Grid, Mixture-Fraction-Based Thermodynamic Equilibrium Model for Gas Phase Combustion in FIRETEC: Development and Results," *International Journal of Wildland Fire*, **19**(2), 202-212 (2010).
- Coen, J. L., M. Cameron, J. Michalakes, E. G. Patton, P. J. Riggan and K. M. Yedinak, "WRF-Fire: Coupled Weather-Wildland Fire Modeling with the Weather Research and Forecasting Model," *Journal of Applied Meteorology and Climatology*, **52**(1), 16-38 (2013).
- Coen, J. L. and P. J. Riggan, "Simulation and Thermal Imaging of the 2006 Esperanza Wildfire in Southern California: Application of a Coupled Weather-Wildland Fire Model," *International Journal of Wildland Fire*, **23**(6), 755-770 (2014).
- Cohen, J. D., "Estimating Fire Behavior with Firecast User's Manual," General Technical Report PSW 90, Pacific Southwest Forest and Range Experiment Station, Berkeley, CA, USDA Forest Service (1986).
- Cohen, J. D. and M. A. Finney, "An Examination of Fuel Particle Heating During Fire Spread," VI International Conference on Forest Fire Research, Coimbra, Portugal (2010).
- Cole, W. J., B. M. Pickett, T. H. Fletcher and D. R. Weise, "A Semi-Empirical Multi-Leaf Model for Fire Spread through a Manzanita Shrub," 6th U.S. National Combustion Meeting, Ann Arbor, MI (2009).
- Cole, W. J., M. H. Dennis, T. H. Fletcher and D. R. Weise, "The Effects of Wind on the Flame Characteristics of Individual Leaves," *International Journal of Wildland Fire*, **2011**(2), 657-667 (2011).
- Countryman, C. M. and C. W. Philpot, "Physical Characteristics of Chamise as a Wildland Fuel," Research Paper PSW 66, Forest and Range Experiment Station, Berkeley, CA, USDA Forest Service (1970).
- Countryman, C. M., "Physical Characteristics of Some Northern California Brush Fuels," General Technical Report PSW-61, Pacific Southwest Forest and Range Experiment Station, Berkeley, CA, USDA Forest Service (1982).
- Cowan, P. D., "Flammability, Physiology and Coexistence in Fire Prone Environments," PhD Dissertation, Integrative Biology, University of California Berkeley (2010).
- Dennison, P. E., G. K. Fryer and T. J. Cova, "Identification of Firefighter Safety Zones Using Lidar," *Environmental Modelling & Software*, **59**, 91-97 (2014).

- Dimitrakopoulos, A. P., "Thermogravimetric Analysis of Mediterranean Plant Species," *Journal of Analytical and Applied Pyrolysis*, **60**(2), 123-130 (2001).
- Dimitrakopoulos, A. P. and K. K. Papaioannou, "Flammability Assessment of Mediterranean Forest Fuels," *Fire Technology*, **37**(2), 143-152 (2001).
- Drysdale, D. D., A. J. R. Macmillan and D. Shilitto, "The Kings-Cross Fire - Experimental-Verification of the Trench Effect," *Fire Safety Journal*, **18**(1), 75-82 (1992).
- Dunlap, F., "The Specific Heat of Wood," *USDA Forest Service Products Laboratory Bulletin*, **110**, 28 (1912).
- Dupuy, J. L., J. Maréchal and D. Morvan, "Fires from a Cylindrical Forest Fuel Burner: Combustion Dynamics and Flame Properties," *Combustion and Flame*, **135**(1-2), 65-76 (2003).
- Elder, T., J. S. Kush and S. M. Hermann, "Thermogravimetric Analysis of Forest Understory Grasses," *Thermochimica Acta*, **512**, 170-177 (2011).
- Engstrom, J. D., J. K. Butler, S. G. Smith, L. L. Baxter, T. H. Fletcher and D. R. Weise, "Ignition Behavior of Live California Chaparral Leaves," *Combustion Science and Technology*, **176**(9), 1577-1591 (2004).
- Etlinger, M. G. and F. C. Beall, "Development of a Laboratory Protocol for Fire Performance of Landscape Plants," *International Journal of Wildland Fire*, **13**(4), 479-488 (2004).
- Fang, J. B. and F. R. Steward, "Flame Spread through Randomly Packed Fuel Particles," *Combustion and Flame*, **13**(4) (1969).
- Ferguson, S. C., A. Dahale, B. Shotorban, S. Mahalingam and D. R. Weise, "The Role of Moisture on Combustion of Pyrolysis Gases in Wildland Fires," *Combustion Science and Technology*, **185**(3), 435-453 (2013).
- Fernandes, P. M. and F. C. Rego, "A New Method to Estimate Fuel Surface Area-to-Volume Ratio Using Water Immersion," *International Journal of Wildland Fire*, **8**(2), 59-66 (1998).
- Finney, M. A., "Farsite: Fire Area Simulator - Model Development and Evaluation," Research Paper RMRS-RP-4 0502-5001, Rocky Mountain Forest and Range Experiment Station, Ogden, UT, USDA Forest Service (1998).
- Finney, M. A., "Fire Growth Using Minimum Travel Time Methods," *Canadian Journal of Forest Research-Revue Canadienne De Recherche Forestiere*, **32**(8), 1420-1424 (2002).
- Finney, M. A., I. C. Grenfell, C. W. McHugh, R. C. Seli, D. Trethewey, R. D. Stratton and S. Brittain, "A Method for Ensemble Wildland Fire Simulation," *Environmental Modeling & Assessment*, **16**(2), 153-167 (2011).

- Finney, M. A., J. D. Cohen, S. S. McAllister and W. M. Jolly, "On the Need for a Theory of Wildland Fire Spread," *International Journal of Wildland Fire*, **22**(1), 25 (2013).
- Finney, M. A., J. D. Cohen, J. M. Forthofer, S. S. McAllister, M. J. Gollner, D. J. Gorham, K. Saito, N. K. Akafuah, B. A. Adam and J. D. English, "Role of Buoyant Flame Dynamics in Wildfire Spread," *Proceedings of the National Academy of Sciences of the United States of America*, **112**(32), 9833-9838 (2015).
- Fire Executive Council, "Guidance for Implementation of Federal Wildland Fire Management Policy," Washington, D.C., USDA and US Department of Interior (2009).
- Flannigan, M., A. S. Cantin, W. J. de Groot, M. Wotton, A. Newbery and L. M. Gowman, "Global Wildland Fire Season Severity in the 21st Century," *Forest Ecology and Management*, **294**, 54-61 (2013).
- Fletcher, T. H., A. R. Kerstein, R. J. Pugmire, M. S. Solum and D. M. Grant, "Chemical Percolation Model for Devolatilization .3. Direct Use of C-13 NMR Data to Predict Effects of Coal Type," *Energy & Fuels*, **6**(4), 414-431 (1992).
- Fletcher, T. H., B. M. Pickett, S. G. Smith, G. S. Spittle, M. M. Woodhouse, E. Haake and D. R. Weise, "Effects of Moisture on Ignition Behavior of Moist California Chaparral and Utah Leaves," *Combustion Science and Technology*, **179**(6), 1183-1203 (2007).
- Fons, W. L., "Analysis of Fire Spread in Light Forest Fuels," *Journal of Agricultural Research*, **72**(13), 93-121 (1946).
- Fons, W. L., "Heating and Ignition of Small Wood Cylinders," *Industrial and Engineering Chemistry*, **42**(10), 2130-2133 (1950).
- Forest Products Laboratory, "Wood Handbook—Wood as an Engineering Material," Madison, WI: U.S., Department of Agriculture, Forest Service, Forest Products Laboratory: 508 (2010).
- Fox, J. S. and J. A. Stewart, "The Influence of the Coanda Effect on Heat Transfer from Combusting Gases," *Combustion Science and Technology*, **19**, 73-75 (1978).
- Frandsen, W. H., "Fire Spread through Porous Fuels from the Conservation of Energy," *Combustion and Flame*, **16**(1), 9-16 (1971).
- Frandsen, W. H., "Modeling Big Sagebrush as a Fuel," *Journal of Range Management*, **36**(5), 596-600 (1983).
- Fryer, G. K., P. E. Dennison and T. J. Cova, "Wildland Firefighter Entrapment Avoidance: Modelling Evacuation Triggers," *International Journal of Wildland Fire*, **22**(7), 883-893 (2013).

- Gao, Z. H., J. Ji, H. X. Wan, K. Y. Li and J. H. Sun, "An Investigation of the Detailed Flame Shape and Flame Length under the Ceiling of a Channel," *Proceedings of the Combustion Institute*, **35**, 2657-2664 (2015).
- Gill, A. M. and P. H. R. Moore, "Ignitability of Leaves of Australian Plants," Centre for Plant Biodiversity Research (1996).
- Gilmore, A. R., "Effects of Soil Moisture Stress on Monoterpenes in Loblolly Pine," *Journal of Chemical Ecology*, **3**, 667-676 (1977).
- Gratkowski, M. T., N. A. Dembsey and C. L. Beyler, "Radiant Smoldering Ignition of Plywood," *Fire Safety Journal*, **41**(6), 427-443 (2006).
- Green, L. R. and H. E. Schimke, "Guides for Fuel-Breaks in the Sierra Nevada Mixed-Conifer Type," Berkeley, CA, USDA Forest Service Pacific Southwest Forest and Range Experiment Station (1971).
- Gujarati, D. N., Basic Econometrics, New York, NY, McGraw-Hill, 363-370 (2003).
- Hamins, A., T. Kashiwagi and R. Buch, "Characteristics of Pool Fire Burning," Fire Resistance of Industrial Fluids, ASTM STP 1284, G. E. Totten and J. Reichel, Philadelphia, PA, American Society for Testing and Materials (1995).
- Haseli, Y., J. A. van Oijen and L. P. H. de Goeij, "Modeling Biomass Particle Pyrolysis with Temperature-Dependent Heat of Reactions," *Journal of Analytical and Applied Pyrolysis*, **90**(2), 140-154 (2011).
- Hawley, L. F., "Theoretical Considerations Regarding the Factors Which Influence Forest Fires," *Journal of Forestry*, **24**, 756-763 (1926).
- Helgeson, O. T., K. Cromack, S. Stafford, R. E. Miller and R. Slagle, "Equations for Estimating above-Ground Components of Young Douglas-Fir and Red Alder in a Coastal Oregon Plantation," *Canadian Journal of Forest Research*, **18**(8), 1082-1085 (1988).
- Henriksen, T. L., T. A. Ring, E. G. Eddings and G. J. Nathan, "Puffing Frequency and Soot Extinction Correlation in JP-8 and Heptane Pool Fires," *Combustion Science and Technology*, **180**(4), 699-712 (2008).
- Heskestad, G., "On  $Q^*$  and the Dynamics of Diffusion Flames," Thirteenth Meeting of the UNJR Panel on Fire Research and Safety, 1 (1996).
- Himoto, K., T. Tsuchihashi, Y. Tanaka and T. Tanaka, "Modeling the Trajectory of Window Flames with Regard to Flow Attachment to the Adjacent Wall," *Fire Safety Journal*, **44**(2), 250-258 (2009).
- Horwitz, W. and G. W. Latimer, Eds., AOAC Official Method 2003.05, Official Methods of Analysis of AOAC International, Gaithersburg, MD, AOAC International (2005).

- Hough, W. A., "Caloric Values of Some Forest Fuels of the Southern United States," Research Note SE-120, Southeastern Forest Experiment Station, Asheville, NC, USDA Forest Service (1969).
- Hu, L. H., F. Tang, M. A. Delichatsios, Q. Wang, K. H. Lu and X. C. Zhang, "Global Behaviors of Enclosure Fire and Facade Flame Heights in Normal and Reduced Atmospheric Pressures at Two Altitudes," *International Journal of Heat and Mass Transfer*, **56**(1-2), 119-126 (2013).
- Hull, M. K., C. A. O'Dell and M. J. Schroeder, "Critical Fire Weather Patterns-Their Frequency and Levels of Fire Danger," Pacific Southwest Forest and Range Experiment Station, Berkeley, CA, USDA Forest Service (1966).
- Incropera, F. P., D. P. Dewitt, T. L. Bergman and A. S. Lavine, Fundamentals of Heat and Mass Transfer, Hoboken, NJ, John Wiley & Sons, 426 (2007).
- Ji, J., C. G. Fan, Y. Z. Li, H. Ingason and J. H. Sun, "Experimental Study of Non-Monotonous Sidewall Effect on Flame Characteristics and Burning Rate of N-Heptane Pool Fires," *Fuel*, **145**, 228-233 (2015).
- Jolly, W. M., A. M. Hadlow and K. Huguet, "De-Coupling Seasonal Changes in Water Content and Dry Matter to Predict Live Conifer Foliar Moisture Content," *International Journal of Wildland Fire*, **23**(4), 480-489 (2014).
- Kainulainen, P., J. Oksanen, V. Palomaki, J. K. Holopainen and T. Holopainen, "Effect of Drought and Waterlogging Stress on Needle Monoterpenes of Picea Abies," *Canadian Journal of Botany*, **70**, 1613-1616 (1992).
- Kozlowsk, T. and J. J. Clausen, "Changes in Moisture Contents and Dry Weights of Buds and Leaves of Forest Trees," *Botanical Gazette*, **126**(1), 20-26 (1965).
- Lalli, F., A. Bruschi, R. Lama, L. Liberti, S. Mandrone and V. Pesarino, "Coanda Effect in Coastal Flows," *Coastal Engineering*, **57**(3), 278-289 (2010).
- LANDFIRE 1.2.0, "Existing Vegetation Type Layer," U. S. Department of Interior, Geological Survey (2010).
- Leroy, V., D. Cancellieri, E. Leoni and J. L. Rossi, "Kinetic Study of Forest Fuels by TGA: Model-Free Kinetic Approach for the Prediction of Phenomena," *Thermochimica Acta*, **497**(1-2), 1-6 (2010).
- Lindenmuth, A. W. J. and J. R. Davis, "Predicting Fire Spread in Arizona's Oak Chaparral," U. S. Service, Rocky Mountain Forest and Range Experiment Station: 1-12 (1973).
- Linn, R., J. Winterkamp, J. J. Colman, C. Edminster and J. D. Bailey, "Modeling Interactions between Fire and Atmosphere in Discrete Element Fuel Beds," *International Journal of Wildland Fire*, **14**(1), 37-48 (2005).

- Linn, R. R., "A Transport Model for Prediction of Wildfire Behavior," Dissertation, Mechanical Engineering, New Mexico State University (1997).
- Linn, R. R. and P. Cunningham, "Numerical Simulations of Grass Fires Using a Coupled Atmosphere-Fire Model: Basic Fire Behavior and Dependence on Wind Speed," *Journal of Geophysical Research-Atmospheres*, **110**(D13) (2005).
- Little, C. H. A., "Seasonal Changes in Carbohydrate and Moisture Content in Needles of Balsam Fir (*Abies-Balsamea*)," *Canadian Journal of Botany*, **48**(11), 2021-& (1970).
- Liu, Y. Q., S. Goodrick and W. Heilman, "Wildland Fire Emissions, Carbon, and Climate: Wildfire-Climate Interactions," *Forest Ecology and Management*, **317**, 80-96 (2014).
- Lozano, J. S., "An Investigation of Surface and Crown Fire Dynamics in Shrub Fuels," PhD Dissertation, Mechanical Engineering, University of California - Riverside (2011).
- Lu, H., J. Scott, B. Ripa, R. Farr and L. L. Baxter, "Effects of Particle Shape and Size on Black Liquor and Biomass Reactivity," Proceedings of Science in Thermal and Chemical Biomass Conversion, Victoria, BC, Canada (2004).
- Ludwig, J. A., J. F. Reynolds and P. D. Whitson, "Size-Biomass Relationships of Several Chihuahuan Desert Shrubs," *American Midland Naturalist*, **94**(2), 451-461 (1975).
- Lyons, P. R. A. and R. O. Weber, "Geometrical Effects on Flame Spread Rate for Wildland Fine Fuels," *Combustion Science and Technology*, **89**(1-4), 153-165 (1993).
- Maditinos, Z. and C. Vassiliadis, "Mega Fires: Can They Be Managed Effectively?," *Disaster Prevention and Management*, **20**(1), 41-52 (2011).
- Mardini, J., A. S. Lavine, V. K. Dhir and E. B. Anderson, "Heat and Mass Transfer in Live Fuel During the Process of Drying, Pyrolysis, and Ignition," Proceedings of the 1989 National Heat Transfer Conference (1989).
- Marino, E., J. L. Dupuy, F. Pimont, M. Guijarro, C. Hernando and R. Linn, "Fuel Bulk Density and Fuel Moisture Content Effects on Fire Rate of Spread: A Comparison between FIRETEC Model Predictions and Experimental Results in Shrub Fuels," *Journal of Fire Sciences*, **30**(4), 277-299 (2012).
- McAllister, S., I. Grenfell, A. Hadlow, W. M. Jolly, M. Finney and J. Cohen, "Piloted Ignition of Live Forest Fuels," *Fire Safety Journal*, **51**, 133-142 (2012).
- McCarter, R. J. and A. Broido, "Radiative and Convective Energy from Wood Crib Fires," *Pyrodynamics*, **2**(1), 65-85 (1965).
- McGrattan, K. B. and G. P. Forney, "Fire Dynamics Simulator (Version 4) - User's Guide," NIST Special Publication 1019, Gaithersburg, Maryland, USA, U.S. Dept. of Commerce, Technology Administration, National Institute of Standards and Technology (2005).

- McLean, D., Understanding Aerodynamics: Arguing from the Real Physics, Hoboken, New Jersey, John Wiley & Sons, 275 (2012).
- Mell, W., J. J. Charney, M. A. Jenkins, P. Cheney and J. Gould, "Numerical Simulations of Grassland Fire Behavior from the LANL - FIRETEC and NIST - WFDS Models," EastFIRE Conference, George Mason University, Fairfax, Virginia, USA (2005).
- Mell, W., M. A. Jenkins, J. Gould and P. Cheney, "A Physics-Based Approach to Modelling Grassland Fires," *International Journal of Wildland Fire*, **16**(1), 1-22 (2007).
- Mell, W. E., S. L. Manzello and A. Maranghides, "Numerical Modeling of Fire Spread through Trees and Shrubs," V International Conference on Forest Fire Research, Coimbra, Portugal (2006).
- Moghtaderi, B., V. Novozhilov, D. F. Fletcher and J. H. Kent, "A New Correlation for Bench-Scale Piloted Ignition Data of Wood," *Fire Safety Journal*, **29**, 41-59 (1997).
- Moodie, K., "The Kings-Cross Fire - Damage Assessment and Overview of the Technical Investigation," *Fire Safety Journal*, **18**(1), 13-33 (1992).
- Morandini, F., P. A. Santoni and J. H. Balbi, "The Contribution of Radiant Heat Transfer to Laboratory-Scale Fire Spread under the Influences of Wind and Slope," *Fire Safety Journal*, **36**, 519-543 (2001).
- Morvan, D. and J. L. Dupuy, "Modeling of Fire Spread through a Forest Fuel Bed Using a Multiphase Formulation," *Combustion and Flame*, **127**, 1981-1994 (2001).
- Morvan, D. and J. L. Dupuy, "Modeling the Propagation of a Wildfire through a Mediterranean Shrub Using a Multiphase Formulation," *Combustion and Flame*, **138**(3), 199-210 (2004).
- Narender, K., A. S. M. Rao, K. G. K. Rao and N. G. Krishna, "Thermo Physical Properties of Wrought Aluminum Alloys 6061, 2219 and 2014 by Gamma Ray Attenuation Method," *Thermochimica Acta*, **569**, 90-96 (2013).
- National Interagency Fire Center, "National Interagency Fire Center: Fire Information: Statistics: Suppression Costs (1985-2014)," Boise, ID, National Interagency Fire Center (2014).
- National Wildfire Coordinating Group, "NWCG Fireline Handbook," NWCG Handbook 3, PMS 410-1, NFES 0065, National Wildfire Coordinating Group, Boise, ID (2004).
- Nunez-Regueira, L., J. A. Rodriguez-Anon, J. Proupin, B. Mourino and R. A.-. Diaz, "Energetic Study of Residual Forest Biomass Using Calorimetry and Thermal Analysis," *Journal of Thermal Analysis and Calorimetry*, **80**, 457-464 (2005).
- Overholt, K. J., J. Cabrera, A. Kurzawski, M. Koopersmith and O. A. Ezekoye, "Characterization of Fuel Properties and Fire Spread Rates for Little Bluestem Grass," *Fire Technology*, **50**(1), 9-38 (2014).

- Owens, M. K., C.-D. Lin, J. Charles A. Taylor and S. G. Whisenant, "Seasonal Patterns of Plant Flammability and Monoterpenoid Content in *Juniperus Ashei*," *Journal of Chemical Ecology*, **24**(12), 2115-2129 (1998).
- Pagni, J., "Flame Spread over Thin Solid Fuels," *Journal of Heat Transfer*, **97**(1), 153-155 (1975).
- Parsons, R. A., W. E. Mell and P. McCauley, "Linking 3D Spatial Models of Fuels and Fire: Effects of Spatial Heterogeneity on Fire Behavior," *Ecological Modelling*, **222**(3), 679-691 (2011).
- Paudel, A., "Application of One Dimensional Turbulence (Odt) to Model Fire Spread through Biomass Fuel Bed," MS Thesis, Chemical Engineering Department, Brigham Young University (2013).
- Pellizzaro, G., P. Duce, A. Ventura and P. Zara, "Seasonal Variations of Live Moisture Content and Ignitability in Shrubs of the Mediterranean Basin," *International Journal of Wildland Fire*, **16**(5), 633-641 (2007).
- Peterson, S. H., "Using HFIRE for Spatial Modeling of Fire in Shrublands," Research Paper PSW-RP 259, Pacific Southwest Research Station, Albany, CA, USDA Forest Service (2009).
- Philpot, C. W., "Seasonal Changes in Heat Content and Ether Extractive Content of Chamise," Research Paper INT 61, Pacific Southwest Forest and Range Experiment Station, Berkely, CA, USDA Forest Service (1969).
- Philpot, C. W. and R. W. Mutch, "The Seasonal Trends in Moisture Content, Ether Extractives, and Energy of Ponderosa Pine and Douglas-Fir Needles," Research Paper PSW 66, Pacific Southwest Forest and Range Experiment Station, Berkely, CA, USDA Forest Service (1970).
- Pickett, B. M., "Effects of Moisture on Combustion of Live Wildland Forest Fuels," PhD Dissertation, Chemical Engineering Department, Brigham Young University (2008).
- Pickett, B. M., C. Isackson, R. Wunder, T. H. Fletcher, B. W. Butler and D. R. Weise, "Flame Interactions and Burning Characteristics of Two Live Leaf Samples," *International Journal of Wildland Fire*, **18**(7), 865-874 (2009).
- Pickett, B. M., C. Isackson, R. Wunder, T. H. Fletcher, B. W. Butler and D. R. Weise, "Experimental Measurements During Combustion of Moist Individual Foliage Samples," *International Journal of Wildland Fire*, **19**, 153-162 (2010).
- Pitts, W. M., "Ignition of Cellulosic Fuels by Heated and Radiative Surfaces," NIST Technical Note 1481, National Institute of Standards and Technology, U. S. Department of Commerce (2007).

- Prince, D. and T. H. Fletcher, "A Combined Experimental and Theoretical Study of the Combustion of Live Vs. Dead Leaves," 8th Meeting of the U. S. Joint Sections of the Combustion Institute, Park City, Utah (2013).
- Prince, D. and A. Lewis, "Proximate Analysis Hints," J. Gallacher (2013).
- Prince, D., "Measurement and Modeling of Fire Behavior in Leaves and Sparse Shrubs," PhD Dissertation, Chemical Engineering, Brigham Young University (2014).
- Prince, D. R., "Modeling a Burning Bush with and without Wind," International Association of Wildland Fire 3rd Fire Behavior and Fuels Conference, Spokane, WA (2010).
- Prince, D. R., M. E. Fletcher, C. Shen and T. H. Fletcher, "Application of L-Systems to Geometrical Construction of Chamise and Juniper Shrubs," *Ecological Modelling*, **273**, 86-95 (2014).
- Prince, D. R. and T. H. Fletcher, "Differences in Burning Behavior of Live and Dead Leaves, Part 1: Measurements," *Combustion Science and Technology*, **186**(12), 1844-1857 (2014).
- Pyne, S. J., P. L. Andrews and R. D. Laven, Introduction to Wildland Fire, New York, John Wiley & Sons, (1996).
- Raimundo, A. M. and A. R. Figueiredo, "Personal Protective Clothing and Safety of Firefighters near a High Intensity Fire Front," *Fire Safety Journal*, **44**(4), 514-521 (2009).
- Rehm, R. and R. McDermott, "Fire-Front Propagation Using the Level Set Method," NIST Technical Note 1611, National Institute of Standards and Technology, Gaithersburg, MD, (2009).
- Reszka, P. and J. L. Torero, "In-Depth Temperature Measurements in Wood Exposed to Intense Radiant Energy," *Experimental Thermal and Fluid Science*, **32**(7), 1405-1411 (2008).
- Rodriguez Anon, J. A., F. F. Lopez, J. P. Castineiras, J. P. Ledo and R. Nuneza, L., "Calorific Values and Flammability for Forest Wastes During the Seasons of the Year," *Bioresource Technology*, **52**, 267-274 (1995).
- Rossi, J. L., A. Simeoni, B. Moretti and V. Leroy-Cancellieri, "An Analytical Model Based on Radiative Heating for the Determination of Safety Distances for Wildland Fires," *Fire Safety Journal*, **46**(8), 520-527 (2011).
- Rothermel, R. C., "A Mathematical Model for Predicting Fire Spread in Wildland Fuels," Research Paper INT-115, Intermountain Forest and Range Experiment Station, Ogden, UT, USDA Forest Service (1972).
- Rothermel, R. C. and C. W. Philpot, "Predicting Changes in Chaparral Flammability," *Journal of Forestry*, **71**, 640-643 (1973).

- Ryan, K. C. and S. G. Pickford, "Physical Properties of Woody Fuels in the Blue Mountains of Oregon and Washington," Research Note PNW-315, Pacific Northwest Forest and Range Experiment Station, Portland, OR, USDA Forest Service (1978).
- Sackett, S. S., "Woody Fuel Particle Size and Specific Gravity of Southwestern Tree Species " Research Note RM-389, Rocky Mountain Forest and Range Experiment Station, Ft. Collins, CO, USDA Forest Service (1980).
- Schlecht, R. M. and D. L. R. Affleck, "Branch Aggregation and Crown Allometry Condition the Precision of Randomized Branch Sampling Estimators of Conifer Crown Mass," *Canadian Journal of Forest Research*, **44**(5), 499-508 (2014).
- Schwilk, D. W., "Flammability Is a Niche Construction Trait: Canopy Architecture Affects Fire Intensity," *American Naturalist*, **162**(6), 725-733 (2003).
- Seielstad, C., C. Stonesifer, E. Rowell and L. Queen, "Deriving Fuel Mass by Size Class in Douglas-Fir (*Pseudotsuga Menziesii*) Using Terrestrial Laser Scanning," *Remote Sensing*, **3**(8), 1691-1709 (2011).
- Shen, C., "Application of Fuel Element Combustion Properties to a Semi-Empirical Flame Propagation Model for Live Wildland Utah Shrubs," MS Thesis, Chemical Engineering, Brigham Young University (2013).
- Shen, C., M. E. Fletcher, J. R. Gallacher, D. R. Prince, T. H. Fletcher, C. A. Seielstad and D. R. Weise, "Experiments and Modeling of Fire Spread in Big Sagebrush and Chamise Shrubs in a Wind Tunnel," Western States Section of the Combustion Institute Fall 2015 Meeting, Provo, UT (2015).
- Shen, C. and T. H. Fletcher, "Fuel Element Combustion Properties for Live Wildland Utah Shrubs," *Combustion Science and Technology*, **187**(3), 428-444 (2015).
- Shu, L., X. Tian and X. Kou, "Studies on Selection of Fire Resistance Tree Species for Sub-Tropical Area of China," Proceedings of 4th Asia-Oceania Symposium on Fire Science & Technology, Tokyo, Japan (2000).
- Silvani, X. and F. Morandini, "Fire Spread Experiments in the Field: Temperature and Heat Fluxes Measurements," *Fire Safety Journal*, **44**(2), 279-285 (2009).
- Simms, L., "Ignition of Cellulosic Materials by Radiation," *Combustion and Flame*, **4**(4), 293-300 (1960).
- Simms, L., "On the Pilot Ignition of Wood by Radiation," *Combustion and Flame*, **7**(3), 253-261 (1963).
- Simms, L. and M. Law, "The Ignition of Wet and Dry Wood by Radiation," *Combustion and Flame*, **11**(5), 377-388 (1967).

- Singh, N. K. and K. Ramamurthi, "Formation of Coanda Jet from Sharp-Edged Swirl Nozzle with Base Plate," *Experimental Thermal and Fluid Science*, **33**(4), 675-682 (2009).
- Skowronski, N., K. Clark, R. Nelson, J. Hom and M. Patterson, "Remotely Sensed Measurements of Forest Structure and Fuel Loads in the Pinelands of New Jersey," *Remote Sensing of Environment*, **108**(2), 123-129 (2007).
- Skowronski, N. S., K. L. Clark, M. Duveneck and J. Hom, "Three-Dimensional Canopy Fuel Loading Predicted Using Upward and Downward Sensing Lidar Systems," *Remote Sensing of Environment*, **115**(2), 703-714 (2011).
- Smith, E. A., D. O'Loughlin, J. R. Buck and S. B. St Clair, "The Influences of Conifer Succession, Physiographic Conditions and Herbivory on Quaking Aspen Regeneration after Fire," *Forest Ecology and Management*, **262**(3), 325-330 (2011).
- Smith, S. G., "Effects of Moisture on Combustion Characteristics of Live California Chaparral and Utah Foliage," MS Thesis, Chemical Engineering Department, Brigham Young University (2005).
- Smith, W. K. and J. B. King, "Surface Temperature of Materials During Radiant Heating to Ignition," *Journal of Fire and Flammability*, **1**, 272-288 (1970).
- Stavros, E. N., J. Abatzoglou, N. K. Larkin, D. McKenzie and E. A. Steel, "Climate and Very Large Wildland Fires in the Contiguous Western USA," *International Journal of Wildland Fire*, **23**(7), 899-914 (2014).
- Steele, J., "Effective Firefighter Safety Zone Size: A Perception of Firefighter Safety," 4th International Wildland Fire Safety Summit, Edmonton, Alberta, Canada (2000).
- Stephens, S. L. and L. W. Ruth, "Federal Forest-Fire Policy in the United States," *Ecological Applications*, **15**, 532-542 (2005).
- Stocks, B. J., M. E. Alexander, B. M. Wotton, C. N. Steffner, M. D. Flannigan, S. W. Taylor, N. Lavoie, J. A. Mason, G. R. Hartley, M. E. Maffey, G. N. Dalrymple, T. W. Blake, M. G. Cruz and R. A. Lanoville, "Crown Fire Behaviour in a Northern Jack Pine Black Spruce Forest," *Canadian Journal of Forest Research*, **34**(8), 1548-1560 (2004).
- Sullivan, A. L., P. F. Ellis and I. K. Knight, "A Review of Radiant Heat Flux Models Used in Bushfire Applications," *International Journal of Wildland Fire*, **12**, 101-110 (2003).
- Sullivan, A. L., "Wildland Surface Fire Spread Modelling, 1990-2007. 1: Physical and Quasi-Physical Models," *International Journal of Wildland Fire*, **18**(4), 349-368 (2009a).
- Sullivan, A. L., "Wildland Surface Fire Spread Modelling, 1990-2007. 2: Empirical and Quasi-Empirical Models," *International Journal of Wildland Fire*, **18**(4), 369-386 (2009b).

- Sullivan, A. L., "Wildland Surface Fire Spread Modelling, 1990-2007. 3: Simulation and Mathematical Analogue Models," *International Journal of Wildland Fire*, **18**(4), 387-403 (2009c).
- Sunol, A., D. Vucinic and S. Vanlanduit, "CFD Modelling of the Coanda Based Thrust Vectoring Nozzle," *Engineering Applications of Computational Fluid Dynamics*, K. Shaari, K. Zilati and M. Awang, New York, New York, Springer International Publishing: 73-84 (2015).
- Susott, R. A., W. F. Degroot and F. Shafizadeh, "Heat Content of Natural Fuels," *Journal of Fire and Flammability*, **6**, 311-325 (1975).
- Susott, R. A., "Thermal Behavior of Conifer Needle Extractives," *Forest Science*, **26**(3), 347-360 (1980).
- Susott, R. A., "Characterization of the Thermal Properties of Forest Fuels by Combustible Gas Analysis," *Forest Science*, **28**(2), 404-420 (1982).
- Tang, F., L. H. Hu, M. A. Delichatsios, K. H. Lu and W. Zhu, "Experimental Study on Flame Height and Temperature Profile of Buoyant Window Spill Plume from an under-Ventilated Compartment Fire," *International Journal of Heat and Mass Transfer*, **55**(1-3), 93-101 (2012).
- Tiaz, L. and E. Zeiger, *Plant Physiology, 5th Ed.*, Sunderland, MA, Sinauer Associates, Inc., (2010).
- Turns, S. R., *An Introduction to Combustion: Concepts and Applications*, New York, NY, McGraw-Hill, 21 (2011).
- van Hooff, T., B. Blocken, T. Defraeye, J. Carmeliet and G. J. F. van Heijst, "PIV Measurements and Analysis of Transitional Flow in a Reduced-Scale Model: Ventilation by a Free Plane Jet with Coanda Effect," *Building and Environment*, **56**, 301-313 (2012).
- Viegas, D. X., "On the Existence of a Steady State Regime for Slope and Wind Driven Fires," *International Journal of Wildland Fire*, **13**(1), 101-117 (2004).
- Vogel, M. and F. R. Williams, "Flame Propagation Along Matchstick Arrays," *Combustion Science and Technology*, **1**, 429-436 (1970).
- Wagtendonk, J. W. v., J. M. Benedict and W. M. Sydoriak, "Physical Properties of Woody Fuel Particles of Sierra Nevada Conifers," *International Journal of Wildland Fire*, **6**(3), 117-123 (1996).
- Wan, H. Y., A. C. Rhodes and S. B. St Clair, "Fire Severity Alters Plant Regeneration Patterns and Defense against Herbivores in Mixed Aspen Forests," *Oikos*, **123**(12), 1479-1488 (2014).

- Weber, R. O., "Modeling Fire Spread through Fuel Beds," *Progress in Energy and Combustion Science*, **17**(1), 67-82 (1991).
- Weise, D. R., R. H. White, F. C. Beall and M. Etlinger, "Use of the Cone Calorimeter to Detect Seasonal Differences in Selected Combustion Characteristics of Ornamental Vegetation," *International Journal of Wildland Fire*, **14**(3), 321-338 (2005a).
- Weise, D. R., X. Zhou, L. Sun and S. Mahalingam, "Fire Spread in Chaparral - "Go or No-Go?"," *International Journal of Wildland Fire*, **14**(1), 99-106 (2005b).
- Weise, D. R. and C. S. Wright, "Wild Land Fire Emissions, Carbon and Climate: Characterizing Wildland Fuels," *Forest Ecology and Management*, **317**, 26-40 (2014).
- Werth, P., "Critical Fire Weather Patterns," Wildland Fire Lessons Learned Center Webinar Series, J. McDaniel (2015).
- White, C. S., "Monoterpenes—Their Effects on Ecosystem Nutrient Cycling," *Journal of Chemical Ecology*, **20**, 1381-1406 (1994).
- White, R. H. and W. C. Zipperer, "Testing and Classification of Individual Plants for Fire Behaviour: Plant Selection for the Wildland-Urban Interface," *International Journal of Wildland Fire*, **19**(2), 213-227 (2010).
- Williams, C. C., "Damage Initiation in Organic Materials Exposed to High-Intensity Thermal Radiation," PhD Dissertation, Chemical Engineering, Massachusetts Institute of Technology (1953).
- Williams, J., "Exploring the Onset of High-Impact Mega-Fires through a Forest Land Management Prism," *Forest Ecology and Management*, **294**, 4-10 (2013).
- Williams, R. A., "Use of Randomized Branch and Importance Sampling to Estimate Loblolly Pine Biomass," *Southern Journal of Applied Forestry*, **13**(4), 181-184 (1989).
- Wotton, B. M., M. E. Alexander and S. W. Taylor, "Updates and Revisions to the 1992 Canadian Forest Fire Behavior Prediction System," Information Report GLC-X-10, Great Lakes Forestry Centre, Canadian Forest Service Natural Resources Canada (2009).
- Wright, C. S., "Fuel Consumption Models for Pine Flatwoods Fuel Types in the Southeastern United States," *Southern Journal of Applied Forestry*, **37**(3), 148-159 (2013).
- Wright, H. A. and A. W. Bailey, Fire Ecology: United States and Southern Canada, New York, John Wiley & Sons, (1982).
- Xanthopoulos, G. and R. H. Wakimoto, "A Time to Ignition-Temperature-Moisture Relationship for Branches of Three Western Conifers," *Canadian Journal of Forest Research*, **23**(253-258) (1993).

Zarate, L., J. Arnaldos and J. Casal, "Establishing Safety Distances for Wildland Fires," *Fire Safety Journal*, **43**(8), 565-575 (2008).



## **APPENDIX**

- A. Preliminary Riverside Results
- B. Prediction Model Parity Plots
- C. Experimental Data
- D. Data Processing and Model Development Algorithms

## **A. PRELIMINARY RIVERSIDE RESULTS**

The following work was presented at the U.S. National Combustion Institute Meeting in Cincinnati, OH in May, 2015. This work was a collaboration between Jonathan Gallacher and Chen Shen. More details will be given regarding experimental and modeling results in Chen Shen's PhD dissertation.

### **A.1 Introduction**

Operational models can be used to predict the spread of wildland fires and prescribed burns. Most current models (e.g. BehavePlus, FARSITE, FlamMap) (Finney, 1998, 2002; Andrews, 2008; Finney et al., 2011) are based on the empirical spread model by Rothermel (1972), which was developed for dead and low-moisture fuels that are contiguous to the ground. These models do not adequately describe fire spread in live fuels such as those found in shrublands and tree crowns. Since much of the western United States is covered by sparsely growing shrubs and small trees (LANDFIRE 1.2.0, 2010), it is imperative that fire models be developed that can describe fire spread in live fuels. Development of a next-generation model is hindered by the lack of fundamental understanding regarding fire behavior in live fuels (McAllister et al., 2012; Finney et al., 2013).

Computational fluid dynamics models (CFD) have also been developed, including FIRETEC and WFDS (Linn, 1997; Mell et al., 2006; Clark et al., 2010). These models solve the governing equations for mass and energy balances rather than using empirical relationships and

thus provide insight into the physics and chemistry that influence fire spread. However, these models are computationally expensive and are generally constrained to 1 – 2 m<sup>3</sup> grid cells for landscape-scale simulations, oversimplifying the combustion process. Additionally, CFD models are restricted by inadequate knowledge regarding solid fuel physical properties (e.g. heat capacity) and surface reactions (Prince, 2014).

This paper describes a semi-empirical, multi-leaf shrub combustion model was developed to fill the gap between current operational models and CFD models. This model is based on individual leaf sample combustion behavior measured with a flat-flame burner (Pickett, 2008; Cole et al., 2009). Flames are simulated using equations based on individual leaf properties and combustion behavior; fire spread is accomplished via flame-fuel overlap. This model is computationally efficient while maintaining the essential components of fire spread models (Prince, 2014). The current model has several fuel models but has only been validated for manzanita.

## **A.2 Experimental Methods**

### **A.2.1 Shrub Combustion Experiment**

Multi-shrub combustion experiments were performed in the wind tunnel (see Figure A-1) at the USDA Forest Service Pacific Southwest Research Station in Riverside, CA. The fuel bed was designed to contain two shrubs in their natural arrangements (nominally 2m long x 1m wide x 1m high). A 200 g, triangular shaped bed of excelsior placed just upwind of the first shrub was used as the ignition source. The shrub closest to the excelsior bed was used as an ignition shrub and the fire was allowed to propagate to the second shrub, with the goal of measuring fire behavior without the influence of the excelsior bed. Continuous mass data were collected using a

Sartorius CPA34001s mass balance ( $< 2$  s response time, 0.1 g resolution). Fuel surface temperature was measured using a FLIR A20M infrared camera; gas temperature was measured using K-type thermocouples spaced throughout the fuel bed. Radiative and total heat flux downwind of the fuel bed was measured using a Hukseflux SBG01-200 heat flux sensor. The terminal end diameter of burned branches was measured as an indicator of fire intensity. The wind tunnel is open-roofed with doors on both sides. The doors on one side were open for video camera and FLIR camera recording. Shrub fuels were collected in the mountains near Riverside, CA.

Fuel density was varied between high and low values to explore the effect of local and overall fuel density on fire spread. Moisture content was also varied between high and low values by performing a set of experiments immediately after fuel collection and again after allowing the fuel to dry for approximately 48 hours in ambient air or one hour in a drying oven at 95 °C. Combustion characteristics and time-dependent fire behavior were measured using three digital camcorders at different locations around the fuel bed. For example, flame angle, fire propagation path, time to burnout and flame length were determined by processing the video image frames by a MATLAB code routine developed. Wind speed was held constant at 1.4 m s<sup>-1</sup>. Ambient temperature and relative humidity were recorded before each experiment. The effect of understory fuel was also explored in some experiments.

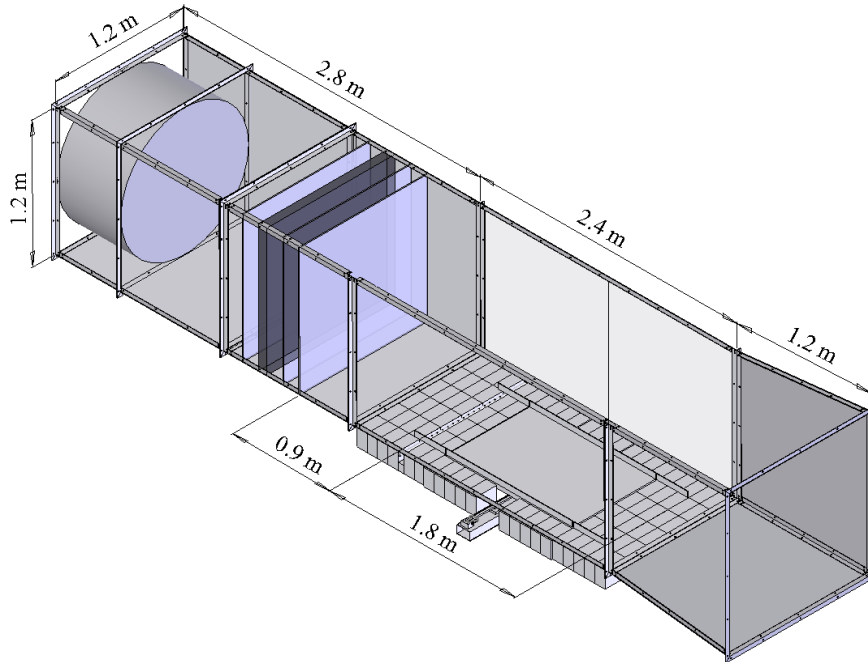


**Figure A-1: Schematic illustration of the wind tunnel at the Pacific Southwest Research Station of Forest service in Riverside, CA (Lozano, 2011)**

### **A. 2.2 Individual Leaf Combustion Experiment**

Individual live fuel sample combustion experiments were conducted for various species on a flat-flame burner (FFB) system (Pickett, 2008). The FFB has a porous surface and produces a 1 mm thin premixed flame ( $\text{CH}_4$ ,  $\text{H}_2$  and air). A glass cage surrounding the FFB prevents entrainment of ambient air. The fuel samples were placed 5 cm above the burner surface and ignited by the post-flame convective gases ( $1000\text{ }^\circ\text{C}$ , 10 mol%  $\text{O}_2$ ). Moisture content and geometric dimensions of each fuel sample were measured. The sample is held above the burner by a holding rod connected to a Mettler Toledo XS204 Cantilever mass balance; mass data are continuously measured using National Instruments Labview 8.6 Software. A K-type thermocouple (0.013 mm diameter, 0.05 s response time) was used to measure the gas temperature. Leaf sample combustion from ignition to burnout was recorded by a video camera. Combustion characteristics (e.g. flame height and time to ignition) were determined by image

analysis using an automated MATLAB code routine. The results of individual live fuel combustion experiments were used to develop statistical, species-specific correlations for combustion characteristics which describe the single flame growth behavior of each fuel element. These correlations were embedded in the semi-empirical, multi-leaf shrub combustion model.

### **A.3 Shrub Combustion Modeling**

The semi-empirical multi-leaf shrub combustion model developed at BYU includes following sections: fuel element locations, fuel element physical properties, fuel element combustion behavior, individual flame volume simulation and flame merging submodel (Engstrom et al., 2004; Smith, 2005; Fletcher et al., 2007; Pickett, 2008; Shen, 2013; Shen and Fletcher, 2015). Pickett developed the first-generation of this shrub combustion model in two dimensions for Manzanita shrubs. The flame merging was based on the two-leaf combustion experiments by Pickett (2008) and was treated as the expansion of each individual flame height when two flames overlapped. An individual leaf is ignited, and the flame height and flame angle is calculated from correlations developed from observations of burning individual leaves. As a neighboring leaf is contacted by a flame, the ignition sequence for that leaf commences, and that leaf ignites. The flames then merge and contact surrounding leaves until burnout occurs. The shrub combustion model was extended to three dimensions and improved through consideration of flame coalescence and wind effects on flame angle and size (Prince, 2010; Cole et al., 2011). Shen (2013) expanded fuel types and modified the individual flame volume simulation method to be capable of handling larger fuel sample flame. More species-specific shapes of fuel element placement were also developed.

Figure A-2 is an example of a manzanita shrub from the southern California and the associated model shrub constructed using an image recognition method. Fuel element detail properties, including total dry mass and number of stems, were determined by empirical correlations developed from either literature data or measurements in the field. Prince (2014) initiated an image recognition method to place the fuel elements. Fuel element placement was random within the project outline of the shrub. Prince also upgraded the flame interaction submodel to include semi-empirical correlations (shown in Equations A-1 through A-3) based on 2D flame merging experimental results reported in the literature. However, he considered both horizontal and vertical separation between leaf flames in three dimensions to approximate the merging flame height in shrub combustion model.

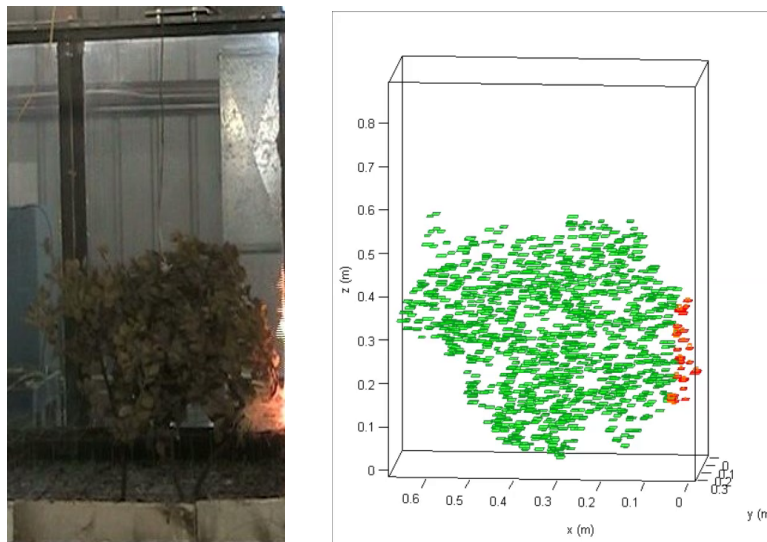


**Figure A-2: Comparison of (a) picture of a manzanita shrub and (b) manzanita shrub simulated.**

$$\left(\frac{L_m}{L_1}\right)_{N_2} - \left(\frac{L_m}{L_1}\right)_{N_1} = c_1 \ln\left(\frac{N_2}{N_1}\right) \quad (\text{A-1})$$

$$\hat{S}_{i,j} = \sqrt{\left(\frac{s_{i,j}}{r_{f,i}+r_{f,j}}\right)^2 + \left(\frac{z_i-z_j}{L_{f,j}}\right)^2} \quad (\text{A-2})$$

$$\frac{L_{f,i}}{L_{1,i}} = \left(\frac{v}{v_0}\right)^{c_3} \sum_{j=2}^{N^*} \left(\frac{c_1 \ln\left(\frac{j}{j-1}\right)}{1+c_2 \hat{S}_{i,j}}\right) + 1 \quad (\text{A-3})$$

In Equations A-1 through A-3,  $N_1$ ,  $N_2$  are number of fuel sources in two groups of flames;  $i, j$  are two different leaves (fuel sources);  $\hat{S}_{i,j}$  is the dimensionless separation distance;  $r$  denotes radius of leaf; and  $c_1$ ,  $c_2$  are coefficients obtained via literature data.

Prince (2014) established a physics-based submodel for scaling flame parameters. This submodel provided a mechanistic description of heat transfer to the leaf surface, tracked the temperature-dependent mass release and held the energy balance of the leaf. A multi-component one-step devolatilization model was used to compute the mass release of the dry matter components from the manzanita leaf. Water release was tracked by a diffusion-limited model. The mass transfer were dependent on the leaf temperature as well. Both convection and radiation were used to determine the elevated temperature of leaf. Finally, the heating of a leaf with the moisture evaporation was solved and the temperature history of a leaf was obtained. Based on this physics submodel, flame parameters (end time of mass release, flame height, etc.) were scaled to match the observed fire spread conditions.

## A.4 Results and Discussion

### A.4.1 Shrub Combustion Experiments

In total, 45 multi-shrub combustion experiments studying chamise and sagebrush were performed over a two-year period from 2012 to 2014. The experimental results presented here are for sagebrush only. Table A-1 shows the average results for 16 experimental runs (2 runs at each condition). In the table, runs that were considered low density are in italics. The average density for no understory experiments was  $17.8 \text{ kg m}^{-3}$  for the high density experiments and  $13.3 \text{ kg m}^{-3}$  for the low density experiments. None of the low density, no understory experiments (four runs) spread successfully. This suggests a spread, no-spread condition corresponding to a critical density. While the local fuel density measurements are still being analyzed, preliminary observations indicate that local fluctuations in fuel density also affect fire spread behavior. These results agree with those published by Parsons et al. (2011). The excelsior understory was meant to approximate grasses and dead fuels found near the base of wildland shrubs and was found to significantly increase flammability. Shrubs burned with an excelsior understory exhibited no “critical density” point—fire spread successfully in all experiments with an understory.

**Table A-1: Experimental data for 16 big sagebrush shrub combustion experiments.**

<b>Shrub Age (days)</b>	<b>Understory (Y/N)</b>	<b>MC (%)</b>	<b>Density (kg/m<sup>3</sup>)</b>	<b>Fraction Burned</b>	<b>Spread Success (Y/N)</b>	<b>Propagation Speed (cm/s)</b>
<i>4</i>	<i>N</i>	<i>14</i>	<i>14.5</i>	<i>0.156</i>	<i>N</i>	--
4	N	14	19.1	0.523	Y	1.3
<i>4</i>	<i>Y</i>	<i>10</i>	<i>12.1</i>	<i>0.701</i>	<i>Y</i>	<i>2.4</i>
4	Y	10	16.5	0.574	Y	2.0
<i>1</i>	<i>N</i>	<i>38</i>	<i>13.8</i>	<i>0.214</i>	<i>N</i>	--
1	N	37	21.0	0.790	Y	1.2
<i>1</i>	<i>Y</i>	<i>52</i>	<i>15.1</i>	<i>0.532</i>	<i>Y</i>	<i>2.2</i>
1	Y	38	15.5	0.594	Y	2.1

Age of the shrub had little effect on burn behavior under these conditions. Propagation speed, defined as the length of the fuel bed divided by the time of active fire spread, showed no difference between 1-day and 4-day shrubs. Propagation speed doubled with the addition of understory fuels, but the speeds themselves were the same between age groups. It is generally accepted that higher moisture content slows fire propagation, but that is not seen here. More work must be done to understand this result.

For analysis purposes, the bush data were divided into four equal, vertical sections and the maximum solid temperature was recorded from each frame for each section, as shown in Figure A-3 for a manzanita shrub burned with no wind. Area 1 was the upwind slice of the bush and area 4 was ignited last. Fuel surface temperatures showed a slow temperature rise until immediately before the fire reached the unburned fuel. Based on this, it was concluded that radiative pre-heating accounted for approximately one-third of the temperature rise prior to ignition.

Chamise stems smaller than  $\frac{1}{4}$  inch diameter burned at almost the same rate as the rest of the chamise shrub. In contrast, it was found that sagebrush stems burned more readily and longer than stems in other species (e.g., chamise). Figure A-4 is an example of burning big sagebrush stem after the leaf element fuel burnout.

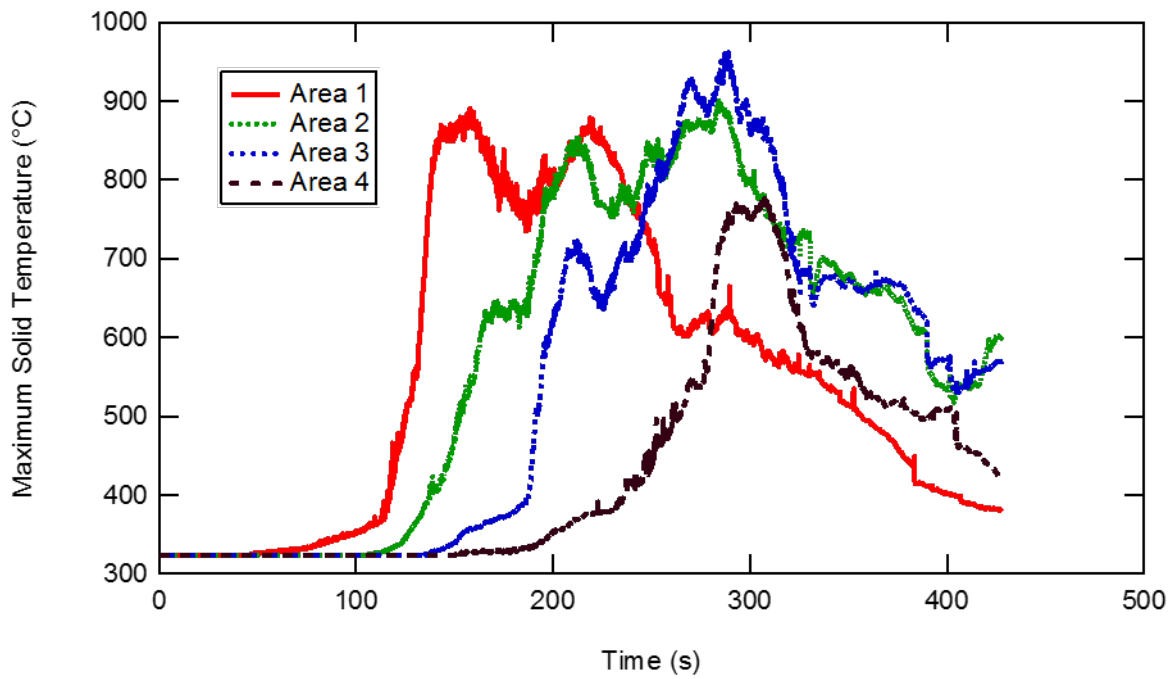


**Figure A-3: Maximum solid temperature of each area with respect to time for a manzanita shrub combustion experiment with no wind.**



**Figure A-4: Burning big sagebrush stems after the foliage burnout.**

#### A. 4.2 Shrub Combustion Modeling

The semi-empirical, multi-leaf shrub combustion model was constructed to model flame propagation through a user-defined manzanita shrub. Species-specific correlations and flame behavior submodels for burning behavior of individual manzanita leaves were incorporated into this model. A few of the flame merging and combustion parameters were tweaked to give good agreement with measured shrub flame behavior (Prince, 2014). The calculated flame height above the shrub ( $\Delta z_{f,max}$ ), fraction of shrub burnt ( $X_s$ ), burn time ( $t_{burn}$ ) as well as flame propagation speed and flame path were all compared with experimental results.

The calculations of  $\Delta z_{f,max}$  was underestimated and decreased with increasing wind speed in the previous shrub combustion model (Pickett, 2008), which contradicted experimental observations. The predicted burn times also did not match the measurements from the wind tunnel experiment well. The current shrub combustion model managed to match the trend of  $\Delta z_{f,max}$  obtained from experiments, as shown in the box plot (Figure A-5). The spread in the calculations was due to 30 different realizations with random placement of fuel elements within the project shrub volume. Predicted  $t_{burn}$  also agreed with the measured values, which was largely due to the physics-based scaling efforts by Prince (2014). The comparison is shown in Figure A-6. Flame merging was improved in the current shrub model by simulating group flames rather than separate individual flames. The flame simulation compared with flame behavior for a manzanita shrub is shown in Figure A-7.

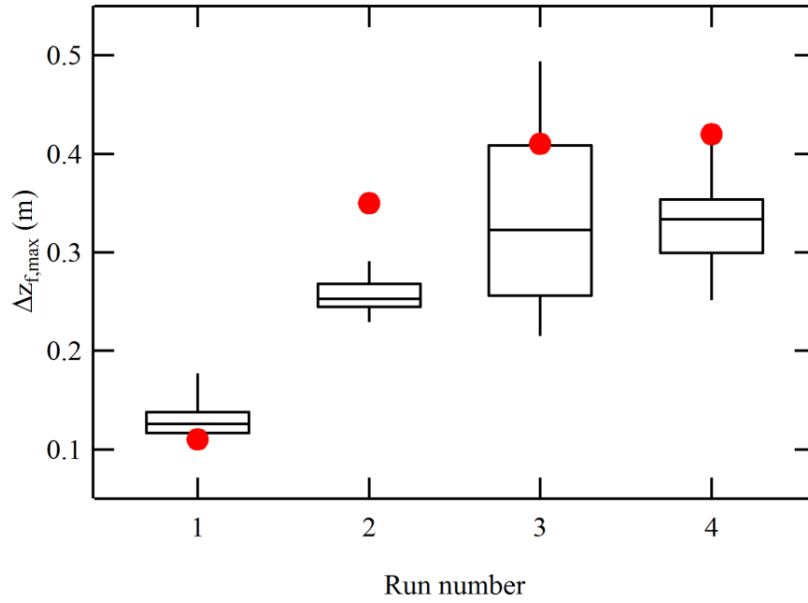


**Figure A-5:  $\Delta z_{f,max}$  comparison of current model (box plots of minimum, first quartile, median, third quartile and maximum) and wind tunnel experiments (dots) (Prince, 2014)**

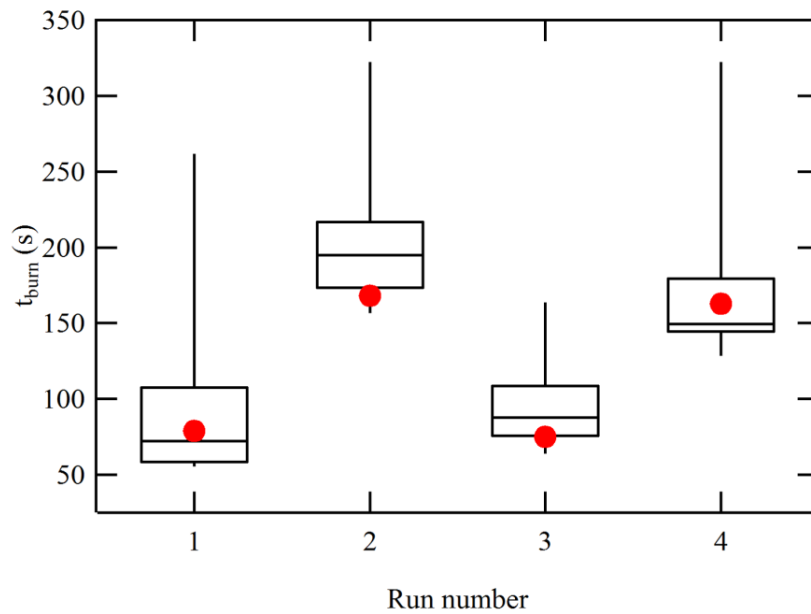


**Figure A-6: Burn time comparison of model simulations (box plots of minimum, first quartile, median, third quartile and maximum) and wind tunnel experiments (dots) (Prince, 2014)**

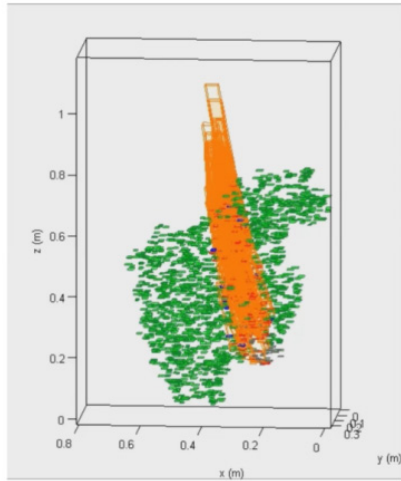


**Figure A-7: Comparison of predicted flame behavior in a manzanita shrub (left) using the semi-empirical shrub combustion model vs. the measured flame behavior in a wind tunnel.**

### **A.5 Future Work**

Fuel element placement was found to be critical to this model. Methods to better incorporate image recognition for fuel placement are being explored. Models for chamise and sagebrush are currently being developed as well. The image recognition will be combined with an L-systems fractal theory approach for chamise (Prince et al., 2014).

### **A.6 Conclusions**

Multi-shrub combustion experiments were performed in a wind tunnel facility at the Pacific Southwest Research Station in Riverside, CA. Bulk density and local fuel density were found to be two major factors in shrub flame propagation. Shrubs with high moisture content were usually observed to burn slower. Infrared observations of solid temperatures ahead of the flame front indicated that radiation heat transfer contributed about one-third of the temperature rise for pre-heating the fuel element prior to ignition. Calculated shrub flame propagation

behavior agreed well with observed flame height, flame tilt, flame path, and extent of burnout. More accurate 3D fuel placement development is currently in progress. Furthermore, a better flame merging submodel is being developed based on 3D flame merging experiments and correlations.

### **A.7 Acknowledgements**

This work was supported in part by JFSP Grant 11-1-2-22 and Brigham Young University. Special thanks to Joey Chong, Gloria Burke and Bonni Corcoran from the USDA Forest Service for collecting samples. Special thanks to Carl Seielstad and Theodore Adams from the University of Montana for helping plan and conduct the experiments. Special thanks to Marianne Fletcher and Victoria Lansigner from BYU for their help in developing the L-systems model and analyzing the experimental data.

## B. PREDICTION MODEL PARITY PLOTS

This appendix contains the parity plots for all the correlations whose parity plots were not shown in the text of the dissertation. The plots for the physical properties models are in Appendix B.1, parity plots for the best overall models are in Appendix B.2 and plots for the models using the most common parameters are in Appendix B.3.

### B.1 Physical Properties Models

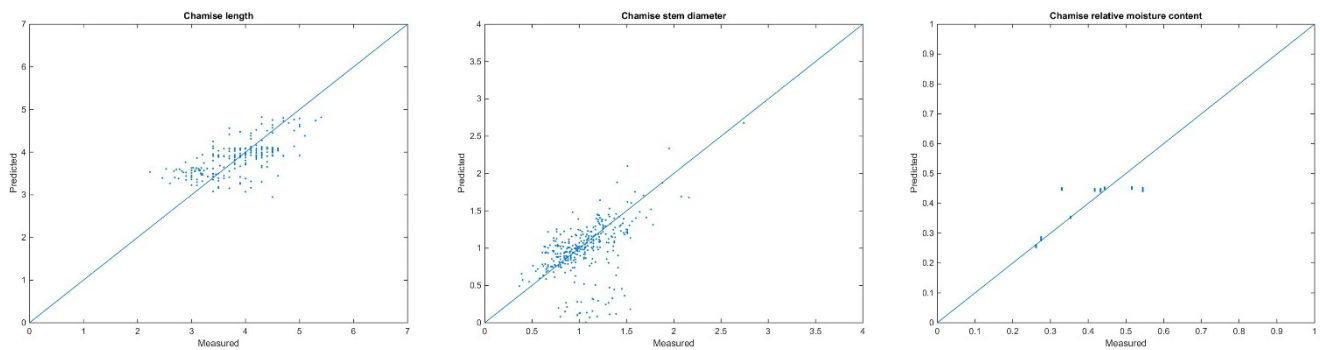


Figure B-1: Parity plots for chamise

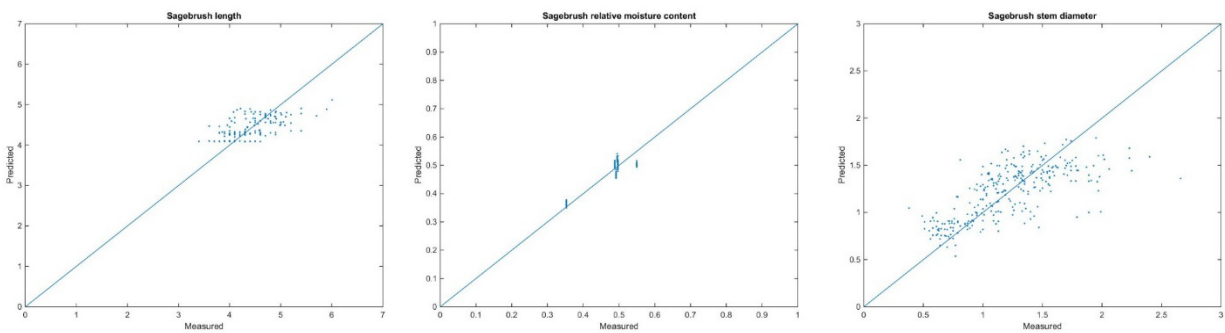
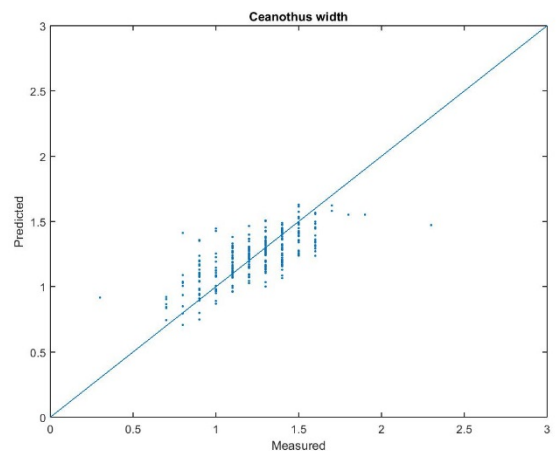
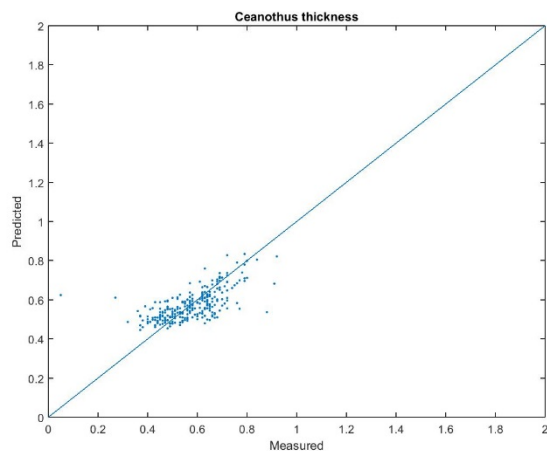
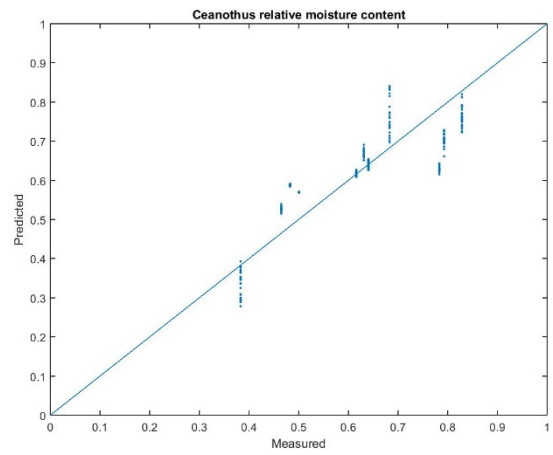
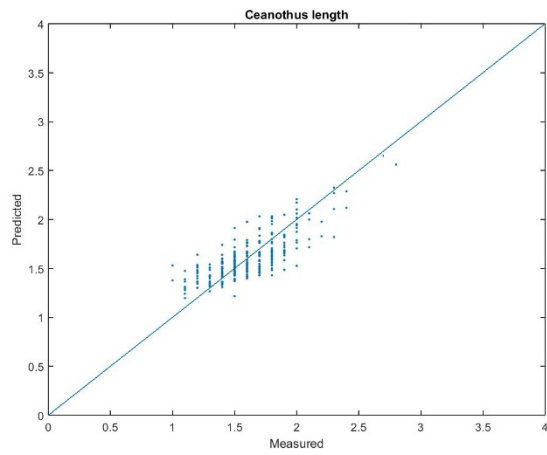
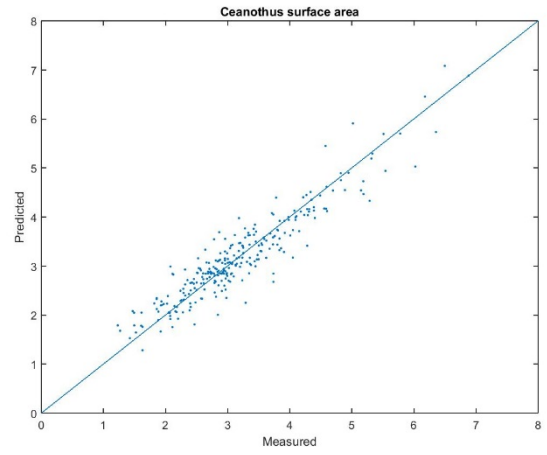
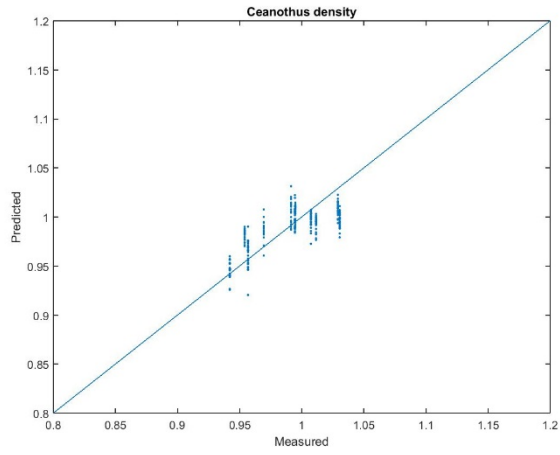
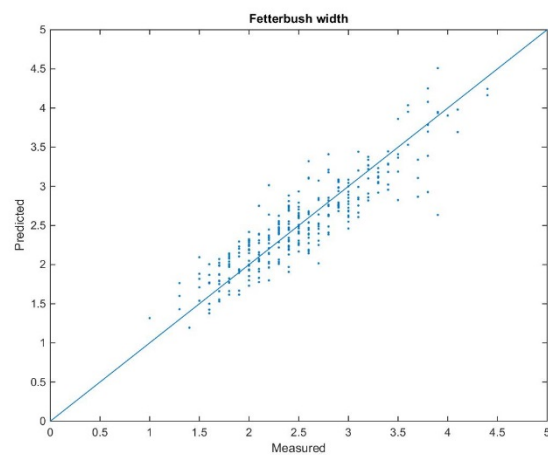
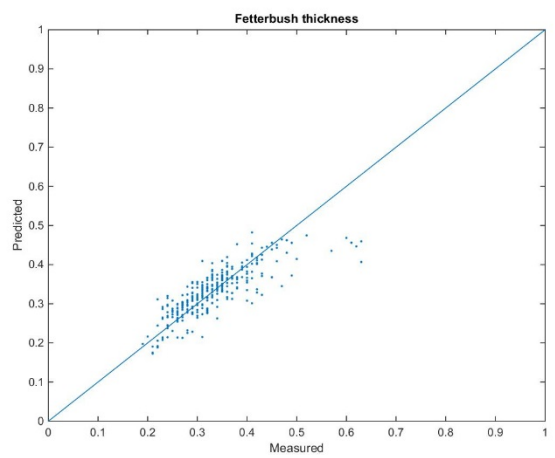
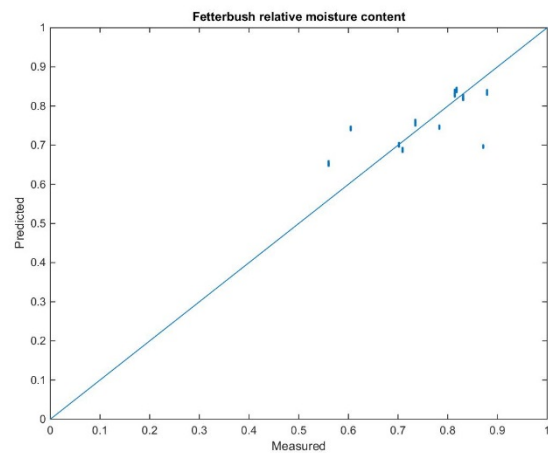
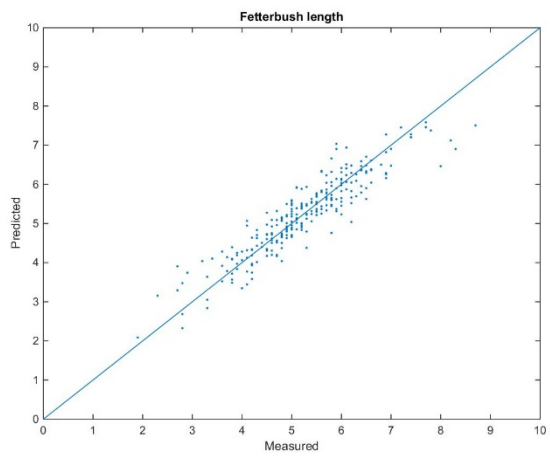
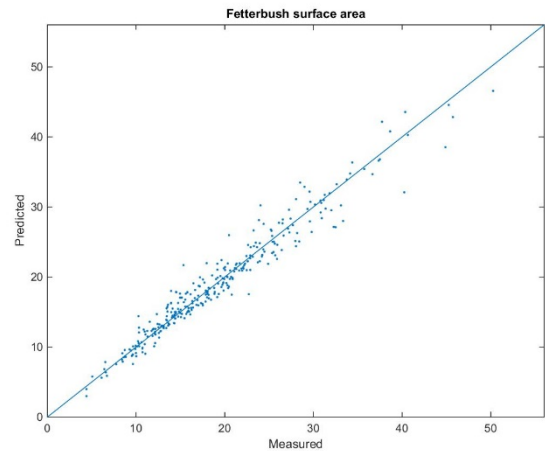
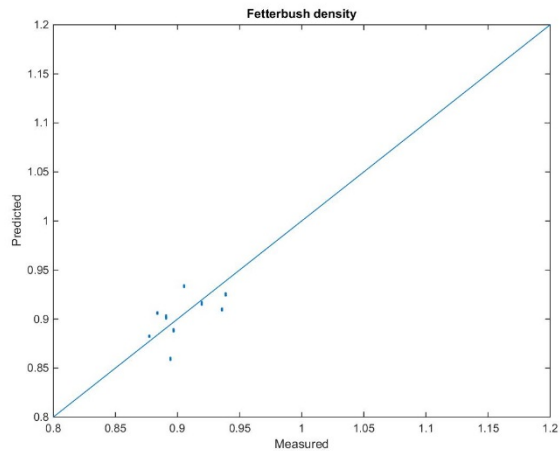


Figure B-2: Parity plots for sagebrush



**Figure B-3: Parity plots for ceanothus**



**Figure B-4: Parity plots for fetterbush**

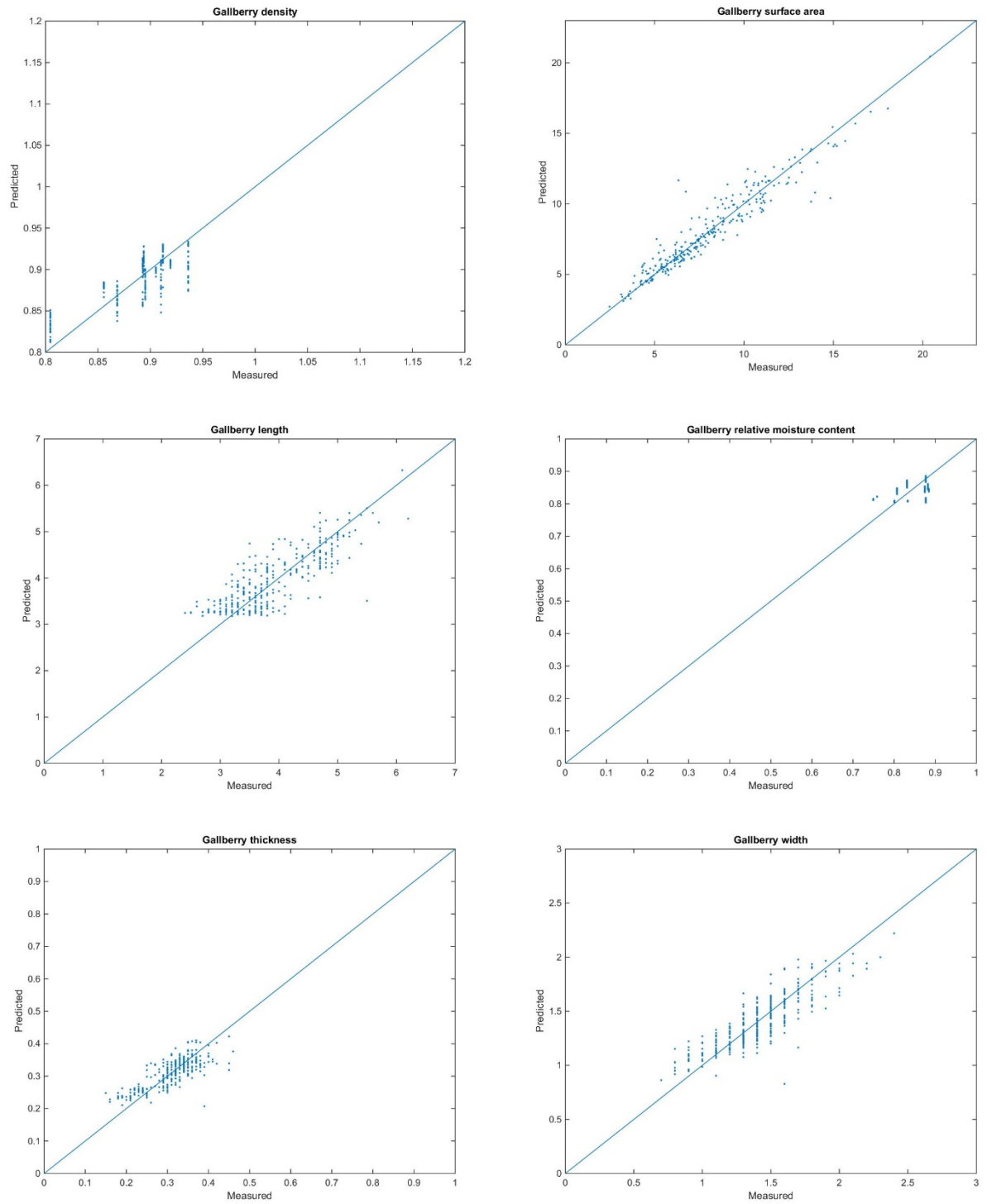


**Figure B-5: Parity plots for gallberry**

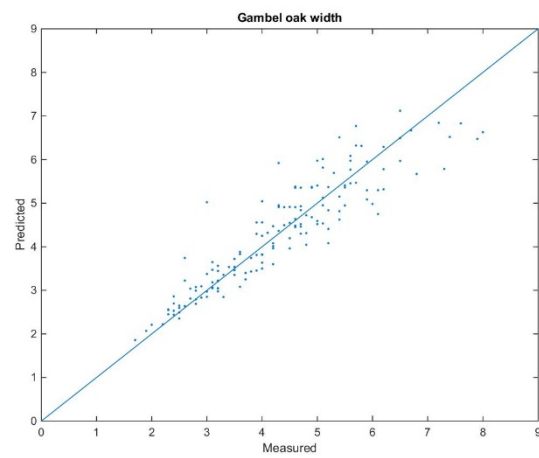
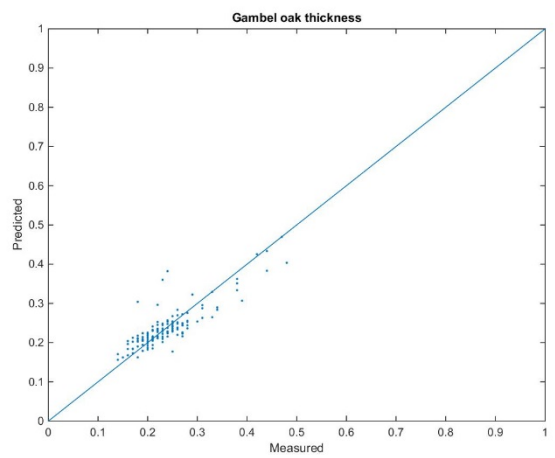
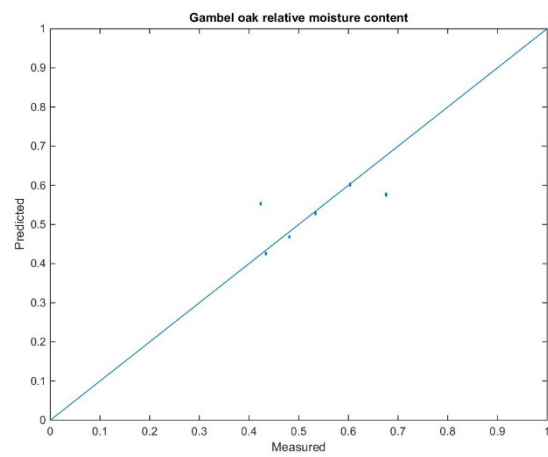
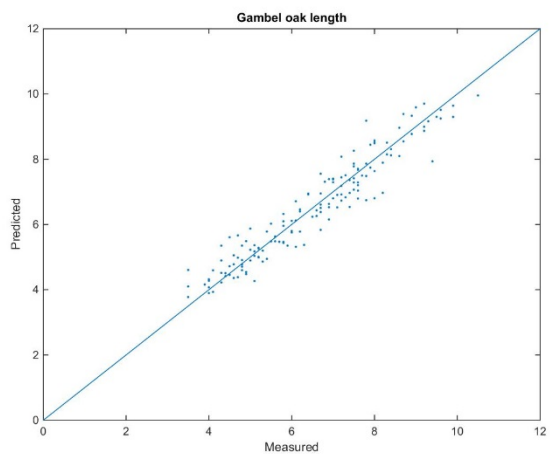
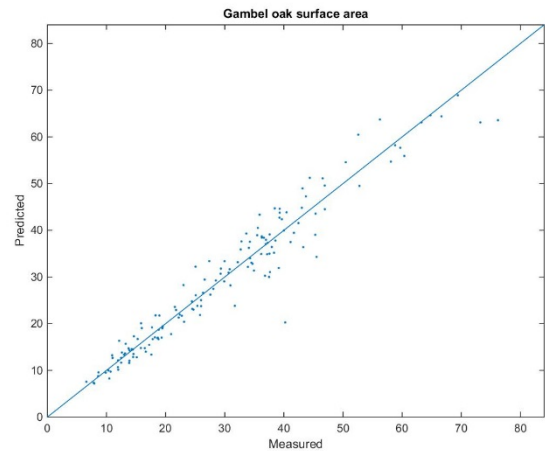
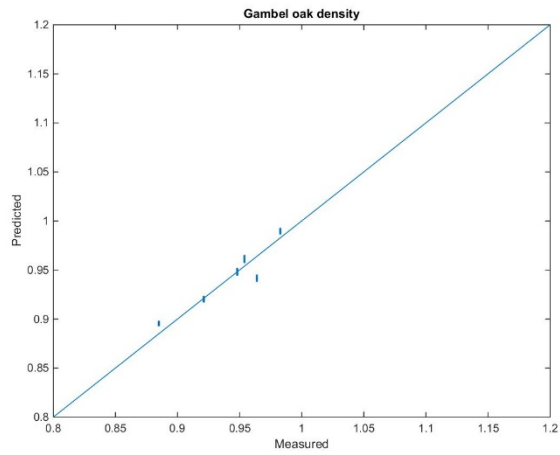


**Figure B-6: Parity plots for Gambel oak**

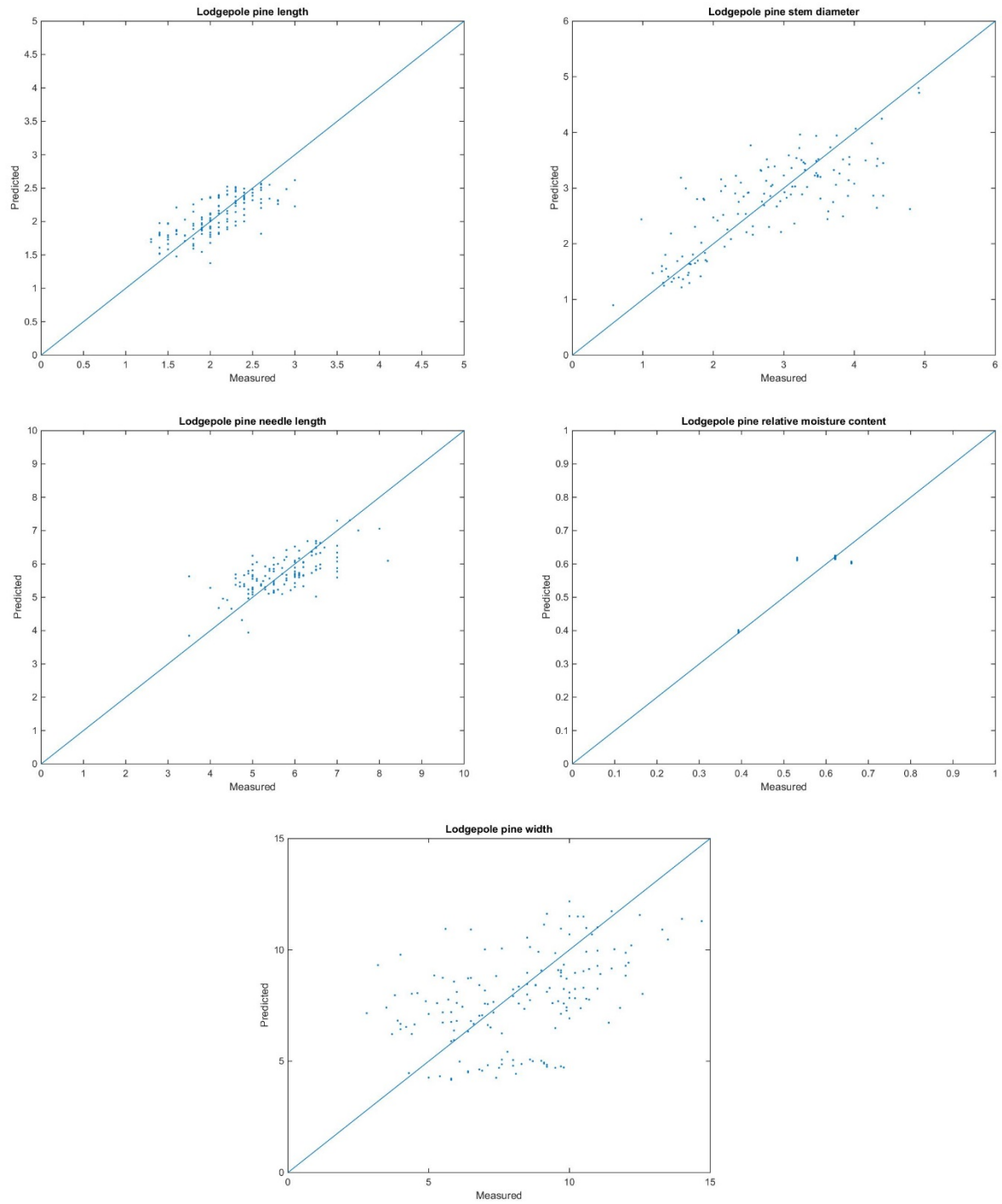


**Figure B-7: Parity plots for lodgepole pine**

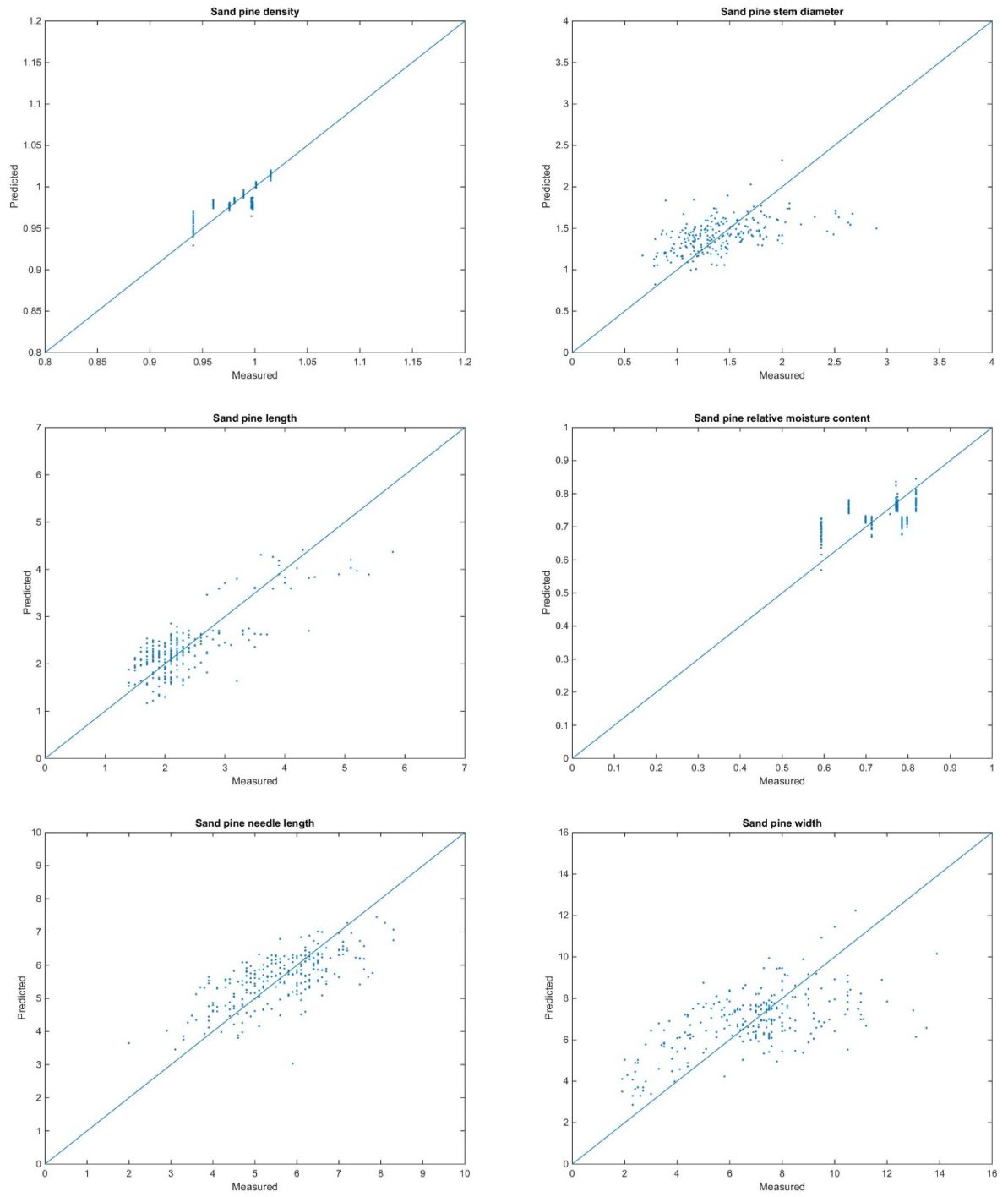


**Figure B-8: Parity plots for sand pine**

## B.2 Ignition and Burning Behavior Models—Best Overall Models

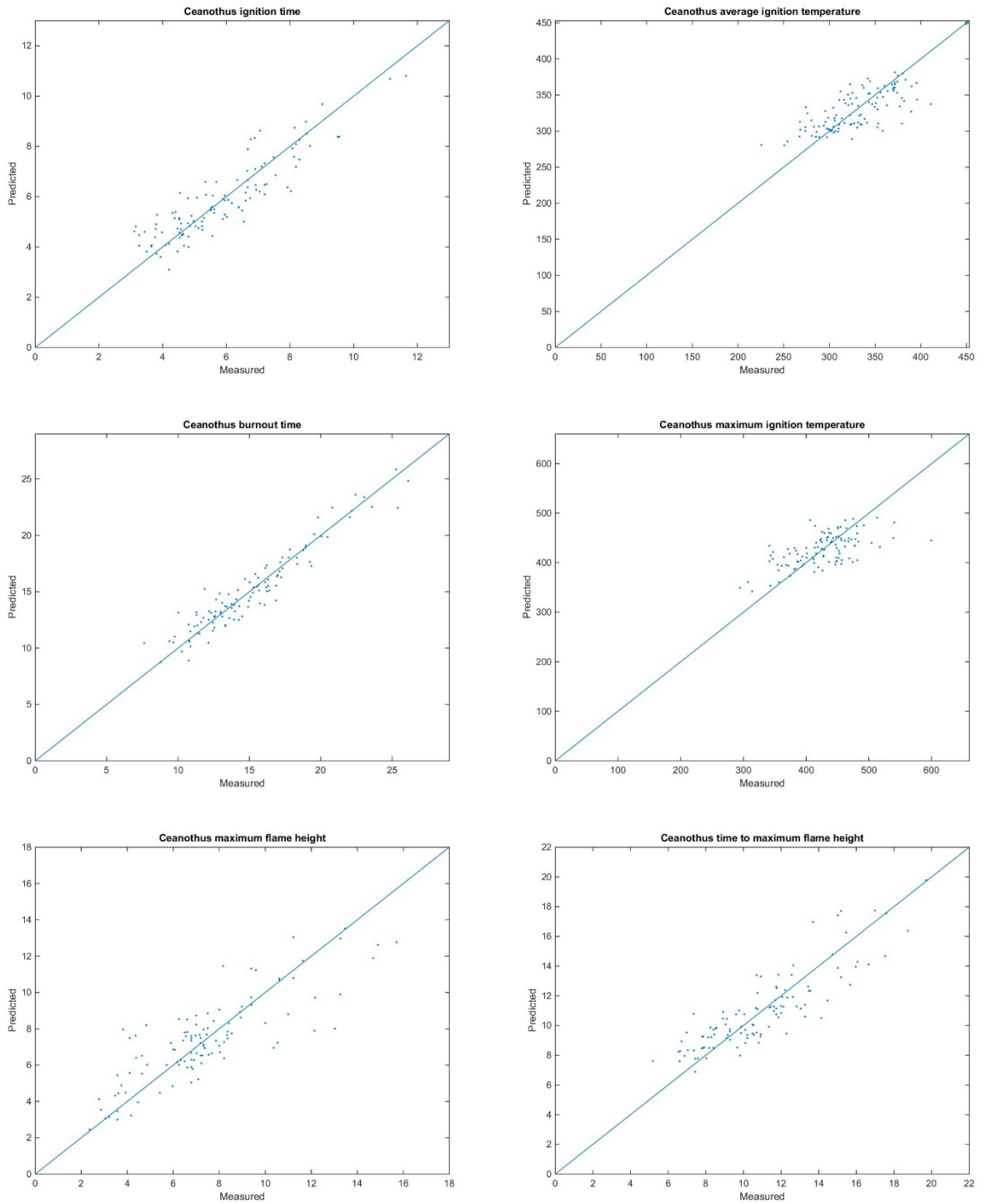
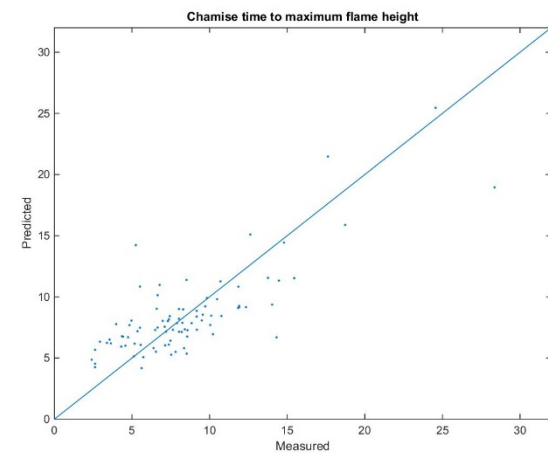
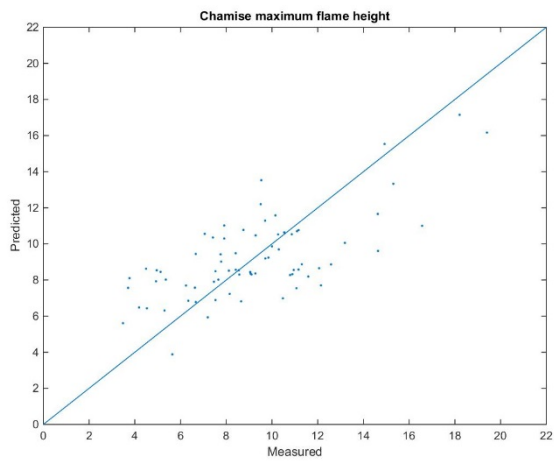
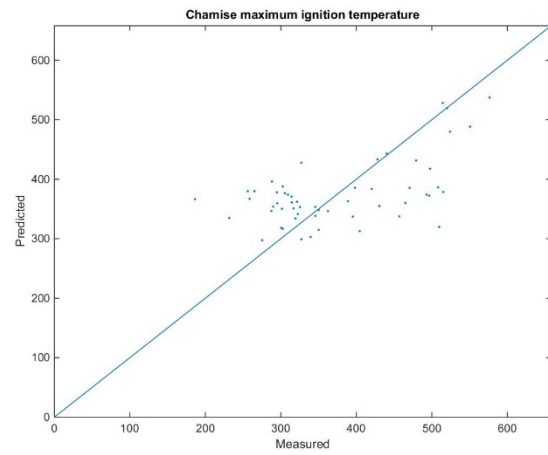
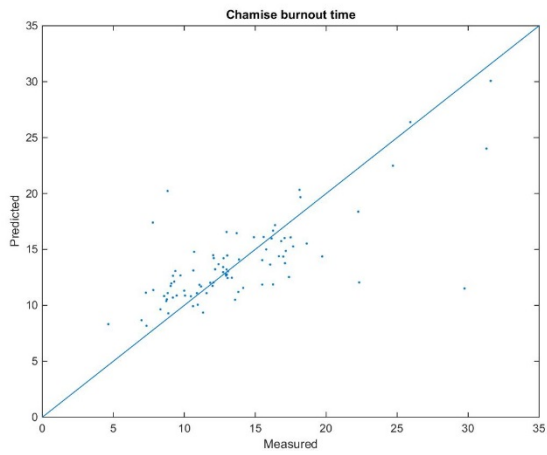
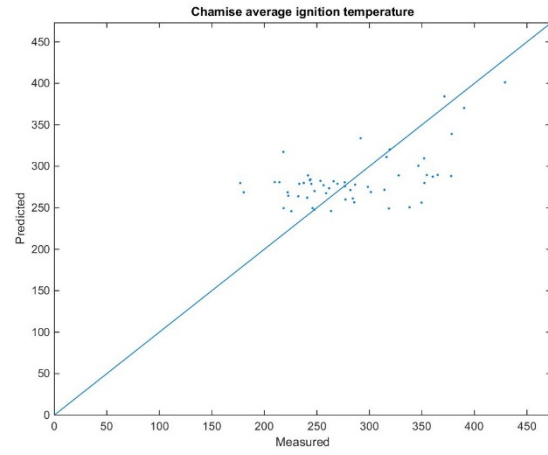
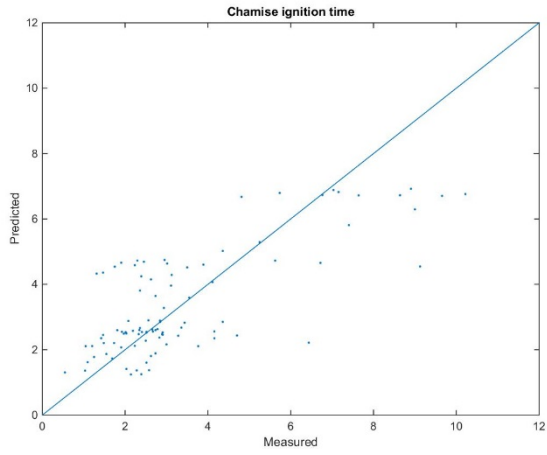
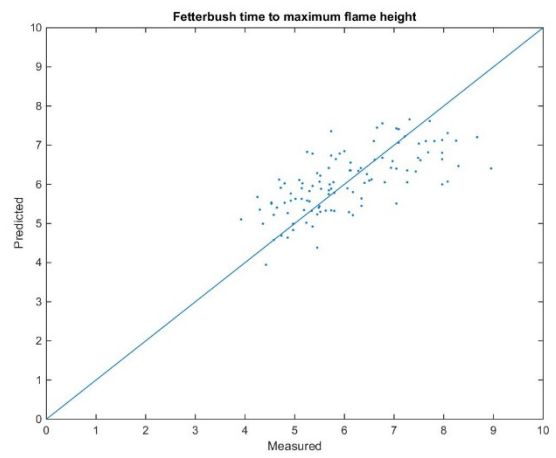
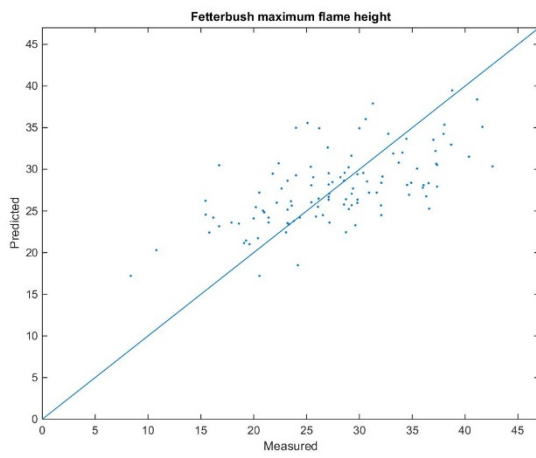
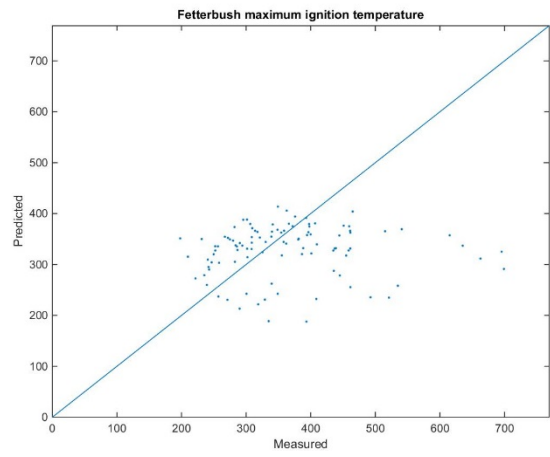
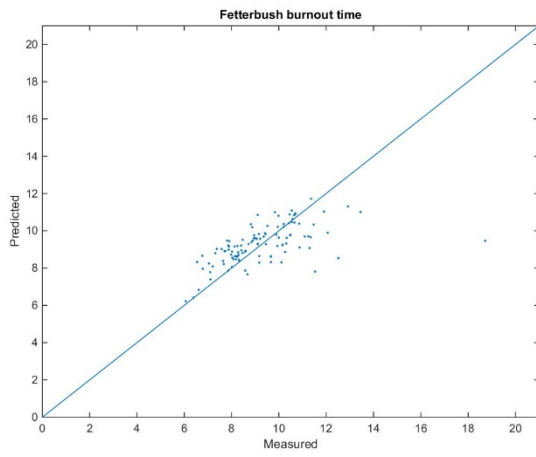
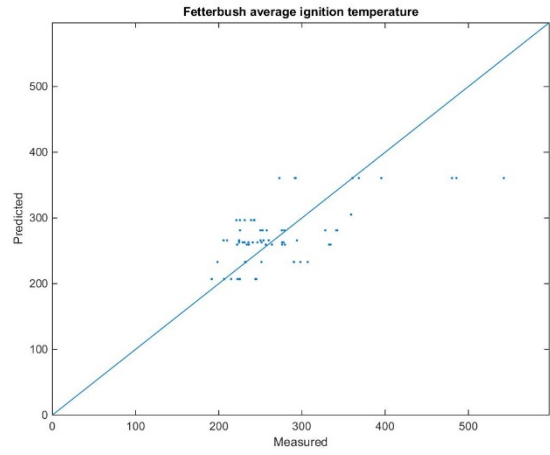
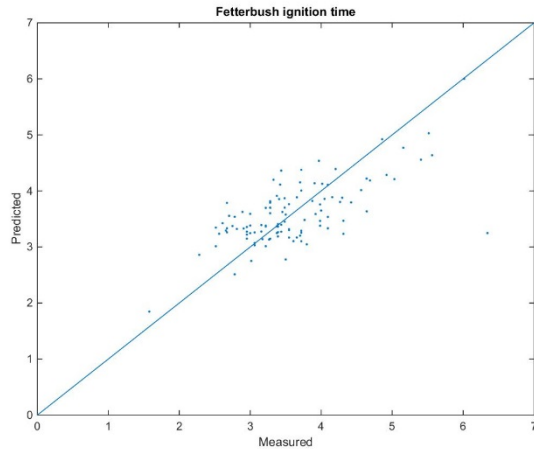


Figure B-9: Parity plots for ceanothus—best overall models



**Figure B-10: Parity plots for chamise—best overall models**



**Figure B-11: Parity plots for fetterbush—best overall models**

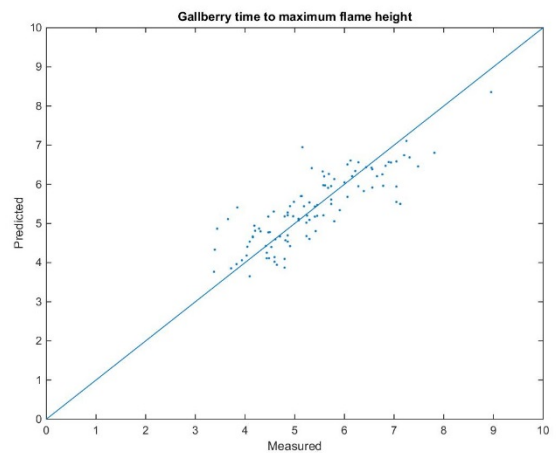
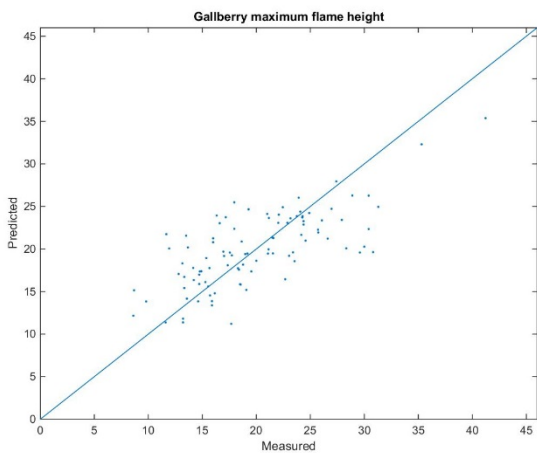
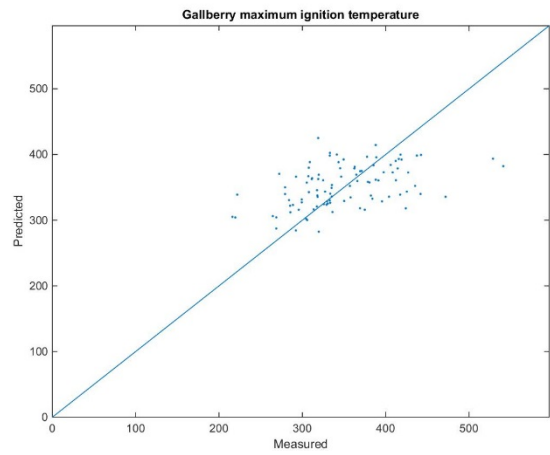
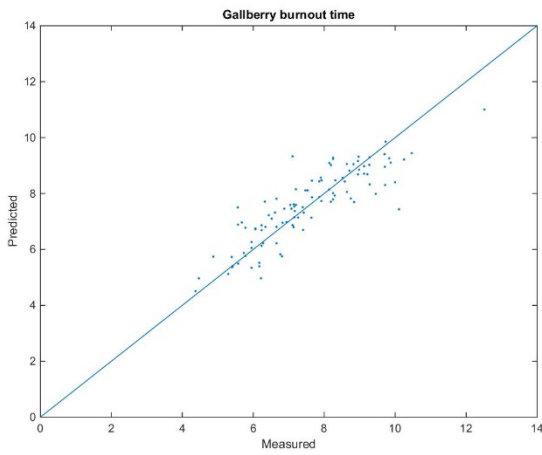
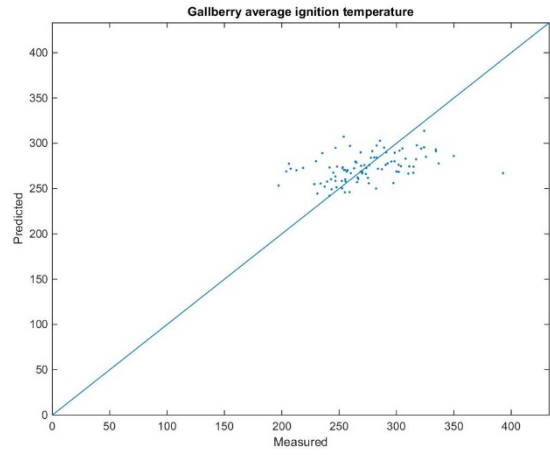
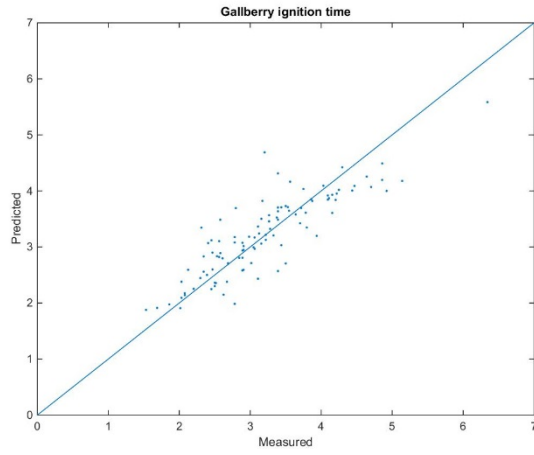


**Figure B-12: Parity plots for gallberry—best overall models**

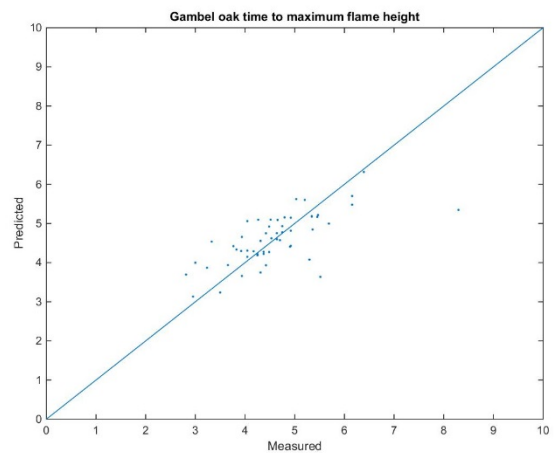
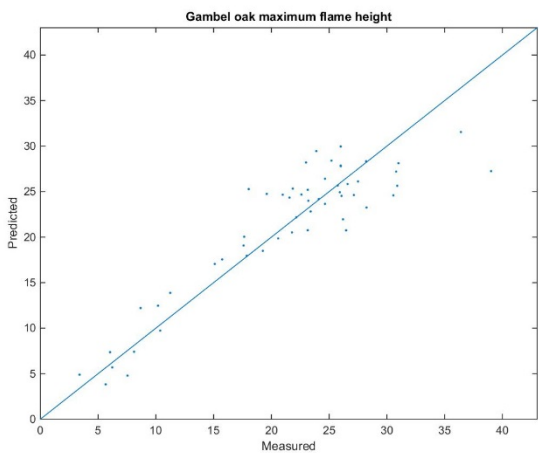
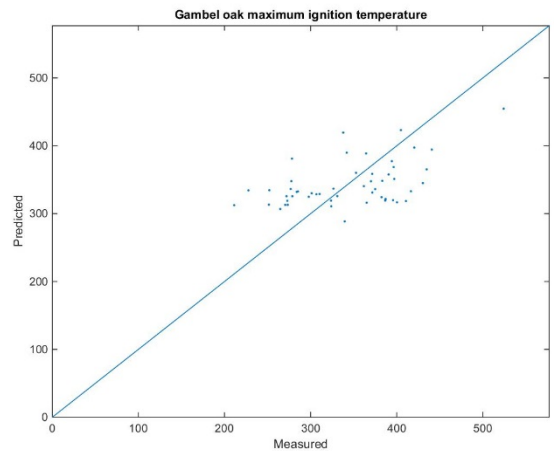
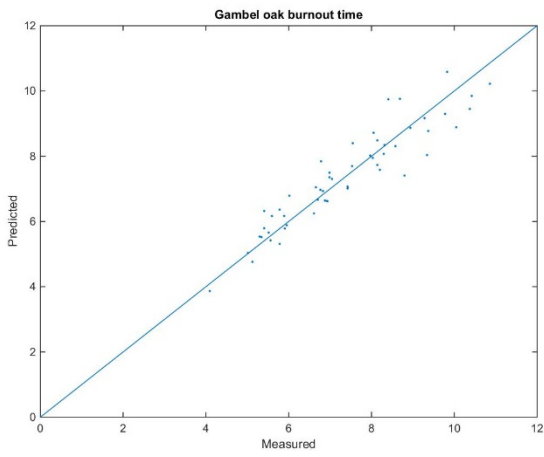
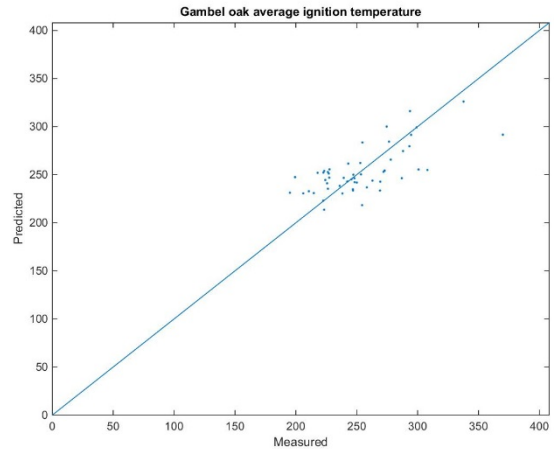
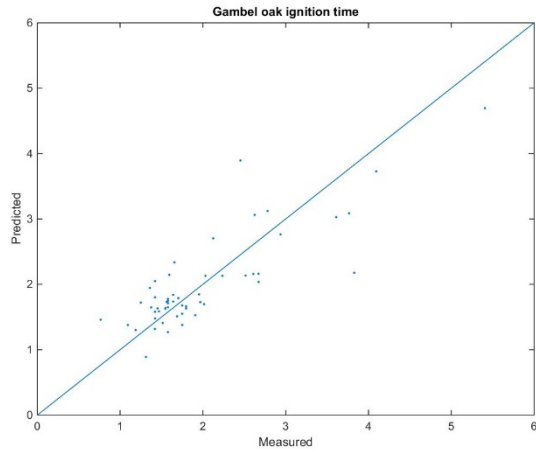


**Figure B-13: Parity plots for Gambel oak—best overall models**

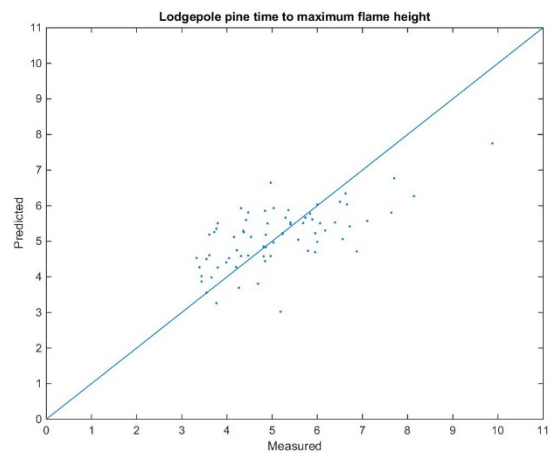
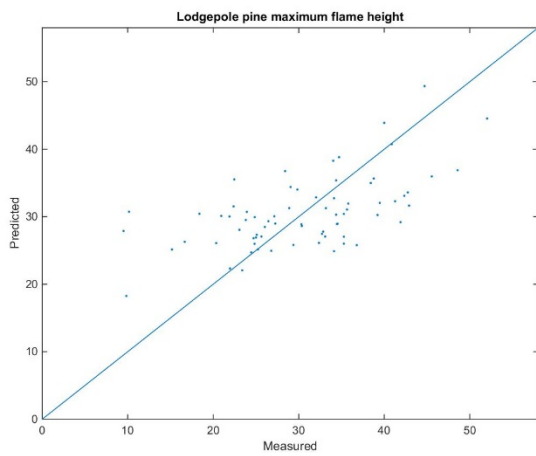
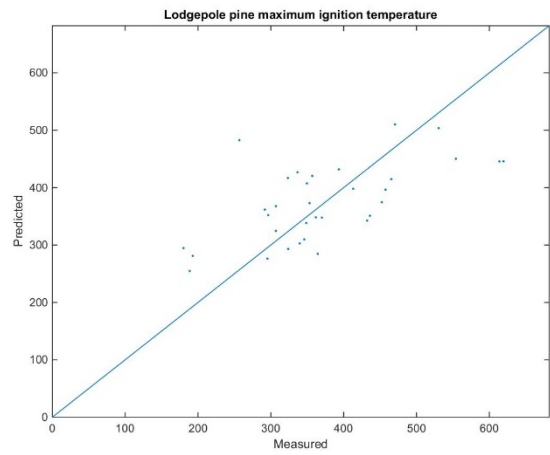
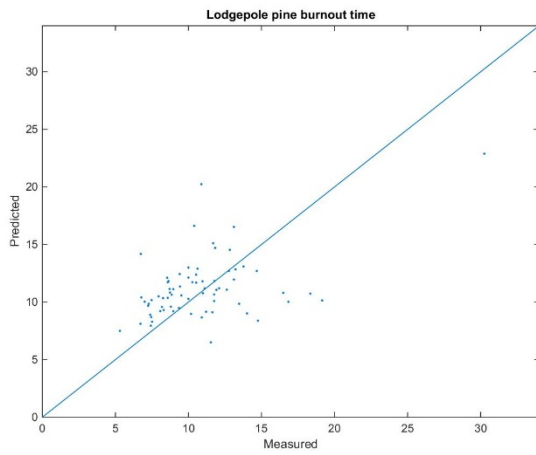
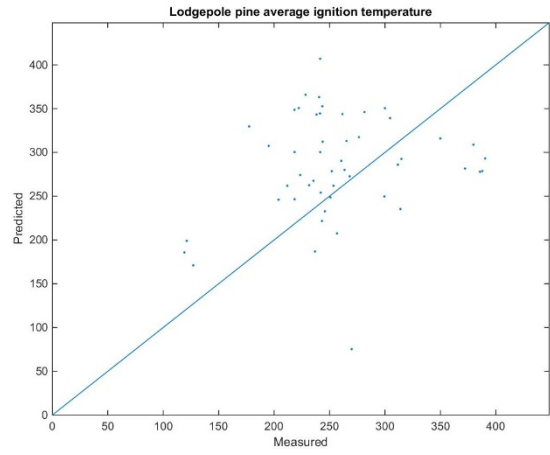
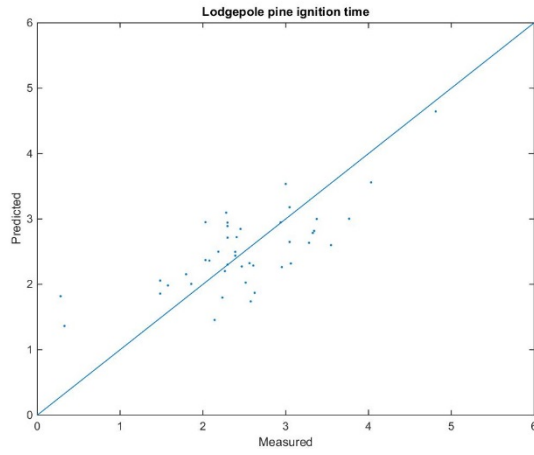


**Figure B-14: Parity plots for lodgepole pine—best overall models**

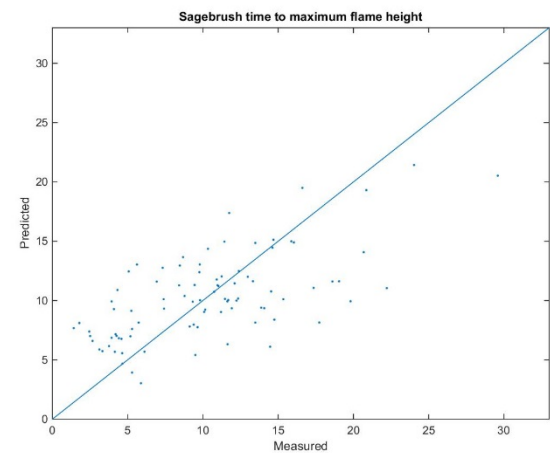
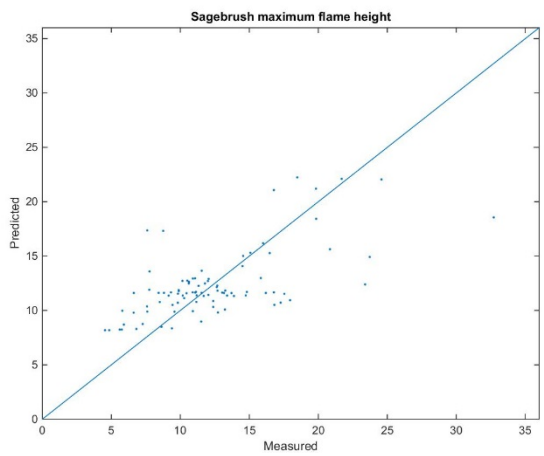
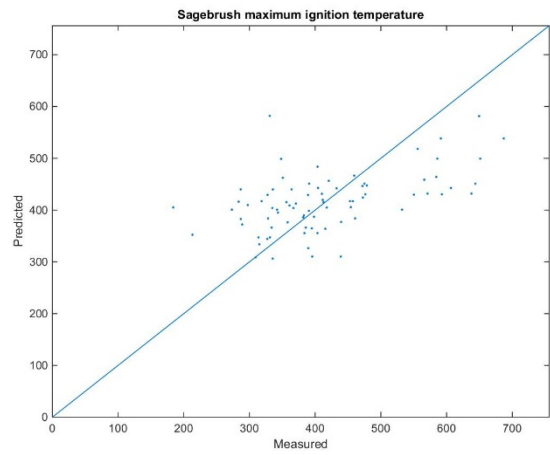
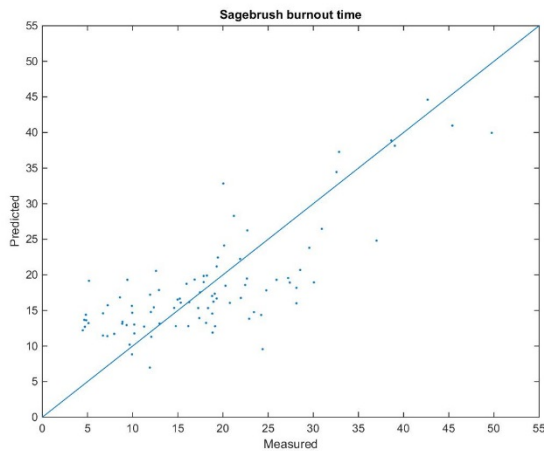
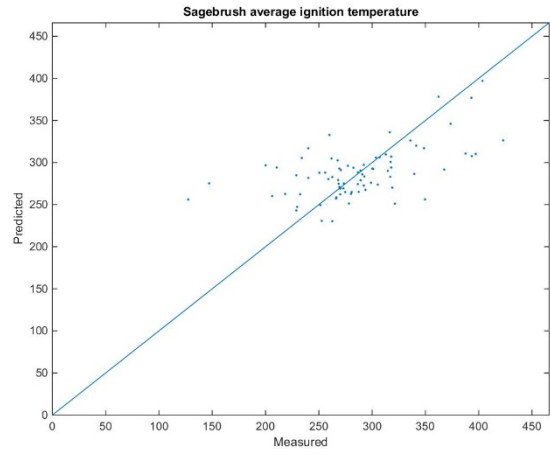
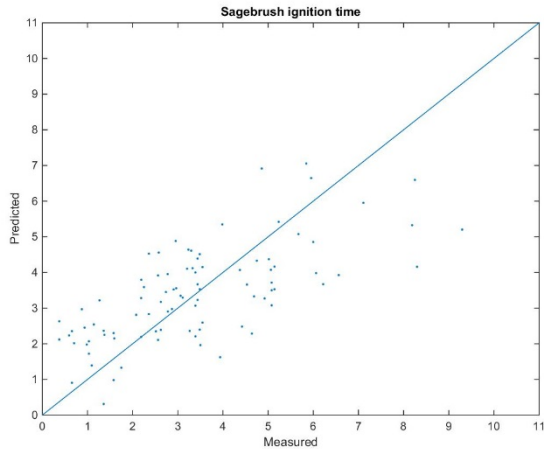


**Figure B-15: Parity plots for sagebrush—best overall models**

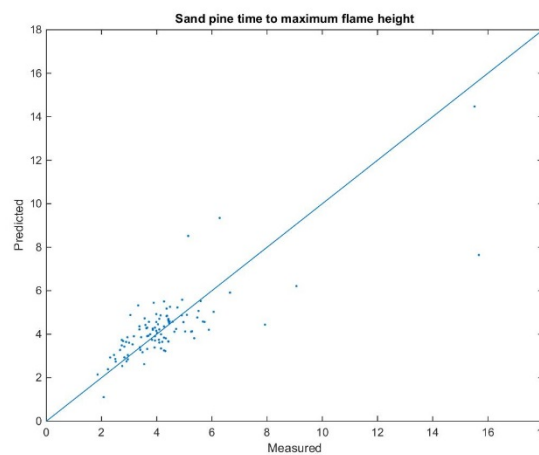
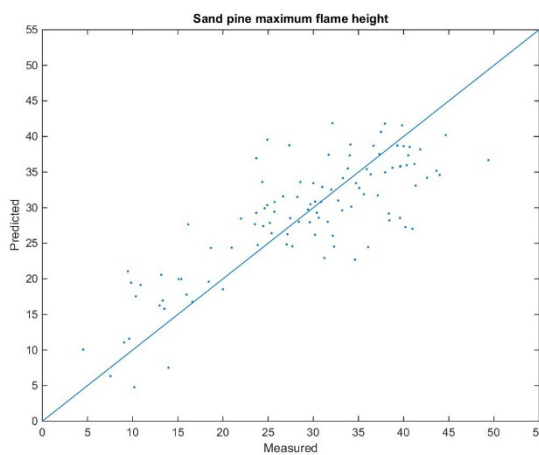
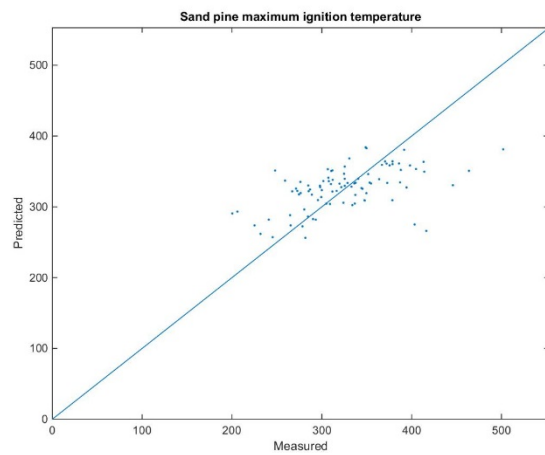
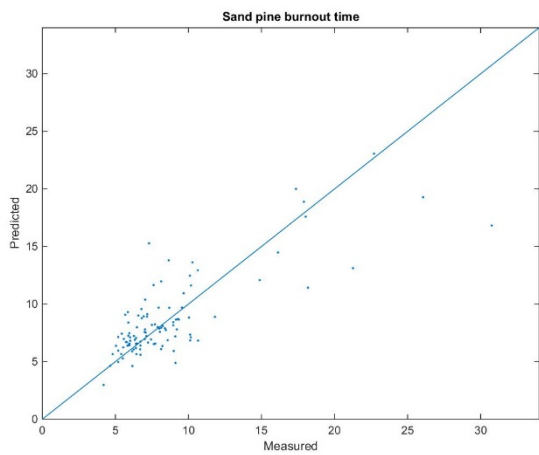
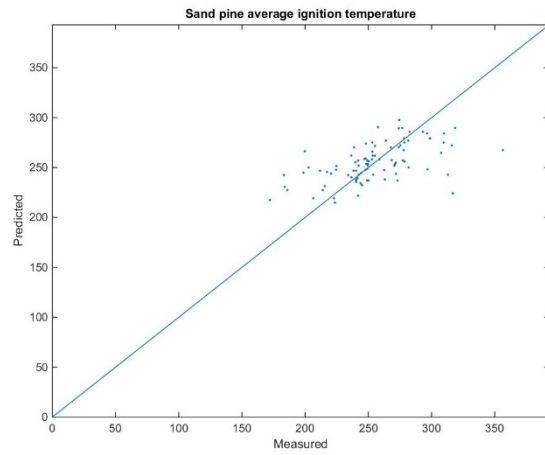
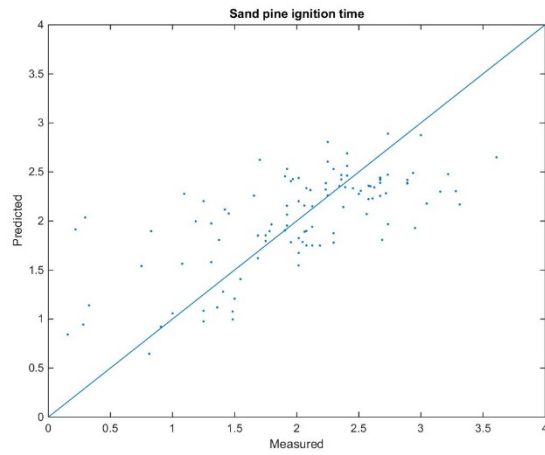


**Figure B-16: Parity plots for sand pine—best overall models**

### B.3 Ignition and Burning Behavior Models—Models Using Most Common Parameters

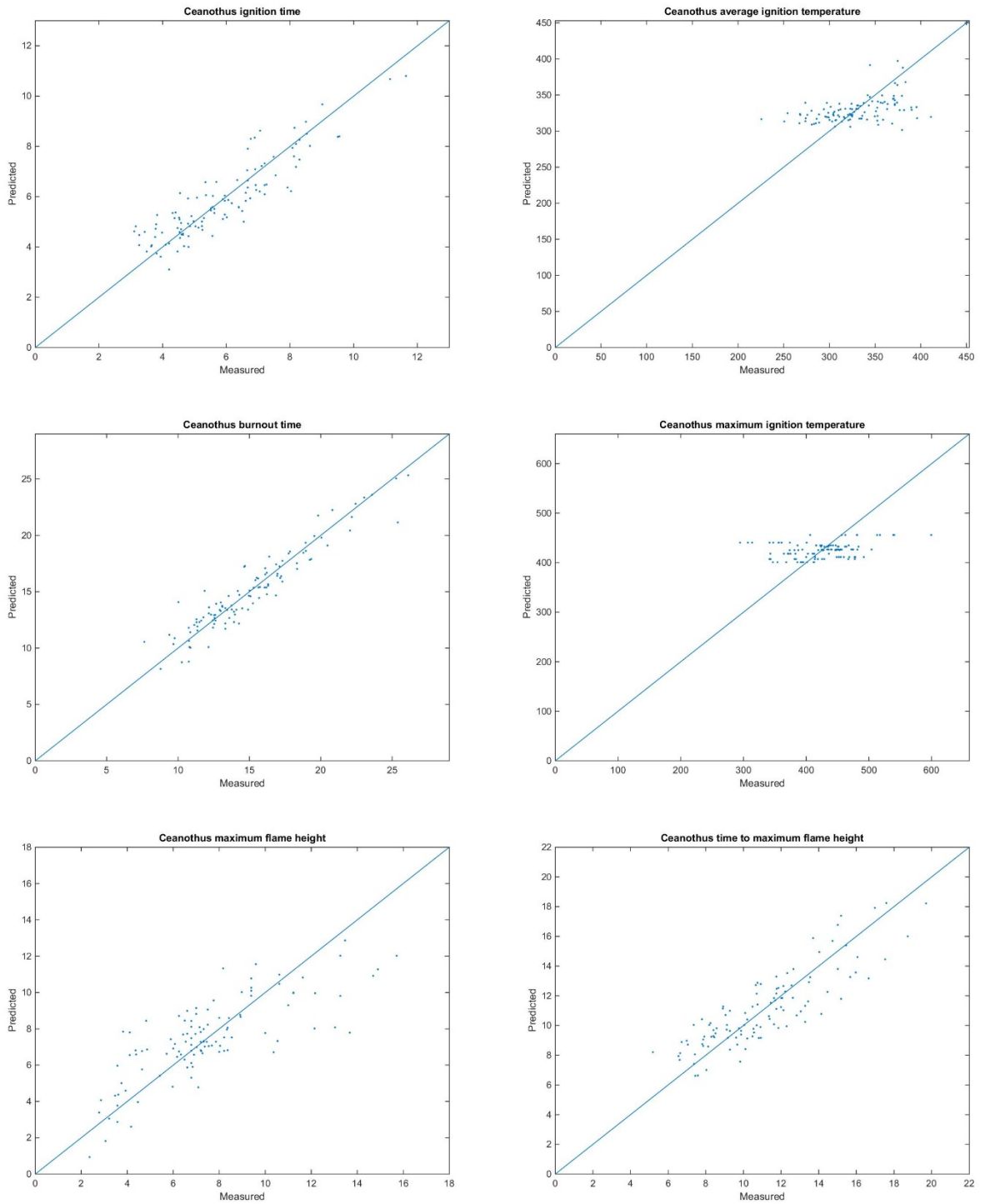
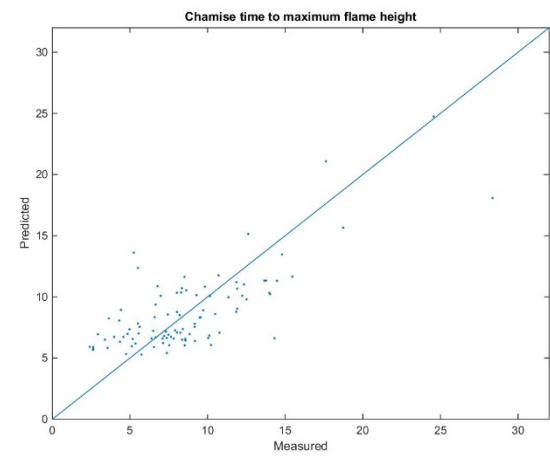
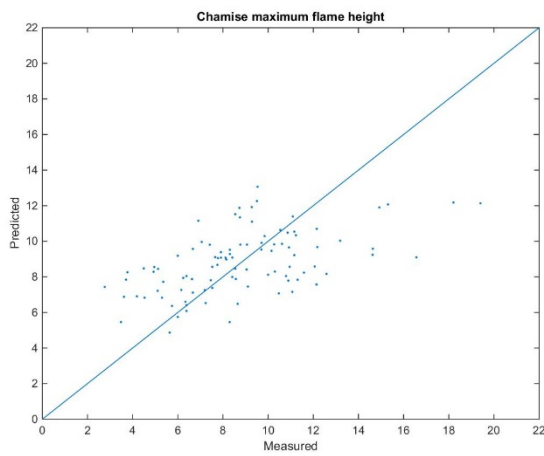
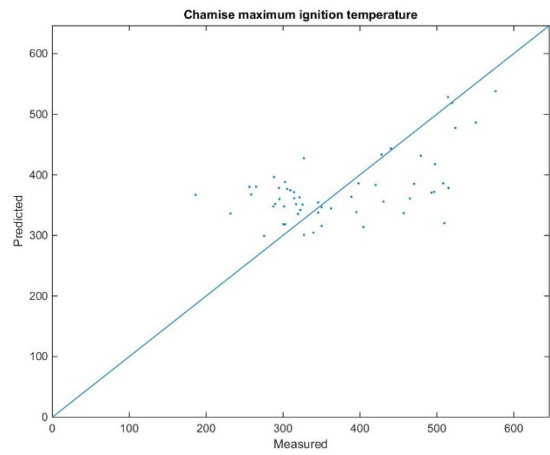
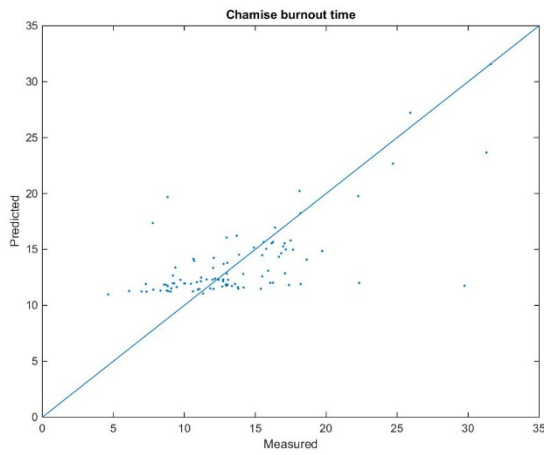
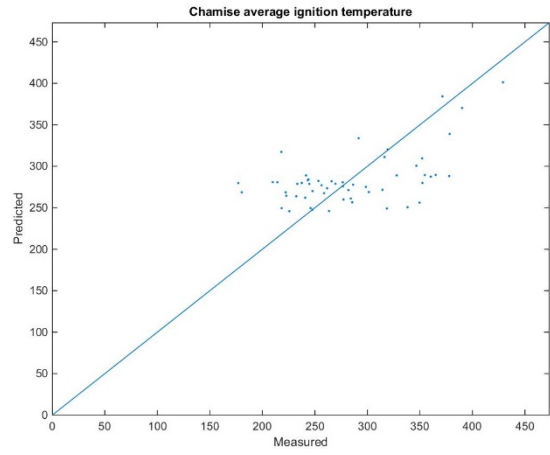
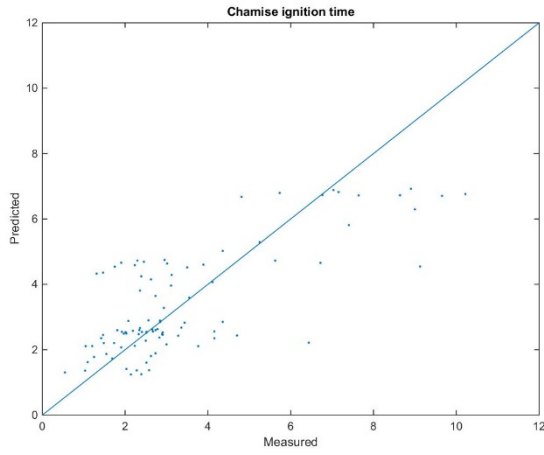
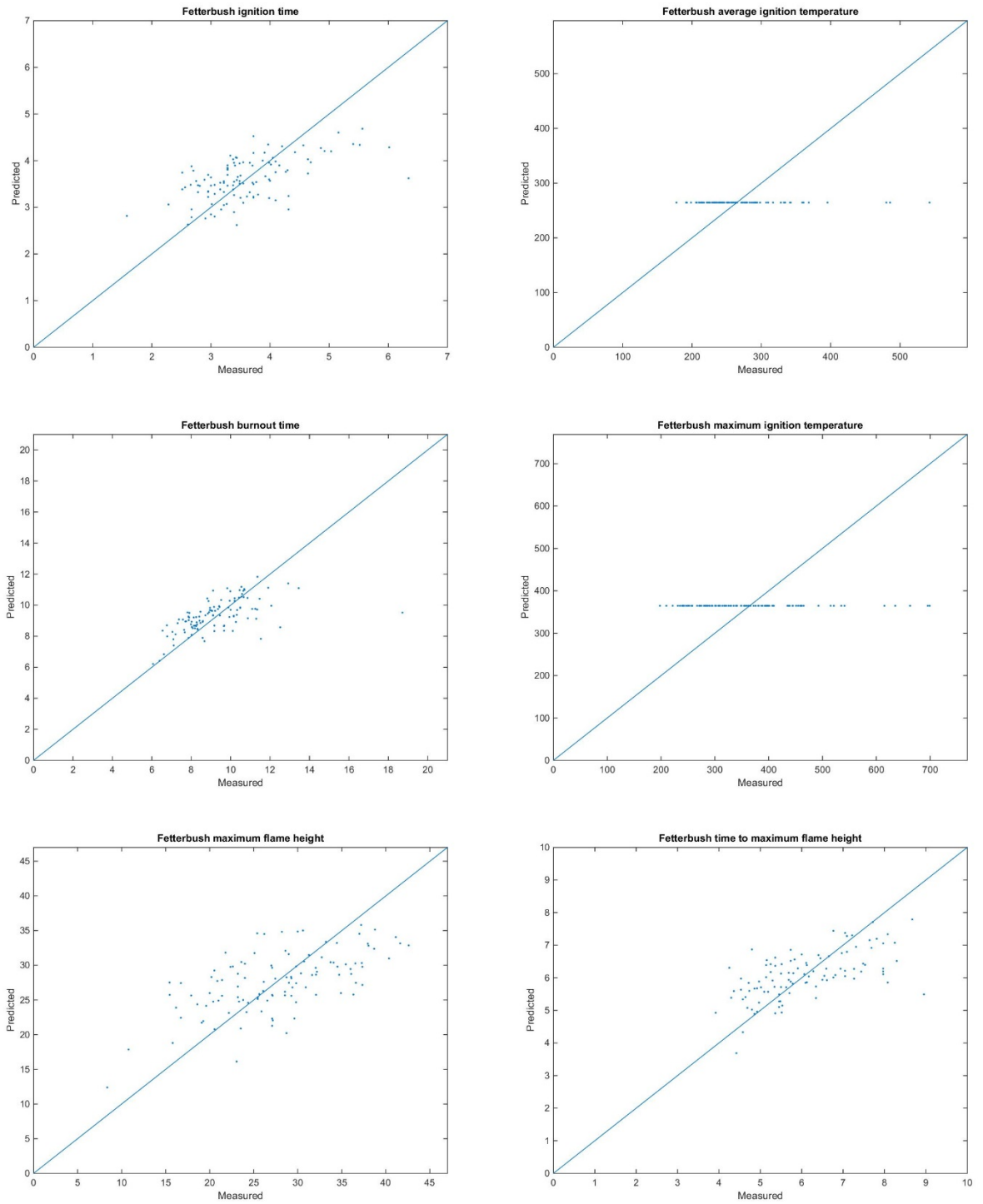


Figure B-17: Parity plots for ceanothus—models using MCP



**Figure B-18: Parity plots for chamise—models using MCP**



**Figure B-19: Parity plots for fetterbush—models using MCP**

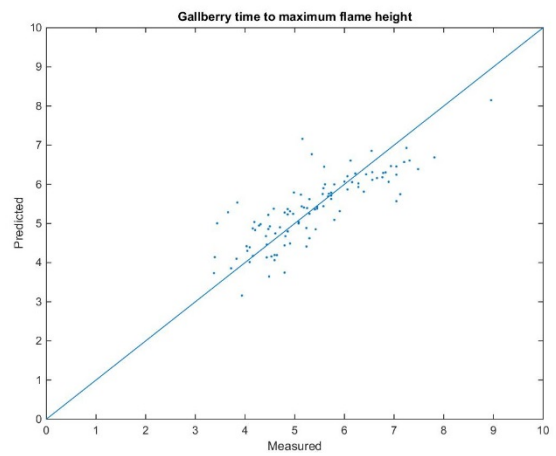
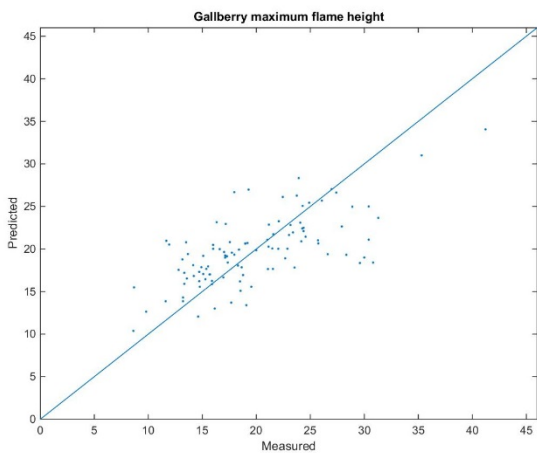
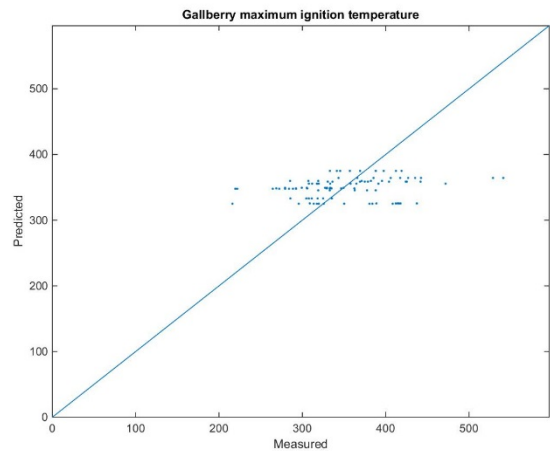
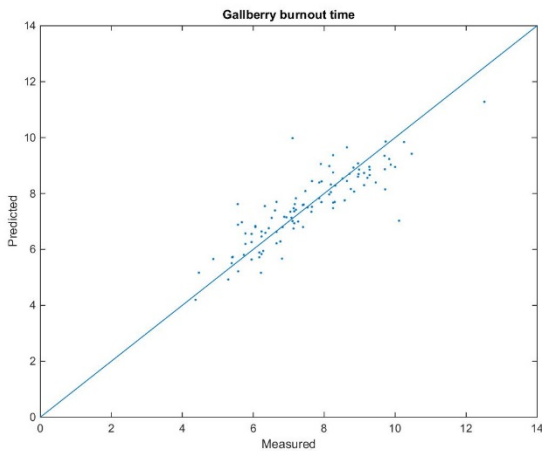
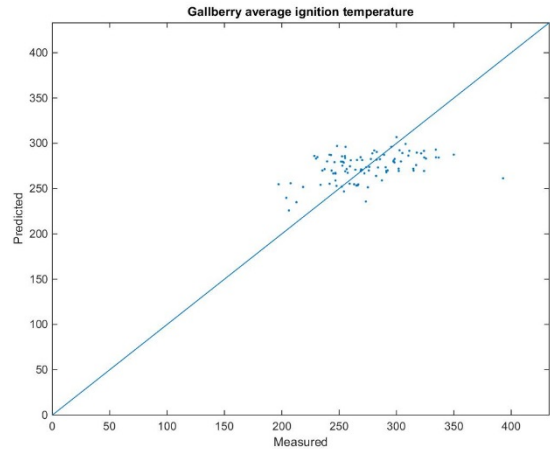
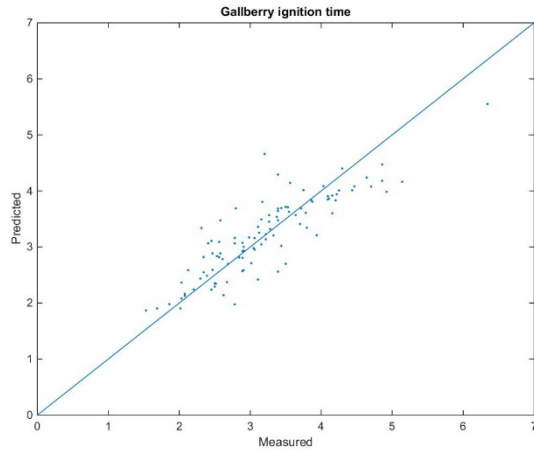


**Figure B-20: Parity plots for gallberry—models using MCP**

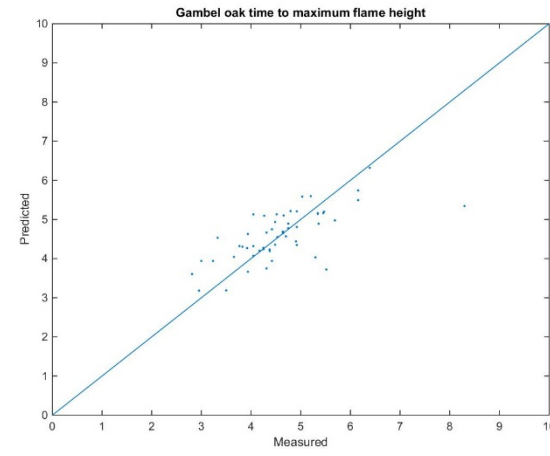
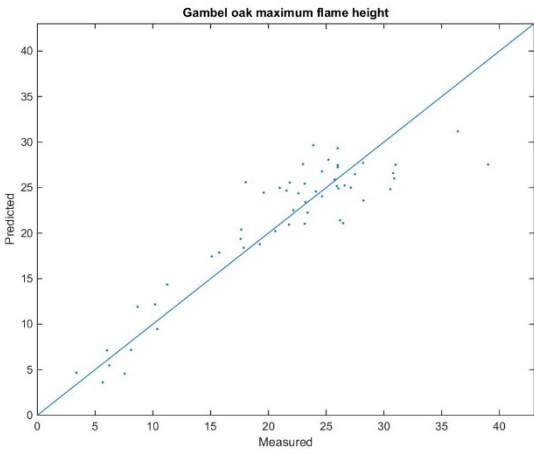
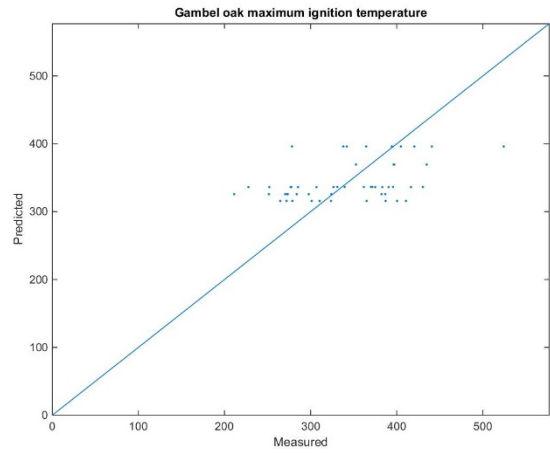
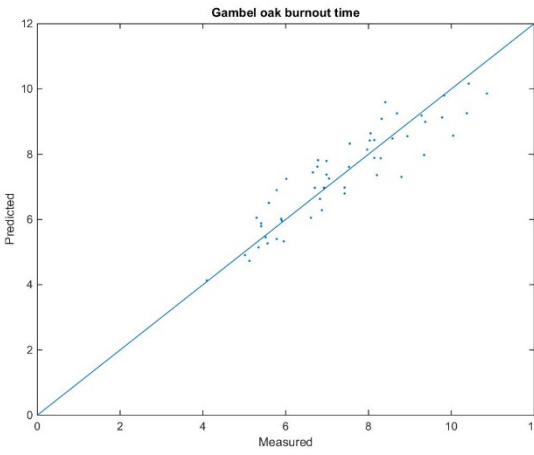
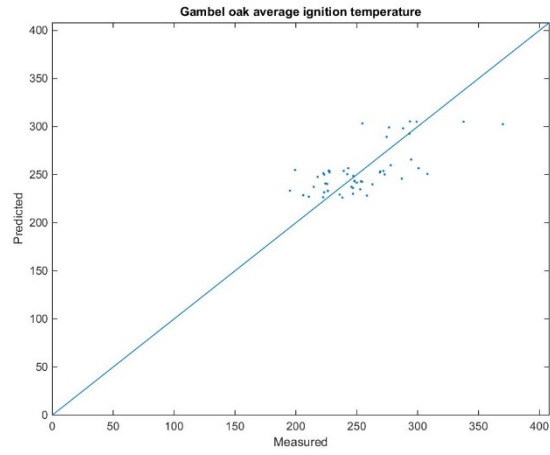
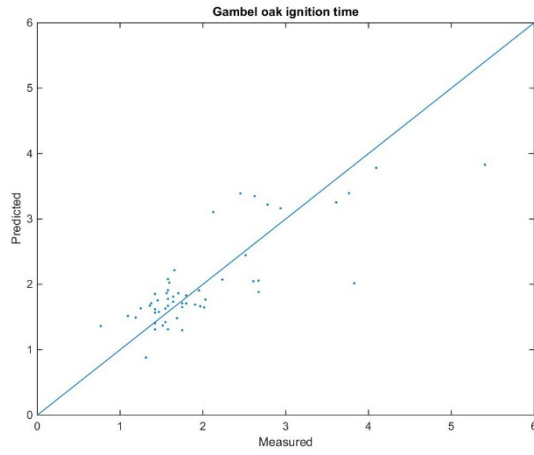


**Figure B-21: Parity plots for Gambel oak—models using MCP**

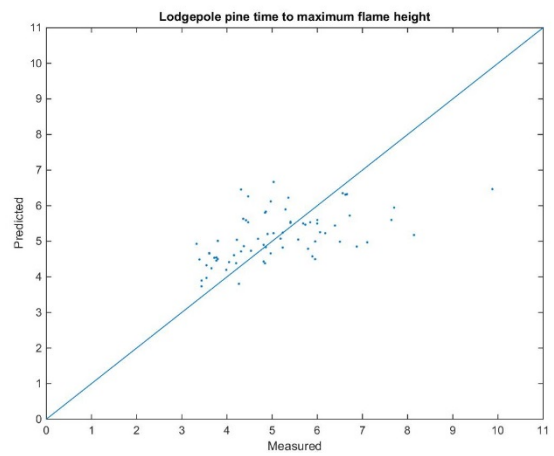
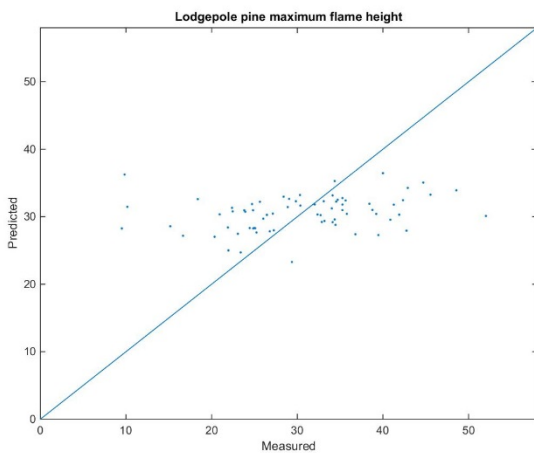
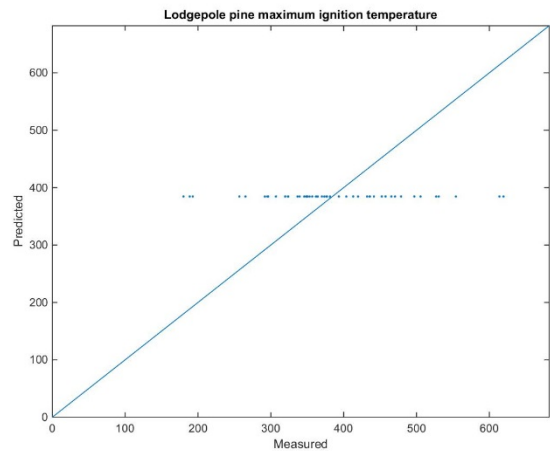
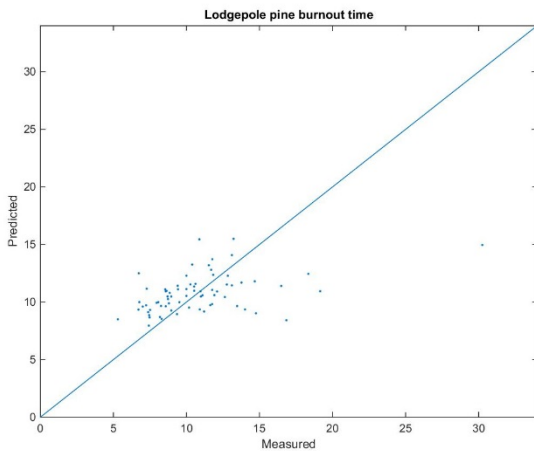
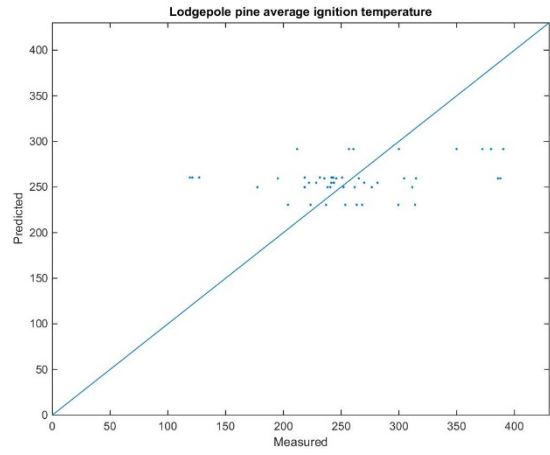
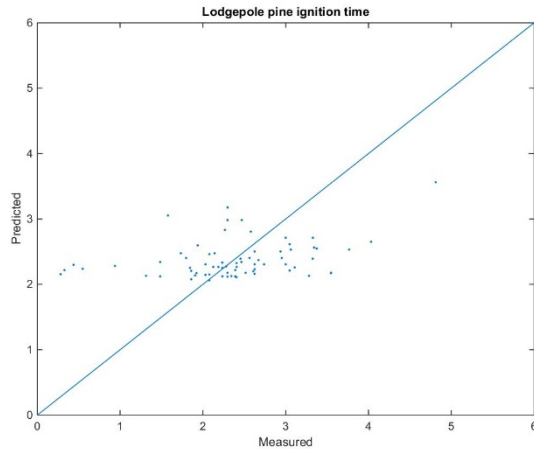


**Figure B-22: Parity plots for lodgepole pine—models using MCP**

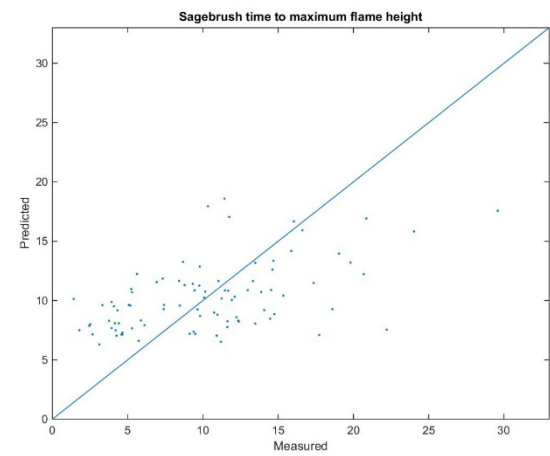
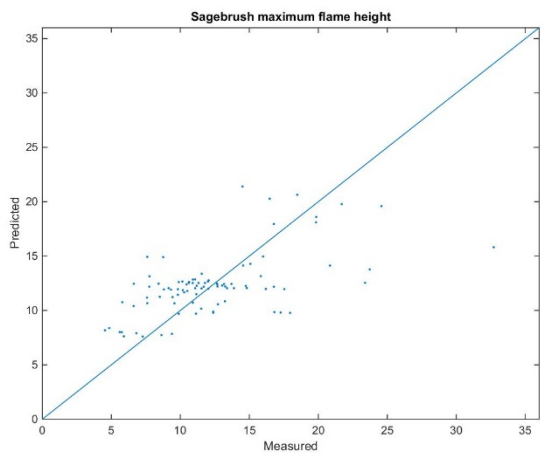
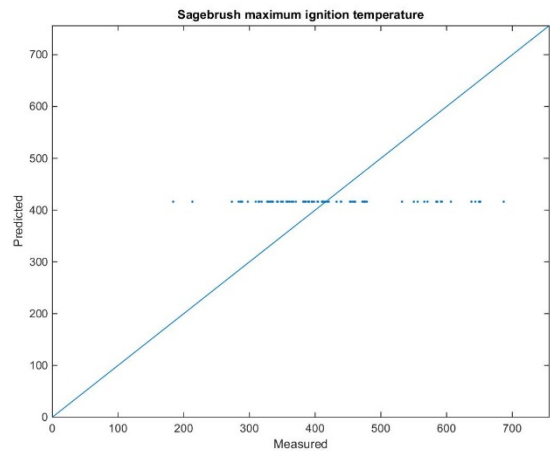
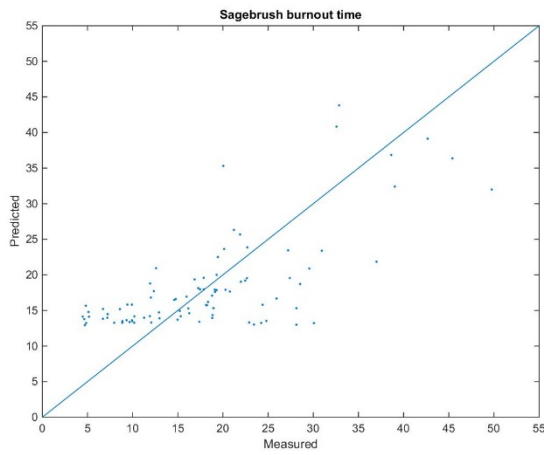
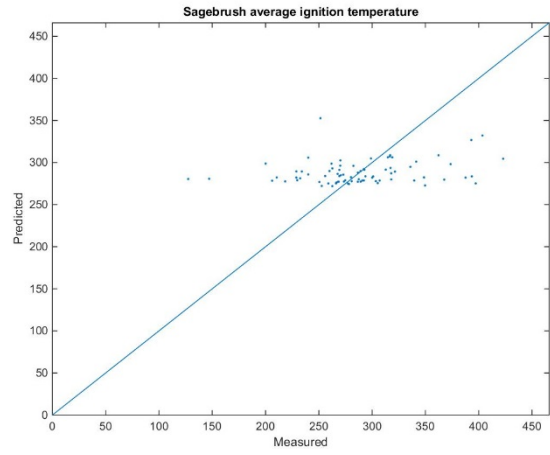
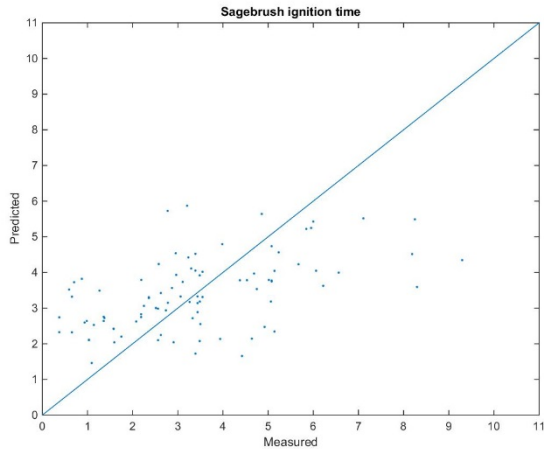


**Figure B-23: Parity plots for sagebrush—models using MCP**

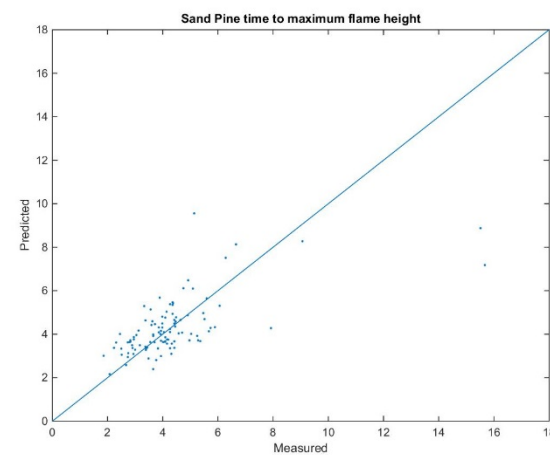
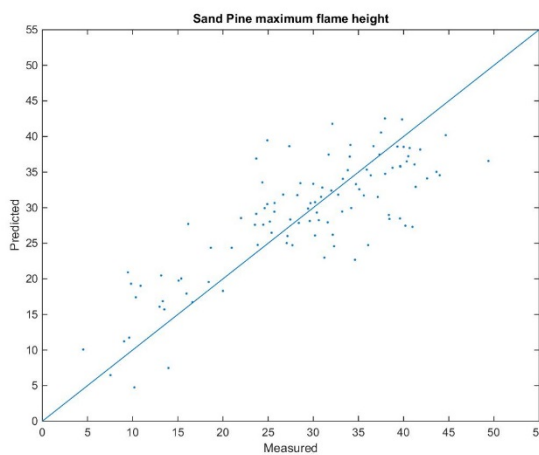
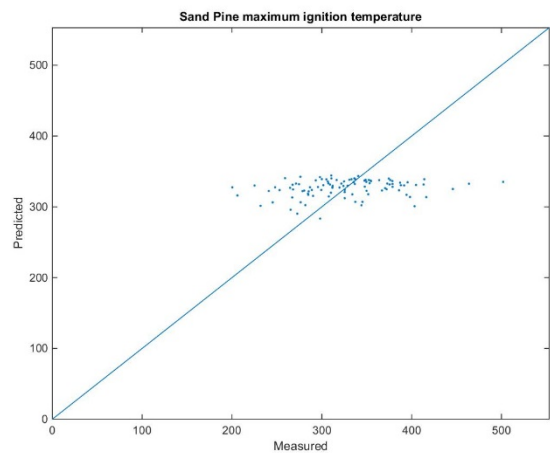
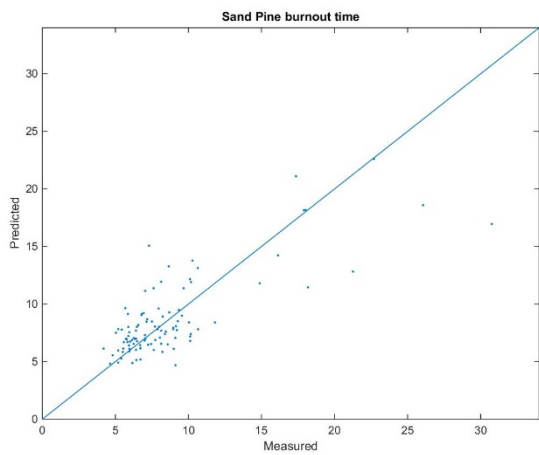
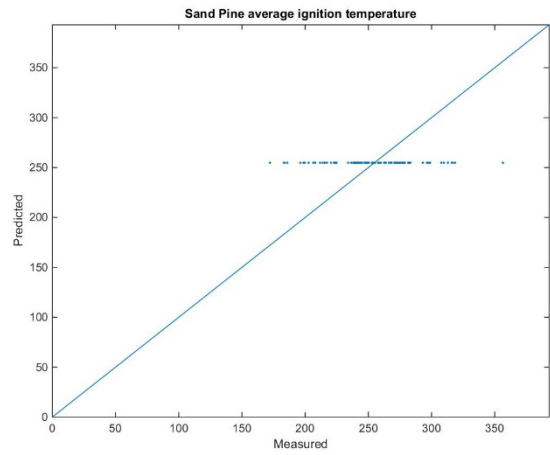
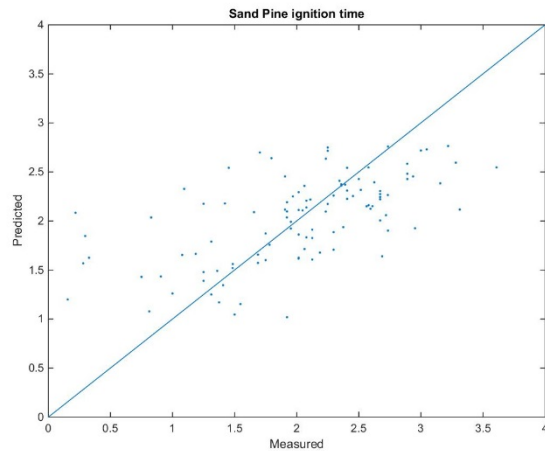


**Figure B-24: Parity plots for sand pine—models using MCP**

## **C. EXPERIMENTAL DATA**

This appendix contains the processed experimental data for the results reported in the text of the dissertation. The physical and chemical properties data are in Appendix C.1, ignition and burning data are in Appendix C.2, the temperature plateau data are in Appendix C.3 and the data for flame behavior near slopes are in Appendix C.4.

### **C.1 Physical and Chemical Properties Data**

The data for the pre-burn measurements can be found on the US Forest Service database using the following citation.

Gallacher, Jonathan R.; Lansinger, Victoria; Hansen, Sydney; Ellsworth, Taylor; Weise, David R.; Fletcher, Thomas H. 2016. Physical and chemical properties of the foliage of 10 live wildland fuels. Fort Collins, CO: USDA Forest Service, Forest Service Research Data Archive.

### **C.2 Ignition and Burning Data**

The processed data for the experiments on the ignition and burning behavior of live fuels can be found on the US Forest Service database using the following citation.

Gallacher, Jonathan R.; Lansinger, Victoria; Hansen, Sydney; Smith, Samantha; Doll, Ashley; Weise, David R.; Fletcher, Thomas H. 2016. Ignition and burning behavior of the foliage of 10 live wildland fuels. Fort Collins, CO: USDA Forest Service, Forest Service Research Data Archive.

### C.3 Temperature Plateau Data

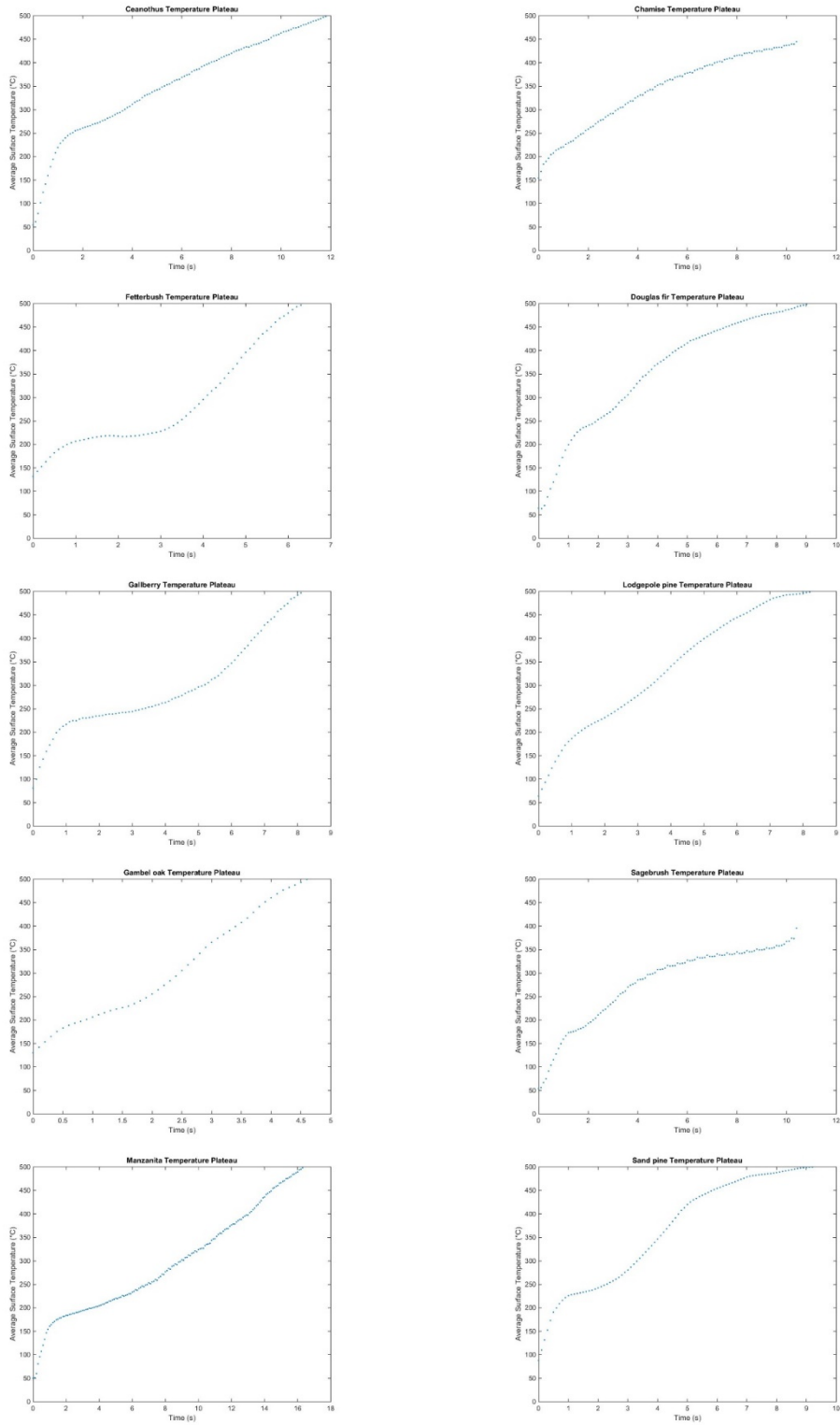


Figure C-1: Sample temperature plateau curves for all ten species. Broadleaf species are in the left column, needle species are in the right column.

#### **C.4 Data for Flame Behavior near Slopes**

The processed data for the experiments on the Coanda effect and flame behavior near slopes are available at the following url:

[http://www.et.byu.edu/~tom/students/Jonathan\\_Gallacher.html](http://www.et.byu.edu/~tom/students/Jonathan_Gallacher.html).

## D. DATA PROCESSING AND MODEL DEVELOPMENT ALGORITHMS

This appendix contains the data processing and model development algorithms for the data and models reported in the text of the dissertation. The surface area measurement algorithm is in Appendix D.1; the physical properties model development algorithm is in Appendix D.2 and the ignition and burning model development algorithm is in Appendix D.3.

### D.1 Surface Area Measurement Algorithm<sup>6</sup>

```
% Calculates surface area of broadleaf species based on 'Run 0' images
% To use: load 'Run 0' image and rename it "I"; enter thickness (in mm)
% where indicated
% create variable thick_mm by copying data from Excel. Access the
desired entry in that vector by changing the value of run.
% create variable I entering the path to the desired image

run = 1;
thick_mm; % units: mm; load vector manually
thick_cm = thick_mm(run)/10;

% Define reference length of 10cm based on user input
num_cm = 10;
imshow(I);
title(['Click ' num2str(num_cm) ' cm interval']);
hold on;
[x1,y1]=ginput(1);
[x2,y2]=ginput(1);
hold off;
close (1)

% Create roipoly mask around individual leaf
Ipoly = roipoly(I);

% Calculate reference length and pixel to cm conversions
ref_length = sqrt((x1-x2)^2+(y1-y2)^2);
cm = ref_length/10;
cm2 = (ref_length^2)/100;
```

---

<sup>6</sup> This algorithm was written by Victoria Lansinger

```

% Convert to B/W
Igray = double(rgb2gray(I));
Inorm = Igray/max(max(Igray));
Ibw = imcomplement(im2bw(Inorm,graythresh(Inorm(Ipoly))));

% Calculate pixel area and perimeter
area = bwarea(Ibw(Ipoly));
p = regionprops(Ibw.*Ipoly,'Perimeter');
perim = p.Perimeter;

% Calculate surface area
SA_cm = 2*area/cm2 + perim/cm*thick_cm;

% Log calculated value
SA_log(run,1) = SA_cm;

```

## D.2 Physical Properties Model Development Algorithm

```

% This script will process the physical properties data
%% Data Organization
cd(['B:\Experiments\Seasonal Moisture Content Project'])
data = xlsread('Physical Properties Data.xlsx'); %data collected during
experiments
%Column Order: Run, MC, RMC, density(g/cm^3), length(cm), width(cm)...
%needle length(cm), thickness(mm), diameter(mm), SA(cm^2), mass(g),
dry mass(g), water mass (g)
%Species Order: Manz, Cean, DF, Goak, Fet, Gal, SP, Cham, Sage, LP
mdry = data(:,11)./(1+data(:,2)); %mdry = mfresh/(1+MC) [=] grams
mwater = data(:,11) - mdry; %mwater = mfresh - mdry
extradata = [data,mdry,mwater];
lndata = log(extradata(:,2:end)); quaddata = (extradata(:,2:end)).^2;
sqrtdata = sqrt(extradata(:,2:end)); %data transformations
alldata = [extradata,lndata,quaddata,sqrtdata]; %concatenate matrices--all
data with which to do the stats

%%%%%%%%%%%%%%%%%%%%%%%%%%%%%%%%%%%%%%%%%%%%%%%%%%%%%%%%%%%%%%%%%%%%%%%%% Organization of ALL DATA %%%%%%%%%%%%%%%%%%%%%%%%%%%%%%%%%%%%%%%%%%%%%%%%%%%%%%%%%%%%%%%%%%%%%%%%%%
% Define species
loc_nan = find(isnan(alldata(:,1)));
manz = alldata(1:loc_nan(1)-1,:); cean = alldata(loc_nan(1)+1:loc_nan(2)-
1,:);
DF = alldata(loc_nan(2)+1:loc_nan(3)-1,:); goak =
alldata(loc_nan(3)+1:loc_nan(4)-1,:);
fet = alldata(loc_nan(4)+1:loc_nan(5)-1,:); gal =
alldata(loc_nan(5)+1:loc_nan(6)-1,:);
SP = alldata(loc_nan(6)+1:loc_nan(7)-1,:); cham =
alldata(loc_nan(7)+1:loc_nan(8)-1,:);
sage = alldata(loc_nan(8)+1:loc_nan(9)-1,:); LP =
alldata(loc_nan(9)+1:end,:);
% Define columns for each dimension
col_run = 1; col_MC = [2,14,26,38]; col_RMC = [3,15,27,39]; col_rho =
[4,16,28,40]; col_len = [5,17,29,41];
col_wid = [6,18,30,42]; col_NL = [7,19,31,43]; col_thick = [8,20,32,44];
col_dia = [9,21,33,45];

```

```

col_SA = [10,22,34,46]; col_mf = [11,23,35,47]; col_md = [12,24,36,48];
col_mw = [13,25,37,49];

%% User Input
best_num = 5; %Number of models from each Criterion collected in best_md
nrns = 500; %Number of iterations using stepwiselm
dim_md_upper = 4; %maximum number of predictors used in the model.
Currently set to increase by 1 each round
type = 'needle'; %species type: broad, needle, cham, sage
species = 'cham'; %input species code: manz, cean, goak, fet, gal, SP, DF,
LP, cham, sage %%ADJ for SP2

%% Set up the loops
if strcmp(type, 'broad') == 1
%   poss_pred = ;%insert the possible predictors here
    if strcmp(species, 'manz') == 1
        response_var1 = manz(:,5); RV1_col = col_len'; RV1 =
'length'; %length
        response_var2 = manz(:,6); RV2_col = col_wid'; RV2 =
'width'; %width
        response_var3 = manz(:,8); RV3_col = col_thick'; RV3 =
'thickness'; %thickness
        response_var4 = [];
        pred_lm = manz(:,11); %length as the one-variable model
        current_range = (1:loc_nan(1)-1)'; %the section of alldata from
which I will pull the data
        elseif strcmp(species, 'cean') == 1
            response_var1 = cean(:,5); RV1_col = col_len'; RV1 =
'length'; %length
            response_var2 = cean(:,6); RV2_col = col_wid'; RV2 =
'width'; %width
            response_var3 = cean(:,8); RV3_col = col_thick'; RV3 =
'thickness'; %thickness
            response_var4 = [];
            pred_lm = cean(:,11); %length as the one-variable model
            current_range = (loc_nan(1)+1:loc_nan(2)-1)';
        elseif strcmp(species, 'goak') == 1
            response_var1 = goak(:,5); RV1_col = col_len'; RV1 =
'length'; %length
            response_var2 = goak(:,6); RV2_col = col_wid'; RV2 =
'width'; %width
            response_var3 = goak(:,8); RV3_col = col_thick'; RV3 =
'thickness'; %thickness
            response_var4 = [];
            pred_lm = goak(:,11); %length as the one-variable model
            current_range = (loc_nan(3)+1:loc_nan(4)-1)';
        elseif strcmp(species, 'fet') == 1
            response_var1 = fet(:,5); RV1_col = col_len'; RV1 =
'length'; %length
            response_var2 = fet(:,6); RV2_col = col_wid'; RV2 =
'width'; %width
            response_var3 = fet(:,8); RV3_col = col_thick'; RV3 =
'thickness'; %thickness
            response_var4 = [];
            pred_lm = fet(:,11); %length as the one-variable model
            current_range = (loc_nan(4)+1:loc_nan(5)-1)';

```

```

elseif strcmp(species, 'gal') == 1
    response_var1 = gal(:,5); RV1_col = col_len'; RV1 =
'length'; %length
    response_var2 = gal(:,6); RV2_col = col_wid'; RV2 =
'width'; %width
    response_var3 = gal(:,8); RV3_col = col_thick'; RV3 =
'thickness'; %thickness
    response_var4 = [];
    pred_lm = gal(:,11); %length as the one-variable model
    current_range = (loc_nan(5)+1:loc_nan(6)-1)';
else
    'You need a different broadleaf species.'
end
elseif strcmp(type, 'needle') == 1 %needles ahve width also
%    poss_pred = ;%insert the possible predictors here
    if strcmp(species, 'DF') == 1
        response_var1 = DF(:,5); RV1_col = col_len'; RV1 =
'length'; %length
        response_var2 = DF(:,6); RV2_col = col_wid'; RV2 = 'width'; %width
        response_var3 = DF(:,7); RV3_col = col_NL'; RV3 = 'needle
length'; %needle length
        response_var4 = DF(:,9); RV4_col = col_dia'; RV4 = 'stem
diameter'; %stem diameter
        pred_lm = DF(:,11); %length as the one-variable model
        current_range = (loc_nan(2)+1:loc_nan(3)-1)';
        elseif strcmp(species, 'SP') == 1 %%ADJ for SP2
            response_var1 = SP(:,5); RV1_col = col_len'; RV1 =
'length'; %length %%ADJ for SP2
            response_var2 = SP(:,6); RV2_col = col_wid'; RV2 =
'width'; %width %%ADJ for SP2
            response_var3 = SP(:,7); RV3_col = col_NL'; RV3 = 'needle
length'; %needle length %%ADJ for SP2
            response_var4 = SP(:,9); RV4_col = col_dia'; RV4 = 'stem
diameter'; %stem diameter %%ADJ for SP2
            pred_lm = SP(:,11); %length as the one-variable model %%ADJ for
SP2
            current_range = (loc_nan(6)+1:loc_nan(7)-1)'; %current_range =
current_range(33:end);%%ADJ for SP2
            elseif strcmp(species, 'LP') == 1
                response_var1 = LP(:,5); RV1_col = col_len'; RV1 =
'length'; %length
                response_var2 = LP(:,6); RV2_col = col_wid'; RV2 = 'width'; %width
                response_var3 = LP(:,7); RV3_col = col_NL'; RV3 = 'needle
length'; %needle length
                response_var4 = LP(:,9); RV4_col = col_dia'; RV4 = 'stem
diameter'; %stem diameter
                pred_lm = LP(:,11); %length as the one-variable model
                current_range = (loc_nan(9)+1:length(alldata))';
            else
                'You need a different needle species.'
            end
        elseif strcmp(type, 'cham') == 1
            response_var1 = cham(:,5); RV1_col = col_len'; RV1 = 'length'; %length
            %    response_var2 = cham(:,7); %needle length
            response_var2 = cham(:,9); RV2_col = col_dia'; RV2 = 'stem
diameter'; %stem diameter
            response_var3 = [];

```

```

    response_var4 = [];
    pred_lm = cham(:,11); %length as the one-variable model
    current_range = (loc_nan(7)+1:loc_nan(8)-1)';
elseif strcmp(type, 'sage') == 1
    response_var1 = sage(:,5); RV1_col = col_len'; RV1 = 'length'; %length
%     response_var2 = cham(:,7); %needle length
    response_var2 = sage(:,9); RV2_col = col_dia'; RV2 = 'stem
diameter'; %stem diameter
    response_var3 = [];
    response_var4 = [];
    pred_lm = sage(:,11); %length as the one-variable model
    current_range = (loc_nan(8)+1:loc_nan(9)-1)';
else
    'you need to specify the type correctly.'
end
end
poss_pred = [2,3,11,12,13; 14,15,23,24,25; 26,27,35,36,37;
38,39,47,48,49]; %The possible variables to be used in the model--sans
density

%% Statistics Round 1
%%%%%%%%%%%%%% RV1 %%%%%%%%%%%%%%%
if isempty(response_var1) == 0
clear predictors coltrack p F response_var i j col
%Linear model
store_RV1_crit = zeros(nruns+1,5); %store_len_crit =
[i,NumCoefficients,R^2,AIC,BIC]
md_RV1_lm = fitlm(pred_lm,response_var1);
store_RV1_crit(1,1) = 1; %first model try
store_RV1_crit(1,2) = size(md_RV1_lm.Coefficients.Estimate,1)-1; %number
of parameters
store_RV1_crit(1,3) = md_RV1_lm.Rsquared.Adjusted; %R^2 value for the
model
[p,F] = coefTest(md_RV1_lm);
store_RV1_info{1,:} = [(LANDFIRE 1.2.0), {p}, {F}, {md_RV1_lm.DFE},
{md_RV1_lm.NumObservations}, {md_RV1_lm.RMSE}, {md_RV1_lm.Coefficients},
{md_RV1_lm.Formula}];
md_RV1{1,:} = md_RV1_lm;
i = 2;
while i <= nruns+1
    %Extract a random subset of variables for use in the model
development
    predictors = zeros(length(response_var1),dim_md_upper); coltrack =
zeros(dim_md_upper,1);
    dmy1 = randsample(1:size(poss_pred,2),dim_md_upper)'; %columns
    dmy2 = ceil(rand(dim_md_upper,1)*size(poss_pred,1)); %rows--always 4
rows in poss_pred
    pairs = [dmy2,dmy1];
    for j = 1:size(predictors,2)
        coltrack(j) = poss_pred(dmy2(j),dmy1(j));
        predictors(:,j) = alldata(current_range,coltrack(j));
    end
end
%Stepwise Model working up from a constant
if i < nruns/2
    md_RV1_su =
stepwiselm(predictors,response_var1,'constant','Upper','interactions','Cri
terion','bic'); %'AdjRsquared');

```

```

        store_RV1_crit(i,:) = [i, md_RV1_su.NumCoefficients,
md_RV1_su.Rsquared.Adjusted, md_RV1_su.ModelCriterion.AIC,
md_RV1_su.ModelCriterion.BIC];
        [p,F] = coefTest(md_RV1_su);
        store_RV1_info{i,:} = {i, p, F, md_RV1_su.DFE,
md_RV1_su.NumObservations, md_RV1_su.RMSE, md_RV1_su.Coefficients,
md_RV1_su.Formula, coltrack};
        md_RV1{i,:} = md_RV1_su;
%Stepwise Model working down from the full model
else
    md_RV1_su =
stepwiselm(predictors,response_var1,'interactions','Upper','interactions',
'Criterion','bic'); %'AdjRsquared');
    store_RV1_crit(i,:) = [i, md_RV1_su.NumCoefficients,
md_RV1_su.Rsquared.Adjusted, md_RV1_su.ModelCriterion.AIC,
md_RV1_su.ModelCriterion.BIC];
    [p,F] = coefTest(md_RV1_su);
    store_RV1_info{i,:} = {i, p, F, md_RV1_su.DFE,
md_RV1_su.NumObservations, md_RV1_su.RMSE, md_RV1_su.Coefficients,
md_RV1_su.Formula, coltrack};
    md_RV1{i,:} = md_RV1_su;
end
i = i+1;
clear coltrack
end

best_RV1_p = sortrows(store_RV1_crit,2); best_RV1_AdjR =
sortrows(store_RV1_crit,-3); best_RV1_aic = sortrows(store_RV1_crit,4);
best_RV1_bic = sortrows(store_RV1_crit,5);
best_RV1_crit = [store_RV1_crit(1,:); best_RV1_p(1:best_num,:)];
best_RV1_AdjR(1:best_num,:); best_RV1_aic(1:best_num,:);
best_RV1_bic(1:best_num,:)];

md_RV1_crit = best_RV1_AdjR(1,:); md_RV1_info =
store_RV1_info{best_RV1_AdjR(1,1),:};
end

%%%%%%%%%%%%% RV2 %%%%%%%%%%%%%%
if isempty(response_var2) == 0
clear predictors coltrack p F i j col
%Linear Model
store_RV2_crit = zeros(nruns+1,5); %store_RV2_crit =
[i,NumCoefficients,R^2,AIC,BIC]
md_RV2_lm = fitlm(pred_lm,response_var2);
store_RV2_crit(1,1) = 1; %first model try
store_RV2_crit(1,2) = size(md_RV2_lm.Coefficients.Estimate,1)-1; %number
of parameters
store_RV2_crit(1,3) = md_RV2_lm.Rsquared.Adjusted; %R^2 value for the
model
[p,F] = coefTest(md_RV2_lm);
store_RV2_info{1,:} = [(LANDFIRE 1.2.0), {p}, {F}, {md_RV2_lm.DFE},
{md_RV2_lm.NumObservations}, {md_RV2_lm.RMSE}, {md_RV2_lm.Coefficients},
{md_RV2_lm.Formula}];
md_RV2{1,:} = md_RV2_lm;
i = 2;
while i <= nruns+1

```

```

    %Extract a random subset of variables for use in the model
    developement
    predictors = zeros(length(response_var2),dim_md_upper); coltrack =
zeros(dim_md_upper,1);
    dmy1 = randsample(1:size(poss_pred,2),dim_md_upper)'; %columns
    dmy2 = ceil(rand(dim_md_upper,1)*size(poss_pred,1)); %rows--always 4
rows in poss_pred
    pairs = [dmy2,dmy1];
    for j = 1:size(predictors,2)
        coltrack(j) = poss_pred(dmy2(j),dmy1(j));
        predictors(:,j) = alldata(current_range,coltrack(j));
    end
%Stepwise Model working up from a constant
if i < nruns/2
    md_RV2_su =
stepwiselm(predictors,response_var2,'constant','Upper','interactions','Cri
terion','bic'); %'AdjRsquared');
    store_RV2_crit(i,:) = [i, md_RV2_su.NumCoefficients,
md_RV2_su.Rsquared.Adjusted, md_RV2_su.ModelCriterion.AIC,
md_RV2_su.ModelCriterion.BIC];
    [p,F] = coefTest(md_RV2_su);
    store_RV2_info{i,:} = {i, p, F, md_RV2_su.DFE,
md_RV2_su.NumObservations, md_RV2_su.RMSE, md_RV2_su.Coefficients,
md_RV2_su.Formula, coltrack};
    md_RV2{i,:} = md_RV2_su;
%Stepwise Model working down from the full model
else
    md_RV2_su =
stepwiselm(predictors,response_var2,'interactions','Upper','interactions',
'Criterion','bic'); %'AdjRsquared');
    store_RV2_crit(i,:) = [i, md_RV2_su.NumCoefficients,
md_RV2_su.Rsquared.Adjusted, md_RV2_su.ModelCriterion.AIC,
md_RV2_su.ModelCriterion.BIC];
    [p,F] = coefTest(md_RV2_su);
    store_RV2_info{i,:} = {i, p, F, md_RV2_su.DFE,
md_RV2_su.NumObservations, md_RV2_su.RMSE, md_RV2_su.Coefficients,
md_RV2_su.Formula, coltrack};
    md_RV2{i,:} = md_RV2_su;
end
i = i+1;
clear coltrack
end

best_RV2_p = sortrows(store_RV2_crit,2); best_RV2_AdjR =
sortrows(store_RV2_crit,-3); best_RV2_aic = sortrows(store_RV2_crit,4);
best_RV2_bic = sortrows(store_RV2_crit,5);
best_RV2_crit = [store_RV2_crit(1,:); best_RV2_p(1:best_num,:);
best_RV2_AdjR(1:best_num,:); best_RV2_aic(1:best_num,:);
best_RV2_bic(1:best_num,:)];

md_RV2_crit = best_RV2_AdjR(1,:); md_RV2_info =
store_RV2_info{best_RV2_AdjR(1,1),:};
end

%%%%%%%%%%%%% RV3 %%%%%%%%%%%%%%
if isempty(response_var3) == 0

```

```

clear predictors coltrack p F i j col
%Linear Model
store_RV3_crit = zeros(nruns+1,5); %store_RV3_crit =
[i,NumCoefficients,R^2,AIC,BIC]
md_RV3_lm = fitlm(pred_lm,response_var3);
store_RV3_crit(1,1) = 1; %first model try
store_RV3_crit(1,2) = size(md_RV3_lm.Coefficients.Estimate,1)-1; %number
of parameters
store_RV3_crit(1,3) = md_RV3_lm.Rsquared.Adjusted; %R^2 value for the
model
[p,F] = coefTest(md_RV3_lm);
store_RV3_info{1,:} = [(LANDFIRE 1.2.0), {p}, {F}, {md_RV3_lm.DFE},
{md_RV3_lm.NumObservations}, {md_RV3_lm.RMSE}, {md_RV3_lm.Coefficients},
{md_RV3_lm.Formula}];
md_RV3{1,:} = md_RV3_lm;
i = 2;
while i <= nruns+1
    %Extract a random subset of variables for use in the model
    developement
    predictors = zeros(length(response_var3),dim_md_upper); coltrack =
zeros(dim_md_upper,1);
    dmy1 = randsample(1:size(poss_pred,2),dim_md_upper)'; %columns
    dmy2 = ceil(rand(dim_md_upper,1)*size(poss_pred,1)); %rows--always 4
rows in poss_pred
    pairs = [dmy2,dmy1];
    for j = 1:size(predictors,2)
        coltrack(j) = poss_pred(dmy2(j),dmy1(j));
        predictors(:,j) = alldata(current_range,coltrack(j));
    end
    %Stepwise Model working up from a constant
    if i < nruns/2
        md_RV3_su =
stepwiselm(predictors,response_var3,'constant','Upper','interactions','Cri
terion','bic'); %'AdjRsquared');
        store_RV3_crit(i,:) = [i, md_RV3_su.NumCoefficients,
md_RV3_su.Rsquared.Adjusted, md_RV3_su.ModelCriterion.AIC,
md_RV3_su.ModelCriterion.BIC];
        [p,F] = coefTest(md_RV3_su);
        store_RV3_info{i,:} = {i, p, F, md_RV3_su.DFE,
md_RV3_su.NumObservations, md_RV3_su.RMSE, md_RV3_su.Coefficients,
md_RV3_su.Formula, coltrack};
        md_RV3{i,:} = md_RV3_su;
    %Stepwise Model working down from the full model
    else
        md_RV3_su =
stepwiselm(predictors,response_var3,'interactions','Upper','interactions',
'Criterion','bic'); %'AdjRsquared');
        store_RV3_crit(i,:) = [i, md_RV3_su.NumCoefficients,
md_RV3_su.Rsquared.Adjusted, md_RV3_su.ModelCriterion.AIC,
md_RV3_su.ModelCriterion.BIC];
        [p,F] = coefTest(md_RV3_su);
        store_RV3_info{i,:} = {i, p, F, md_RV3_su.DFE,
md_RV3_su.NumObservations, md_RV3_su.RMSE, md_RV3_su.Coefficients,
md_RV3_su.Formula, coltrack};
        md_RV3{i,:} = md_RV3_su;
    end
    i = i+1;

```

```

clear coltrack
end

best_RV3_p = sortrows(store_RV3_crit,2); best_RV3_AdjR =
sortrows(store_RV3_crit,-3); best_RV3_aic = sortrows(store_RV3_crit,4);
best_RV3_bic = sortrows(store_RV3_crit,5);
best_RV3_crit = [store_RV3_crit(1,:); best_RV3_p(1:best_num,:);
best_RV3_AdjR(1:best_num,:); best_RV3_aic(1:best_num,:);
best_RV3_bic(1:best_num,:)];
md_RV3_crit = best_RV3_AdjR(1,:); md_RV3_info =
store_RV3_info{best_RV3_AdjR(1,1),:};
end

%%%%%%%%%%%%%% RV4 %%%%%%%%%%%%%%%
if isempty(response_var4) == 0
clear predictors coltrack p F i j col
%Linear Model
store_RV4_crit = zeros(nruns+1,5); %store_RV4_crit =
[i,NumCoefficients,R^2,AIC,BIC]
md_RV4_lm = fitlm(pred_lm,response_var4);
store_RV4_crit(1,1) = 1; %first model try
store_RV4_crit(1,2) = size(md_RV4_lm.Coefficients.Estimate,1)-1; %number
of parameters
store_RV4_crit(1,3) = md_RV4_lm.Rsquared.Adjusted; %R^2 value for the
model
[p,F] = coefTest(md_RV4_lm);
store_RV4_info{1,:} = [(LANDFIRE 1.2.0), {p}, {F}, {md_RV4_lm.DFE},
{md_RV4_lm.NumObservations}, {md_RV4_lm.RMSE}, {md_RV4_lm.Coefficients},
{md_RV4_lm.Formula}];
md_RV4{1,:} = md_RV4_lm;
i = 2;
while i <= nruns+1
    %Extract a random subset of variables for use in the model
development
    predictors = zeros(length(response_var4),dim_md_upper); coltrack =
zeros(dim_md_upper,1);
    dmy1 = randsample(1:size(poss_pred,2),dim_md_upper)'; %columns
    dmy2 = ceil(rand(dim_md_upper,1)*size(poss_pred,1)); %rows--always 4
rows in poss_pred
    pairs = [dmy2,dmy1];
    for j = 1:size(predictors,2)
        coltrack(j) = poss_pred(dmy2(j),dmy1(j));
        predictors(:,j) = alldata(current_range,coltrack(j));
    end
end
%Stepwise Model working up from a constant
if i < nruns/2
    md_RV4_su =
stepwiselm(predictors,response_var4,'constant','Upper','interactions','Cri
terion','bic'); %'AdjRsquared');
    store_RV4_crit(i,:) = [i, md_RV4_su.NumCoefficients,
md_RV4_su.Rsquared.Adjusted, md_RV4_su.ModelCriterion.AIC,
md_RV4_su.ModelCriterion.BIC];
    [p,F] = coefTest(md_RV4_su);
    store_RV4_info{i,:} = {i, p, F, md_RV4_su.DFE,
md_RV4_su.NumObservations, md_RV4_su.RMSE, md_RV4_su.Coefficients,
md_RV4_su.Formula, coltrack};
end

```

```

    md_RV4{i,:} = md_RV4_su;
%Stepwise Model working down from the full model
else
    md_RV4_su =
stepwiselm(predictors,response_var4,'interactions','Upper','interactions',
'Criterion','bic'); %'AdjRsquared');
    store_RV4_crit(i,:) = [i, md_RV4_su.NumCoefficients,
md_RV4_su.Rsquared.Adjusted, md_RV4_su.ModelCriterion.AIC,
md_RV4_su.ModelCriterion.BIC];
    [p,F] = coefTest(md_RV4_su);
    store_RV4_info{i,:} = {i, p, F, md_RV4_su.DFE,
md_RV4_su.NumObservations, md_RV4_su.RMSE, md_RV4_su.Coefficients,
md_RV4_su.Formula, coltrack};
    md_RV4{i,:} = md_RV4_su;
end
i = i+1;
clear coltrack
end

best_RV4_p = sortrows(store_RV4_crit,2); best_RV4_AdjR =
sortrows(store_RV4_crit,-3); best_RV4_aic = sortrows(store_RV4_crit,4);
best_RV4_bic = sortrows(store_RV4_crit,5);
best_RV4_crit = [store_RV4_crit(1,:); best_RV4_p(1:best_num,:);
best_RV4_AdjR(1:best_num,:); best_RV4_aic(1:best_num,:);
best_RV4_bic(1:best_num,:)];
md_RV4_crit = best_RV4_AdjR(1,:); md_RV4_info =
store_RV4_info{best_RV4_AdjR(1,1),:};
end

if isempty(response_var1) == 1
    best_md1(1) = 0;
else
    best_md1(1) = best_RV1_AdjR(1,3);
end
if isempty(response_var2) == 1
    best_md1(2) = 0;
else
    best_md1(2) = best_RV2_AdjR(1,3);
end
if isempty(response_var3) == 1
    best_md1(3) = 0;
else
    best_md1(3) = best_RV3_AdjR(1,3);
end
if isempty(response_var4) == 1
    best_md1(4) = 0;
else
    best_md1(4) = best_RV4_AdjR(1,3);
end
if max(best_md1) == best_md1(1)
    order(LANDFIRE 1.2.0) = 'RV1';
    response_var1 = [];
    poss_pred = [poss_pred, RV1_col];
elseif max(best_md1) == best_md1(2)
    order(LANDFIRE 1.2.0) = 'RV2';
    response_var2 = [];

```

```

    poss_pred = [poss_pred, RV2_col];
elseif max(best_md1) == best_md1(3)
    order(LANDFIRE 1.2.0) = 'RV3';
    response_var3 = [];
    poss_pred = [poss_pred, RV3_col];
elseif max(best_md1) == best_md1(4)
    order(LANDFIRE 1.2.0) = 'RV4';
    response_var4 = [];
    poss_pred = [poss_pred, RV4_col];
else
    'best unknown R1'
    break
end

'Finished round 1. -----'

%% Statistics Round 2
dim_md_upper = dim_md_upper + 1; %maximum number of predictors used in the
model

%%%%%%%%%%%%%% RV11 %%%%%%%%%%%%%%%
if isempty(response_var1) == 0
clear predictors coltrack p F i j col
i = 1;
while i <= nruns+1
    %Extract a random subset of variables for use in the model
    development
    predictors = zeros(length(response_var1),dim_md_upper); coltrack =
zeros(dim_md_upper,1);
    dmy1 = randsample(1:size(poss_pred,2),dim_md_upper)'; %columns
    dmy2 = ceil(rand(dim_md_upper,1)*size(poss_pred,1)); %rows--always 4
rows in poss_pred
    pairs = [dmy2,dmy1];
    for j = 1:size(predictors,2)
        coltrack(j) = poss_pred(dmy2(j),dmy1(j));
        predictors(:,j) = alldata(current_range,coltrack(j));
    end
    %Stepwise Model working up from a constant
    if i < nruns/2
        md_RV11_su =
stepwiselm(predictors,response_var1,'constant','Upper','interactions','Cri
terion','bic'); %'AdjRsquared');
        store_RV11_crit(i,:) = [i, md_RV11_su.NumCoefficients,
md_RV11_su.Rsquared.Adjusted, md_RV11_su.ModelCriterion.AIC,
md_RV11_su.ModelCriterion.BIC];
        [p,F] = coefTest(md_RV11_su);
        store_RV11_info{i,:} = {i, p, F, md_RV11_su.DFE,
md_RV11_su.NumObservations, md_RV11_su.RMSE, md_RV11_su.Coefficients,
md_RV11_su.Formula, coltrack};
        md_RV11{i,:} = md_RV11_su;
    %Stepwise Model working down from the full model
    else
        md_RV11_su =
stepwiselm(predictors,response_var1,'interactions','Upper','interactions',
'Criterion','bic'); %'AdjRsquared');

```

```

    store_RV11_crit(i,:) = [i, md_RV11_su.NumCoefficients,
md_RV11_su.Rsquared.Adjusted, md_RV11_su.ModelCriterion.AIC,
md_RV11_su.ModelCriterion.BIC];
    [p,F] = coefTest(md_RV11_su);
    store_RV11_info{i,:} = {i, p, F, md_RV11_su.DFE,
md_RV11_su.NumObservations, md_RV11_su.RMSE, md_RV11_su.Coefficients,
md_RV11_su.Formula, coltrack};
    md_RV11{i,:} = md_RV11_su;
end
i = i+1;
clear coltrack
end

best_RV11_p = sortrows(store_RV11_crit,2); best_RV11_AdjR =
sortrows(store_RV11_crit,-3); best_RV11_aic = sortrows(store_RV11_crit,4);
best_RV11_bic = sortrows(store_RV11_crit,5);
best_RV11_crit = [store_RV11_crit(1,:); best_RV11_p(1:best_num,:);
best_RV11_AdjR(1:best_num,:); best_RV11_aic(1:best_num,:);
best_RV11_bic(1:best_num,:)];

md_RV11_crit = best_RV11_AdjR(1,:); md_RV11_info =
store_RV11_info{best_RV11_AdjR(1,1),:};
end

%%%%%%%%%%%% RV22 %%%%%%%%%%%%%
if isempty(response_var2) == 0
clear predictors coltrack p F i j col
i = 1;
while i <= nruns+1
    %Extract a random subset of variables for use in the model
    development
    predictors = zeros(length(response_var2),dim_md_upper); coltrack =
zeros(dim_md_upper,1);
    dmy1 = randsample(1:size(poss_pred,2),dim_md_upper)'; %columns
    dmy2 = ceil(rand(dim_md_upper,1)*size(poss_pred,1)); %rows--always 4
    rows in poss_pred
    pairs = [dmy2,dmy1];
    for j = 1:size(predictors,2)
        coltrack(j) = poss_pred(dmy2(j),dmy1(j));
        predictors(:,j) = alldata(current_range,coltrack(j));
    end
    %Stepwise Model working up from a constant
    if i < nruns/2
        md_RV22_su =
stepwiselm(predictors,response_var2,'constant','Upper','interactions','Cri
terion','bic'); %'AdjRsquared');
        store_RV22_crit(i,:) = [i, md_RV22_su.NumCoefficients,
md_RV22_su.Rsquared.Adjusted, md_RV22_su.ModelCriterion.AIC,
md_RV22_su.ModelCriterion.BIC];
        [p,F] = coefTest(md_RV22_su);
        store_RV22_info{i,:} = {i, p, F, md_RV22_su.DFE,
md_RV22_su.NumObservations, md_RV22_su.RMSE, md_RV22_su.Coefficients,
md_RV22_su.Formula, coltrack};
        md_RV22{i,:} = md_RV22_su;
    %Stepwise Model working down from the full model
    else

```

```

md_RV22_su =
stepwiselm(predictors,response_var2,'interactions','Upper','interactions',
'Criterion','bic'); %'AdjRsquared');
store_RV22_crit(i,:) = [i, md_RV22_su.NumCoefficients,
md_RV22_su.Rsquared.Adjusted, md_RV22_su.ModelCriterion.AIC,
md_RV22_su.ModelCriterion.BIC];
[p,F] = coefTest(md_RV22_su);
store_RV22_info{i,:} = {i, p, F, md_RV22_su.DFE,
md_RV22_su.NumObservations, md_RV22_su.RMSE, md_RV22_su.Coefficients,
md_RV22_su.Formula, coltrack};
md_RV22{i,:} = md_RV22_su;
end
i = i+1;
clear coltrack
end

best_RV22_p = sortrows(store_RV22_crit,2); best_RV22_AdjR =
sortrows(store_RV22_crit,-3); best_RV22_aic = sortrows(store_RV22_crit,4);
best_RV22_bic = sortrows(store_RV22_crit,5);
best_RV22_crit = [store_RV22_crit(1,:); best_RV22_p(1:best_num,:);
best_RV22_AdjR(1:best_num,:); best_RV22_aic(1:best_num,:);
best_RV22_bic(1:best_num,:)];

md_RV22_crit = best_RV22_AdjR(1,:); md_RV22_info =
store_RV22_info{best_RV22_AdjR(1,1),:};
end

%%%%%%%%%%%%%% RV33 %%%%%%%%%%%%%%%
if isempty(response_var3) == 0
clear predictors coltrack p F i j col
i = 1;
while i <= nruns+1
%Extract a random subset of variables for use in the model
development
predictors = zeros(length(response_var3),dim_md_upper); coltrack =
zeros(dim_md_upper,1);
dmy1 = randsample(1:size(poss_pred,2),dim_md_upper)'; %columns
dmy2 = ceil(rand(dim_md_upper,1)*size(poss_pred,1)); %rows--always 4
rows in poss_pred
pairs = [dmy2,dmy1];
for j = 1:size(predictors,2)
coltrack(j) = poss_pred(dmy2(j),dmy1(j));
predictors(:,j) = alldata(current_range,coltrack(j));
end
%Stepwise Model working up from a constant
if i < nruns/2
md_RV33_su =
stepwiselm(predictors,response_var3,'constant','Upper','interactions','Cri
terion','bic'); %'AdjRsquared');
store_RV33_crit(i,:) = [i, md_RV33_su.NumCoefficients,
md_RV33_su.Rsquared.Adjusted, md_RV33_su.ModelCriterion.AIC,
md_RV33_su.ModelCriterion.BIC];
[p,F] = coefTest(md_RV33_su);
store_RV33_info{i,:} = {i, p, F, md_RV33_su.DFE,
md_RV33_su.NumObservations, md_RV33_su.RMSE, md_RV33_su.Coefficients,
md_RV33_su.Formula, coltrack};

```

```

    md_RV33{i,:} = md_RV33_su;
%Stepwise Model working down from the full model
else
    md_RV33_su =
stepwiselm(predictors,response_var3,'interactions','Upper','interactions',
'Criterion','bic'); %'AdjRsquared');
    store_RV33_crit(i,:) = [i, md_RV33_su.NumCoefficients,
md_RV33_su.Rsquared.Adjusted, md_RV33_su.ModelCriterion.AIC,
md_RV33_su.ModelCriterion.BIC];
    [p,F] = coefTest(md_RV33_su);
    store_RV33_info{i,:} = {i, p, F, md_RV33_su.DFE,
md_RV33_su.NumObservations, md_RV33_su.RMSE, md_RV33_su.Coefficients,
md_RV33_su.Formula, coltrack};
    md_RV33{i,:} = md_RV33_su;
end
i = i+1;
clear coltrack
end

best_RV33_p = sortrows(store_RV33_crit,2); best_RV33_AdjR =
sortrows(store_RV33_crit,-3); best_RV33_aic = sortrows(store_RV33_crit,4);
best_RV33_bic = sortrows(store_RV33_crit,5);
best_RV33_crit = [store_RV33_crit(1,:); best_RV33_p(1:best_num,:);
best_RV33_AdjR(1:best_num,:); best_RV33_aic(1:best_num,:);
best_RV33_bic(1:best_num,:)];
md_RV33_crit = best_RV33_AdjR(1,:); md_RV33_info =
store_RV33_info{best_RV33_AdjR(1,1),:};
end

%%%%%%%%%%%%%%%%%%%%%%%%%%%%%%%%%%%%%%%%%%%%%%%%%%%%%%%%%%%%%%%%%%%%%%%% RV44 %%%%%%%%%%%%%%%%%%%%%%%%%%%%%%%%%%%%%%%%%%%%%%%%%%%%%%%%%%%%%%%%%%%%%%%%%
if isempty(response_var4) == 0
clear predictors coltrack p F i j col
i = 1;
while i <= nruns+1
    %Extract a random subset of variables for use in the model
development
    predictors = zeros(length(response_var4),dim_md_upper); coltrack =
zeros(dim_md_upper,1);
    dmy1 = randsample(1:size(poss_pred,2),dim_md_upper)'; %columns
    dmy2 = ceil(rand(dim_md_upper,1)*size(poss_pred,1)); %rows--always 4
rows in poss_pred
    pairs = [dmy2,dmy1];
    for j = 1:size(predictors,2)
        coltrack(j) = poss_pred(dmy2(j),dmy1(j));
        predictors(:,j) = alldata(current_range,coltrack(j));
    end
end
%Stepwise Model working up from a constant
if i < nruns/2
    md_RV44_su =
stepwiselm(predictors,response_var4,'constant','Upper','interactions','Cri
terion','bic'); %'AdjRsquared');
    store_RV44_crit(i,:) = [i, md_RV44_su.NumCoefficients,
md_RV44_su.Rsquared.Adjusted, md_RV44_su.ModelCriterion.AIC,
md_RV44_su.ModelCriterion.BIC];
    [p,F] = coefTest(md_RV44_su);

```

```

        store_RV44_info{i,:} = {i, p, F, md_RV44_su.DFE,
md_RV44_su.NumObservations, md_RV44_su.RMSE, md_RV44_su.Coefficients,
md_RV44_su.Formula, coltrack};
        md_RV44{i,:} = md_RV44_su;
%Stepwise Model working down from the full model
else
        md_RV44_su =
stepwiselm(predictors,response_var4,'interactions','Upper','interactions',
'Criterion','bic'); %'AdjRsquared');
        store_RV44_crit(i,:) = [i, md_RV44_su.NumCoefficients,
md_RV44_su.Rsquared.Adjusted, md_RV44_su.ModelCriterion.AIC,
md_RV44_su.ModelCriterion.BIC];
        [p,F] = coefTest(md_RV44_su);
        store_RV44_info{i,:} = {i, p, F, md_RV44_su.DFE,
md_RV44_su.NumObservations, md_RV44_su.RMSE, md_RV44_su.Coefficients,
md_RV44_su.Formula, coltrack};
        md_RV44{i,:} = md_RV44_su;
end
i = i+1;
clear coltrack
end

best_RV44_p = sortrows(store_RV44_crit,2); best_RV44_AdjR =
sortrows(store_RV44_crit,-3); best_RV44_aic = sortrows(store_RV44_crit,4);
best_RV44_bic = sortrows(store_RV44_crit,5);
best_RV44_crit = [store_RV44_crit(1,:); best_RV44_p(1:best_num,:);
best_RV44_AdjR(1:best_num,:); best_RV44_aic(1:best_num,:);
best_RV44_bic(1:best_num,:)];

md_RV44_crit = best_RV44_AdjR(1,:); md_RV44_info =
store_RV44_info{best_RV44_AdjR(1,1),:};
end

%Determine best prediction from second round
if isempty(response_var1) == 1
        best_md2(1) = 0;
else
        best_md2(1) = best_RV11_AdjR(1,3);
end
if isempty(response_var2) == 1
        best_md2(2) = 0;
else
        best_md2(2) = best_RV22_AdjR(1,3);
end
if isempty(response_var3) == 1
        best_md2(3) = 0;
else
        best_md2(3) = best_RV33_AdjR(1,3);
end
if isempty(response_var4) == 1
        best_md2(4) = 0;
else
        best_md2(4) = best_RV44_AdjR(1,3);
end
if max(best_md2) == best_md2(1)
        order{2} = 'RV11';

```

```

        response_var1 = [];
        poss_pred = [poss_pred, RV1_col];
elseif max(best_md2) == best_md2(2)
    order{2} = 'RV22';
    response_var2 = [];
    poss_pred = [poss_pred, RV2_col];
elseif max(best_md2) == best_md2(3)
    order{2} = 'RV33';
    response_var3 = [];
    poss_pred = [poss_pred, RV3_col];
elseif max(best_md2) == best_md2(4)
    order{2} = 'RV44';
    response_var4 = [];
    poss_pred = [poss_pred, RV4_col];
else
    'best unknown R2'
    break
end
'Finished round 2. -----'

%% Statistics Round 3
dim_md_upper = dim_md_upper + 1; %maximum number of predictors used in the
model

%%%%%%%%%%%%%% RV111 %%%%%%%%%%%%%%%
if isempty(response_var1) == 0
clear predictors coltrack p F i j col
i = 1;
while i <= nruns+1
    %Extract a random subset of variables for use in the model
    development
        predictors = zeros(length(response_var1),dim_md_upper); coltrack =
zeros(dim_md_upper,1);
        dmy1 = randsample(1:size(poss_pred,2),dim_md_upper)'; %columns
        dmy2 = ceil(rand(dim_md_upper,1)*size(poss_pred,1)); %rows--always 4
rows in poss_pred
        pairs = [dmy2,dmy1];
        for j = 1:size(predictors,2)
            coltrack(j) = poss_pred(dmy2(j),dmy1(j));
            predictors(:,j) = alldata(current_range,coltrack(j));
        end
    %Stepwise Model working up from a constant
    if i < nruns/2
        md_RV111_su =
stepwiselm(predictors,response_var1,'constant','Upper','interactions','Cri
terion','bic'); %'AdjRsquared');
        store_RV111_crit(i,:) = [i, md_RV111_su.NumCoefficients,
md_RV111_su.Rsquared.Adjusted, md_RV111_su.ModelCriterion.AIC,
md_RV111_su.ModelCriterion.BIC];
        [p,F] = coefTest(md_RV111_su);
        store_RV111_info{i,:} = {i, p, F, md_RV111_su.DFE,
md_RV111_su.NumObservations, md_RV111_su.RMSE, md_RV111_su.Coefficients,
md_RV111_su.Formula, coltrack};
        md_RV111{i,:} = md_RV111_su;
    %Stepwise Model working down from the full model
    else

```

```

md_RV111_su =
stepwiselm(predictors,response_var1,'interactions','Upper','interactions',
'Criterion','bic'); %'AdjRsquared');
store_RV111_crit(i,:) = [i, md_RV111_su.NumCoefficients,
md_RV111_su.Rsquared.Adjusted, md_RV111_su.ModelCriterion.AIC,
md_RV111_su.ModelCriterion.BIC];
[p,F] = coefTest(md_RV111_su);
store_RV111_info{i,:} = {i, p, F, md_RV111_su.DFE,
md_RV111_su.NumObservations, md_RV111_su.RMSE, md_RV111_su.Coefficients,
md_RV111_su.Formula, coltrack};
md_RV111{i,:} = md_RV111_su;
end
i = i+1;
clear coltrack
end

best_RV111_p = sortrows(store_RV111_crit,2); best_RV111_AdjR =
sortrows(store_RV111_crit,-3); best_RV111_aic =
sortrows(store_RV111_crit,4); best_RV111_bic =
sortrows(store_RV111_crit,5);
best_RV111_crit = [store_RV111_crit(1,:); best_RV111_p(1:best_num,:);
best_RV111_AdjR(1:best_num,:); best_RV111_aic(1:best_num,:);
best_RV111_bic(1:best_num,:)];

md_RV111_crit = best_RV111_AdjR(1,:); md_RV111_info =
store_RV111_info{best_RV111_AdjR(1,1),:};
end

%%%%%%%%%%%% RV222 %%%%%%%%%%%%%
if isempty(response_var2) == 0
clear predictors coltrack p F i j col
i = 1;
while i <= nruns+1
%Extract a random subset of variables for use in the model
development
predictors = zeros(length(response_var2),dim_md_upper); coltrack =
zeros(dim_md_upper,1);
dmy1 = randsample(1:size(poss_pred,2),dim_md_upper)'; %columns
dmy2 = ceil(rand(dim_md_upper,1)*size(poss_pred,1)); %rows--always 4
rows in poss_pred
pairs = [dmy2,dmy1];
for j = 1:size(predictors,2)
coltrack(j) = poss_pred(dmy2(j),dmy1(j));
predictors(:,j) =
alldata(current_range,coltrack(j)); %%%%%%%%%%%%%This needs to change
end
%Stepwise Model working up from a constant
if i < nruns/2
md_RV222_su =
stepwiselm(predictors,response_var2,'constant','Upper','interactions','Cri
terion','bic'); %'AdjRsquared');
store_RV222_crit(i,:) = [i, md_RV222_su.NumCoefficients,
md_RV222_su.Rsquared.Adjusted, md_RV222_su.ModelCriterion.AIC,
md_RV222_su.ModelCriterion.BIC];
[p,F] = coefTest(md_RV222_su);

```

```

        store_RV222_info{i,:} = {i, p, F, md_RV222_su.DFE,
md_RV222_su.NumObservations, md_RV222_su.RMSE, md_RV222_su.Coefficients,
md_RV222_su.Formula, coltrack};
        md_RV222{i,:} = md_RV222_su;
%Stepwise Model working down from the full model
else
        md_RV222_su =
stepwiselm(predictors,response_var2,'interactions','Upper','interactions',
'Criterion','bic'); %'AdjRsquared');
        store_RV222_crit(i,:) = [i, md_RV222_su.NumCoefficients,
md_RV222_su.Rsquared.Adjusted, md_RV222_su.ModelCriterion.AIC,
md_RV222_su.ModelCriterion.BIC];
        [p,F] = coefTest(md_RV222_su);
        store_RV222_info{i,:} = {i, p, F, md_RV222_su.DFE,
md_RV222_su.NumObservations, md_RV222_su.RMSE, md_RV222_su.Coefficients,
md_RV222_su.Formula, coltrack};
        md_RV222{i,:} = md_RV222_su;
end
i = i+1;
clear coltrack
end

best_RV222_p = sortrows(store_RV222_crit,2); best_RV222_AdjR =
sortrows(store_RV222_crit,-3); best_RV222_aic =
sortrows(store_RV222_crit,4); best_RV222_bic =
sortrows(store_RV222_crit,5);
best_RV222_crit = [store_RV222_crit(1,:); best_RV222_p(1:best_num,:);
best_RV222_AdjR(1:best_num,:); best_RV222_aic(1:best_num,:);
best_RV222_bic(1:best_num,:)];

md_RV222_crit = best_RV222_AdjR(1,:); md_RV222_info =
store_RV222_info{best_RV222_AdjR(1,1),:};
end

%%%%%%%%%%%%%% RV333 %%%%%%%%%%%%%%%
if isempty(response_var3) == 0
clear predictors coltrack p F i j col
i = 1;
while i <= nruns+1
        %Extract a random subset of variables for use in the model
development
        predictors = zeros(length(response_var3),dim_md_upper); coltrack =
zeros(dim_md_upper,1);
        dmy1 = randsample(1:size(poss_pred,2),dim_md_upper)'; %columns
        dmy2 = ceil(rand(dim_md_upper,1)*size(poss_pred,1)); %rows--always 4
rows in poss_pred
        pairs = [dmy2,dmy1];
        for j = 1:size(predictors,2)
                coltrack(j) = poss_pred(dmy2(j),dmy1(j));
                predictors(:,j) = alldata(current_range,coltrack(j)); %%
        end
%Stepwise Model working up from a constant
if i < nruns/2
        md_RV333_su =
stepwiselm(predictors,response_var3,'constant','Upper','interactions','Cri
terion','bic'); %'AdjRsquared');

```

```

        store_RV333_crit(i,:) = [i, md_RV333_su.NumCoefficients,
md_RV333_su.Rsquared.Adjusted, md_RV333_su.ModelCriterion.AIC,
md_RV333_su.ModelCriterion.BIC];
        [p,F] = coefTest(md_RV333_su);
        store_RV333_info{i,:} = {i, p, F, md_RV333_su.DFE,
md_RV333_su.NumObservations, md_RV333_su.RMSE, md_RV333_su.Coefficients,
md_RV333_su.Formula, coltrack};
        md_RV333{i,:} = md_RV333_su;
%Stepwise Model working down from the full model
else
    md_RV333_su =
stepwiselm(predictors,response_var3,'interactions','Upper','interactions',
'Criterion','bic'); %'AdjRsquared');
    store_RV333_crit(i,:) = [i, md_RV333_su.NumCoefficients,
md_RV333_su.Rsquared.Adjusted, md_RV333_su.ModelCriterion.AIC,
md_RV333_su.ModelCriterion.BIC];
    [p,F] = coefTest(md_RV333_su);
    store_RV333_info{i,:} = {i, p, F, md_RV333_su.DFE,
md_RV333_su.NumObservations, md_RV333_su.RMSE, md_RV333_su.Coefficients,
md_RV333_su.Formula, coltrack};
    md_RV333{i,:} = md_RV333_su;
end
i = i+1;
clear coltrack
end

best_RV333_p = sortrows(store_RV333_crit,2); best_RV333_AdjR =
sortrows(store_RV333_crit,-3); best_RV333_aic =
sortrows(store_RV333_crit,4); best_RV333_bic =
sortrows(store_RV333_crit,5);
best_RV333_crit = [store_RV333_crit(1,:); best_RV333_p(1:best_num,:)];
best_RV333_AdjR(1:best_num,:); best_RV333_aic(1:best_num,:);
best_RV333_bic(1:best_num,:)];

md_RV333_crit = best_RV333_AdjR(1,:); md_RV333_info =
store_RV333_info{best_RV333_AdjR(1,1),:};
end

%%%%%%%%%%%% RV444 %%%%%%%%%%%%%
if isempty(response_var4) == 0
clear predictors coltrack p F i j col
i = 1;
while i <= nruns+1
    %Extract a random subset of variables for use in the model
development
    predictors = zeros(length(response_var4),dim_md_upper); coltrack =
zeros(dim_md_upper,1);
    dmy1 = randsample(1:size(poss_pred,2),dim_md_upper)'; %columns
    dmy2 = ceil(rand(dim_md_upper,1)*size(poss_pred,1)); %rows--always 4
rows in poss_pred
    pairs = [dmy2,dmy1];
    for j = 1:size(predictors,2)
        coltrack(j) = poss_pred(dmy2(j),dmy1(j));
        predictors(:,j) = alldata(current_range,coltrack(j));
    end
end
%Stepwise Model working up from a constant

```

```

if i < nruns/2
    md_RV444_su =
stepwiselm(predictors,response_var4,'constant','Upper','interactions','Cri
terion','bic'); %'AdjRsquared');
    store_RV444_crit(i,:) = [i, md_RV444_su.NumCoefficients,
md_RV444_su.Rsquared.Adjusted, md_RV444_su.ModelCriterion.AIC,
md_RV444_su.ModelCriterion.BIC];
    [p,F] = coefTest(md_RV444_su);
    store_RV444_info{i,:} = {i, p, F, md_RV444_su.DFE,
md_RV444_su.NumObservations, md_RV444_su.RMSE, md_RV444_su.Coefficients,
md_RV444_su.Formula, coltrack};
    md_RV444{i,:} = md_RV444_su;
%Stepwise Model working down from the full model
else
    md_RV444_su =
stepwiselm(predictors,response_var4,'interactions','Upper','interactions',
'Criterion','bic'); %'AdjRsquared');
    store_RV444_crit(i,:) = [i, md_RV444_su.NumCoefficients,
md_RV444_su.Rsquared.Adjusted, md_RV444_su.ModelCriterion.AIC,
md_RV444_su.ModelCriterion.BIC];
    [p,F] = coefTest(md_RV444_su);
    store_RV444_info{i,:} = {i, p, F, md_RV444_su.DFE,
md_RV444_su.NumObservations, md_RV444_su.RMSE, md_RV444_su.Coefficients,
md_RV444_su.Formula, coltrack};
    md_RV444{i,:} = md_RV444_su;
end
i = i+1;
clear coltrack
end

best_RV444_p = sortrows(store_RV444_crit,2); best_RV444_AdjR =
sortrows(store_RV444_crit,-3); best_RV444_aic =
sortrows(store_RV444_crit,4); best_RV444_bic =
sortrows(store_RV444_crit,5);
best_RV444_crit = [store_RV444_crit(1,:); best_RV444_p(1:best_num,:);
best_RV444_AdjR(1:best_num,:); best_RV444_aic(1:best_num,:);
best_RV444_bic(1:best_num,:)];

md_RV444_crit = best_RV444_AdjR(1,:); md_RV444_info =
store_RV444_info{best_RV444_AdjR(1,1),:};
end

%Determine best prediction from second round
if isempty(response_var1) == 1
    best_md3(1) = 0;
else
    best_md3(1) = best_RV111_AdjR(1,3);
end
if isempty(response_var2) == 1
    best_md3(2) = 0;
else
    best_md3(2) = best_RV222_AdjR(1,3);
end
if isempty(response_var3) == 1
    best_md3(3) = 0;
else

```

```

        best_md3(3) = best_RV333_AdjR(1,3);
end
if isempty(response_var4) == 1
    best_md3(4) = 0;
else
    best_md3(4) = best_RV444_AdjR(1,3);
end
if max(best_md3) == best_md3(1)
    order{3} = 'RV111';
    response_var1 = [];
    poss_pred = [poss_pred, RV1_col];
elseif max(best_md3) == best_md3(2)
    order{3} = 'RV222';
    response_var2 = [];
    poss_pred = [poss_pred, RV2_col];
elseif max(best_md3) == best_md3(3)
    order{3} = 'RV333';
    response_var3 = [];
    poss_pred = [poss_pred, RV3_col];
elseif max(best_md3) == best_md3(4)
    order{3} = 'RV444';
    response_var4 = [];
    poss_pred = [poss_pred, RV4_col];
else
    'best unknown R3'
    break
end
'Finished round 3. -----'

%% Statistics Round 4
dim_md_upper = dim_md_upper + 1; %maximum number of predictors used in the
model

%%%%%%%%%%%%%% RV1111 %%%%%%%%%%%%%%%
if isempty(response_var1) == 0
clear predictors coltrack p F i j col
i = 1;
while i <= nruns+1
    %Extract a random subset of variables for use in the model
    developement
        predictors = zeros(length(response_var1),dim_md_upper); coltrack =
zeros(dim_md_upper,1);
        dmy1 = randsample(1:size(poss_pred,2),dim_md_upper)'; %columns
        dmy2 = ceil(rand(dim_md_upper,1)*size(poss_pred,1)); %rows--always 4
rows in poss_pred
        pairs = [dmy2,dmy1];
        for j = 1:size(predictors,2)
            coltrack(j) = poss_pred(dmy2(j),dmy1(j));
            predictors(:,j) = alldata(current_range,coltrack(j));
        end
    %Stepwise Model working up from a constant
    if i < nruns/2
        md_RV1111_su =
stepwiselm(predictors,response_var1,'constant','Upper','interactions','Cri
terion','bic'); %'AdjRsquared');

```

```

        store_RV1111_crit(i,:) = [i, md_RV1111_su.NumCoefficients,
md_RV1111_su.Rsquared.Adjusted, md_RV1111_su.ModelCriterion.AIC,
md_RV1111_su.ModelCriterion.BIC];
        [p,F] = coefTest(md_RV1111_su);
        store_RV1111_info{i,:} = {i, p, F, md_RV1111_su.DFE,
md_RV1111_su.NumObservations, md_RV1111_su.RMSE,
md_RV1111_su.Coefficients, md_RV1111_su.Formula, coltrack};
        md_RV1111{i,:} = md_RV1111_su;
%Stepwise Model working down from the full model
else
    md_RV1111_su =
stepwiselm(predictors,response_var1,'interactions','Upper','interactions',
'Criterion','bic'); %'AdjRsquared');
    store_RV1111_crit(i,:) = [i, md_RV1111_su.NumCoefficients,
md_RV1111_su.Rsquared.Adjusted, md_RV1111_su.ModelCriterion.AIC,
md_RV1111_su.ModelCriterion.BIC];
    [p,F] = coefTest(md_RV1111_su);
    store_RV1111_info{i,:} = {i, p, F, md_RV1111_su.DFE,
md_RV1111_su.NumObservations, md_RV1111_su.RMSE,
md_RV1111_su.Coefficients, md_RV1111_su.Formula, coltrack};
    md_RV1111{i,:} = md_RV1111_su;
end
i = i+1;
clear coltrack
end

best_RV1111_p = sortrows(store_RV1111_crit,2); best_RV1111_AdjR =
sortrows(store_RV1111_crit,-3); best_RV1111_aic =
sortrows(store_RV1111_crit,4); best_RV1111_bic =
sortrows(store_RV1111_crit,5);
best_RV1111_crit = [store_RV1111_crit(1,:); best_RV1111_p(1:best_num,:);
best_RV1111_AdjR(1:best_num,:); best_RV1111_aic(1:best_num,:);
best_RV1111_bic(1:best_num,:)];

md_RV1111_crit = best_RV1111_AdjR(1,:); md_RV1111_info =
store_RV1111_info{best_RV1111_AdjR(1,1),:};
end

%%%%%%%%%% RV2222 %%%%%%%%%%%
if isempty(response_var2) == 0
clear predictors coltrack p F i j col
i = 1;
while i <= nruns+1
    %Extract a random subset of variables for use in the model
development
    predictors = zeros(length(response_var2),dim_md_upper); coltrack =
zeros(dim_md_upper,1);
    dmy1 = randsample(1:size(poss_pred,2),dim_md_upper)'; %columns
    dmy2 = ceil(rand(dim_md_upper,1)*size(poss_pred,1)); %rows--always 4
rows in poss_pred
    pairs = [dmy2,dmy1];
    for j = 1:size(predictors,2)
        coltrack(j) = poss_pred(dmy2(j),dmy1(j));
        predictors(:,j) =
alldata(current_range,coltrack(j)); %%%%%%%%%%%This needs to change
    end
end

```

```

%Stepwise Model working up from a constant
if i < nruns/2
    md_RV2222_su =
stepwiselm(predictors,response_var2,'constant','Upper','interactions','Cri
terion','bic'); %'AdjRsquared');
    store_RV2222_crit(i,:) = [i, md_RV2222_su.NumCoefficients,
md_RV2222_su.Rsquared.Adjusted, md_RV2222_su.ModelCriterion.AIC,
md_RV2222_su.ModelCriterion.BIC];
    [p,F] = coefTest(md_RV2222_su);
    store_RV2222_info{i,:} = {i, p, F, md_RV2222_su.DFE,
md_RV2222_su.NumObservations, md_RV2222_su.RMSE,
md_RV2222_su.Coefficients, md_RV2222_su.Formula, coltrack};
    md_RV2222{i,:} = md_RV2222_su;
%Stepwise Model working down from the full model
else
    md_RV2222_su =
stepwiselm(predictors,response_var2,'interactions','Upper','interactions',
'Criterion','bic'); %'AdjRsquared');
    store_RV2222_crit(i,:) = [i, md_RV2222_su.NumCoefficients,
md_RV2222_su.Rsquared.Adjusted, md_RV2222_su.ModelCriterion.AIC,
md_RV2222_su.ModelCriterion.BIC];
    [p,F] = coefTest(md_RV2222_su);
    store_RV2222_info{i,:} = {i, p, F, md_RV2222_su.DFE,
md_RV2222_su.NumObservations, md_RV2222_su.RMSE,
md_RV2222_su.Coefficients, md_RV2222_su.Formula, coltrack};
    md_RV2222{i,:} = md_RV2222_su;
end
i = i+1;
clear coltrack
end

best_RV2222_p = sortrows(store_RV2222_crit,2); best_RV2222_AdjR =
sortrows(store_RV2222_crit,-3); best_RV2222_aic =
sortrows(store_RV2222_crit,4); best_RV2222_bic =
sortrows(store_RV2222_crit,5);
best_RV2222_crit = [store_RV2222_crit(1,:); best_RV2222_p(1:best_num,:);
best_RV2222_AdjR(1:best_num,:); best_RV2222_aic(1:best_num,:);
best_RV2222_bic(1:best_num,:)];

md_RV2222_crit = best_RV2222_AdjR(1,:); md_RV2222_info =
store_RV2222_info{best_RV2222_AdjR(1,1),:};
end

%%%%%%%%%%%% RV3333 %%%%%%%%%%%%%
if isempty(response_var3) == 0
clear predictors coltrack p F i j col
i = 1;
while i <= nruns+1
    %Extract a random subset of variables for use in the model
developement
    predictors = zeros(length(response_var3),dim_md_upper); coltrack =
zeros(dim_md_upper,1);
    dmy1 = randsample(1:size(poss_pred,2),dim_md_upper)'; %columns
    dmy2 = ceil(rand(dim_md_upper,1)*size(poss_pred,1)); %rows--always 4
rows in poss_pred
    pairs = [dmy2,dmy1];

```

```

    for j = 1:size(predictors,2)
        coltrack(j) = poss_pred(dmy2(j),dmy1(j));
        predictors(:,j) = alldata(current_range,coltrack(j)); %%
    end
    %Stepwise Model working up from a constant
    if i < nruns/2
        md_RV3333_su =
        stepwiselm(predictors,response_var3,'constant','Upper','interactions','Cri
        terion','bic'); %'AdjRsquared');
        store_RV3333_crit(i,:) = [i, md_RV3333_su.NumCoefficients,
        md_RV3333_su.Rsquared.Adjusted, md_RV3333_su.ModelCriterion.AIC,
        md_RV3333_su.ModelCriterion.BIC];
        [p,F] = coefTest(md_RV3333_su);
        store_RV3333_info{i,:} = {i, p, F, md_RV3333_su.DFE,
        md_RV3333_su.NumObservations, md_RV3333_su.RMSE,
        md_RV3333_su.Coefficients, md_RV3333_su.Formula, coltrack};
        md_RV3333{i,:} = md_RV3333_su;
    %Stepwise Model working down from the full model
    else
        md_RV3333_su =
        stepwiselm(predictors,response_var3,'interactions','Upper','interactions',
        'Criterion','bic'); %'AdjRsquared');
        store_RV3333_crit(i,:) = [i, md_RV3333_su.NumCoefficients,
        md_RV3333_su.Rsquared.Adjusted, md_RV3333_su.ModelCriterion.AIC,
        md_RV3333_su.ModelCriterion.BIC];
        [p,F] = coefTest(md_RV3333_su);
        store_RV3333_info{i,:} = {i, p, F, md_RV3333_su.DFE,
        md_RV3333_su.NumObservations, md_RV3333_su.RMSE,
        md_RV3333_su.Coefficients, md_RV3333_su.Formula, coltrack};
        md_RV3333{i,:} = md_RV3333_su;
    end
    i = i+1;
    clear coltrack
end

best_RV3333_p = sortrows(store_RV3333_crit,2); best_RV3333_AdjR =
sortrows(store_RV3333_crit,-3); best_RV3333_aic =
sortrows(store_RV3333_crit,4); best_RV3333_bic =
sortrows(store_RV3333_crit,5);
best_RV3333_crit = [store_RV3333_crit(1,:); best_RV3333_p(1:best_num,:);
best_RV3333_AdjR(1:best_num,:); best_RV3333_aic(1:best_num,:);
best_RV3333_bic(1:best_num,:)];

md_RV3333_crit = best_RV3333_AdjR(1,:); md_RV3333_info =
store_RV3333_info{best_RV3333_AdjR(1,1),:};
end

%%%%%%%%%%%%%% RV4444 %%%%%%%%%%%%%%%
if isempty(response_var4) == 0
clear predictors coltrack p F i j col
i = 1;
while i <= nruns+1
    %Extract a random subset of variables for use in the model
    development
    predictors = zeros(length(response_var4),dim_md_upper); coltrack =
zeros(dim_md_upper,1);

```

```

    dmy1 = randsample(1:size(poss_pred,2),dim_md_upper)'; %columns
    dmy2 = ceil(rand(dim_md_upper,1)*size(poss_pred,1)); %rows--always 4
rows in poss_pred
    pairs = [dmy2,dmy1];
    for j = 1:size(predictors,2)
        coltrack(j) = poss_pred(dmy2(j),dmy1(j));
        predictors(:,j) = alldata(current_range,coltrack(j));
    end
%Stepwise Model working up from a constant
if i < nruns/2
    md_RV4444_su =
stepwiselm(predictors,response_var4,'constant','Upper','interactions','Cri
terion','bic'); %'AdjRsquared');
    store_RV4444_crit(i,:) = [i, md_RV4444_su.NumCoefficients,
md_RV4444_su.Rsquared.Adjusted, md_RV4444_su.ModelCriterion.AIC,
md_RV4444_su.ModelCriterion.BIC];
    [p,F] = coefTest(md_RV4444_su);
    store_RV4444_info{i,:} = {i, p, F, md_RV4444_su.DFE,
md_RV4444_su.NumObservations, md_RV4444_su.RMSE,
md_RV4444_su.Coefficients, md_RV4444_su.Formula, coltrack};
    md_RV4444{i,:} = md_RV4444_su;
%Stepwise Model working down from the full model
else
    md_RV4444_su =
stepwiselm(predictors,response_var4,'interactions','Upper','interactions',
'Criterion','bic'); %'AdjRsquared');
    store_RV4444_crit(i,:) = [i, md_RV4444_su.NumCoefficients,
md_RV4444_su.Rsquared.Adjusted, md_RV4444_su.ModelCriterion.AIC,
md_RV4444_su.ModelCriterion.BIC];
    [p,F] = coefTest(md_RV4444_su);
    store_RV4444_info{i,:} = {i, p, F, md_RV4444_su.DFE,
md_RV4444_su.NumObservations, md_RV4444_su.RMSE,
md_RV4444_su.Coefficients, md_RV4444_su.Formula, coltrack};
    md_RV4444{i,:} = md_RV4444_su;
end
i = i+1;
clear coltrack
end

best_RV4444_p = sortrows(store_RV4444_crit,2); best_RV4444_AdjR =
sortrows(store_RV4444_crit,-3); best_RV4444_aic =
sortrows(store_RV4444_crit,4); best_RV4444_bic =
sortrows(store_RV4444_crit,5);
best_RV4444_crit = [store_RV4444_crit(1,:); best_RV4444_p(1:best_num,:);
best_RV4444_AdjR(1:best_num,:); best_RV4444_aic(1:best_num,:);
best_RV4444_bic(1:best_num,:)];

md_RV4444_crit = best_RV4444_AdjR(1,:); md_RV4444_info =
store_RV4444_info{best_RV4444_AdjR(1,1),:};
end

%Determine best prediction from second round
if isempty(response_var1) == 1
    best_md4(1) = 0;
else
    best_md4(1) = best_RV1111_AdjR(1,3);
end

```

```

end
if isempty(response_var2) == 1
    best_md4(2) = 0;
else
    best_md4(2) = best_RV2222_AdjR(1,3);
end
if isempty(response_var3) == 1
    best_md4(3) = 0;
else
    best_md4(3) = best_RV3333_AdjR(1,3);
end
if isempty(response_var4) == 1
    best_md4(4) = 0;
else
    best_md4(4) = best_RV4444_AdjR(1,3);
end
if max(best_md4) == best_md4(1)
    order{4} = 'RV1111';
    response_var1 = [];
    poss_pred = [poss_pred, RV1_col];
elseif max(best_md4) == best_md4(2)
    order{4} = 'RV2222';
    response_var2 = [];
    poss_pred = [poss_pred, RV2_col];
elseif max(best_md4) == best_md4(3)
    order{4} = 'RV3333';
    response_var3 = [];
    poss_pred = [poss_pred, RV3_col];
elseif max(best_md4) == best_md4(4)
    order{4} = 'RV4444';
    response_var4 = [];
    poss_pred = [poss_pred, RV4_col];
else
    'best unknown R4'
    break
end
'Finished round 4. -----'

%% Save model information and write to and Excel file
save([species '.mat'], 'md_RV*', 'store_RV*', 'best_*',
'alldata', 'manz', 'cean', ...
'DF', 'goak', 'fet', 'gal', 'SP', 'cham', 'sage', 'LP');

```

### D.3 Ignition and Burning Model Development Algorithm

```

%% Data Organization
% cd('B:\Experiments\Seasonal Moisture Content Project')
% %Column Order: Run, MC, RMC, density(g/cm^3), length(cm), width(cm)...
%     %needle length(cm), thickness(mm), diameter(mm), SA(cm^2),
%     mass(g), dry mass(g), water mass (g)
% %Species Order: Manz, Cean, DF, Goak, Fet, Gal, SP, Cham, Sage, LP
load 'All Data.mat'
%%%%%%%%%%%%%%%%%%%%%%%%%%%%%%%%%%%%%%%%%%%%%%%%%%%%%%%%%%%%%%%%%%%%%%%% Organization of ALL DATA %%%%%%%%%%
alldata = [alldata, 20./alldata(:,8)]; %adding approximate SA:V ratio--it
simplifies to 20/t[mm] = [cm^-1].

```

```

% find locations for species, month, heating mode and new or old
loc_nan = find(isnan(alldata(:,1)));
loc_new = find(alldata(:,49)==2); loc_old = find(alldata(:,49)==1);
loc_conv = find(alldata(:,48)==1); loc_comb = find(alldata(:,48)==2); loc_rad
= find(alldata(:,48)==3);
loc_jan = find(alldata(:,47)==10); loc_feb = find(alldata(:,47)==11); loc_mar
= find(alldata(:,47)==12); loc_apr1 = find(alldata(:,47)==1); loc_apr2 =
find(alldata(:,47)==13); loc_may = find(alldata(:,47)==2); loc_jun =
find(alldata(:,47)==3); loc_jul = find(alldata(:,47)==4); loc_aug =
find(alldata(:,47)==5); loc_sep = find(alldata(:,47)==6); loc_oct =
find(alldata(:,47)==7); loc_nov = find(alldata(:,47)==8); loc_dec =
find(alldata(:,47)==9); %Two aprils because there we did experiments for year
2 from April to April--13 months

% Define each species by month
DF_apr1 = alldata(loc_apr1(loc_apr1<loc_nan(1)),:); DF_may =
alldata(loc_may(loc_may<loc_nan(1)),:); DF_jun =
alldata(loc_jun(loc_jun<loc_nan(1)),:); DF_jul =
alldata(loc_jul(loc_jul<loc_nan(1)),:); DF_aug =
alldata(loc_aug(loc_aug<loc_nan(1)),:); DF_sep =
alldata(loc_sep(loc_sep<loc_nan(1)),:);
DF_oct = alldata(loc_oct(loc_oct<loc_nan(1)),:); DF_nov =
alldata(loc_nov(loc_nov<loc_nan(1)),:); DF_dec =
alldata(loc_dec(loc_dec<loc_nan(1)),:); DF_jan =
alldata(loc_jan(loc_jan<loc_nan(1)),:); DF_feb =
alldata(loc_feb(loc_feb<loc_nan(1)),:); DF_mar =
alldata(loc_mar(loc_mar<loc_nan(1)),:); DF_apr2 =
alldata(loc_apr2(loc_apr2<loc_nan(1)),:);
i = 1;
manz_apr1 = alldata(loc_apr1(loc_apr1>loc_nan(i) & loc_apr1<loc_nan(i+1)),:);
manz_may = alldata(loc_may(loc_may>loc_nan(i) & loc_may<loc_nan(i+1)),:);
manz_jun = alldata(loc_jun(loc_jun>loc_nan(i) & loc_jun<loc_nan(i+1)),:);
manz_jul = alldata(loc_jul(loc_jul>loc_nan(i) & loc_jul<loc_nan(i+1)),:);
manz_aug = alldata(loc_aug(loc_aug>loc_nan(i) & loc_aug<loc_nan(i+1)),:);
manz_sep = alldata(loc_sep(loc_sep>loc_nan(i) & loc_sep<loc_nan(i+1)),:);
manz_oct = alldata(loc_oct(loc_oct>loc_nan(i) & loc_oct<loc_nan(i+1)),:);
manz_nov = alldata(loc_nov(loc_nov>loc_nan(i) & loc_nov<loc_nan(i+1)),:);
manz_dec = alldata(loc_dec(loc_dec>loc_nan(i) & loc_dec<loc_nan(i+1)),:);
manz_jan = alldata(loc_jan(loc_jan>loc_nan(i) & loc_jan<loc_nan(i+1)),:);
manz_feb = alldata(loc_feb(loc_feb>loc_nan(i) & loc_feb<loc_nan(i+1)),:);
manz_mar = alldata(loc_mar(loc_mar>loc_nan(i) & loc_mar<loc_nan(i+1)),:);
manz_apr2 = alldata(loc_apr2(loc_apr2>loc_nan(i) & loc_apr2<loc_nan(i+1)),:);
i = 2;
cean_apr1 = alldata(loc_apr1(loc_apr1>loc_nan(i) & loc_apr1<loc_nan(i+1)),:);
cean_may = alldata(loc_may(loc_may>loc_nan(i) & loc_may<loc_nan(i+1)),:);
cean_jun = alldata(loc_jun(loc_jun>loc_nan(i) & loc_jun<loc_nan(i+1)),:);
cean_jul = alldata(loc_jul(loc_jul>loc_nan(i) & loc_jul<loc_nan(i+1)),:);
cean_aug = alldata(loc_aug(loc_aug>loc_nan(i) & loc_aug<loc_nan(i+1)),:);
cean_sep = alldata(loc_sep(loc_sep>loc_nan(i) & loc_sep<loc_nan(i+1)),:);
cean_oct = alldata(loc_oct(loc_oct>loc_nan(i) & loc_oct<loc_nan(i+1)),:);
cean_nov = alldata(loc_nov(loc_nov>loc_nan(i) & loc_nov<loc_nan(i+1)),:);
cean_dec = alldata(loc_dec(loc_dec>loc_nan(i) & loc_dec<loc_nan(i+1)),:);
cean_jan = alldata(loc_jan(loc_jan>loc_nan(i) & loc_jan<loc_nan(i+1)),:);
cean_feb = alldata(loc_feb(loc_feb>loc_nan(i) & loc_feb<loc_nan(i+1)),:);
cean_mar = alldata(loc_mar(loc_mar>loc_nan(i) & loc_mar<loc_nan(i+1)),:);
cean_apr2 = alldata(loc_apr2(loc_apr2>loc_nan(i) & loc_apr2<loc_nan(i+1)),:);
i = 3;

```



```

cham_apr1 = alldata(loc_apr1(loc_apr1>loc_nan(i) & loc_apr1<loc_nan(i+1)),:);
cham_may = alldata(loc_may(loc_may>loc_nan(i) & loc_may<loc_nan(i+1)),:);
cham_jun = alldata(loc_jun(loc_jun>loc_nan(i) & loc_jun<loc_nan(i+1)),:);
cham_jul = alldata(loc_jul(loc_jul>loc_nan(i) & loc_jul<loc_nan(i+1)),:);
cham_aug = alldata(loc_aug(loc_aug>loc_nan(i) & loc_aug<loc_nan(i+1)),:);
cham_sep = alldata(loc_sep(loc_sep>loc_nan(i) & loc_sep<loc_nan(i+1)),:);
cham_oct = alldata(loc_oct(loc_oct>loc_nan(i) & loc_oct<loc_nan(i+1)),:);
cham_nov = alldata(loc_nov(loc_nov>loc_nan(i) & loc_nov<loc_nan(i+1)),:);
cham_dec = alldata(loc_dec(loc_dec>loc_nan(i) & loc_dec<loc_nan(i+1)),:);
cham_jan = alldata(loc_jan(loc_jan>loc_nan(i) & loc_jan<loc_nan(i+1)),:);
cham_feb = alldata(loc_feb(loc_feb>loc_nan(i) & loc_feb<loc_nan(i+1)),:);
cham_mar = alldata(loc_mar(loc_mar>loc_nan(i) & loc_mar<loc_nan(i+1)),:);
cham_apr2 = alldata(loc_apr2(loc_apr2>loc_nan(i) & loc_apr2<loc_nan(i+1)),:);
i = 8;
sage_apr1 = alldata(loc_apr1(loc_apr1>loc_nan(i) & loc_apr1<loc_nan(i+1)),:);
sage_may = alldata(loc_may(loc_may>loc_nan(i) & loc_may<loc_nan(i+1)),:);
sage_jun = alldata(loc_jun(loc_jun>loc_nan(i) & loc_jun<loc_nan(i+1)),:);
sage_jul = alldata(loc_jul(loc_jul>loc_nan(i) & loc_jul<loc_nan(i+1)),:);
sage_aug = alldata(loc_aug(loc_aug>loc_nan(i) & loc_aug<loc_nan(i+1)),:);
sage_sep = alldata(loc_sep(loc_sep>loc_nan(i) & loc_sep<loc_nan(i+1)),:);
sage_oct = alldata(loc_oct(loc_oct>loc_nan(i) & loc_oct<loc_nan(i+1)),:);
sage_nov = alldata(loc_nov(loc_nov>loc_nan(i) & loc_nov<loc_nan(i+1)),:);
sage_dec = alldata(loc_dec(loc_dec>loc_nan(i) & loc_dec<loc_nan(i+1)),:);
sage_jan = alldata(loc_jan(loc_jan>loc_nan(i) & loc_jan<loc_nan(i+1)),:);
sage_feb = alldata(loc_feb(loc_feb>loc_nan(i) & loc_feb<loc_nan(i+1)),:);
sage_mar = alldata(loc_mar(loc_mar>loc_nan(i) & loc_mar<loc_nan(i+1)),:);
sage_apr2 = alldata(loc_apr2(loc_apr2>loc_nan(i) & loc_apr2<loc_nan(i+1)),:);
i = 9;
LP_apr1 = alldata(loc_apr1(loc_apr1>loc_nan(i)),:); LP_may =
alldata(loc_may(loc_may>loc_nan(i)),:); LP_jun =
alldata(loc_jun(loc_jun>loc_nan(i)),:); LP_jul =
alldata(loc_jul(loc_jul>loc_nan(i)),:);
LP_aug = alldata(loc_aug(loc_aug>loc_nan(i)),:); LP_sep =
alldata(loc_sep(loc_sep>loc_nan(i)),:); LP_oct =
alldata(loc_oct(loc_oct>loc_nan(i)),:); LP_nov =
alldata(loc_nov(loc_nov>loc_nan(i)),:);
LP_dec = alldata(loc_dec(loc_dec>loc_nan(i)),:); LP_jan =
alldata(loc_jan(loc_jan>loc_nan(i)),:); LP_feb =
alldata(loc_feb(loc_feb>loc_nan(i)),:); LP_mar =
alldata(loc_mar(loc_mar>loc_nan(i)),:); LP_apr2 =
alldata(loc_apr2(loc_apr2>loc_nan(i)),:);

% Define each species by heating mode
DF_conv = alldata(loc_conv(loc_conv<loc_nan(1)),:); DF_comb =
alldata(loc_comb(loc_comb<loc_nan(1)),:); DF_rad =
alldata(loc_rad(loc_rad<loc_nan(1)),:);
i = 1;manz_conv = alldata(loc_conv(loc_conv>loc_nan(i) &
loc_conv<loc_nan(i+1)),:); manz_comb = alldata(loc_comb(loc_comb>loc_nan(i) &
loc_comb<loc_nan(i+1)),:); manz_rad = alldata(loc_rad(loc_rad>loc_nan(i) &
loc_rad<loc_nan(i+1)),:);
i = 2;cean_conv = alldata(loc_conv(loc_conv>loc_nan(i) &
loc_conv<loc_nan(i+1)),:); cean_comb = alldata(loc_comb(loc_comb>loc_nan(i) &
loc_comb<loc_nan(i+1)),:); cean_rad = alldata(loc_rad(loc_rad>loc_nan(i) &
loc_rad<loc_nan(i+1)),:);
i = 3;goak_conv = alldata(loc_conv(loc_conv>loc_nan(i) &
loc_conv<loc_nan(i+1)),:); goak_comb = alldata(loc_comb(loc_comb>loc_nan(i) &

```

```

loc_comb<loc_nan(i+1),:); goak_rad = alldata(loc_rad(loc_rad>loc_nan(i) &
loc_rad<loc_nan(i+1),:);
i = 4;fet_conv = alldata(loc_conv(loc_conv>loc_nan(i) &
loc_conv<loc_nan(i+1),:); fet_comb = alldata(loc_comb(loc_comb>loc_nan(i) &
loc_comb<loc_nan(i+1),:); fet_rad = alldata(loc_rad(loc_rad>loc_nan(i) &
loc_rad<loc_nan(i+1),:);
i = 5;gal_conv = alldata(loc_conv(loc_conv>loc_nan(i) &
loc_conv<loc_nan(i+1),:); gal_comb = alldata(loc_comb(loc_comb>loc_nan(i) &
loc_comb<loc_nan(i+1),:); gal_rad = alldata(loc_rad(loc_rad>loc_nan(i) &
loc_rad<loc_nan(i+1),:);
i = 6;SP_conv = alldata(loc_conv(loc_conv>loc_nan(i) &
loc_conv<loc_nan(i+1),:); SP_comb = alldata(loc_comb(loc_comb>loc_nan(i) &
loc_comb<loc_nan(i+1),:); SP_rad = alldata(loc_rad(loc_rad>loc_nan(i) &
loc_rad<loc_nan(i+1),:);
i = 7;cham_conv = alldata(loc_conv(loc_conv>loc_nan(i) &
loc_conv<loc_nan(i+1),:); cham_comb = alldata(loc_comb(loc_comb>loc_nan(i) &
loc_comb<loc_nan(i+1),:); cham_rad = alldata(loc_rad(loc_rad>loc_nan(i) &
loc_rad<loc_nan(i+1),:);
i = 8;sage_conv = alldata(loc_conv(loc_conv>loc_nan(i) &
loc_conv<loc_nan(i+1),:); sage_comb = alldata(loc_comb(loc_comb>loc_nan(i) &
loc_comb<loc_nan(i+1),:); sage_rad = alldata(loc_rad(loc_rad>loc_nan(i) &
loc_rad<loc_nan(i+1),:);
i = 9;LP_conv = alldata(loc_conv(loc_conv>loc_nan(i)),:); LP_comb =
alldata(loc_comb(loc_comb>loc_nan(i)),:); LP_rad =
alldata(loc_rad(loc_rad>loc_nan(i)),:);

```

*% Define each species by age*

```

DF_new = alldata(loc_new(loc_new<loc_nan(1)),:); DF_old =
alldata(loc_old(loc_old<loc_nan(1)),:);
i = 1;manz_new = alldata(loc_new(loc_new>loc_nan(i) &
loc_new<loc_nan(i+1),:); manz_old = alldata(loc_old(loc_old>loc_nan(i) &
loc_old<loc_nan(i+1),:);
i = 2;cean_new = alldata(loc_new(loc_new>loc_nan(i) &
loc_new<loc_nan(i+1),:); cean_old = alldata(loc_old(loc_old>loc_nan(i) &
loc_old<loc_nan(i+1),:);
i = 3;goak_new = alldata(loc_new(loc_new>loc_nan(i) &
loc_new<loc_nan(i+1),:); goak_old = alldata(loc_old(loc_old>loc_nan(i) &
loc_old<loc_nan(i+1),:);
i = 4;fet_new = alldata(loc_new(loc_new>loc_nan(i) &
loc_new<loc_nan(i+1),:); fet_old = alldata(loc_old(loc_old>loc_nan(i) &
loc_old<loc_nan(i+1),:);
i = 5;gal_new = alldata(loc_new(loc_new>loc_nan(i) &
loc_new<loc_nan(i+1),:); gal_old = alldata(loc_old(loc_old>loc_nan(i) &
loc_old<loc_nan(i+1),:);
i = 6;SP_new = alldata(loc_new(loc_new>loc_nan(i) & loc_new<loc_nan(i+1)),:);
SP_old = alldata(loc_old(loc_old>loc_nan(i) & loc_old<loc_nan(i+1)),:);
i = 7;cham_new = alldata(loc_new(loc_new>loc_nan(i) &
loc_new<loc_nan(i+1),:); cham_old = alldata(loc_old(loc_old>loc_nan(i) &
loc_old<loc_nan(i+1),:);
i = 8;sage_new = alldata(loc_new(loc_new>loc_nan(i) &
loc_new<loc_nan(i+1),:); sage_old = alldata(loc_old(loc_old>loc_nan(i) &
loc_old<loc_nan(i+1),:);
i = 9;LP_new = alldata(loc_new(loc_new>loc_nan(i)),:); LP_old =
alldata(loc_old(loc_old>loc_nan(i)),:);

```

*%Define each species by month, heating mode and age*

```

%Douglas-fir
DF_apr1_conv = DF_apr1(1:10,:); DF_apr1_comb = DF_apr1(11:20,:); DF_apr1_rad
= DF_apr1(21:25,:); DF_may_conv = DF_may(1:10,:); DF_may_comb =
DF_may(11:20,:); DF_may_rad = DF_may(21:25,:);
DF_jun_conv = DF_jun(1:10,:); DF_jun_comb = DF_jun(11:20,:); DF_jun_rad =
DF_jun(21:25,:); DF_jul_conv = DF_jul(1:10,:); DF_jul_comb = DF_jul(11:20,:);
DF_jul_rad = DF_jul(21:25,:);
DF_aug_conv = DF_aug(1:10,:); DF_aug_comb = DF_aug(11:20,:); DF_aug_rad =
DF_aug(21:25,:); DF_sep_conv = DF_sep(1:10,:); DF_sep_comb = DF_sep(11:20,:);
DF_sep_rad = DF_sep(21:25,:);
DF_oct_conv = []; DF_oct_comb = []; DF_oct_rad = []; DF_nov_conv =
DF_nov(1:10,:); DF_nov_comb = DF_nov(11:20,:); DF_nov_rad = DF_nov(21:25,:);
DF_dec_conv = DF_dec(1:10,:); DF_dec_comb = DF_dec(11:20,:); DF_dec_rad =
DF_dec(21:25,:); DF_jan_conv = DF_jan(1:10,:); DF_jan_comb = DF_jan(11:20,:);
DF_jan_rad = DF_jan(21:25,:);
DF_feb_conv = []; DF_feb_comb = []; DF_feb_rad = []; %DF_mar_conv =
DF_mar(1:10,:); DF_mar_comb = DF_mar(11:20,:); DF_mar_rad = DF_mar(21:25,:);
DF_apr2_conv = DF_apr2(1:10,:); DF_apr2_comb = DF_apr2(11:20,:); DF_apr2_rad
= DF_apr2(21:25,:);
DF_mar_new = DF_mar([1:2 5:6 8:9 14 16:19 22 24:25],:); DF_mar_old =
DF_mar([3:4 7 10:13 15 20:21 23],:);
DF_mar_conv_new = DF_mar([1:2 5:6 8:9],:); DF_mar_comb_new = DF_mar([14
16:19],:); DF_mar_rad_new = DF_mar([22 24:25],:);
DF_mar_conv_old = DF_mar([3:4 7 10],:); DF_mar_comb_old = DF_mar([11:13 15
20],:); DF_mar_rad_old = DF_mar([21 23],:);
%Manzanita
manz_apr1_conv = manz_apr1(1:10,:); manz_apr1_comb = manz_apr1(11:20,:);
manz_apr1_rad = manz_apr1(21:25,:); manz_may_conv = manz_may(1:10,:);
manz_may_comb = manz_may(11:20,:); manz_may_rad = manz_may(21:25,:);
manz_jun_conv = manz_jun(1:10,:); manz_jun_comb = manz_jun(11:20,:);
manz_jun_rad = manz_jun(21:25,:); manz_jul_conv = manz_jul(1:10,:);
manz_jul_comb = manz_jul(11:20,:); manz_jul_rad = manz_jul(21:25,:);
manz_aug_conv = manz_aug(1:10,:); manz_aug_comb = manz_aug(11:20,:);
manz_aug_rad = manz_aug(21:25,:); manz_sep_conv = manz_sep(1:10,:);
manz_sep_comb = manz_sep(11:20,:); manz_sep_rad = manz_sep(21:25,:);
manz_oct_conv = []; manz_oct_comb = []; manz_oct_rad = []; manz_nov_conv =
manz_nov(1:10,:); manz_nov_comb = manz_nov(11:20,:); manz_nov_rad =
manz_nov(21:25,:);
manz_dec_conv = manz_dec(1:10,:); manz_dec_comb = manz_dec(11:20,:);
manz_dec_rad = manz_dec(21:25,:); manz_jan_conv = manz_jan(1:10,:);
manz_jan_comb = manz_jan(11:20,:); manz_jan_rad = manz_jan(21:25,:);
manz_feb_conv = manz_feb(1:10,:); manz_feb_comb = manz_feb(11:20,:);
manz_feb_rad = manz_feb(21:25,:); manz_mar_conv = manz_mar(1:10,:);
manz_mar_comb = manz_mar(11:20,:); manz_mar_rad = manz_mar(21:25,:);
manz_apr2_conv = manz_apr2(1:10,:); manz_apr2_comb = manz_apr2(11:20,:);
manz_apr2_rad = manz_apr2(21:25,:);
%Ceanothus
cean_apr1_conv = []; cean_apr1_comb = []; cean_apr1_rad = []; cean_may_conv =
cean_may(1:10,:); cean_may_comb = cean_may(12:21,:); cean_may_rad =
cean_may([11 22:25],:);
cean_jun_conv = cean_jun(1:10,:); cean_jun_comb = cean_jun(11:20,:);
cean_jun_rad = cean_jun(21:25,:); cean_jul_conv = cean_jul(1:10,:);
cean_jul_comb = cean_jul(11:20,:); cean_jul_rad = cean_jul(21:25,:);
cean_aug_conv = cean_aug(1:10,:); cean_aug_comb = cean_aug(11:20,:);
cean_aug_rad = cean_aug(21:25,:); cean_sep_conv = cean_sep(1:10,:);
cean_sep_comb = cean_sep(11:20,:); cean_sep_rad = cean_sep(21:25,:);

```

```

cean_oct_conv = []; cean_oct_comb = []; cean_oct_rad = []; cean_nov_conv =
cean_nov(1:10,:); cean_nov_comb = cean_nov(11:20,:); cean_nov_rad =
cean_nov(21:25,:);
cean_dec_conv = cean_dec(1:10,:); cean_dec_comb = cean_dec(11:20,:);
cean_dec_rad = cean_dec(21:25,:); cean_jan_conv = cean_jan(1:10,:);
cean_jan_comb = cean_jan(11:20,:); cean_jan_rad = cean_jan(21:25,:);
cean_feb_conv = cean_feb(1:10,:); cean_feb_comb = cean_feb(11:20,:);
cean_feb_rad = cean_feb(21:25,:); cean_mar_conv = cean_mar(1:10,:);
cean_mar_comb = cean_mar(11:20,:); cean_mar_rad = cean_mar(21:25,:);
cean_apr2_conv = cean_apr2(1:10,:); cean_apr2_comb = cean_apr2(11:20,:);
cean_apr2_rad = cean_apr2(21:25,:);
%Gambel Oak
goak_apr1_conv = []; goak_apr1_comb = []; goak_apr1_rad = []; goak_may_conv =
goak_may(1:10,:); goak_may_comb = goak_may(11:20,:); goak_may_rad =
goak_may(21:25,:);
goak_jun_conv = goak_jun(1:10,:); goak_jun_comb = goak_jun(11:20,:);
goak_jun_rad = goak_jun(21:25,:); goak_jul_conv = goak_jul(1:10,:);
goak_jul_comb = goak_jul(11:20,:); goak_jul_rad = goak_jul(21:25,:);
goak_aug_conv = goak_aug(1:10,:); goak_aug_comb = goak_aug(11:20,:);
goak_aug_rad = goak_aug(21:25,:); goak_sep_conv = goak_sep(1:10,:);
goak_sep_comb = goak_sep(11:20,:); goak_sep_rad = goak_sep(21:25,:);
% goak_oct_conv = goak_oct(1:10,:); goak_oct_comb = goak_oct(11:20,:);
goak_oct_rad = goak_oct(21:25,:);
goak_nov_conv = []; goak_nov_comb = []; goak_nov_rad = [];
goak_dec_conv = []; goak_dec_comb = []; goak_dec_rad = []; goak_jan_conv =
[]; goak_jan_comb = []; goak_jan_rad = [];
goak_feb_conv = []; goak_feb_comb = []; goak_feb_rad = []; goak_mar_conv =
[]; goak_mar_comb = []; goak_mar_rad = [];
goak_apr2_conv = []; goak_apr2_comb = []; goak_apr2_rad = [];
goak_oct_new = goak_oct([1:5 11:15 21:22],:); goak_oct_old = goak_oct([6:10
16:20 23:25],:);
goak_oct_conv_new = goak_oct(1:5,:); goak_oct_comb_new = goak_oct(11:15,:);
goak_oct_rad_new = goak_oct(21:22,:);
goak_oct_conv_old = goak_oct(6:10,:); goak_oct_comb_old = goak_oct(16:20,:);
goak_oct_rad_old = goak_oct(23:25,:);
%Fetterbush
fet_apr1_conv = fet_apr1(1:10,:); fet_apr1_comb = fet_apr1(11:20,:);
fet_apr1_rad = fet_apr1(21:25,:); fet_may_conv = fet_may(1:10,:);
fet_may_comb = fet_may(12:21,:); fet_may_rad = fet_may([11 22:25],:);
fet_jun_conv = fet_jun(1:10,:); fet_jun_comb = fet_jun(11:20,:); fet_jun_rad
= fet_jun(21:25,:); fet_jul_conv = fet_jul(1:10,:); fet_jul_comb =
fet_jul(11:20,:); fet_jul_rad = fet_jul(21:25,:);
fet_aug_conv = fet_aug(1:10,:); fet_aug_comb = fet_aug(11:20,:); fet_aug_rad
= fet_aug(21:25,:); fet_sep_conv = fet_sep(1:10,:); fet_sep_comb =
fet_sep(11:20,:); fet_sep_rad = fet_sep(21:25,:);
fet_oct_conv = fet_oct(1:10,:); fet_oct_comb = fet_oct(11:20,:); fet_oct_rad
= fet_oct(21:25,:); fet_nov_conv = fet_nov(1:10,:); fet_nov_comb =
fet_nov(11:16,:); fet_nov_rad = [];
fet_dec_conv = fet_dec(1:10,:); fet_dec_comb = fet_dec(11:20,:); fet_dec_rad
= fet_dec(21:25,:); fet_jan_conv = []; fet_jan_comb = []; fet_jan_rad = [];
fet_feb_conv = fet_feb(1:10,:); fet_feb_comb = fet_feb(11:20,:); fet_feb_rad
= fet_feb(21:25,:); fet_mar_conv = fet_mar(1:10,:); fet_mar_comb =
fet_mar(11:20,:); fet_mar_rad = fet_mar(21:25,:);
fet_apr2_conv = fet_apr2(1:10,:); fet_apr2_comb = fet_apr2(11:20,:);
fet_apr2_rad = fet_apr2(21:25,:);
%Galberry

```

```

gal_apr1_conv = gal_apr1(1:10,:); gal_apr1_comb = gal_apr1(11:20,:);
gal_apr1_rad = gal_apr1(21:25,:); gal_may_conv = gal_may(1:10,:);
gal_may_comb = gal_may(11:20,:); gal_may_rad = gal_may(21:25,:);
gal_jun_conv = gal_jun(1:10,:); gal_jun_comb = gal_jun(11:20,:); gal_jun_rad
= gal_jun(21:25,:); gal_jul_conv = gal_jul(1:10,:); gal_jul_comb =
gal_jul(11:20,:); gal_jul_rad = gal_jul(21:25,:);
gal_aug_conv = gal_aug(1:10,:); gal_aug_comb = gal_aug(11:20,:); gal_aug_rad
= gal_aug(21:25,:); gal_sep_conv = gal_sep(1:10,:); gal_sep_comb =
gal_sep(11:20,:); gal_sep_rad = gal_sep(21:25,:);
gal_oct_conv = gal_oct(1:10,:); gal_oct_comb = gal_oct(11:20,:); gal_oct_rad
= gal_oct(21:25,:); gal_nov_conv = gal_nov(1:10,:); gal_nov_comb =
gal_nov(11:20,:); gal_nov_rad = gal_nov(21:25,:);
gal_dec_conv = gal_dec(1:10,:); gal_dec_comb = gal_dec(11:20,:); gal_dec_rad
= gal_dec(21:25,:); gal_jan_conv = []; gal_jan_comb = []; gal_jan_rad = [];
gal_feb_conv = gal_feb(1:10,:); gal_feb_comb = gal_feb(11:20,:); gal_feb_rad
= gal_feb(21:25,:); gal_mar_conv = gal_mar(1:10,:); gal_mar_comb =
gal_mar(11:20,:); gal_mar_rad = gal_mar(21:25,:);
gal_apr2_conv = gal_apr2(1:10,:); gal_apr2_comb = gal_apr2(11:20,:);
gal_apr2_rad = gal_apr2(21:25,:);
%Sand Pine
% SP_apr1_conv = SP_apr1(1:10,:); SP_apr1_comb = SP_apr1(11:20,:);
SP_apr1_rad = [];
SP_may_conv = SP_may(1:10,:); SP_may_comb = SP_may(11:20,:); SP_may_rad =
SP_may(21:25,:);
SP_jun_conv = SP_jun(1:10,:); SP_jun_comb = SP_jun(11:20,:); SP_jun_rad =
SP_jun(21:25,:); SP_jul_conv = SP_jul(1:10,:); SP_jul_comb = SP_jul(11:20,:);
SP_jul_rad = SP_jul(21:25,:);
SP_aug_conv = SP_aug(1:10,:); SP_aug_comb = SP_aug(11:20,:); SP_aug_rad =
SP_aug(21:25,:); SP_sep_conv = SP_sep(1:10,:); SP_sep_comb = SP_sep(11:20,:);
SP_sep_rad = SP_sep(21:25,:);
SP_oct_conv = SP_oct(1:10,:); SP_oct_comb = SP_oct(11:20,:); SP_oct_rad =
SP_oct(21:25,:); SP_nov_conv = SP_nov(1:10,:); SP_nov_comb = SP_nov(11:20,:);
SP_nov_rad = SP_nov(21:25,:);
SP_dec_conv = SP_dec(1:10,:); SP_dec_comb = SP_dec(11:20,:); SP_dec_rad =
SP_dec(21:25,:); SP_jan_conv = []; SP_jan_comb = []; SP_jan_rad = [];
SP_feb_conv = SP_feb(1:10,:); SP_feb_comb = SP_feb([11:13 15:19],:);
SP_feb_rad = SP_feb(14,:); SP_mar_conv = SP_mar(1:10,:); SP_mar_comb =
SP_mar(11:20,:); SP_mar_rad = SP_mar(21:25,:);
% SP_apr2_conv = SP_apr2(1:10,:); SP_apr2_comb = SP_apr2(11:20,:);
SP_apr2_rad = SP_apr2(21:25,:);
SP_apr1_new = SP_apr1(1:8,:); SP_apr1_old = SP_apr1(9:15,:);
SP_apr1_conv_new = SP_apr1(1:4,:); SP_apr1_comb_new = SP_apr1(5:8,:);
SP_apr1_rad_new = [];
SP_apr1_conv_old = SP_apr1(9:12,:); SP_apr1_comb_old = SP_apr1(13:15,:);
SP_apr1_rad_old = [];
SP_apr2_new = SP_apr2([1:5 11:15 21:25],:); SP_apr2_old = SP_apr2([6:10
16:20],:);
SP_apr2_conv_new = SP_apr2(6:10,:); SP_apr2_comb_new = SP_apr2(16:20,:);
SP_apr2_rad_new = [];
SP_apr2_conv_old = SP_apr2(1:5,:); SP_apr2_comb_old = SP_apr2(11:15,:);
SP_apr2_rad_old = SP_apr2(21:25,:);
%Chamise
cham_apr1_conv = []; cham_apr1_comb = []; cham_apr1_rad = []; cham_may_conv =
cham_may(1:10,:); cham_may_comb = cham_may(11:20,:); cham_may_rad =
cham_may(21:30,:);

```

```

cham_jun_conv = cham_jun(1:10,:); cham_jun_comb = cham_jun(12:2:30,:);
cham_jun_rad = cham_jun(11:2:29,:); %cham_jul_conv = cham_jul(1:10,:);
cham_jul_comb = cham_jul(11:2:29,:); cham_jul_rad = cham_jul(12:2:30,:);
cham_aug_conv = cham_aug(1:10,:); cham_aug_comb = cham_aug(11:2:29,:);
cham_aug_rad = cham_aug(12:2:30,:); %cham_sep_conv = cham_sep(1:10,:);
cham_sep_comb = cham_sep(11:2:29,:); cham_sep_rad = cham_sep(12:2:30,:);
%cham_oct_conv = cham_oct(1:10,:); cham_oct_comb = cham_oct(11:2:29,:);
cham_oct_rad = cham_oct(12:2:30,:); cham_nov_conv = cham_nov(1:10,:);
cham_nov_comb = cham_nov(11:20,:); cham_nov_rad = cham_nov(21:25,:);
cham_dec_conv = cham_dec(1:10,:); cham_dec_comb = cham_dec(11:20,:);
cham_dec_rad = []; cham_jan_conv = cham_jan(1:10,:); cham_jan_comb =
cham_jan(11:20,:); cham_jan_rad = [];
cham_feb_conv = cham_feb(1:10,:); cham_feb_comb = cham_feb(11:20,:);
cham_feb_rad = cham_feb(21:23,:); cham_mar_conv = cham_mar(1:10,:);
cham_mar_comb = cham_mar(11:20,:); cham_mar_rad = cham_mar(21:25,:);
cham_apr2_conv = cham_apr2(1:10,:); cham_apr2_comb = cham_apr2(11:20,:);
cham_apr2_rad = cham_apr2(21:25,:);
cham_jul_new = cham_jul([2:2:10 13:14 17:18 21:22 25:26 29:30],:);
cham_jul_old = cham_jul([1:2:9 11:12 15:16 19:20 23:24 27:28],:);
cham_jul_conv_new = cham_jul(2:2:10,:); cham_jul_comb_new = cham_jul([13 17
21 25 29],:); cham_jul_rad_new = cham_jul([14 18 22 26 30],:);
cham_jul_conv_old = cham_jul(1:2:9,:); cham_jul_comb_old = cham_jul([11 15 19
23 27],:); cham_jul_rad_old = cham_jul([12 16 20 24 28],:);
cham_sep_new = cham_sep([1:5 11:20],:); cham_sep_old = cham_sep([6:10
21:30],:);
cham_sep_conv_new = cham_sep(1:5,:); cham_sep_comb_new = cham_sep(11:2:19,:);
cham_sep_rad_new = cham_sep(12:2:20,:);
cham_sep_conv_old = cham_sep(6:10,:); cham_sep_comb_old =
cham_sep(21:2:29,:); cham_sep_rad_old = cham_sep(22:2:30,:);
cham_oct_new = cham_oct([6:10 13:14 17:18 21:22 25:26 29:30],:); cham_oct_old
= cham_oct([1:5 11:12 15:16 19:20 23:24 27:28],:);
cham_oct_conv_new = cham_oct(6:10,:); cham_oct_comb_new = cham_oct([13 17 21
25 29],:); cham_oct_rad_new = cham_oct([14 18 22 26 30],:);
cham_oct_conv_old = cham_oct(1:5,:); cham_oct_comb_old = cham_oct([11 15 19
23 27],:); cham_oct_rad_old = cham_oct([12 16 20 24 28],:);
cham_nov_new = cham_nov([2:2:10 13:14 17:18 21:22 25:26 29:30],:);
cham_nov_old = cham_nov([1:2:9 11:12 15:16 19:20 23:24 27:28],:);
cham_nov_conv_new = cham_nov(2:2:10,:); cham_nov_comb_new = cham_nov([13 17
21 25 29],:); cham_nov_rad_new = cham_nov([14 18 22 26 30],:);
cham_nov_conv_old = cham_nov(1:2:9,:); cham_nov_comb_old = cham_nov([11 15 19
23 27],:); cham_nov_rad_old = cham_nov([12 16 20 24 28],:);
%Sagebrush
sage_apr1_conv = []; sage_apr1_comb = []; sage_apr1_rad = []; sage_may_conv =
sage_may(1:10,:); sage_may_comb = sage_may(11:2:29,:); sage_may_rad =
sage_may(12:2:30,:);
sage_jun_conv = sage_jun(1:10,:); sage_jun_comb = sage_jun(11:2:29,:);
sage_jun_rad = sage_jun(12:2:30,:); sage_jul_conv = sage_jul(1:10,:);
sage_jul_comb = sage_jul(12:2:30,:); sage_jul_rad = sage_jul(11:2:29,:);
sage_aug_conv = sage_aug(1:10,:); sage_aug_comb = sage_aug(11:2:29,:);
sage_aug_rad = sage_aug(12:2:30,:); sage_sep_conv = sage_sep(1:10,:);
sage_sep_comb = sage_sep(11:2:29,:); sage_sep_rad = sage_sep(12:2:30,:);
% sage_oct_conv = sage_oct(1:10,:); sage_oct_comb = sage_oct(11:2:29,:);
sage_oct_rad = sage_oct(12:2:30,:);
sage_nov_conv = sage_nov(1:10,:); sage_nov_comb = sage_nov(11:2:29,:);
sage_nov_rad = sage_nov(12:2:30,:);

```

```

sage_dec_conv = sage_dec(1:10,:); sage_dec_comb = []; sage_dec_rad = [];
sage_jan_conv = sage_jan(1:10,:); sage_jan_comb = sage_jan(11:20,:);
sage_jan_rad = [];
sage_feb_conv = sage_feb(1:10,:); sage_feb_comb = sage_feb(11:20,:);
sage_feb_rad = sage_feb(21:25,:); sage_mar_conv = sage_mar(1:10,:);
sage_mar_comb = sage_mar(11:20,:); sage_mar_rad = sage_mar(21:25,:);
sage_apr2_conv = []; sage_apr2_comb = []; sage_apr2_rad = [];
sage_oct_new = sage_oct([1:6 8 10 12:14 16:19 25:26],:); sage_oct_old =
sage_oct([7 9 11 15 20:24 27:30],:);
sage_oct_conv_new = sage_oct([1:6 8 10],:); sage_oct_comb_new = sage_oct([13
17 19 25],:); sage_oct_rad_new = sage_oct([12 14 16 18 26],:);
sage_oct_conv_old = sage_oct([7 9],:); sage_oct_comb_old = sage_oct([11 15 21
23 27 29],:); sage_oct_rad_old = sage_oct([20 22 24 28 30],:);
%Lodgepole Pine
LP_apr1_conv = []; LP_apr1_comb = []; LP_apr1_rad = []; LP_may_conv =
LP_may(1:10,:); LP_may_comb = LP_may(12:2:30,:); LP_may_rad =
LP_may(11:2:29,:);
LP_jun_conv = LP_jun(1:10,:); LP_jun_comb = LP_jun(11:2:29,:); LP_jun_rad =
LP_jun(12:2:30,:); LP_jul_conv = LP_jul(1:10,:); LP_jul_comb =
LP_jul(12:2:30,:); LP_jul_rad = LP_jul(11:2:29,:);
LP_aug_conv = LP_aug(1:10,:); LP_aug_comb = LP_aug(11:2:29,:); LP_aug_rad =
LP_aug(12:2:30,:); LP_sep_conv = LP_sep(1:10,:); LP_sep_comb =
LP_sep(11:30,:); LP_sep_rad = [];
LP_oct_conv = LP_oct(1:10,:); LP_oct_comb = LP_oct(11:2:29,:); LP_oct_rad =
LP_oct(12:2:30,:); LP_nov_conv = []; LP_nov_comb = []; LP_nov_rad = [];
LP_dec_conv = []; LP_dec_comb = []; LP_dec_rad = []; LP_jan_conv = [];
LP_jan_comb = []; LP_jan_rad = [];
LP_feb_conv = LP_feb(1:10,:); LP_feb_comb = LP_feb(11:20,:); LP_feb_rad = [];
LP_mar_conv = LP_mar(1:10,:); LP_mar_comb = LP_mar(11:20,:); LP_mar_rad = [];
LP_apr2_conv = []; LP_apr2_comb = []; LP_apr2_rad = [];

%% User Defined Information
species = 'manz'; %input code for species: manz, cean, DF, goak, fet, gal,
SP, cham, sage, LP
type = 'overall'; %input type of model developed: overall, month(specify),
season(summer, winter)
heat = 'conv'; %input heating mode: conv, comb, rad, all(all the data for
the month)
age = 'old_Redo'; %input age: new, old, both %Is age necessary?
nreps = 500;
dim_md_upper = 4; %maximum number of predictors used in the model.
best_num = 5;
md_ceil = 'linear'; %goes with Name-Value pair Upper in stepwiselm. Use
'interactions' or 'linear'

dataused = [manz_apr1_conv; manz_may_conv; manz_jun_conv; manz_jul_conv;
manz_aug_conv; manz_sep_conv; manz_oct_conv; manz_nov_conv; manz_dec_conv;
manz_jan_conv; manz_feb_conv; manz_mar_conv; manz_apr2_conv];

%%%%%%%% Season Definition %%%%%%%%%%
% California summer (manz, cean, cham) = March - December
% Utah summer (sage, goak) = May - Oct
% Montana summer (DF, LP) = June - Oct
% Florida summer (fet, gal ,SP) = March - Nov

```

```

poss_pred = [2:11, 44:45]; %Column numbers of the predictor variables
poss_pred_pca = [2:11, 40:45, 53];%Column numbers of the predictor variables
plus chemical analysis
store_p = ones(poss_pred_pca(end),11)*NaN;
%% One predictor models
for i = poss_pred_pca
    try
        md_tig{i} = fitlm(dataused(:,i),dataused(:,12)); [p,F] =
coefTest(md_tig{i});
        store_md_tig{i} = [md_tig{i}.Rsquared.Adjusted, p, F, md_tig{i}.DFE,
md_tig{i}.RMSE, md_tig{i}.NumObservations, md_tig{i}.NumPredictors,
md_tig{i}.NumCoefficients];
        store_p(i,1) = p;
    catch
        disp(['tig: Column ' num2str(i) ' is empty for this predictor']);
    end
    try
        md_tmfh{i} = fitlm(dataused(:,i),dataused(:,17)); [p,F] =
coefTest(md_tmfh{i});
        store_md_tmfh{i} = [md_tmfh{i}.Rsquared.Adjusted, p, F, md_tmfh{i}.DFE,
md_tmfh{i}.RMSE, md_tmfh{i}.NumObservations, md_tmfh{i}.NumPredictors,
md_tmfh{i}.NumCoefficients];
        store_p(i,2) = p;
    catch
        disp(['tmfh: Column ' num2str(i) ' is empty for this predictor']);
    end
    try
        md_tbo{i} = fitlm(dataused(:,i),dataused(:,19)); [p,F] =
coefTest(md_tbo{i});
        store_md_tbo{i} = [md_tbo{i}.Rsquared.Adjusted, p, F, md_tbo{i}.DFE,
md_tbo{i}.RMSE, md_tbo{i}.NumObservations, md_tbo{i}.NumPredictors,
md_tbo{i}.NumCoefficients];
        store_p(i,3) = p;
    catch
        disp(['tbo: Column ' num2str(i) ' is empty for this predictor']);
    end
    try
        md_Tig{i} = fitlm(dataused(:,i),dataused(:,13)); [p,F] =
coefTest(md_Tig{i});
        store_md_Tig{i} = [md_Tig{i}.Rsquared.Adjusted, p, F, md_Tig{i}.DFE,
md_Tig{i}.RMSE, md_Tig{i}.NumObservations, md_Tig{i}.NumPredictors,
md_Tig{i}.NumCoefficients];
        store_p(i,4) = p;
    catch
        disp(['Tig: Column ' num2str(i) ' is empty for this predictor']);
    end
    try
        md_Tigmax{i} = fitlm(dataused(:,i),dataused(:,14)); [p,F] =
coefTest(md_Tigmax{i});
        store_md_Tigmax{i} = [md_Tigmax{i}.Rsquared.Adjusted, p, F,
md_Tigmax{i}.DFE, md_Tigmax{i}.RMSE, md_Tigmax{i}.NumObservations,
md_Tigmax{i}.NumPredictors, md_Tigmax{i}.NumCoefficients];
        store_p(i,5) = p;
    catch
        disp(['Tigmax: Column ' num2str(i) ' is empty for this predictor']);
    end
end
try

```

```

    md_Tigmode{i} = fitlm(dataused(:,i),dataused(:,16)); [p,F] =
coefTest(md_Tigmode{i});
    store_md_Tigmode{i} = [md_Tigmode{i}.Rsquared.Adjusted, p, F,
md_Tigmode{i}.DFE, md_Tigmode{i}.RMSE, md_Tigmode{i}.NumObservations,
md_Tigmode{i}.NumPredictors, md_Tigmode{i}.NumCoefficients];
    store_p(i,6) = p;
    catch
    disp(['Tigmode: Column ' num2str(i) ' is empty for this predictor']);
    end
    try
    md_mfh{i} = fitlm(dataused(:,i),dataused(:,20)); [p,F] =
coefTest(md_mfh{i});
    store_md_mfh{i} = [md_mfh{i}.Rsquared.Adjusted, p, F, md_mfh{i}.DFE,
md_mfh{i}.RMSE, md_mfh{i}.NumObservations, md_mfh{i}.NumPredictors,
md_mfh{i}.NumCoefficients];
    store_p(i,7) = p;
    catch
    disp(['mfh: Column ' num2str(i) ' is empty for this predictor']);
    end
    try
    md_mfa{i} = fitlm(dataused(:,i),dataused(:,23)); [p,F] =
coefTest(md_mfa{i});
    store_md_mfa{i} = [md_mfa{i}.Rsquared.Adjusted, p, F, md_mfa{i}.DFE,
md_mfa{i}.RMSE, md_mfa{i}.NumObservations, md_mfa{i}.NumPredictors,
md_mfa{i}.NumCoefficients];
    store_p(i,8) = p;
    catch
    disp(['mfa: Column ' num2str(i) ' is empty for this predictor']);
    end
    try
    md_igmfrac{i} = fitlm(dataused(:,i),dataused(:,31)); [p,F] =
coefTest(md_igmfrac{i});
    store_md_igmfrac{i} = [md_igmfrac{i}.Rsquared.Adjusted, p, F,
md_igmfrac{i}.DFE, md_igmfrac{i}.RMSE, md_igmfrac{i}.NumObservations,
md_igmfrac{i}.NumPredictors, md_igmfrac{i}.NumCoefficients];
    store_p(i,9) = p;
    catch
    disp(['igmfrac: Column ' num2str(i) ' is empty for this predictor']);
    end
    try
    md_igdevol{i} = fitlm(dataused(:,i),dataused(:,32)); [p,F] =
coefTest(md_igdevol{i});
    store_md_igdevol{i} = [md_igdevol{i}.Rsquared.Adjusted, p, F,
md_igdevol{i}.DFE, md_igdevol{i}.RMSE, md_igdevol{i}.NumObservations,
md_igdevol{i}.NumPredictors, md_igdevol{i}.NumCoefficients];
    store_p(i,10) = p;
    catch
    disp(['igdevol: Column ' num2str(i) ' is empty for this predictor']);
    end
    try
    md_igdevolfrac{i} = fitlm(dataused(:,i),dataused(:,46)); [p,F] =
coefTest(md_igdevolfrac{i});
    store_md_igdevolfrac{i} = [md_igdevolfrac{i}.Rsquared.Adjusted, p, F,
md_igdevolfrac{i}.DFE, md_igdevolfrac{i}.RMSE,
md_igdevolfrac{i}.NumObservations, md_igdevolfrac{i}.NumPredictors,
md_igdevolfrac{i}.NumCoefficients];
    store_p(i,11) = p;

```

```

    catch
    disp(['igdevol: Column ' num2str(i) ' is empty for this predictor']);
    end
end
k=1;
for i = poss_pred_pca
    try
    tbl_R2(1,k) = store_md_tig{i}(1); %all tig models
    tbl_R2(2,k) = store_md_tmfh{i}(1); %all tmfh models
    tbl_R2(3,k) = store_md_tbo{i}(1);
    tbl_R2(4,k) = store_md_Tig{i}(1);
    tbl_R2(5,k) = store_md_Tigmax{i}(1);
    tbl_R2(6,k) = store_md_mfh{i}(1);
    tbl_R2(7,k) = store_md_igmfrac{i}(1);
    tbl_R2(8,k) = store_md_igdevol{i}(1);
    tbl_R2(9,k) = store_md_igdevolfrac{i}(1);

    tbl_F(1,k) = store_md_tig{i}(3); %all tig models
    tbl_F(2,k) = store_md_tmfh{i}(3); %all tmfh models
    tbl_F(3,k) = store_md_tbo{i}(3);
    tbl_F(4,k) = store_md_Tig{i}(3);
    tbl_F(5,k) = store_md_Tigmax{i}(3);
    tbl_F(6,k) = store_md_mfh{i}(3);
    tbl_F(7,k) = store_md_igmfrac{i}(3);
    tbl_F(8,k) = store_md_igdevol{i}(3);
    tbl_F(9,k) = store_md_igdevolfrac{i}(3);

    tbl_p(1,k) = store_md_tig{i}(2); %all tig models
    tbl_p(2,k) = store_md_tmfh{i}(2); %all tmfh models
    tbl_p(3,k) = store_md_tbo{i}(2);
    tbl_p(4,k) = store_md_Tig{i}(2);
    tbl_p(5,k) = store_md_Tigmax{i}(2);
    tbl_p(6,k) = store_md_mfh{i}(2);
    tbl_p(7,k) = store_md_igmfrac{i}(2);
    tbl_p(8,k) = store_md_igdevol{i}(2);
    tbl_p(9,k) = store_md_igdevolfrac{i}(2);
    k=k+1;
    catch
    end
end

%% Stepwise Models
g1 = [2 3 45];    g2 = [11 44];    g3 = [4 7 8 9];    g4 = [5 6 10]; g5 =
40:43;
% [MC, RMC, m.water] [m.fresh, m.dry] [rho,NL,thick,dia] [L,W,SA]
[lipid,vol,FC,ash];
if strcmp(species, 'manz')==1 || strcmp(species, 'fet')==1 || strcmp(species,
'goak')==1
    g1 = [2 3 45]; g2 = [11 44]; g3 = [4 8]; g4 = [5 6 10]; g5 = 40:43; numg =
5;
elseif strcmp(species, 'cean')==1 || strcmp(species, 'gal')==1
    g1 = [2 3 45]; g2 = [11 44]; g3 = [4 8]; g4 = [5 6 10]; numg = 4;
elseif strcmp(species, 'DF')==1
    g1 = [2 3 45]; g2 = [11 44]; g3 = [4 7 9]; g4 = [5 6]; g5 = 40:43; numg =
5;
elseif strcmp(species, 'SP')==1

```

```

    g1 = [2 3 45]; g2 = [11 44]; g3 = [4 7 9]; g4 = [5 6]; numg = 4;
elseif strcmp(species, 'LP')==1
    g1 = [2 3 45]; g2 = [11 44]; g3 = [7 9]; g4 = [5 6]; numg = 4;
elseif strcmp(species, 'cham')==1 || strcmp(species, 'sage')==1
    g1 = [2 3 45]; g2 = [11 44]; g3 = [5 9]; numg = 3; %g4 = [5]; numg = 4;
end

numNaN = 0; %counter for the number of times that a model didn't work because
of a column of NaNs
i = 1;
while i <= nreps
    %Extract a random subset of variables for use in the model development
    predictors = zeros(size(dataused,1),dim_md_upper); coltrack =
zeros(dim_md_upper,2);
    dmy3 = randsample(numg,dim_md_upper);
    a = eval(['g' num2str(dmy3(1))]); dmy1(1) = randsample(a,1); b =
eval(['g' num2str(dmy3(2))]); dmy1(2) = randsample(b,1); c = eval(['g'
num2str(dmy3(3))]); dmy1(3) = randsample(c,1); d = eval(['g'
num2str(dmy3(4))]); dmy1(4) = randsample(d,1);
    dmy2 = randi(5,[dim_md_upper 1]); %This will generate a vector with
for j = 1:size(predictors,2)
    coltrack(j,:) = [dmy1(j),dmy2(j)];
    if dmy2(j) == 1; predictors(:,j) = dataused(:,dmy1(j)); elseif
dmy2(j) == 2; predictors(:,j) = log(dataused(:,dmy1(j)));
    elseif dmy2(j) == 3; predictors(:,j) = (dataused(:,dmy1(j))).^2;
elseif dmy2(j) == 4; predictors(:,j) = sqrt(dataused(:,dmy1(j)));
    elseif dmy2(j) == 5; predictors(:,j) = (dataused(:,dmy1(j))).^(-1);
    end
end

%Stepwise Model working up from a constant
if i < nreps/2
try
    tig =
stepwiselm(predictors,dataused(:,12),'constant','Upper',md_ceil,'Criterion','
bic'); %'AdjRsquared');
    store_tig_crit(i,:) = [i, tig.NumCoefficients, tig.Rsquared.Adjusted,
tig.ModelCriterion.AIC, tig.ModelCriterion.BIC, tig.NumObservations];
    [p,F] = coefTest(tig); store_tig_info{i,:} = {i, p, F, tig.DFE,
tig.NumObservations, tig.RMSE, tig.Coefficients, tig.Formula, coltrack};
    md_tig_sw{i,:} = tig;
    Tig =
stepwiselm(predictors,dataused(:,13),'constant','Upper',md_ceil,'Criterion','
bic'); %'AdjRsquared');
    store_Tig_crit(i,:) = [i, Tig.NumCoefficients, Tig.Rsquared.Adjusted,
Tig.ModelCriterion.AIC, Tig.ModelCriterion.BIC, Tig.NumObservations];
    [p,F] = coefTest(Tig); store_Tig_info{i,:} = {i, p, F, Tig.DFE,
Tig.NumObservations, Tig.RMSE, Tig.Coefficients, Tig.Formula, coltrack};
    md_Tig_sw{i,:} = Tig;
    MFHt =
stepwiselm(predictors,dataused(:,17),'constant','Upper',md_ceil,'Criterion','
bic'); %'AdjRsquared');
    store_MFHt_crit(i,:) = [i, MFHt.NumCoefficients, MFHt.Rsquared.Adjusted,
MFHt.ModelCriterion.AIC, MFHt.ModelCriterion.BIC, MFHt.NumObservations];
    [p,F] = coefTest(MFHt); store_MFHt_info{i,:} = {i, p, F, MFHt.DFE,
MFHt.NumObservations, MFHt.RMSE, MFHt.Coefficients, MFHt.Formula, coltrack};

```

```

    md_MFHT_sw{i,:} = MFHT;
    BOT =
stepwiselm(predictors,dataused(:,19),'constant','Upper',md_ceil,'Criterion','
bic'); %'AdjRsquared');
    store_BOT_crit(i,:) = [i, BOT.NumCoefficients, BOT.Rsquared.Adjusted,
BOT.ModelCriterion.AIC, BOT.ModelCriterion.BIC, BOT.NumObservations];
    [p,F] = coefTest(BOT); store_BOT_info{i,:} = {i, p, F, BOT.DFE,
BOT.NumObservations, BOT.RMSE, BOT.Coefficients, BOT.Formula, coltrack};
    md_BOT_sw{i,:} = BOT;
    MFH =
stepwiselm(predictors,dataused(:,20),'constant','Upper',md_ceil,'Criterion','
bic'); %'AdjRsquared');
    store_MFH_crit(i,:) = [i, MFH.NumCoefficients, MFH.Rsquared.Adjusted,
MFH.ModelCriterion.AIC, MFH.ModelCriterion.BIC, MFH.NumObservations];
    [p,F] = coefTest(MFH); store_MFH_info{i,:} = {i, p, F, MFH.DFE,
MFH.NumObservations, MFH.RMSE, MFH.Coefficients, MFH.Formula, coltrack};
    md_MFH_sw{i,:} = MFH;
    MFA =
stepwiselm(predictors,dataused(:,23),'constant','Upper',md_ceil,'Criterion','
bic'); %'AdjRsquared');
    store_MFA_crit(i,:) = [i, MFA.NumCoefficients, MFA.Rsquared.Adjusted,
MFA.ModelCriterion.AIC, MFA.ModelCriterion.BIC, MFA.NumObservations];
    [p,F] = coefTest(MFA); store_MFA_info{i,:} = {i, p, F, MFA.DFE,
MFA.NumObservations, MFA.RMSE, MFA.Coefficients, MFA.Formula, coltrack};
    md_MFA_sw{i,:} = MFA;
    Tigmax =
stepwiselm(predictors,dataused(:,14),'constant','Upper',md_ceil,'Criterion','
bic'); %'AdjRsquared');
    store_Tigmax_crit(i,:) = [i, Tigmax.NumCoefficients,
Tigmax.Rsquared.Adjusted, Tigmax.ModelCriterion.AIC,
Tigmax.ModelCriterion.BIC, Tigmax.NumObservations];
    [p,F] = coefTest(Tigmax); store_Tigmax_info{i,:} = {i, p, F, Tigmax.DFE,
Tigmax.NumObservations, Tigmax.RMSE, Tigmax.Coefficients, Tigmax.Formula,
coltrack};
    md_Tigmax_sw{i,:} = Tigmax;
    Tigmode =
stepwiselm(predictors,dataused(:,16),'constant','Upper',md_ceil,'Criterion','
bic'); %'AdjRsquared');
    store_Tigmode_crit(i,:) = [i, Tigmode.NumCoefficients,
Tigmode.Rsquared.Adjusted, Tigmode.ModelCriterion.AIC,
Tigmode.ModelCriterion.BIC, Tigmode.NumObservations];
    [p,F] = coefTest(Tigmode); store_Tigmode_info{i,:} = {i, p, F,
Tigmode.DFE, Tigmode.NumObservations, Tigmode.RMSE, Tigmode.Coefficients,
Tigmode.Formula, coltrack};
    md_Tigmode_sw{i,:} = Tigmode;
    i = i+1;
    clear coltrack
catch
    i = i; numNaN = numNaN + 1;
end
[i numNaN]
%Stepwise Model working down from the full model
else
try
    tig =
stepwiselm(predictors,dataused(:,12),md_ceil,'Upper',md_ceil,'Criterion','bic
'); %'AdjRsquared');

```

```

    store_tig_crit(i,:) = [i, tig.NumCoefficients, tig.Rsquared.Adjusted,
tig.ModelCriterion.AIC, tig.ModelCriterion.BIC, tig.NumObservations];
    [p,F] = coefTest(tig); store_tig_info{i,:} = {i, p, F, tig.DFE,
tig.NumObservations, tig.RMSE, tig.Coefficients, tig.Formula, coltrack};
    md_tig_sw{i,:} = tig;
    Tig =
stepwiselm(predictors,dataused(:,13),md_ceil,'Upper',md_ceil,'Criterion','bic
'); %'AdjRsquared');
    store_Tig_crit(i,:) = [i, Tig.NumCoefficients, Tig.Rsquared.Adjusted,
Tig.ModelCriterion.AIC, Tig.ModelCriterion.BIC, Tig.NumObservations];
    [p,F] = coefTest(Tig); store_Tig_info{i,:} = {i, p, F, Tig.DFE,
Tig.NumObservations, Tig.RMSE, Tig.Coefficients, Tig.Formula, coltrack};
    md_Tig_sw{i,:} = Tig;
    MFHt =
stepwiselm(predictors,dataused(:,17),md_ceil,'Upper',md_ceil,'Criterion','bic
'); %'AdjRsquared');
    store_MFHt_crit(i,:) = [i, MFHt.NumCoefficients, MFHt.Rsquared.Adjusted,
MFHt.ModelCriterion.AIC, MFHt.ModelCriterion.BIC, MFHt.NumObservations];
    [p,F] = coefTest(MFHt); store_MFHt_info{i,:} = {i, p, F, MFHt.DFE,
MFHt.NumObservations, MFHt.RMSE, MFHt.Coefficients, MFHt.Formula, coltrack};
    md_MFHt_sw{i,:} = MFHt;
    BOT =
stepwiselm(predictors,dataused(:,19),md_ceil,'Upper',md_ceil,'Criterion','bic
'); %'AdjRsquared');
    store_BOT_crit(i,:) = [i, BOT.NumCoefficients, BOT.Rsquared.Adjusted,
BOT.ModelCriterion.AIC, BOT.ModelCriterion.BIC, BOT.NumObservations];
    [p,F] = coefTest(BOT); store_BOT_info{i,:} = {i, p, F, BOT.DFE,
BOT.NumObservations, BOT.RMSE, BOT.Coefficients, BOT.Formula, coltrack};
    md_BOT_sw{i,:} = BOT;
    MFH =
stepwiselm(predictors,dataused(:,20),md_ceil,'Upper',md_ceil,'Criterion','bic
'); %'AdjRsquared');
    store_MFH_crit(i,:) = [i, MFH.NumCoefficients, MFH.Rsquared.Adjusted,
MFH.ModelCriterion.AIC, MFH.ModelCriterion.BIC, MFH.NumObservations];
    [p,F] = coefTest(MFH); store_MFH_info{i,:} = {i, p, F, MFH.DFE,
MFH.NumObservations, MFH.RMSE, MFH.Coefficients, MFH.Formula, coltrack};
    md_MFH_sw{i,:} = MFH;
    MFA =
stepwiselm(predictors,dataused(:,23),md_ceil,'Upper',md_ceil,'Criterion','bic
'); %'AdjRsquared');
    store_MFA_crit(i,:) = [i, MFA.NumCoefficients, MFA.Rsquared.Adjusted,
MFA.ModelCriterion.AIC, MFA.ModelCriterion.BIC, MFA.NumObservations];
    [p,F] = coefTest(MFA); store_MFA_info{i,:} = {i, p, F, MFA.DFE,
MFA.NumObservations, MFA.RMSE, MFA.Coefficients, MFA.Formula, coltrack};
    md_MFA_sw{i,:} = MFA;
    Tigmax =
stepwiselm(predictors,dataused(:,14),md_ceil,'Upper',md_ceil,'Criterion','bic
'); %'AdjRsquared');
    store_Tigmax_crit(i,:) = [i, Tigmax.NumCoefficients,
Tigmax.Rsquared.Adjusted, Tigmax.ModelCriterion.AIC,
Tigmax.ModelCriterion.BIC, Tigmax.NumObservations];
    [p,F] = coefTest(Tigmax); store_Tigmax_info{i,:} = {i, p, F, Tigmax.DFE,
Tigmax.NumObservations, Tigmax.RMSE, Tigmax.Coefficients, Tigmax.Formula,
coltrack};
    md_Tigmax_sw{i,:} = Tigmax;

```

```

Tigmode =
stepwiselm(predictors,dataused(:,16),md_ceil,'Upper',md_ceil,'Criterion','bic
'); %'AdjRsquared');
    store_Tigmode_crit(i,:) = [i, Tigmode.NumCoefficients,
Tigmode.Rsquared.Adjusted, Tigmode.ModelCriterion.AIC,
Tigmode.ModelCriterion.BIC, Tigmode.NumObservations];
    [p,F] = coefTest(Tigmode); store_Tigmode_info{i,:} = {i, p, F,
Tigmode.DFE, Tigmode.NumObservations, Tigmode.RMSE, Tigmode.Coefficients,
Tigmode.Formula, coltrack};
    md_Tigmode_sw{i,:} = Tigmode;
    i = i+1;
    clear coltrack
catch
    i = i; numNaN = numNaN + 1;
end
[i numNaN]
end

end
%Sort models
best_tig_p = sortrows(store_tig_crit,2); best_tig_AdjR =
sortrows(store_tig_crit,-3); best_tig_aic = sortrows(store_tig_crit,4);
best_tig_bic = sortrows(store_tig_crit,5); best_tig_obs =
sortrows(store_tig_crit,-6);
best_tig_crit = [store_tig_crit(1,:); best_tig_p(1:best_num,:);
best_tig_AdjR(1:best_num,:); best_tig_aic(1:best_num,:);
best_tig_bic(1:best_num,:); best_tig_obs(1:best_num,:)];
md_tig_crit = best_tig_AdjR(1,:); md_tig_info =
store_tig_info{best_tig_AdjR(1,1),:};
best_Tig_p = sortrows(store_Tig_crit,2); best_Tig_AdjR =
sortrows(store_Tig_crit,-3); best_Tig_aic = sortrows(store_Tig_crit,4);
best_Tig_bic = sortrows(store_Tig_crit,5);best_Tig_obs =
sortrows(store_Tig_crit,-6);
best_Tig_crit = [store_Tig_crit(1,:); best_Tig_p(1:best_num,:);
best_Tig_AdjR(1:best_num,:); best_Tig_aic(1:best_num,:);
best_Tig_bic(1:best_num,:); best_Tig_obs(1:best_num,:)];
md_Tig_crit = best_Tig_AdjR(1,:); md_Tig_info =
store_Tig_info{best_Tig_AdjR(1,1),:};
best_Tigmax_p = sortrows(store_Tigmax_crit,2); best_Tigmax_AdjR =
sortrows(store_Tigmax_crit,-3); best_Tigmax_aic =
sortrows(store_Tigmax_crit,4); best_Tigmax_bic =
sortrows(store_Tigmax_crit,5);best_Tigmax_obs = sortrows(store_Tigmax_crit,-
6);
best_Tigmax_crit = [store_Tigmax_crit(1,:); best_Tigmax_p(1:best_num,:);
best_Tigmax_AdjR(1:best_num,:); best_Tigmax_aic(1:best_num,:);
best_Tigmax_bic(1:best_num,:); best_Tigmax_obs(1:best_num,:)];
md_Tigmax_crit = best_Tigmax_AdjR(1,:); md_Tigmax_info =
store_Tigmax_info{best_Tigmax_AdjR(1,1),:};
best_Tigmode_p = sortrows(store_Tigmode_crit,2); best_Tigmode_AdjR =
sortrows(store_Tigmode_crit,-3); best_Tigmode_aic =
sortrows(store_Tigmode_crit,4); best_Tigmode_bic =
sortrows(store_Tigmode_crit,5);best_Tigmode_obs =
sortrows(store_Tigmode_crit,-6);
best_Tigmode_crit = [store_Tigmode_crit(1,:); best_Tigmode_p(1:best_num,:);
best_Tigmode_AdjR(1:best_num,:); best_Tigmode_aic(1:best_num,:);
best_Tigmode_bic(1:best_num,:); best_Tigmode_obs(1:best_num,:)];

```

```

md_Tigmode_crit = best_Tigmode_AdjR(1,:); md_Tigmode_info =
store_Tigmode_info{best_Tigmode_AdjR(1,1),:};
best_MFHT_p = sortrows(store_MFHT_crit,2); best_MFHT_AdjR =
sortrows(store_MFHT_crit,-3); best_MFHT_aic = sortrows(store_MFHT_crit,4);
best_MFHT_bic = sortrows(store_MFHT_crit,5);best_MFHT_obs =
sortrows(store_MFHT_crit,-6);
best_MFHT_crit = [store_MFHT_crit(1,:); best_MFHT_p(1:best_num,:);
best_MFHT_AdjR(1:best_num,:); best_MFHT_aic(1:best_num,:);
best_MFHT_bic(1:best_num,:); best_MFHT_obs(1:best_num,:)];
md_MFHT_crit = best_MFHT_AdjR(1,:); md_MFHT_info =
store_MFHT_info{best_MFHT_AdjR(1,1),:};
best_BOT_p = sortrows(store_BOT_crit,2); best_BOT_AdjR =
sortrows(store_BOT_crit,-3); best_BOT_aic = sortrows(store_BOT_crit,4);
best_BOT_bic = sortrows(store_BOT_crit,5);best_BOT_obs =
sortrows(store_BOT_crit,-6);
best_BOT_crit = [store_BOT_crit(1,:); best_BOT_p(1:best_num,:);
best_BOT_AdjR(1:best_num,:); best_BOT_aic(1:best_num,:);
best_BOT_bic(1:best_num,:); best_BOT_obs(1:best_num,:)];
md_BOT_crit = best_BOT_AdjR(1,:); md_BOT_info =
store_BOT_info{best_BOT_AdjR(1,1),:};
best_MFH_p = sortrows(store_MFH_crit,2); best_MFH_AdjR =
sortrows(store_MFH_crit,-3); best_MFH_aic = sortrows(store_MFH_crit,4);
best_MFH_bic = sortrows(store_MFH_crit,5);best_MFH_obs =
sortrows(store_MFH_crit,-6);
best_MFH_crit = [store_MFH_crit(1,:); best_MFH_p(1:best_num,:);
best_MFH_AdjR(1:best_num,:); best_MFH_aic(1:best_num,:);
best_MFH_bic(1:best_num,:); best_MFH_obs(1:best_num,:)];
md_MFH_crit = best_MFH_AdjR(1,:); md_MFH_info =
store_MFH_info{best_MFH_AdjR(1,1),:};
best_MFA_p = sortrows(store_MFA_crit,2); best_MFA_AdjR =
sortrows(store_MFA_crit,-3); best_MFA_aic = sortrows(store_MFA_crit,4);
best_MFA_bic = sortrows(store_MFA_crit,5);best_MFA_obs =
sortrows(store_MFA_crit,-6);
best_MFA_crit = [store_MFA_crit(1,:); best_MFA_p(1:best_num,:);
best_MFA_AdjR(1:best_num,:); best_MFA_aic(1:best_num,:);
best_MFA_bic(1:best_num,:); best_MFA_obs(1:best_num,:)];
md_MFA_crit = best_MFA_AdjR(1,:); md_MFA_info =
store_MFA_info{best_MFA_AdjR(1,1),:};

save(['B:\Experiments\Seasonal Moisture Content Project\Files for Seasonal
Paper\' species '_' type '_' heat '_' age '.mat']);

```